UNIVERSITÉ DE SHERBROOKE
Faculté de génie
Département de génie mécanique

# Système intégré de stockage de l'électricité renouvelable par air comprimé

## Integrated storage system for renewable electricity by compressed air

Thèse de doctorat
Spécialité : Génie Mécanique

Mohamad Cheayb

Sherbrooke, Québec, Canada

January 2020

# Jury members

Prof. Sébastien Poncet (Université de Sherbrooke)
Supervisor
Prof. Mohand Tazerout (IMT Atalantique), supervisor
Supervisor

Dr Mylène Marin Gallego (IMT Atalantique)
Co-supervisor

Prof. Hachimi Fellouah (Université de Sherbrooke)
Rapporteur
Prof. Yann Bartosiewicz (Université catholique de Louvain)
Examiner
Prof. Stéphane Hallé (École de Technologie Supérieure)
Examiner

# RÉSUMÉ

De nos jours, en raison des préoccupations liées à la protection de l'environnement et à la sécurité énergétique, l'utilisation des énergies renouvelables (ER) est en pleine croissance. L'intégration actuelle et future des ER entraîne des déséquilibres importants entre la production et la consommation d'électricité ainsi que des problèmes liés à la flexibilité et à la fiabilité de la gestion du réseau électrique. Dans ce contexte, les technologies de stockage de l'énergie électrique (SEE) s'avèrent être l'élément clé pour relever ces défis. En outre, dans les sites hors réseau qui ont recours aux moteurs diesel, les systèmes SEE sont essentiels pour accroître le taux de pénétration des énergies renouvelables et réduire la consommation d'énergie combustible.

De nouvelles évolutions dans le domaine du stockage d'énergie par air comprimé CAES (compressed air energy storage) ont été effectuées en utilisant la chaleur produite durant la phase de compression et en employant des réservoirs de stockage artificiels indépendamment de la disponibilité des cavernes souterraines. Grâce à ces améliorations, le CAES se révèle être une technologie prometteuse pour des applications pratiques. Récemment, le concept de stockage d'énergie trigénérative à air comprimé T-CAES (énergie thermique, mécanique et frigorifique) a été introduit. De nombreuses études soulignent la faisabilité et les avantages de ce système pour être implanté au niveau du consommateur.

Les objectifs de ce projet de recherche sont d'examiner les configurations du système T-CAES, de l'étudier par une approche couplée expériences/modélisations, ainsi que d'effectuer une optimisation technico-économique pour des systèmes à petite échelle, généralement inférieure à 500 kW.

En partant d'un modèle thermodynamique simplifié, les différentes configurations du système ont été étudiées et les paramètres clés ayant une influence dominante sur l'efficacité du système ont été identifiés. Cette analyse permet de mieux comprendre les principes fondamentaux et le concept thermodynamique de notre système, ainsi que de déduire deux configurations de base du système. Ensuite, un modèle thermodynamique détaillé de ces configurations a été développé incluant les aspects technologiques existants et les interrelations entre les composants.

Un banc expérimental a été utilisé pour valider le modèle des composants côté air et pour étudier l'effet des paramètres de fonctionnement sur l'efficacité du système. Les prédictions du modèle sont conformes aux mesures expérimentales pendant les phases de charge, de stockage et de décharge. De plus, il a été constaté que la chute de température à travers le régulateur de pression ne doit pas être ignorée et elle est régie par l'effet de Joule-Thomson. Par ailleurs, il a été observé que la température d'entrée du moteur pneumatique doit être étudiée pour évaluer de futures configurations.

L'étude se concentre ensuite sur l'étude des effets mutuels des paramètres de conception et de leur influence sur les performances du système, la densité énergétique et l'empreinte des échangeurs de chaleur via une étude paramétrique. Il est ressorti de cette analyse que la température du stockage d'énergie thermique, le nombre d'étages de compression et l'efficacité des échangeurs de chaleur devraient être choisis comme compromis entre l'efficacité du système, l'empreinte des échangeurs

de chaleur et le nombre requis d'étages de détente. Par contre, le choix de la pression maximale de stockage est un compromis à faire entre l'augmentation de la densité énergétique ou l'augmentation de l'efficacité du système. Une ligne directrice pour la conception optimale des paramètres clés mentionnés précédemment est ensuite fournie. Cette directive, la méthodologie et la procédure développée peuvent être étendues pour optimiser le système adiabatique A-CAES avec des changements mineurs. En se basant sur les technologies existantes et en utilisant une sélection optimale des paramètres, le rendement électrique de notre système à micro-échelle, généralement quelques kW, reste faible à 17%, tandis que l'efficacité du système augmente de 10.2% en ajoutant l'énergie électrique équivalente de production de froid et d'énergie thermique. Les faibles performances sont principalement liées aux pertes éxergétiques dans la vanne de détente et aux faibles rendements des machines à petites échelles.

L'étude a été complétée par l'élaboration d'un modèle économique du système en fonction de son échelle de puissance et d'énergie. Les résultats montrent que le coût des réservoirs de stockage d'air représente le coût le plus élevé et que la plage technico-économique optimale de la pression maximale de stockage se situe entre 120 et 200 bars. En outre, malgré les faibles performances du système, il a été constaté qu'il pourrait être compétitif à long terme avec les batteries électrochimiques en termes de coûts d'investissement, en particulier après avoir comptabilisé les coûts de production des énergies de chauffage et de refroidissement.

Les travaux futurs devraient être orientés vers l'amélioration de l'efficacité du système par l'étude du potentiel d'intégration des tubes à vortex et le développement technologique des machines de détente. De plus, les recherches futures peuvent envisager de réduire les coûts de stockage de l'air en intégrant les réservoirs sous pression en acier/béton qui sont en cours de développement.

**Mots-clés**: Stockage par air comprimé, trigénération, étude expérimentale, modèle thermodynamique, optimisation technico-économique, étude paramétrique.

# ABSTRACT

Nowadays, as a result of environmental and energy security concerns, the use of renewable energy (RE) is growing rapidly. The actual and prospective integration of RE results in significant imbalances between electricity production and consumption as well as problems related to the flexibility and reliability of grid operations. Here, electrical energy storage (EES) technologies turn out to be the key element to address these challenges. In addition, in off-grid sites relying originally on diesel engine, EES is a critical point in order to increase the penetration rate of RE and to reduce fuel energy consumption.

New advances in compressed air energy storage (CAES) have been made in the use of heat generated from compression and the use of artificial storage reservoirs independently from the availability of underground caverns. Such improvements make CAES a promising technology for practical applications. Recently, the concept of trigenerative compressed air energy storage T-CAES (heat energy, mechanical energy and cooling power) was introduced. Many studies highlight the feasibility and the benefits of this system to be placed close to the energy demand.

The aims of this research project are to examine the T-CAES system configurations, to study it by a coupled experimental/modeling approach, as well as to conduct its techno-economic optimizations and economic feasibility at a small-scale, typically less than 500 kW.

Starting from a simplified thermodynamic model, the different configurations of the system was investigated and the key parameters having dominant influences on the system efficiency were identified. This analysis enhances the fundamental understanding and the thermodynamic concept of our system and enabled to conclude two main basic configurations. Then, a whole detailed thermodynamic model of the system configurations was developed including the existing technological aspects and the relations between components.

An experimental bench was used to validate the model of air side components and to investigate the effect of operating parameters on the system efficiency and the model accuracy.
Model predictions were consistent with experimental measurements during charge, storage and discharge phases. It has been found that the temperature drop across the pressure regulator should not be ignored and is governed by the Joule-Thomson effect. Besides, it has been observed that the input temperature of the air motor must be accounted for in the assessment of future improved configurations.

The study then focuses on investigating the mutual effects of the design parameters and their influences on the system performances, energy density and heat exchanger footprints via a parametric study. From this analysis, it is found that the temperature of the thermal energy storage, the number of compression stages and the effectiveness of heat exchangers should be selected as a trade-off between the system efficiencies, heat exchangers footprints and the required number of expansion stages. Meanwhile, the selection of the maximum storage pressure is a choice whether to increase the energy density or the system efficiencies. An optimal design guideline of the above key parameters is then provided. This guideline, the method and the procedure developed can be applied to the optimization of the trigenerative compressed air energy storage and could be

extended for the adiabatic one with minor changes. Based on existing technologies and using an optimal set of parameters, the round-trip electrical efficiency of our system at micro-scale, typically a few of kW remains low at 17%, while the system efficiency increases by 10.2% by adding the equivalent electric energy of cooling and heating energy productions. The poor performances are mainly linked to the exergy losses in the throttling valve and the low values of the component efficiencies at a micro-scale.

The study was extended by developing an economic model of the system as a function of its power and energy scale. The results show that the cost of air storage tanks accounts for the highest cost, and the optimal techno-economical range of the maximum storage pressure is [120 bars-200 bars]. Besides, regardless of the low efficiency of the system, it was found that it could be competitive with electrochemical batteries in terms of investments cost at long terms, especially when accounting for the free-cost of cooling and heating energy production.

Future work should focus on the improvement of the efficiency of the system by investigating the potential of integrating of vortex tube, and on technology development of expander machineries. In addition, future research can consider reducing the air storage cost by integrating the under-development steel/concrete pressure vessels.

**Keywords:** Compressed air energy storage, trigeneration, experimental study, thermodynamic model, techno-economic optimization, parametric study.

# ACKNOWLEDGEMENTS

I would like to sincerely thank my supervisors Prof. Sébastien Poncet and Prof. Mohand Tazerout for providing me an opportunity to do this project. Thankfulness to Prof. Poncet, for his support, guidance, scientific vision and trust. My gratitude to Prof. Tazerout for his useful guidance, insight comments and his expertise. I am grateful to my co-supervisor Dr. Mylene Marin-Gallego for her valuable support, encouragement and understanding.

I would like to express my profound gratitude to the members of the jury, for their time to assess my work and their insightful suggestions and comments to improve it.

I would like to express my special thanks for our industrial partner Sigma Energy Storage, especially Dr. Richard Boudreault, not only for providing a part of the funding, but for his critical thinking and his professional cooperation.

Last, but not least, I owe my deep gratitude to the Conseil Régional d'Ile-de-France, for my previous Master Scholarship which allows me to enrich my education and my professional career.

# Table of Contents

CHAPTER 1 - INTRODUCTION ..... 1
1.1 Background and motivation ..... 1
1.2 Objectives and approach ..... 4
1.3 Outlines ..... 5
CHAPTER 2 – STATE OF ART ON ELECTRICAL ENERGY STORAGE TECHNOLOGIES 6
2.1 Overview on Electrical Energy Storage technologies ..... 6
2.1.1 Hydraulic Pumped Energy Storage ..... 6
2.1.2 Compressed Air Energy Storage ..... 7
2.1.3 Thermal Energy Storage ..... 8
2.1.4 Electrochemical batteries ..... 10
2.1.5 Chemical storage: Fuel cell ..... 11
2.1.6 Other Storage Systems ..... 12
2.2 Comparison and evaluation of EES technologies ..... 12
2.2.1 Maturity ..... 15
2.2.2 Power and energy scale ..... 15
2.2.3 Efficiency ..... 15
2.2.4 Energy and power density ..... 15
2.2.5 Time of storage and self-discharge ..... 16
2.2.6 Response time ..... 16
2.2.7 Lifetime ..... 16
2.2.8 Cost ..... 17
2.2.9 Environmental impacts ..... 17
2.2.10 Global synthesis on EES ..... 17
2.3 General working principle and classifications of CAES technologies ..... 18
2.3.1 Working principle ..... 18
2.3.2 Classifications ..... 19
2.4 Conventional/Diabatic compressed air energy storage D-CAES ..... 22
2.5 Adiabatic compressed air energy storage A-CAES ..... 23
2.5.1 A-CAES at high TES temperature ..... 24
2.5.2 A-CAES at medium TES temperature ..... 25
2.5.3 A-CAES at low TES temperature ..... 26

2.6 Trigenerative Compressed Air Energy Storage T-CAES ..... 29
2.6.1 Evaluation of the performances of T-CAES ..... 35
2.6.2 Optimization studies on Adiabatic and T-CAES. ..... 37
2.7 Conclusions and Problematic ..... 38
CHAPTER 3 - THERMODYNAMIC CONCEPT AND ENERGETIC ANALYSIS OF THE TRIGENERATIVE COMPRESSED AIR ENERGY STORAGE ..... 40
3.1 Objectives and originality ..... 40
3.2 Methodology ..... 40
3.3 Governing thermodynamic equations ..... 41
3.3.1 Charging phase ..... 41
3.3.2 Discharging phase ..... 43
3.3.3 Global system assessment ..... 44
3.4 Thermodynamic concept ..... 45
3.4.1 Adiabatic concept ..... 45
3.4.2 Trigenerative concept ..... 47
3.5 Trigenerative Compressed Air Energy Storage possible configurations ..... 49
3.5.1 Energy analysis method ..... 49
3.5.2 Possible configurations ..... 50
3.5.3 Basic configurations ..... 52
3.6 Conclusion ..... 53
CHAPTER 4 – DESCRIPTION AND MODELLING OF THE TRIGENERATIVE COMPRESSED AIR ENERGY STORAGE. ..... 55
4.1 Objectives ..... 55
4.2 System description ..... 55
4.3 Modeling of the T-CAES process ..... 58
4.3.1 Modeling assumptions ..... 58
4.3.2 Modelling of the charge phase ..... 59
4.3.3 Modelling of the discharge phase ..... 62
4.3.4 Modelling of heat exchangers and thermal energy storage ..... 68
4.4 Evaluation criteria ..... 73
4.5 Conclusion ..... 74
CHAPTER 5 - EXPERIMENTAL TESTS AND MODEL VALIDATION OF A SMALL SCALE TRIGENERATIVE COMPRESSED AIR ENERGY STORAGE SYSTEM ..... 76

5.1 . Objectives and originality ..... 76
5.2 Experimental Setup ..... 76
5.2.1 . General description ..... 76
5.2.2 . Compressor chain ..... 78
5.2.3 . Storage reservoir ..... 79
5.2.4 . Air motor and pressure regulator ..... 79
5.3 . Experimental results and model validation ..... 80
5.3.1 . Charge phase ..... 81
5.3.2 . Storage phase ..... 84
5.3.3 . Discharge phase ..... 84
5.4 Experimental Focus on the throttling valve and the air motor ..... 87
5.4.1 . Throttling valve ..... 87
5.4.2 . Air Motor ..... 87
5.5 . Conclusions and perspectives ..... 88
CHAPTER 6 - PARAMETRIC OPTIMIZATION OF SMALL SCALE TRIGENERATIVE COMPRESSED AIR ENERGY STORAGE ..... 91
6.1 Objectives and originality ..... 91
6.2 Methodology of the parametric optimization ..... 91
6.3 . Results and discussions ..... 93
6.3.1 . Effects of the temperature of the thermal energy storage ..... 93
6.3.2 . Effects of the number of compression stages ..... 95
6.3.3 . Effect of the effectiveness of intercooling HEX ..... 97
6.3.4 . Effect of the effectiveness of discharge phase HEX ..... 99
6.3.5 . Effect of the maximum storage pressure ..... 101
6.3.6 . Effect of the cooling energy ..... 104
6.4 . Characteristics of the micro-scale T-CAES ..... 104
6.5 . Conclusions and perspectives ..... 106
CHAPTER 7 - TECHNO ECONOMIC STUDY OF T-CAES ..... 109
7.1 . Introduction ..... 109
7.2 . Economic Modeling of the components of the T-CAES ..... 110
7.2.1 . General Method ..... 110
7.2.2 . Application of the method on T-CAES plant. ..... 112
7.3 . Methodology of the technoeconomic analysis and cost model validation ..... 115

7.3.1 . Methodology ..... 115
7.3.2 . Model reliability ..... 117
7.4 . Results and discussions ..... 118
7.4.1 . Optimal storage pressure range ..... 118
7.4.2 . Cost of the components and the plant ..... 119
7.4.3 . Comparison of the T-CAES with batteries ..... 123
7.5 Conclusions and Perspectives ..... 125
CHAPTER 8 – CONCLUSIONS AND PRESPECTIVES ..... 126
8.1 Conclusions (en français) ..... 126
8.2 . Conclusions (in English) ..... 130

# LIST OF TABLES

*Table 2.1: Thermo-physical proprieties of sensible heat TES materials (synthetized from [27,28] and [29])..... 9*
*Table 2.2: Thermo-physical proprieties of PCM for TES (collected from [28] and [30]). ..... 10*
*Table 2.3: Comparison of the evaluation criteria of EES technologies (collected from [2,4]). ..... 13*
*Table 2.4: Characteristics of the Huntorf and McIntosh power plants [9,10]. ..... 23*
*Table 2.5: Main characteristics of LT-A-CAES as proposed by relevant research studies..... 30*
*Table 2.6: Operation parameters of air side components of T-CAES as proposed by related authors. .... 34*
*Table 2.7: Characteristics of TES components of T-CAES as proposed by the mentioned authors. ..... 35*
*Table 2.8: Performances achieved by the studies conducted on T-CAES ..... 36*
*Table 3.1: Numerical example of an ideal A-CAES. ..... 46*
*Table 3.2: Imposed parameters to study the T-CAES..... 47*
*Table 3.3: Numerical values of energy flows of an ideal T-CAES. ..... 50*
*Table 3.4: Numerical values of energy streams of the first basic configuration..... 53*
*Table 5.1: Experimental characteristics of compression chain. ..... 79*
*Table 5.2: Experimental characteristics of the discharge phase ..... 80*
*Table 5.3: Experimental and model results of the charge phase. ..... 81*
*Table 5.4: Experimental and model results of the discharge phase. ..... 85*
*Table 5.5: Power and pressure output of the air motor for different operating conditions. ..... 88*
*Table 6.1: Fixed parameters and variable parameters of the parametric study. ..... 92*
*Table 6.2: Optimal solution of the design parameters. ..... 104*
*Table 6.3: Energy outputs, efficiencies and total HEX footprints of the two configurations with and without enabling the cooling energy. ..... 104*
*Table 6.4: Output parameters of the charge phase for the first configuration. ..... 105*
*Table 6.5: Output parameters of the discharge phase for the first configuration..... 106*
*Table 6.6: Main output parameters of the model for the first configuration. ..... 106*
*Table 7.1: Coefficients required for the calculation of capital cost of mechanical components (base year 2001 for compressors and HEX [6]). ..... 114*
*Table 7.2: Comparison between the results of the cost model and cost data of Matches Company. ..... 118*
*Table 7.3: Round trip electric efficiency and comprehensive efficiency of the proposed system..... 120*

# LIST OF FIGURES

*Figure 1.1: The main applications of electrical energy storage (EES).* ..... 2
*Figure 1.2: Distribution of isolated sites (left [9]) and wind farms in Canada (right, taken from Canadian Wind Energy Atlas).* ..... 3
*Figure 2.1: Schematic of pumped hydroelectric storage plant [2].* ..... 6
*Figure 2.2: Representative diagram of compressed air storage systems [2].* ..... 7
*Figure 2.3: Scheme of the application of TES in the power plant "Solar Power Tres"[26].* ..... 8
*Figure 2.4: General schematic of operation of electrochemical batteries [2].* ..... 11
*Figure 2.5: Classifications of compressed air energy storage systems [31].* ..... 19
*Figure 2.6: Representative scheme of isobaric CAES concept (a) [32] and the Hydrostor demonstration project (b) [33].* ..... 21
*Figure 2.7: Process operation of combined isobaric-CAES and PHS system proposed by Kim et al. [32].* ..... 22
*Figure 2.8: Basic concept of A-CAES [31].* ..... 23
*Figure 2.9: Schematic diagram of A-CAES at high TES temperature [31],[42].* ..... 25
*Figure 2.10: Block diagram of A-CAES at medium TES temperature [31].* ..... 26
*Figure 2.11: Schematic of A-CAES at low temperature of TES [31].* ..... 26
*Figure 2.12: Detailed schematic diagram of the experimental pilot "TIC-500", Chinese Academy of Sciences [39].* ..... 27
*Figure 2.13: T-CAES without preheating as proposed by Facci et al.[13], Lv et al.[19], Liu and Wang [20]and Arabkoohsar et al.[50].* ..... 31
*Figure 2.14: T-CAES with preheating as proposed by Jannelli et al.[16], Li et al. [21] and Han and Guo [51].* ..... 32
*Figure 3.1: Scheme of the charging phase.* ..... 41
*Figure 3.2: Scheme of the discharging phase.* ..... 42
*Figure 3.3: Block diagram of the thermodynamic equations of the T-CAES.* ..... 45
*Figure 3.4: A-CAES representation on the Clapeyron diagram.* ..... 47
*Figure 3.5: Input and Output temperature variation (left figure) and energy distribution as a function of the heat recuperated to stored ratio.* ..... 48
*Figure 3.6: Electrical efficiency variation as a function of the heat recuperated to stored ratio.* ..... 48
*Figure 3.7: Resolution algorithm to derive the possible configurations of the T-CAES.* ..... 50
*Figure 3.8: Discharging phase of the three configurations of the T-CAES.* ..... 52
*Figure 3.9: General basic configurations deduced for T-CAES.* ..... 54
*Figure 4.1: Schematic diagram of the proposed trigenerative compressed air energy system with the notations.* ..... 57
*Figure 4.2: Schematic diagram of the last expansion stage subsystem (the air motor AM) and temperature levels of streams for the first configuration (a) and the second configuration (b).* ..... 58
*Figure 4.3: Block diagram of the model of air side of the charge and storage phase.* ..... 63
*Figure 4.4: Algorithm developed to select the optimal number of expansion stages.* ..... 66
*Figure 4.5: Block diagram of the model for the air side of discharge phase.* ..... 68
*Figure 4.6. variation of temperature of air and water flow versus heat duty for the first configuration (a) and second configuration (b).* ..... 69
*Figure 4.7: Block diagram of the thermodynamic model of the whole T-CAES system with main input parameters (black) and output parameters (red).* ..... 75
*Figure 5.1: Photograph of the CAES pilot unit at IMT Atlantique, France.* ..... 77
*Figure 5.2: PID of the CAES pilot unit at IMT Atlantique, France.* ..... 77

*Figure 5.3: Representative scheme of the intercooled air compressor. ..... 78*
*Figure 5.4: Pressure variations during the charge phase (lines represent the model and points for experimental). ..... 82*
*Figure 5.5: Input and output temperatures of each component during the charge phase (lines represent the model and points for experimental)..... 83*
*Figure 5.6: Air mass flow and compressor power during the charge phase (lines represent the model and points for experimental)..... 83*
*Figure 5.7: Pressure and temperature of the stored air during the storage phase. ..... 84*
*Figure 5.8: Pressure variations during the discharge phase (lines represent the model and points for experimental). ..... 86*
*Figure 5.9: Input and output temperatures of each component during the discharge phase(lines represent the model and points for experimental).. ..... 86*
*Figure 5.10: Isenthalpic curves of throttling in the pressure regulator (lines represent the model and points for experimental)..... 87*
*Figure 5.11: Power versus RPM of the air motor (left) and thermodynamic to electrical conversion (right) (lines represent the model and points the experimental). ..... 89*
*Figure 6.1: Effect of the thermal energy storage temperature..... 95*
*Figure 6.2: Effect of the number of compression stages. ..... 97*
*Figure 6.3: Effect of the effectiveness of intercooling HEX..... 99*
*Figure 6.4: Effect of the effectiveness of discharging HEX. ..... 101*
*Figure 6.5: Effect of the maximum storage pressure. ..... 103*
*Figure 6.6: Comprehensive efficiency (left axis) and energy density (right axis) at constant maximum to minimum pressure ratio as a function of the maximum storage pressure (the variation of the minimum storage pressure is shown in the secondary x-axis on the top) ..... 103*
*Figure 7.1: Variation of cost pressure factor of tank versus maximum storage pressure (fixing the tank diameter at 0.21 m). ..... 113*
*Figure 7.2: Values and interpolated function of the cost of micro-turbines versus shaft power. ..... 114*
*Figure 7.3: Algorithm of finding the expansion mass flowrate for an imposed power output..... 116*
*Figure 7.4: Variation of reservoir number as a function of maximum storage pressure (output energy of 30 kWh)..... 119*
*Figure 7.5: Variation of reservoir costs and electric efficiency as a function of maximum storage pressure (output energy of 30 kWh)..... 119*
*Figure 7.6: Variation of reservoir costs as a function of maximum storage pressure and output energy. ..... 119*
*Figure 7.7: Variation of the output power and the cost of each component as a function of the output energy with a discharge to charge ratio of 0.21..... 120*
*Figure 7.8: The cost of caverns in large scale CAES (y axis is the y-axis is either cost/£106 or cost per unit/£ (kWh) [11]..... 121*
*Figure 7.9: Variation of the output power and the cost of each component as a function of the output energy with a discharge to charge ratio of 0.75 ..... 122*
*Figure 7.10: Variation of the total costs of the plant as a function of the output energy. ..... 123*
*Figure 7.11: Capital cost of Pb-Acid batteries against typical capacity (on logarithmic scale) as reported by companies(black) and according to industry standards (blue). ..... 123*
*Figure 7.12: Capital cost of lead acid battery and T-CAES against electric energy output, without considering the heating energy(left) and with taking the equivalent electric energy of this latter (right). ..... 124*

*Figure 7.13: Capital cost of lead acid battery and T-CAES against electric energy output, with a power range higher than 30 kW.* ..... *125*

# NOMENCLATURE

| | |
|---|---|
| $T$ | Temperature (˚C) |
| $P$ | Pressure (bar) |
| $\Delta P_l$ | Pressure losses (bar) |
| $C_p$ | Heat capacity ($kJ.kg^{-1}.˚C^{-1}$) |
| $\mu_T$ | Joule Thomson coefficient (°C/bar) |
| $N_c$ | Number of compression stages |
| $N_e$ | Number of turbines |
| $n$ | Polytropic coefficient |
| $\beta_c$ | Compression ratio |
| $\beta_{AM}$ | Expansion ratio of air motor |
| $\beta_e$ | Expansion ratio of turbine |
| $\dot{W}$ | Power (kW) |
| $\dot{m}$ | Mass flow rate ($kg.s^{-1}$) |
| $\varepsilon$ | Heat exchanger effectiveness |
| $m_s$ | Stored mass (kg) |
| $\delta$ | Maximum to minimum pressure ratio |
| $V$ | Volume ($m^3$) |
| $t$ | Time (s) |
| $N_{res}$ | Number of air storage tanks |
| $N_u$ | Nusselt number |
| $R_a$ | Rayleigh number |
| $h$ | Heat convection coefficient ($W.m^{-2}.K^{-1}$) |
| $H$ | Height (m) |
| $d$ | Thickness (m) |
| $D$ | Internal diameter (m) |
| $R_{th}$ | Thermal resistance ($W^{-1}.m.K$) |
| $\lambda$ | Thermal conductivity ($W.m^{-1}.K^{-1}$) |
| $Q_r$ | Thermal energy recuperated used on preheating of the compressed air (kWh) |
| $Q_{cool}$ | Cooling energy (kWh) |
| $Q_{heat}$ | Heating energy (kWh) |
| $Q_s$ | Thermal energy stored (kWh) |
| $C_{rs}$ | Heat recuperated to heat stored ratio |
| UA | Heat exchanger footprint ($W.K^{-1}$) |
| $E_d$ | Energy density ($kWh.m^{-3}$) |
| COP | Coefficient of performance |
| $\eta$ | Efficiency |
| $\eta_g$ | Comprehensive efficiency |
| Pinch | Pinch point temperature difference |
| I.CH.S | Initial charging state |
| I.DIS.S | Initial discharge state |
| $\alpha$ | Time of discharge to time of charge ratio |
| $C_A$ | Cost of a certain component (USD) |

# NOMENCLATURE

| | |
|---|---|
| $C_A^0$ | Cost at base conditions (USD) |
| $F_p$ | Bare module factor of operating pressure |
| $F_M$ | Bare module factor of Materials |
| $I_{yi}$ | Cost index |

# ABBREVIATIONS

| | |
|---|---|
| EES | Electrical Energy Storage |
| PHS | Pumped Hydraulic Storage |
| CAES | Compressed Air Energy Storage |
| C-CAES | Conventional CAES |
| A-CAES | Adiabatic CAES |
| T-CAES | Trigererative CAES |
| TES | Thermal Energy Storage |
| AM | Compressed Air Motor |
| HEX | Heat exchanger |

# SUBSCRIPTS

| | |
|---|---|
| c | compression |
| e | expansion |
| i | Compression stage or heat exchanger number i |
| j | Expansion stage or heat exchanger number j |
| out | output |
| in | input |
| amb | Ambient |
| d | Expansion valve |
| el | electrical |
| m | mechanical |
| th | thermodynamic |
| th,m | Thermodynamic to mechanical conversion |
| tt | Total to total |
| ts | Total to static |
| s | isentropic |
| 0 | stagnation |
| rem | remaining |
| cold,TES | Cold thermal energy storage |
| h,TES | Hot thermal energy storage |
| ch | charge |
| dis | discharge |
| a | air |

# SUBSCRIPTS

| | |
|---|---|
| w | water |
| res | reservoir |
| max | Maximum pressure |
| min | Minimum pressure |
| A | Component capacity such as power, volume or surface |
| yi | year i |

# CHAPTER 1 - INTRODUCTION

## 1.1 Background and motivation

The demand for electrical energy continues to grow and is projected to increase by 56% between 2010 and 2040 per person [1]. This increase is mainly met by thermal and nuclear power plants [2,3]. The most frequent problems arising from fossil fuels are mainly:

- Economic: they are exhaustible sources and their prices are in rise.
- Environmental: they are the main cause of greenhouse gas emissions.

Nowadays, with the concerns about the environment and energy security, the use of renewable energies (RE) is becoming increasingly important [4] and the electricity market is experiencing major changes by integrating these resources. In this context, many countries policies purpose is to encourage RE investments by utilities implement policies such as feed-in tariffs, carbon taxes and/or renewable portfolio standards [5].

On the other hand, Increased penetration of renewable energies leads to significant imbalances between instantaneous electricity production and consumption. Therefore, Electrical energy storage (EES) is becoming a vital aspect to meet these challenges [2,3,4]. The fundamental idea of EES is to recover excess energy supply over demand, store it and deliver it during the period of insufficient energy production.

Primarily, EES is used to supply high peaks in demand that exceed the production capacity of power plants [3,6]. This prevents the installation of an additional power plant, which is better than oversizing the power plants and operating it at part-load with low performance far from the design conditions. Now, Electrical Energy Storage (EES) plays a key role in integrating renewable energy sources [2,4]. Besides, EES systems ensure the flexibility and reliability of grid operations especially smart grids [7].

Referring to Wolf [3], Chen et al. [4] and Ibrahim [6], the application of EES (Figure 1) takes place at several levels as follows:

Generation: normally on a large or medium scale, energy is stored during the off-peak period (night) for use in the peak period (day).

Consumption: the reduction of the peak load can also be achieved at the consumer level. In addition, in order to reduce consumer dependence on the electricity grid, renewable energies can be integrated into their own facilities. Hence, EES serves to manage power flows.

Off-Grid Sites: they are communities that are not connected to national electricity transmission grids. In most of these communities, power is provided by diesel generators. With the integration of renewable energies, EES is necessary to increase the penetration rate of renewable energies, or even to pursue energy self-sufficiency.

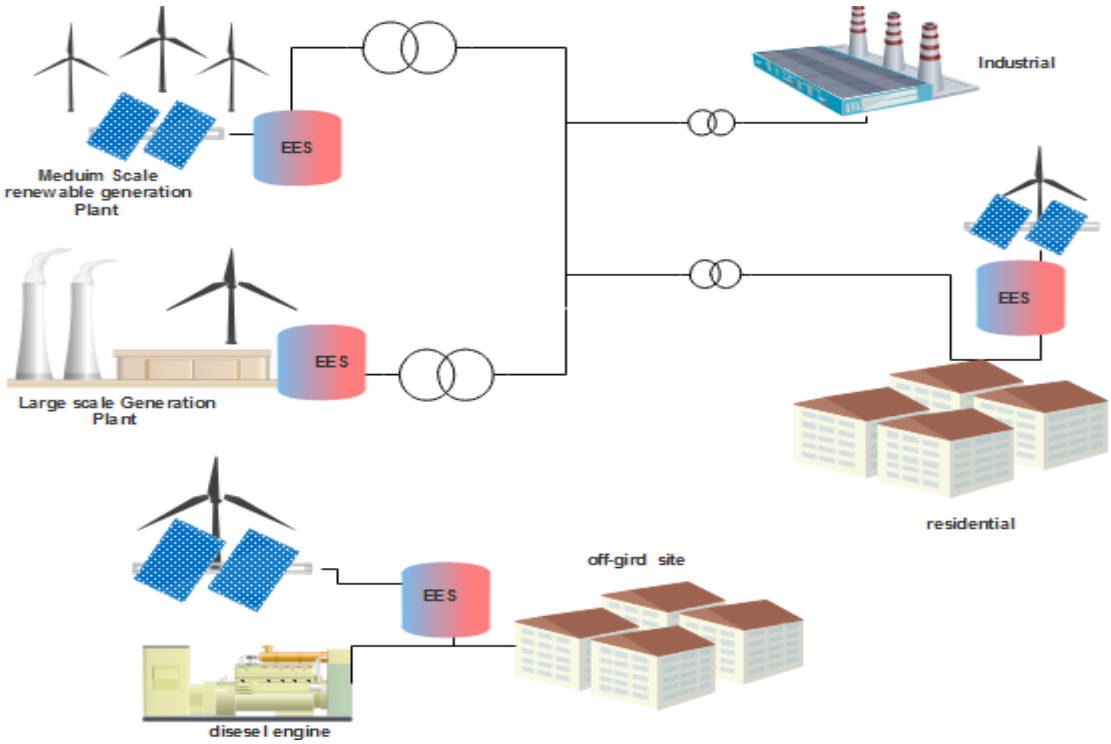


*Figure 1.1: The main applications of electrical energy storage (EES).*

Concerning Off-Grid sites, the number of populations living in isolated communities or who use unreliable networks is estimated at 1.2 billion people worldwide [8] (a number comparable to the population of China). In Canada, there are approximately 292 remote communities, including 44 in Quebec, with a total population of 194,281, including 34,729 in Quebec [9].

The connection of these communities to public electricity grids results in significant power losses, so local production is a necessity. The diesel engine is the most popular solution in Quebec. The total installed capacity in all these communities is estimated at 128 MW, of which 107 MW is diesel-powered. In addition to the disadvantages of using fossil fuels, a second challenge resides in the high costs of transporting diesel fuel to remote locations [6].

On the other hand, most sites in Canada have significant wind potential given their near-shore or mountainous locations (see Figure 1.2). Similarly, in the world, the majority of islands (such as the Greek or Canary Islands) [10,11] also have significant wind resources. Moreover, the populations located in Africa, South Asia and East Asia benefit from a very large solar resource (this population represents 95% of the 1.2 billion people disconnected through the main electricity grids) [8]. Consequently, the integration of renewable energies appears a very interesting solution.

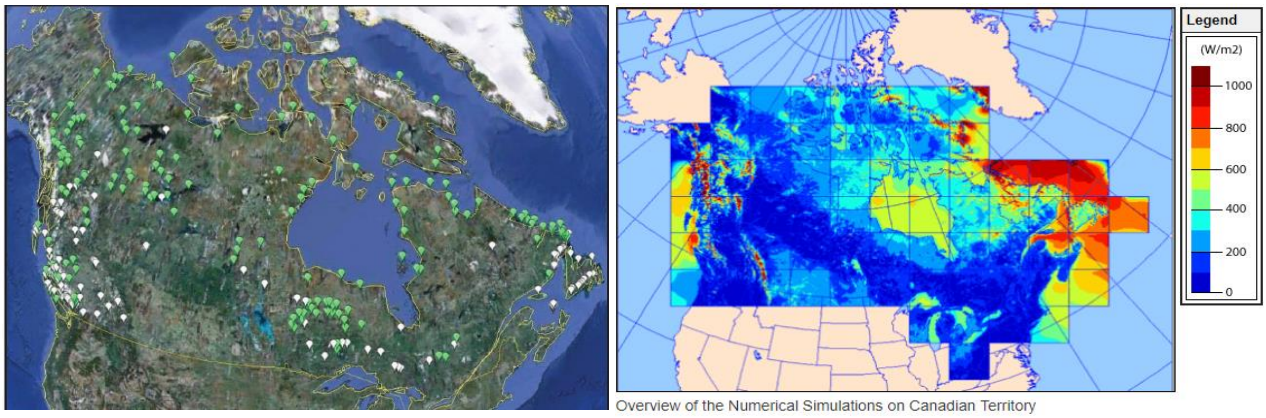


*Figure 1.2: Distribution of isolated sites (left [9]) and wind farms in Canada (right, taken from Canadian Wind Energy Atlas).*

Once the renewable energy production is incorporated with the initial production provided by diesel engine, this latter will function at partial loads which means at low efficiency. Adding to that, it should operate above 30% of its nominal power in order to ensure a proper lubrication [6,12]. As a result, these conditions force to reject a significant percentage of the electrical energy produced (unloaded energy) and prevent a high penetration of renewable, solar or wind energy [6,12,13].

Another challenge that leads to the difficult market penetration of wind/diesel production systems is the dynamic variations in wind speed. The diesel engine is started for safety reasons even if the wind production is higher than 10% -15% of the load [6,14] which leads to the increase in start/stop cycles and consequently cause wears of engine parts, and increases its maintenance cost.

In order to overcome these problems, EES becomes a key solution to increase the penetration rate and the profitability of renewable energy integration, and to recover the unloaded energy.

Several EES such as pumped hydroelectric (PHS), compressed air energy storage (CAES), thermal energy storage (TES), chemical or electrochemical batteries, flywheel, capacitor and supercapacitor have been developed so far. Each system has certain advantages and limitations based on different criteria such as efficiency, energy density, power range, time of response and investment cost [2]. Among EES technologies, compressed air energy storage CAES is considered a very promising technology. At a large scale on the level of producer, it is a strong alternative to the pumped hydroelectric when nearby mountains are not available [2,4] while underground reservoirs such as saline dome caverns, porous rock formation or old mines are accessible [12,15]. Meanwhile, at smaller scales on the level of consumer, CAES attracted recently more attention in favor of the possibility of using overground pressure vessel reservoirs [13,16] and their potential applications especially for off-grid sites [1,6,15].

Until now, only two commercial Compressed Air Energy Storage (CAES) installations have been operated. They have been built to minimize the fuel consumption in conventional gas turbine cycles during high demand periods [1,12,17]. In fact, in this simple concept of CAES called diabatic (D-CAES), the heat produced during the compression phase is wasted leading to moderate

efficiencies (42%-54%) [12]. Recently, this technology regained attention with a major improvement, namely the use of the heat from the compression process in the expansion phase. This second generation recognized as adiabatic compressed air energy storage (A-CAES) could be competitive with others EES [18], thanks to its high availability and starting reliability, environmentally benign, long life, low operation and maintenance costs [12,18,19].

Previously, it has been demonstrated that CAES is adaptable to produce supplementary heating and cooling energy which improves further its round trip efficiency [13,20,21]. Hence the trigenerative compressed air energy storage T-CAES has been introduced. In other words, the T-CAES is based on using the compression heat directly as a heating energy or as a preheating energy in the expansion phase to increase the electrical efficiency. Furthermore, the production of cooling is possible because of the partial use of the compression heat.

The development of small scale T-CAES to be placed close to energy demand (off-grid sites or at the consumer level) is of great interest [13], given the technical ease of transfer of thermal and chilling energy at short distances. However, limited number of studies has been conducted on this system and they mostly focused on demonstrating its concept and its adaptability to specific applications.

## 1.2 Objectives and approach

The aim of this research project is to study this new generation of compressed air storage technology at small scales. The present work is besides part of a joined research project undergoing in IMT Atlantique (France) and Université de Sherbrooke (Canada) dedicated to the implementation of small-scale T-CAES close to energy demand or in off-grid sites especially in remote communities in the North of Québec.

The main objective of this project is the analysis of the T-CAES from a theoretical and experimental perspectives and the techno-economic optimization of the system to propose an efficient design guideline.

The general objective includes the following specific objectives:

- Conducting a thermodynamic and energetic analysis of the system in order to gain a better understanding of the process and deduce its possible configurations.
- Developing a detailed thermodynamic model of each component which leads to elaborate a global model to predict its performances.
- Performing experimental tests to validate the simulation model as well as to investigate its operation and thermal behaviors.
- Carrying out a thermodynamic optimisation via parametric study, including economic criteria, with investigating the mutual effects of design parameters.
- Developing an economical model to estimate the capital cost of the system as well as to compare it with its alternative electrical energy storage system.
- Identifying prospective solutions to make the T-CAES as a competitive EES solution.

## 1.3 Outlines

The thesis is divided on six chapters:

**Chapter 2** presents a literature review on different technologies of electrical energy storage and interprets its evaluation criteria. The particular emphasis will be placed on compressed air energy storage, its principles and system configurations, its modeling and analysis methods aspect as well as past achievements and results of previous related studies. This helps to locate the gabs on our research field and to elaborate the clear methodology essential to examine the T-CAES.

Each of the following chapters includes each of the objectives presented above with a detailed explication of the work methodology.

**Chapter 3** presents the fundamental principle of the T-CAES system based on the first law of thermodynamic. In line with this, a simplified thermodynamic model is developed in order to deduce the different possible configurations of the T-CAES and to identify the key elements that influence the system performances.

Then, in **Chapter 4** a detailed thermodynamic model of the plant is developed with taking into account the technological aspects and technical constraints of each component.

**In Chapter 5** the industrial experimental pilot unit implemented in GEPEA laboratory at the IMT Atlantique, France is described. Afterward, the model developed in chapter 3 for air-side components is validated experimentally by paying a careful attention to each component.

**Chapter 6** focuses on the assessment of the effect of the most relevant design parameters on the system performance and operation via a parametric study. Along with this, the effect of each design parameter on the others as well as economic considerations are investigated. As a conclusion, an optimal design guideline is provided.

**In Chapter 7** an economical model of the system is developed and an optimal techno-economic design solution is deduced. Then, the cost of the system as a function of its power scale is discussed and compared to batteries.

# CHAPTER 2 – STATE OF ART ON ELECTRICAL ENERGY STORAGE TECHNOLOGIES

As mentioned in the last chapter, Electrical Energy Storage (EES) is becoming a vital aspect to ensure the balance between energy production and demand [2,4,22,23] and to deal with the intermittent nature of solar or wind energy sources. Moreover, in off-grid sites, EES appears as a key component to achieve a sufficient penetration of renewable energy resources [10,15]. Electrical Energy Storage technologies are declined into 4 categories: mechanical energy, electrochemical energy, thermal energy and chemical energy.

This chapter is composed of 2 main parts:

- In the first part, the principle of the various storage systems and their evaluation criteria are briefly presented in order to draw an overall conclusion on the position of compressed air storage in relation to other EES.
- In the second part: compressed air storage technologies will be described in depth, paying attention to the various studies recently published on this subject.

## 2.1 Overview on Electrical Energy Storage technologies

### 2.1.1 Hydraulic Pumped Energy Storage

Hydraulic pumped energy storage (PHS) is based on storing the electrical energy in the form of gravitational energy. As shown in Figure 2.1, it includes 2 reservoirs at different elevations (higher and lower reservoir). When excess electricity is produced, the water from the lower reservoir is pumped to the upper one. As needed, water is turned back on a turbine to produce electrical power.

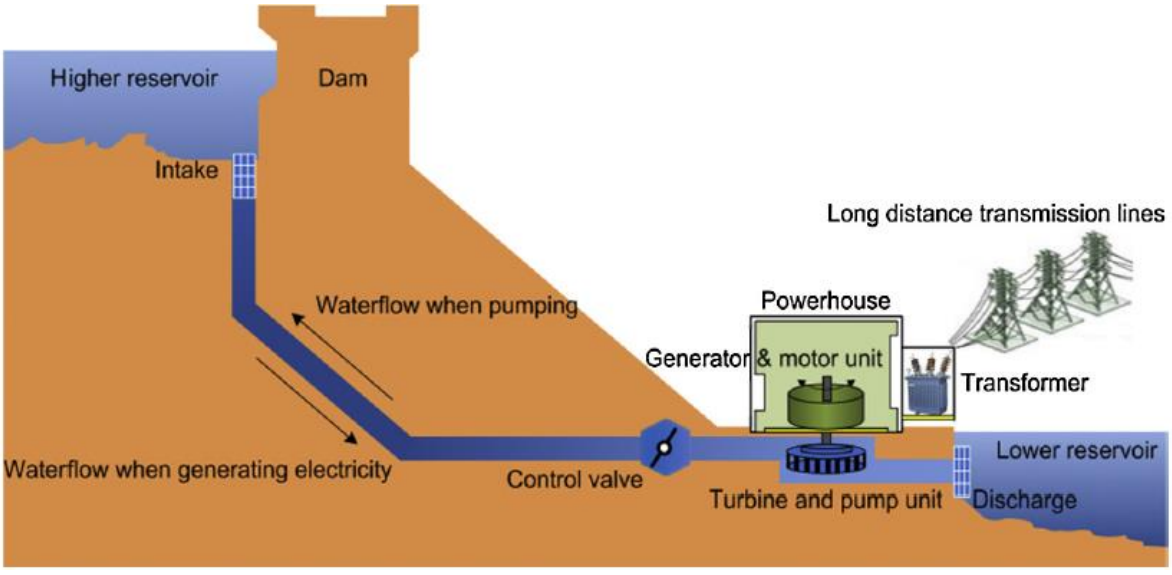


*Figure 2.1: Schematic of pumped hydroelectric storage plant [2].*

PHS is the most widely deployed technology at large scales with high efficiency of 85%. Nevertheless, it requires considerable investments, a specific geographical context mainly mountain areas, and a long time of construction [4].

The installed capacity of hydropower station achieved 1267 GW in the world by the end of 2017, which represents 16.4% of the total renewable energy production [24]. As for the application of this technology in EES, it represents 94 % of global electricity storage by capacity with a value of 153 GW [24].

The contribution of PH in electricity production is 11 % in France, while it is 62% in Canada [25]. In Québec, this contribution is very high which achieves 97% [25]. However, isolated sites still rely on diesel engine as the main electricity producer.

### 2.1.2 Compressed Air Energy Storage

In addition to PHS, Compressed Air Energy Storage (CAES) is implemented at large scale which can provide a capacity over 100 MW. It involves mainly two generations:

1 The conventional CAES (C-CAES) which is a mature and commercialized technology.
2 The under-development system recognized as Advanced Adiabatic compressed air energy storage (AA-CAES) or simply adiabatic (A-CAES), and the recently introduced system called Trigenerative-CAES (T-CAES).

Figure 2.2 presents a general diagram describing different CAES principles. C-CAES stands on the basis of the gas turbine cycle with the difference that the compression and expansion phases are time-delayed. The thermodynamic process in a conventional CAES may be described as follows: during the period of excess energy production, ambient air is compressed via a multi-stage compressor with intercooling. The associated compression heat is lost to the environment. Compressed air is stored in underground reservoirs (in the case of large scale) or in overground tanks (for small scale). During the period of high energy demand, the mechanical energy is converted again into electrical energy by expansion. Stored air is released, heated by means of combustion before expanding into the gas turbine to generate electricity.

The aim of the A-CAES concept is to recuperate the lost heat and use it in the expansion stages. A detailed description of this generation and the trigenerative concept will be presented in the next parts of this chapter.

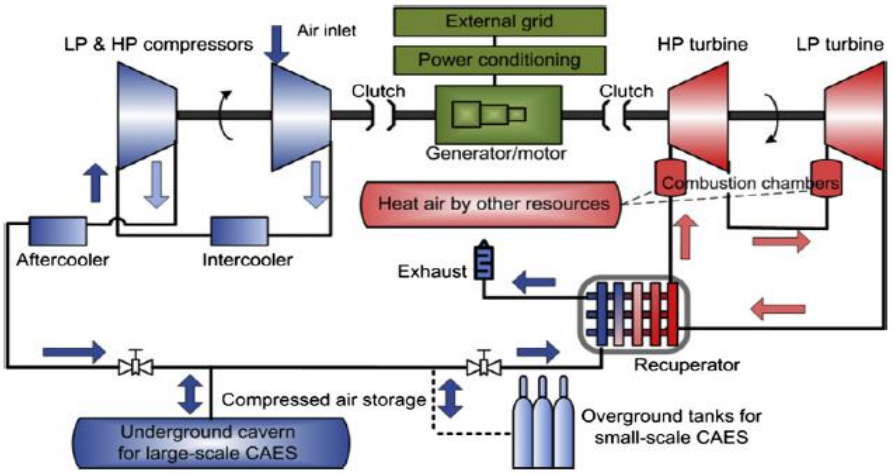


*Figure 2.2: Representative diagram of compressed air storage systems [2].*

CAES is mainly applied to large-scale applications (tens or hundreds of MW). Recently, for small scale applications, by using overground pressure vessel reservoir. CAES is considered as a very promising alternative solution for energy storage in remote areas [6], and especially small scale Trigenerative-CAES (T-CAES) to replace diesel power stations used by small housing groups.

### 2.1.3 Thermal Energy Storage

Thermal Energy Storage (TES) consists in storing energy by cooling, heating, melting, or vaporizing a material [6]. This energy will be available once the process is reversed [2,6]. TES is used in a wide range of applications, mainly for heating and cooling in buildings as well as for electricity production.

Heat sources come either directly from renewable energy (solar energy or from electricity by means of electrical resistance [4,6]) or from unavoidable heat resulting from industries (gas-fired power plants, incineration plants, processes) [6]. The stored thermal energy is converted into electrical form by the use of classical engine cycles. As an application of TES, Figure 2.3 shows the scheme of Solar Tres power plant, Spain. the solar heat is stored by molten salt materials, then the heat is used to produce the superheated steam needed in the Rankine cycle to produce the electric energy.

The storage materials are selected according to the temperature level of the process and material properties such as: thermal inertia, heat capacity and mass density. The storage materials can be classified according to (1) sensible heat storage or (2) latent heat storage material.

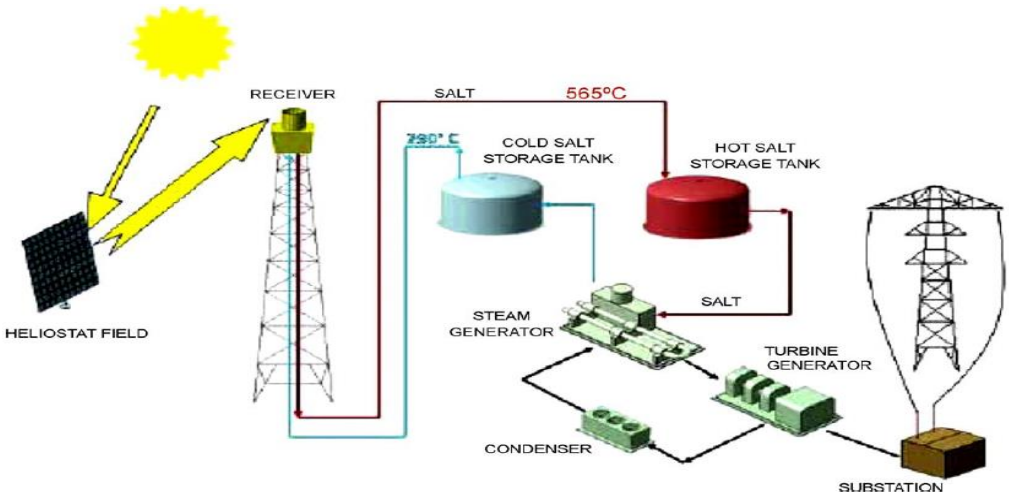


*Figure 2.3: Scheme of the application of TES in the power plant "Solar Power Tres"[26].*

#### *Sensible heat storage materials*

The common materials used are presented as follows:

1. Solid media: these include underground rocks (Borehole Thermal Energy Storage) and natural aquifers (Aquifer Thermal Energy Storage) for large scale applications, and surface

tanks containing solid materials such as concrete [4] or ceramic [3] for small-scales applications. It is important to note that underground rocks and aquifers are intended for daily (day/night) or seasonal (summer/winter) storage at intermediate temperature levels (<80ºC) [4].

2. Liquid media: the commonly used materials are thermal oils and pressurized water. On the other hand, there is a growing interest in molten salt and ionic liquids, more specifically Room Temperature Ionic Liquids RITL [4]. These latter are characterized by a freezing point below 25ºC without risk of decomposition at high temperatures [4].

Table 2.1 presents a comparison of the thermo-physical properties of the most common TES materials.

*Table 2.1: Thermo-physical proprieties of sensible heat TES materials (synthetized from [27,28] and [29]).*

| | Freezing temperature (ºC) | Maximal Temperature (ºC) | Mass density (kg/m$^3$) | Conductivity (W/m.K) | Calorific Capacity (kJ/kg.K) |
|---|---|---|---|---|---|
| **Rock** | --- | 300 | 1700 | 1 | 1.3 |
| **Concrete** | --- | 400 | 2200 | 1.5 | 0.85 |
| **Salt (NaCl)** | --- | 500 | 2160 | 7 | 0.85 |
| **Steel** | --- | 400 | 7200 | 37 | 0.56 |
| **Nitrate salt** | 220 | 500 | 1870 | 0.52 | 1.5 |
| **Ionic Liquids (ex : [C$_8$MIM][PF$_6$])** | -75 | 416 | 1400 | High | 2.5 |
| **Synthetic Oil** | 13 | 395 | 770 | 0.12 | 2.6 |
| **Mineral Oil** | -10 | 300 | 900 | 0.11 | 2.3 |
| **Silicone Oil** | -40 | 400 | 900 | 0.1 | 2.1 |

It is obvious that for temperatures below 100ºC, water is still the best choice due to its high calorific capacity and thermal conductivity and its very low cost.
For high temperature values, nitrate salt (molten salt) and thermal oils are the most commonly used [27,28,30]. The main drawback of nitrate salt is its high freezing temperature (even above room temperature). Besides, thermal oil has low thermal conductivity and mass density values.

Ionic liquids have an interesting thermal property and can be used for low and high temperatures of storage. Although, they have not yet been used in practical applications [28].

### *Latent heat storage materials*

Phase change materials (PCMs) offer valuable benefits since they store energy at a well-defined temperature and perform a high energy density. In counterpart, they require a heat transfer fluid cycle to transmit the thermal energy [4], which increases the system cost. There are several PCM materials such as paraffin, organics or inorganics materials as well as eutectic mixtures. Table 2.2 lists some used or potentially applicable PCMs materials for relatively low or medium temperatures (less than 200˚C).

*Table 2.2: Thermo-physical proprieties of PCM for TES (collected from [28] and [30]).*

| Materials | Melting temperature | Latent heat | Thermal conductivity |
|---|---|---|---|
| | (˚C) | (kJ/kg) | (W/m.K) |
| | **Organic** | | |
| Erythritol | 118 | 89.9 | --- |
| Trans-1,4-polybutadien | 145 | 144 | --- |
| | **Paraffin** | | |
| $C_{22}$-$C_{33}$ | 67 | 189 | --- |
| Paraffin Waxes | 64 | 173.6 | --- |
| | **Inorganic** | | |
| $MgCl_2.6H_2O$ | 117 | 168.6 | --- |
| Mg $(NO_3)_2.2H_2O$ | 130 | 275 | --- |
| | **Inorganic eutectic** | | |
| 48%Ca $(NO_3)_2$-25%$KNO_3$-7%$NaNO_3$ | 140 | | 0.519 |
| $KNO_3$—$NaNO_2$—$NaNO_3$ | 142 | 84 | 0.6 |
| 40% $KNO_3$-60%$NaNO_3$ (Molten Salt) | 222 | | |
| | **inorganic eutectic + Lithium** | | |
| $LiNO_3$ + $NaNO_2$ + $NaNO_3$ + $KNO_2$ +$KNO_3$ | 95.7 | 100<$L_v$<300 or above 300 | |
| $KNO_3$ + $LiNO_3$ + $NaNO_3$ | 117 | 100<$L_v$<<300 or above 300 | |

The materials are characterized by their latent heat, melting temperature levels and thermal conductivity. The latent heat is relatively high but the low values of thermal conductivity is a challenge to overcome and has been the focus of ongoing research projects [28]. It should be noted that the addition of lithium to molten salts lowers their melting points, which allow their use as phase change materials (see the last three lines of Table 2.2). This makes these products more and more popular [28].

### 2.1.4 Electrochemical batteries

The electrochemical storage is based on the transformation of the chemical energy to electrical energy (during the discharge phase) which results from electrochemical reactions and vice versa (during the charge phase). A wide variety of batteries have been used, while the most common are: Lead-acid and Lithium-ion batteries.

As shown in Figure 2.4, batterie contains two electrodes (anode and cathode) with an electrolyte which promotes the movement of ions between these electrodes. During the discharge phase, the electrons move from the anodes to the cathodes in the external circuit, while the electrochemical reaction occurs at the two electrodes. The reaction is reserved in the charging phase. In order to illustrate the battery functioning, the chemical reactions of Lead acid battery are presented as follow:

Reaction at the Anode (negative plate): $P_b + HSO_4^- \underset{charging}{\overset{discharging}{\longleftrightarrow}} P_bSO_4 + H^+ + 2e^-$

Reaction at the cathode (positive plate): $P_bO_2 + HSO_4^- + 3H^+ + 2e^- \underset{charging}{\overset{discharging}{\longleftrightarrow}} P_bSO_4 + 2H_2O$

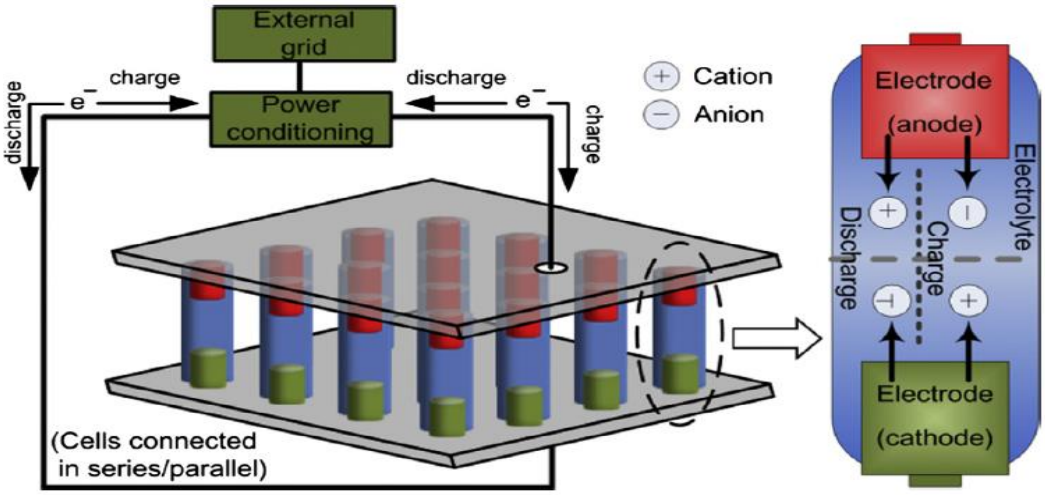


*Figure 2.4: General schematic of operation of electrochemical batteries [2].*

Electrochemical batteries are rather mature and very well established for building or small communities' applications. Their attractiveness is driven by their high roundtrip efficiency (60%-90%), their flexibility and high responsiveness (short response time), thereby enhancing the stability of electricity networks.

On the other hand, batteries have a short lifetime and a low energy density (which explains their applications in installations of several kW [6]). In addition, most batteries contain toxic materials. Batteries covers several types: lead-acid, nickel-cadmium, sodium-sulfur and lithium-ion batteries [4].

### 2.1.5 Chemical storage: Fuel cell

As its name indicates, the electricity storage is powered by the use of a fuel and an oxidant. The basic principle is as follows: the discharge phase consists of consuming a fuel A (e.g. $H_2$) to produce electricity and a chemical product B (e. g. $H_2O$). Chemical A is regenerated by consuming electricity while B acts as a reagent (during the charging phase) as follow:

$Charging\ phase: B + Energy \longrightarrow A$

$Ex: 2H_2O + Energy \longrightarrow 2\,H_2 + O_2$

$Discharging\ phase: A \longrightarrow B + Energy$

$Ex: 2\,H_2 + O_2 \longrightarrow 2\,H_2O + Energy$

Fuels encompass using dihydrogen, hydrocarbons, alcohols and even some metals [4]. Dioxygen is not the only oxidant, chlorine and chlorine dioxide can also be used [4]. However, the focus has been on hydrogen fuel cells in which the electrical energy is stored by the electrolysis of water [3,6]. These cells provide intrinsic advantages such as scalability and high energy density [2,4]. Regardless of these advantages, this technology has a low efficiency and remains expensive at the moment [4].

### 2.1.6 Other Storage Systems

It is intended here to be of the short storage time solutions (a few minutes or hours) such as the superconductor and the flywheel storage systems. Flywheel accumulators include a flywheel associated with a motor-generator. In this way, energy is stored in the form of kinetic energy. While the energy in superconducting Magnetic Energy Storage (SMES) is stored in the form of a magnetic field in favor of the almost zero electrical resistance of the superconducting coils. Besides, the inductor is maintained in a superconducting state by a liquid helium magnetic conductor.

## 2.2 Comparison and evaluation of EES technologies

The ideal EES solution applicable to every energy context does not exist. Rather, the choice of the suitable technology depends on the application requirements on one hand, and the characteristics of each EES technologies on the other hand. In this part, the evaluation criteria of EES are defined and presented in Tables 2.3 and 2.4. Then, for each criterion a comparison between these technologies is carried out in order to highlight the usefulness of the CAES technology and existing data relevant to small-scale CAES.

*Table 2.3: Comparison of the evaluation criteria of EES technologies (collected from [2,4]).*

| | Efficiency (%) | Power (MW) | Energy density (kWh/m³) | Maturity |
|---|---|---|---|---|
| **PHS** | 70-85<br>High | 100-5000<br>Large scale | 0.5-1.5 | Mature |
| **Underground CAES** | 42,54<br>Moderate | 110-290<br>Large scale | 3-6 | Commercialized |
| **Underground A-CAES** | 70 expected | Tens or hundreds of MW<br>Medium-Large scale | Similar to CAES | Under development |
| **Aboveground-CAES** | Not evaluated | 0 -3<br>Small scale | Higher than underground CAES<br>High | Under development |
| **TES** | 30-60<br>Relatively low | 0-300<br>Small or high scale | 80-500<br>Medium | Under development/early commercialized |
| **Electrochemical batteries** | 60-90<br>Depends on battery type | 0-0.3; 0-40<br>Depends on battery type | 50-80<br>(200-400 for some types) | Commercialized |
| **Hydrogen fuel cell** | High<br>20-50 | Small or medium scale<br>0-50 | With a low or medium power density<br>500-3000 | Some types are under development<br>Under development /demonstration projects |
| **Flywheel** | Relatively low<br>90-95 | Small to medium scale<br>0-0.25 | High<br>20-80 | Early commercialized |
| **SMES** | Very high<br>95-97<br>Very high | Small scale<br>0.1-10<br>Small-medium scale | With high power density<br>0.2-2.5<br>With high power density | Demonstration/under development |

*Table 2.3 (continued): Comparison of the evaluation criteria of EES technologies.*

| | Time of response | Storage duration | Life time (years) | Cost ($/kWh) | Specific Cost ($/kWh per cycle) |
|---|---|---|---|---|---|
| **PHS** | Minutes<br>Not fast | Hours-Month<br>Long term | 40-60 | 5-100<br>Medium | 0.1-1.4 |
| **Underground CAES** | Minutes<br>Medium | Hours-Month<br>Long term | 20-40 | 2-50<br>Low | 2-4 |
| **Underground A-CAES** | Minutes<br>Medium | Hours-Month<br>Long term | 20-40 | | |
| **Aboveground-CAES** | Seconds-Minutes | Hours-Month<br>Long term | More than 23 | 200-250 | 8-10 |
| **TES** | | Minutes-Days<br>(Months for HT-TES) | 10-30 | 3-30 | 2-4 |
| **Electrochemical batteries** | Milliseconds<br>Fast | Minutes-Days<br>(Month for some types)<br>Short and medium terms<br>(long for some types) | 5-15 | 100-400<br>(300-500 for some types) | 20-100<br>(8-20 for some types) |
| **Hydrogen fuel cell** | Seconds<br>Fast | Hours-Month | 5-15 | High | |
| **Flywheel** | Seconds<br>Fast | Seconds-Minutes<br>Short term | 15-20 | 250-350 | 3-25 |
| **SMES** | Milliseconds<br>Very fast | Minutes-hours<br>Short term | More than 20 | 200-300 | |

### 2.2.1 Maturity

Maturity indicates the level of commercialization which exhibits technological barriers, technical reliability, economic profitability as well as research and development needs. EES can be classified into 3 categories:

1. Mature technologies: Hydraulically pumped energy storage (PHS), C-CAES and lead-acid batteries are widely recognized and commercialized [4].
2. Developed technologies: Conventional CAES, flux batteries, SMES, TES and flywheel are technically developed and available on the market, but they are not yet widespread because they require further improvements to be more cost-effective and reliable [4].
3. Under development technologies: It includes fuel cells, A-CAES and the trigenerative CAES system targeted in this study.

### 2.2.2 Power and energy scale

This criterion is defined by the capacity generation of the system in terms of power and energy and reflects the size of the components of the storage system.

Referring to Table 2.3, PHS and CAES are the most suitable for large-scale applications (>100 MW). Some types of electrochemical batteries on its development stage (such as flux batteries), fuel cells, TES and CAES systems are compatible with medium-scale applications (5-100 MW). Conventional electrochemical batteries, fuel cells and recently the trigenerative CAES system studied in this thesis are adaptable for small-scale applications (<5 MW).

### 2.2.3 Efficiency

It is the ratio of the output energy produced to the input absorbed energy. The overall efficiency is governed by energy losses and the conversion efficiency of energy forms during charging and discharging phases (e.g. the conversion efficiency of electrical energy into mechanical energy). Generally speaking, the efficiency at design condition is often provided in the literature without taking into account partial loads operations [9].

PHS and electrochemical batteries accounts for the highest efficiency (71%-85% for PHS and 60-90% for batteries). CAES (even for A-CAES) have lower efficiency with a maximum expected value of 70%, while CAES technology maintains a high value of efficiency at partial load operations as reported by Luo and Wang [17]. TES and hydrogen storage have the lowest efficiency values (<60%).

Finally, it is important to notice from Table 2.3 that the efficiency of CAES at small scales has not been confirmed and reported in the literature.

### 2.2.4 Energy and power density

Energy density is defined by the available energy stored per unit mass or volume, while the power density represents the ratio of the delivered power per unit mass or volume. These two terms should not be confused, energy density reveals the volume or mass required to satisfy energy needs, a higher value means a more compact system. This is particularly sought for on-board applications [9], which can also lead to a lower cost. Nevertheless, a higher energy density does not mean a

higher power density and vice-versa. This later gives further an idea on how the stored energy can be released.

As it can be seen from Table 2.3, PHS and CAES are characterized by a low energy density so that they require large natural reservoirs and they are designed for stationary applications at large scales. As for TES, it shows a medium energy and power densities. The power density here has no importance because it is in line with the energy density.

Electrochemical batteries have moderate energy density, which explains their on-board applications. Although, the power density does not achieve high values expect for lithium-ion batteries. These latter are considered as a very promising technology for transport applications, especially the heavy ones. Flywheel and SMES have moderate and low energy density respectively. By contrast, their power density is very high which explains their relevance for high power appliances with short discharge time.

With regards to small scale CAES, it is characterized by high energy density since the air is stored at high pressure in artificial tanks which overcomes the need of natural reservoirs. However, the value of the density has not been rigorously accounted.

### 2.2.5 Time of storage and self-discharge

The self-discharge is defined by the ratio of the energy dissipated to the energy stored during a given storage period. The possible time of storage is basically driven by the self-discharge [2,4, 6]. The energy is lost according to the process type via heat transfer, electrochemical losses, or air leaks emphasizing that this energy does not include the conversion energy losses as it the case in accounting the efficiency.

Compressed air, pumped hydraulic and dihydrogen can be stored for long periods of time (up to seasons) compared to other technologies.

### 2.2.6 Response time

This criterion is defined by the time required to generate the required power. Flywheel, SMES and batteries have relatively short response times (<1 second) compared to other technologies, making them attractive for usage for the stability of electrical networks [3, 4]. But, CAES and PHS have moderate response time.

### 2.2.7 Lifetime

The lifetime is quantified by the cyclic longevity of the storage system or in another term the number of charge-discharge cycles it can undergo before its performances degrades. It is related to fatigue, wear and tear or deterioration of system components. It is expressed by the number of years, or more rigorously by the number of cycles. Beyond this number of cycles, the system becomes unable to meet the needs or the costs associated with the maintenance increase, for example, after a certain number of years, electrochemical batteries cannot deliver the same level of energy for which they were designed and its capacity degrade.

Thermal and mechanical storage systems (TES, PHS, Flywheel and CAES) have a long lifespan, which could extend to 60 years. On the contrary, chemical and electrochemical storages suffer

from low lifetime. For instance, conventional batteries (lead-acid batteries) last on average 5 years or less due to chemical or electrochemical degradation.

### 2.2.8 Cost

The cost encompasses the investment, the maintenance and the operation costs. It is expressed per kWh of output energy. However, it is more appropriate to accounts for the lifetime when the cost is calculated so that it is often expressed as cost/kWh/cycle. The cost is very important in technology selection for the manufacturer [3], as well as for the consumer [9]. Industrial producers adopt cost-competitive technology, meanwhile user does not invest in a solution which does not provide economical profitability.

The cost values presented in Table 2.3 account for the capital cost and do not include maintenance, operating and installation costs. CAES, PHS and TES systems are the most cost-effective in terms of costs per kWh and per kWh per cycle. On the other hand, Electrochemical batteries are low-cost technologies for the short term (in terms of $/kWh) but they have a limited lifetime, which makes them expensive and uneconomical for the long term (in terms of $/kWh/cycle).

As a first evaluation of small-scale CAES, it appears to be costly in the short term, nonetheless the cost per cycle seems to be interesting and sufficiently higher than that of batteries. Note that the cost values presented in Table 2.3 are not based on detailed study of the system.

### 2.2.9 Environmental impacts

Despite the fact that energy storage promotes the integration of renewable energy, some technologies still have negative impacts on the environment. As an illustration, conventional CAES involves fuel combustion and the majority of electrochemical batteries contain toxic substances that may remain for long time. On the contrary, the new generations of CAES, TES and flywheel are environmentally friendly.

### 2.2.10 Global synthesis on EES

Energy storage techniques are very wide. There is no single optimum technology that can combine high efficiency, cost-effectiveness, longevity or all the other criteria mentioned above. The suitable technology depends mainly on its application.

Generally speaking, EES has not been reached technical maturity expect for lead-acid batteries, PHS and conventional CAES. Indeed, research and development has been very active in recent years especially for batteries, fuel cells and CAES.

At large scale, PHS is the most widely implemented. It is technically mature with good efficiency (70-85%), long storage time and high lifetime. Besides, compressed air energy storage (CAES) has a strong potential especially after ongoing research to improve its efficiency by introducing the adiabatic-CAES concept. At small scale, electrochemical batteries remain the most commonly used technology. However, they have been suffering from low lifetime and they entail using toxic materials and chemical wastes that remain for a long time.

Currently, there is an emphasis on small-scale air compression storage. The major attractions lie in the ability to store air in artificial tanks that can be installed at any site, and in the possibility to

apply the development made for A-CAES as well as the opportunity to produce supplementary heating and cooling energy as it will be described in the following sections. In addition, small-scale SS-CAES system appears to be encouraging and even competitive with batteries by virtue of:

1 Prolonged storage time.
2 High energy density.
3 A long lifetime with a very low maintenance cost.
4 Acceptable response time.

Most of the evaluation criteria of the SS-CAES in the literature, in particular the efficiency and the energy density have not been rigorously studied and accounted. Consequently, it is worth to put forward research effort to examine this system and precisely asses its evaluation criteria.

## 2.3 General working principle and classifications of CAES technologies

As mentioned in chapter 1 and earlier in this chapter, the attractiveness of CAES mainly rely on its long lifetime, low operation and maintenance costs and being environmentally benign. Although, the main drawback of the conventional CAES is its low round-trip efficiency (42%-54% [1,17]). Recently, CAES has regain the attention of academic and industrial research which is driven by three main factors: recovering the heat produced during compression to preheat the air during expansion which increases the global efficiency (adiabatic concept), the possibility of using artificial reservoirs (site-independent application) and the flexibility of the system to produce cooling and heating energy (the trigenerative concept). Adding to this, CAES is adaptable to absorb renewable electrical power fluctuations and the storage efficiency of thermal energy storage component is high (70%-95%).

This part presents a detailed review on the different types of CAES focusing on the adiabatic and tri-generative concepts. The review includes as well: illustration of the principle, previous studies aspects, the methodologies used for the evaluation of the systems and recent results and achievements.

### 2.3.1 Working principle

The different types of CAES was already shown depicted in Figure 2.1. The underlying principle is as follows:

During the charge phase: the surplus of electrical power drives a multi-stage compressor with intercooling to increase the compression efficiency [6,12]. Then, the air is cooled before it is stored in order to increase the energy density [6]. The heat is lost to the environment in the conventional CAES, while in the adiabatic or trigenerative CAES, it is stored in a thermal energy storage (TES). Compressed air is stored for large scale applications at moderate pressure (typically between 40 and 80 bars [12,18]) in underground reservoirs such as saline dome caverns [3,31], porous rock formation or old mines [12]. For small-scale applications, air is stored at higher pressure (62 bars [14], 93 bars [14] or up to 300 bars [21]) in aboveground tanks such as spherical or cylindrical tanks [13,31], or steel pipes [6].

During the discharge phase: the energy demand is ensured by expanding the air via multistage turbine. The air is preheated by different heat source according to its type:

1. External heat: this involves the combustion of fossil fuels (typically gas) in the conventional CAES system.
2. Internal heat: this means the heat stored during the charge phase in the adiabatic and trigenerative CAES. In the latter system, the internal heat is used additionally for heating needs, and also the compressed air can be applied for cooling production.

### 2.3.2 Classifications

CAES systems are various and includes further types more than those cited above. Figure 2.5 shows the different systems and their classifications as stated by Wolf [12] and Budt et al. [19]. They are not only distinguished by the way in which the compression heat is used or the system scale, but also according to the thermodynamic of compression and expansion process and the way of storing the air. The classifications are as follow:

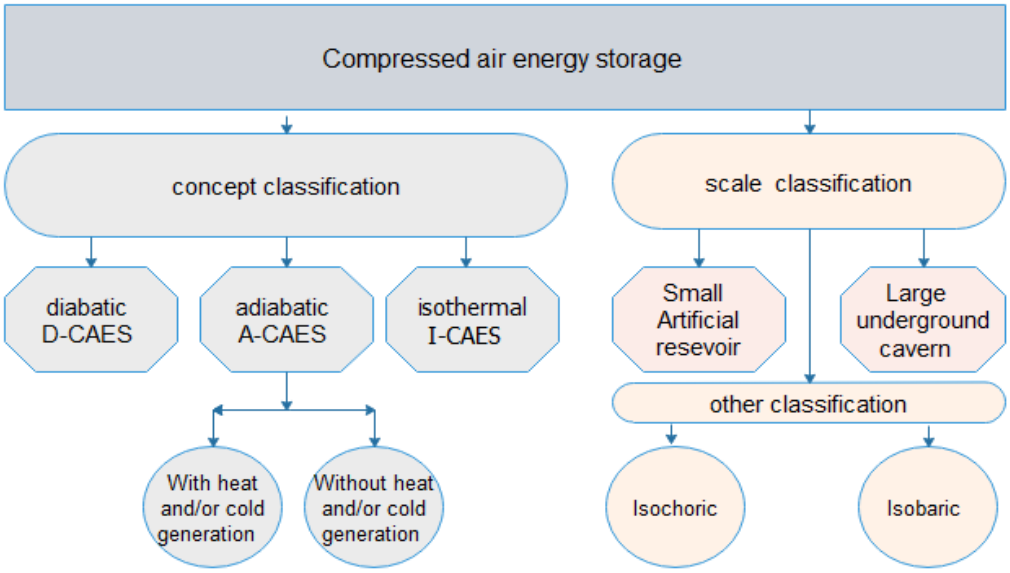


*Figure 2.5: Classifications of compressed air energy storage systems [31].*

#### *Use of compression heat*

Preheating the air in the discharge phase is imperative technically to prevent ice formation in expansion machinery [12], as well to enhance the efficiency of the system. As mentioned early, the type and the employment of the compression heat arise in three types of CAES:

- In Diabatic CAES (D-CAES), the compression heat is wasted and external heat via combustion takes place.

- In A-CAES, the expansion preheating is originated from the compression heat which is an internal source of the system making it as adiabatic.

- In A-CAES with cogeneration of heat and cold energy, or another term the trigenerative CAES (T-CAES) the stored heat of compression is handled by employing part or none of it in the expansion, which makes it convenient for cooling energy production while, at the same time the other part of the heat stored is used for heating purposes.

### *Thermodynamic process of compression/expansion*

In conventional machinery (volumetric or rotary), compression and expansion are irreversible adiabatic or polytropic, which is the case of the D-CAES and A-CAES. In order to overcome the inefficiency associated with irreversibility a new research and development projects aims to target a quasi-isothermal thermodynamic process by using liquid-piston or spraying water during the compression and expansion [12]. This new generation is named the isothermal CAES (I-CAES).

### *Mode of storage*

Depending on the application scale the air is stored in underground reservoirs at large scale and in artificial tanks at small scale. Besides, the air can be stored at constant pressure or constant volume as discussed in the following.

1. **Isochoric storage**

The air is stored at a constant volume and the air pressure vary along the charge and discharge phase so that the mass stored is related to the maximum storage pressure. Notwithstanding, the pressure input of expander must be regulated or more precisely reduced for many reasons : the higher energy density is achieved through this pressure difference, the pressure input should be adaptable to technical specifications of the expander [3, 10, 16] and to seek an optimal operations of this latter at design conditions [14, 17]. The pressure at the inlet of the regulator can be flexible over a certain pressure range but without being able to change it according to the tank pressure which entails a loss of energy.

2. **Isobaric storage**

The air is stored here at constant pressure and the volume changes, while the higher energy density is ensured by a high storage pressure. The idea behind this concept is to omit the energy losses caused by the pressure difference between compression and expansion and to maintain the optimal operating conditions of the expander.

Figure 2.6 (right) shows a representative scheme of the isobaric storage. This concept is feasible by applying a water reservoir at ground level with a water column to the underground deep cavern, where the hydrostatic pressure of water column acts as a pressure regulator of the compressed air. In other words, the height of water column can compensate the pressure variations in the air caverns. Nevertheless, accounting for the pressure to hydraulic height conversion (1 bar corresponds to 10 m height) the water height needed is very high [32], which increases the investment cost [6]. To date, there is only one project in service in Toronto, Canada applied by Hydrostor Company [33] (see Figure 2.6 (left)).

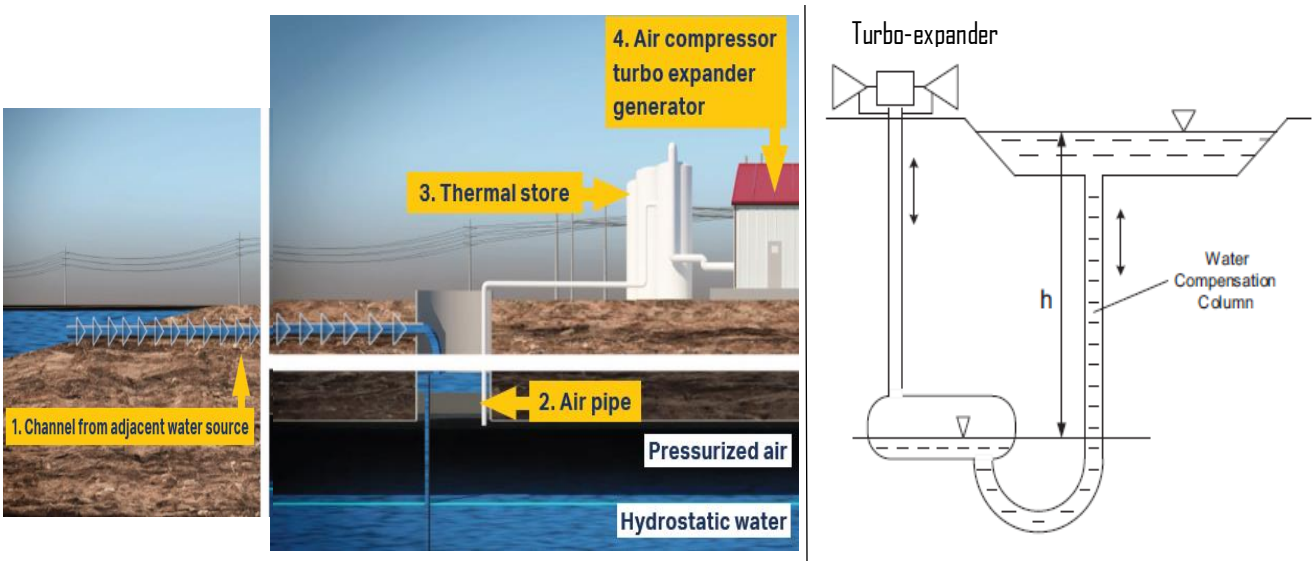


*Figure 2.6: Representative scheme of isobaric CAES concept (right) [32] and the Hydrostor demonstration project (left) [33].*

Owing to the fact the previous solution is restrained by specific geological specifications, high depth and it could not be applied to small scale applications. Recently, in order to overcome this problems, new innovative solutions have been proposed.

Kim et al. [32] proposed a patented constant-pressure CAES system combined with pumped hydro storage as shown in Figure 2.7. In brief, during the charge phase the air is stored at constant pressure Ps in the tank (A), while the water is pumped to the tank (B), compressing at the same time the air in this tank .Here, the water is forcibly transferred by pumping power and the sealed compressed air at the top of tank (B) (which means the air volume V at pressure P or volume V2 at pressure P2 in Figure 2.7) plays the role of the compensation water height in the previous described system. In the discharge phase the process is reserved by flowing the air in the expander and the water through hydraulic turbine. It should be mentioned that there is many versions of this system proposed by researchers such as Wang et al. [34] and Yao et al. [35].

Camargos et al. [36] proofed this concept by an experimental setup which is formed by a water tank, a compressor and air tank instead of the sealed air of the system of Kim et al. [32], a water pump and Pelton turbine. The round-trip efficiency was found close to 30%.

Odukamaiya et al. [37] introduced a configuration similar to that comes up by Kim et al. [32], but without including the turbo expander and setting the pressure Ps equal to the ambient pressure. An experimental setup with power scale of around 6 kW was built by Odukamaiya et al. [37].The roundtrip electrical efficiency was investigated and found experimentally at 24%.this low value is mainly attributed to low conversion efficiency of pump and turbines at small-scale.

This chapter will not enter into details upon these systems, having that they are more engaged to PHS rather than CAES.

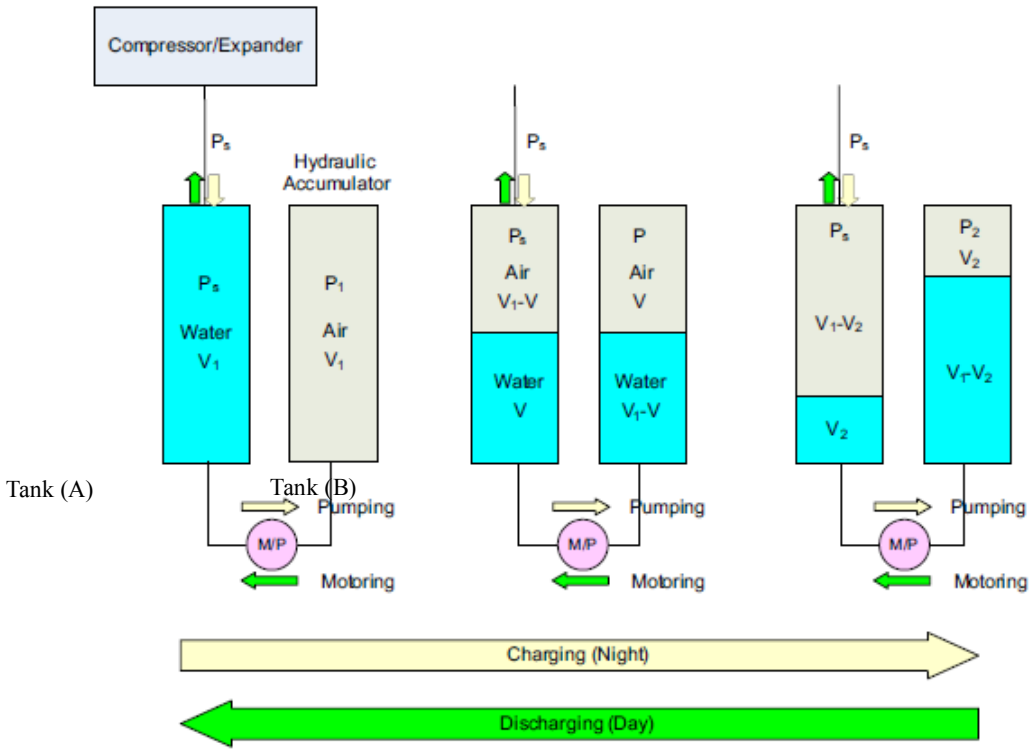


*Figure 2.7: Process operation of combined isobaric-CAES and PHS system proposed by Kim et al. [32].*

## 2.4 Conventional/Diabatic compressed air energy storage D-CAES

As already mentioned, D-CAES is derived from gas turbine power plant technology.The two commercial operating power plants are the Huntorf plant (Germany) and the McIntosh plant (USA) with a round-trip efficiency of 42% and 54% respectively [12]. The efficiency here is defined by the ratio of the output electrical energy (provided by the turbine) to the sum of the compression electrical energy and the heat of combustion. The main elements of these plants are:

1 A multi-stage intercooled compression chain.
2 An underground cavern.
3 A clutching mechanism that connects/disconnects the compressor and the turbine according to whether the system operates in conventional compression or expansion.
4 Classically, combustion chamber located before the turbine.
5 For better conversion efficiency of the expansion phase, it is composed from two turbines, one high-pressure and the second low- pressure.
6 Complementary air preheating is provided by exhaust gases before combustion in the McIntosh installation.

The main characteristics of Huntorf and McIntosh installations are shown in Table 2.4 [12,18]. In both installations, the pressure levels in the caverns are similar. The overall round-trip efficiency of the McIntosh plant is greater than that of Huntorf due to the heat recovery unit of the former. Besides, it is marked by a higher storage capacity and a lower nominal power which leads to an

extended time of discharge. Both installations have high start-up and operation reliabilities [12,31] with a response time faster than conventional gas turbine [31].

*Table 2.4: Characteristics of the Huntorf and McIntosh power plants [9,10].*

| Power plant characteristics | HUNTORF | McIntosh |
|---|---|---|
| **Power (MW)** | 290 | 110 |
| **Cavern volume ($m^3$)** | 310,000 | 500,000 |
| **Cavern depth (m)** | 650 | 450 |
| **Minimum Pressure (bar)** | 45 - 48 | 45 |
| **Maximum Pressure (bar)** | 66 -70 | 74 -75 |
| **Round-trip efficiency (%)** | 42 | 54 |
| **Discharge time (hours)** | 2 to 3 | 26 |

## 2.5 Adiabatic compressed air energy storage A-CAES

As can be seen D-CAES enables reducing fuel consumption and does not mark an encouraging efficiency. In order to overcome these limitations, the concept of adiabatic compressed air energy storage (A-CAES) has been proposed. As shown in Figure 2.8, the main feature of A-CAES is to recover heat produced during compression, store by thermal energy storage device (TES) and use it to preheat the air during expansion, hence it eliminates the need for fossil fuels and promotes a clean technology.

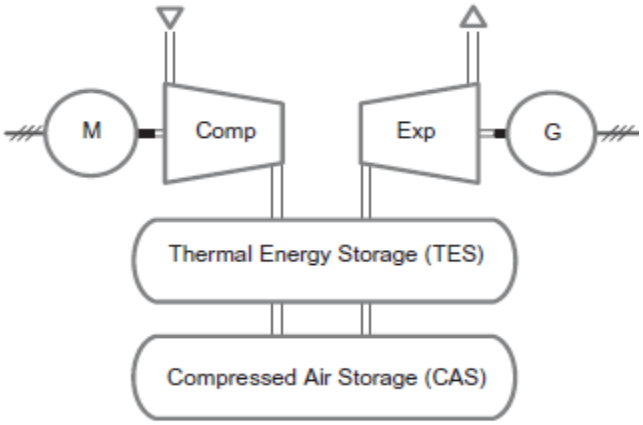


*Figure 2.8: Basic concept of A-CAES [31].*

The first research works conducted on this system was undertaken by Pacific Northwest National Laboratory in the United States from the late 1970s to early 1980's [31]. PNNL judged A-CAES to be a very promising technology [3,31]. From that time to early years of the 20$^{th}$ century, research work was restrained.

In recent years, research and development on A-CAES has been very active, but it has not been built at the utility scale. Although, many projects are in progress and also, aboveground and underground pilot plants have been tested. The main demonstration projects are the ongoing European project "ADELE-ING" [31] which expects the system efficiency to be 70% [38], the pilot plant "TICC-500" designed by the Chinese Academy of Sciences [39] and recently the pilot utility of underground A-CAES developed in Switzerland [40,41].

Before we proceed to present previous theoretical and experimental works, it is convenient to discuss key factors leading to have many types of A-CAES and to adopt different system configurations in the literature, as will be seen later. Based on the studies conducted by Wolf [3], Ibrahim [6] and Budt et al. [31]. These factors can be deduced as follows:

**Capital cost.**

**Response time:** in the context of CAES, it is mainly related to the thermal energy storage TES such as its type (solid, liquid or PCM) and thermal diffusivity of the material used.

**Ease of control:** this aspect is very important in choosing the system components and arrangement. It is strongly linked to the type of TES.

**Efficiency:** which is the most obvious aspect in the design of thermal systems.

**Technological aspects and operational constraints:** This include the selection of the compliant technology of machinery (volumetric, centrifugal or axial turbo-machinery) along with respecting the technical constraints of selected compounds such as the maximum allowable pressure and temperature.

It can be established that TES is the key factor for the above aspects. Hence A-CAES are classified in three types on the basis of the temperature level of TES, as stated by Budt et al. [31]:

3. A-CAES at high TES temperature, above 400°C.
4. A-CAES at medium TES temperature, between 200°C and 400°C.
5. A-CAES at low TES temperature, below 200°C.

The characteristics and the related studies of each type are discussed in the following sections.

### 2.5.1 A-CAES at high TES temperature

Figure 2.9 illustrates a functional schematic of this system type. The air is compressed in 2 stages to 2.4 bars and 65 bars respectively [31]. The heat induced by the first stage is lost to the environment (this is to avoid excessive temperatures in the process [42]), while the heat induced by the second stage is stored in solid materials, more precisely a regenerator or packed bed thermal energy storage [3,42].

Packed bed TES is formed by a tank containing solid compacted solid pieces such as rocks, ceramic bricks or steel slabs [3]. Contrary to conventional heat exchangers, heat transfer is carried out directly between air and solid at high temperature of 580˚C. Owing to the high thermal capacity and mass density of solids, the input temperature of turbines still high (around 570˚C [3]).

The main advantageous of this technology its low cost [31,42] and its high efficiency (up to 70% [31]), thanks to the high effectiveness of direct contact HEX and the low cost of related TES materials. Although, the main drawback are the following:

1. Compressors operating at such high temperatures are technologically unavailable [31].
2. Long response time (10-15 minutes) [31].
3. High pressure losses due to the channels formed between solid shapes [3].
4. Potential failure of materials of TES because of thermal stratifications [3].

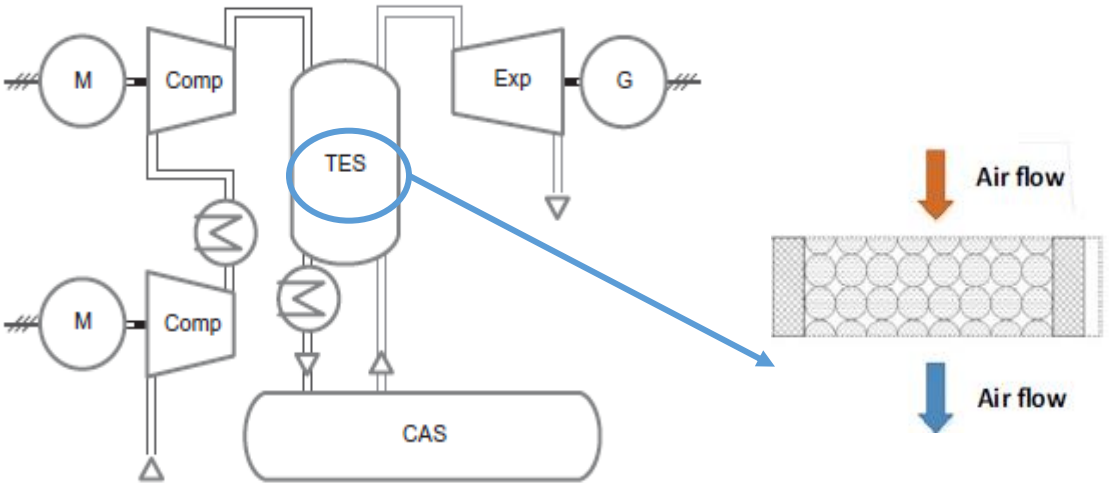


*Figure 2.9: Schematic diagram of A-CAES at high TES temperature [31,42].*

However, the parts of the Swiss pilot plant mentioned earlier is based on this technology, Geissbühler et al. [40] tested an unused tunnel behaviors as a storage volume with a maximum air storage pressure of 7 bars and high temperature up to 550˚C under different charging/discharging frequency, the round trip efficiency was calculated theotrically supposing a variable compression and expansion ratio and it was found in the range of 63%-74%. Here, it is important to mention that the high value of compressed air temperature is not ensured by a new technology of compressors with high compression ratio and working temperature but rather by a heater installed between compressor and TES. For the same plant, Becattini et al. [41] examined a combined sensible/latent TES formed by Al–Cu–Si alloy and packed bed of rocks with compressed air temperature at 566˚C, and their results showed a high TES efficiency ranging from 77% to 91%.

Finally, for the knowledge of the reader, there is many simulation and modeling studies of this system in the literature which is not reported in this thesis.

### 2.5.2 A-CAES at medium TES temperature

In order to overcome the problems associated with the previous system, mainly to reduce research effort to develop a new compressor technology, this type of A-CAES has been proposed.

Figure 2.10 shows the schematic of this system. The difference between the previous one relies on diminishing the temperature level by dividing the second compression stage into two stages. Thus, the compression chain is composed by three stages: the first with compression ratio of 2.4, while the second and the third have an outlet pressure and temperature of (19 bars; 280°C) and (65 bars; 380°C) respectively [31]. The two temperature levels result on having two TES components, each one is linked to a compression stage (upstream) and an expansion stage (downstream). As for TES materials, variety of them can be used such as: Thermal oil, Molten Salt and PCM [3,31].

The efficiency of this type is a little lower than the previous one with high response time. In addition, it is not widely addressed and investigated in the literature.

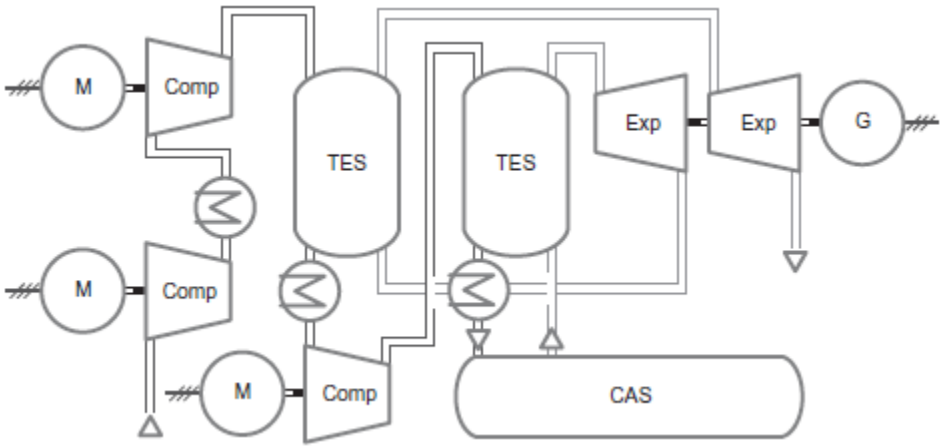


*Figure 2.10: Block diagram of A-CAES at medium TES temperature [31].*

### 2.5.3 A-CAES at low TES temperature

Presently, research and developments on A-CAES has been oriented towards this type on which the TES temperature can vary in the range of 80˚C-200˚C [31,39,43,44,45] and even achieve 300˚C-350˚C [46,47]. The main idea behind establishing this system is that from an ideal thermodynamic view the temperature of TES does not affect the overall efficiency as demonstrated by Wolf and Budt [44]. Note that a particular attention will be paid to this point in the next chapter.

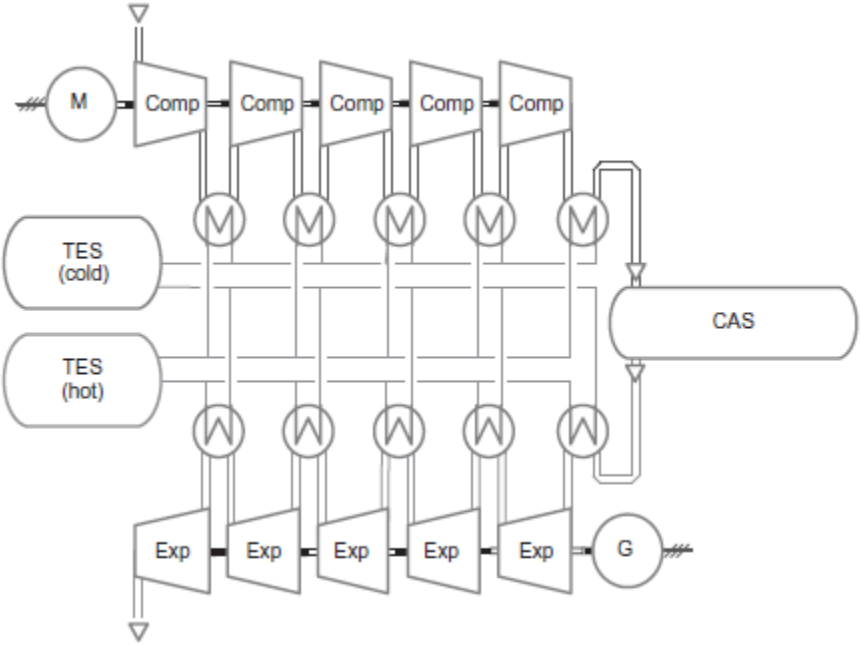


*Figure 2.11: Schematic of A-CAES at low temperature of TES [31].*

The basic principle is outlined in Figure 2.11 It consists of a multi-stage compression and expansion chain, on which the compressed air is cooled after each compression stage and reciprocally reheated before each expansion stage via indirect contact heat exchangers. Hence, it can be applied independently of the required storage pressure via varying the number of compression/expansion stages.

The particular attractiveness to this type rely on these two points [31]:

1 Using multi-stage intercooling compressors enables to reduce the compression work.
2 Using liquid heat transfer medium offer the possibility to use cheap TES materials (as water) and allows the application of flexible control system.
3 Short response time (below 5 minutes).

On the other hand, the low temperature of TES leads to a lower output power delivered by the turbine, which makes the energy density at low values. Besides, the electrical efficiency of this system is slightly lower than of the previous ones due to the irreversibilities induced by the increase of heat exchange process.

The research and development on A-CAES at low TES temperature have been very active in recent years. The following paragraphs discuss theoretical studies conducted on this system, as well as the experimental set-up of Wang et al. [39] shown in Figure 2.12. The optimisation studies on the A-CAES and T-CAES will be presented later in a separate paragraph since these two systems have similar thermodynamic and thermal concepts.

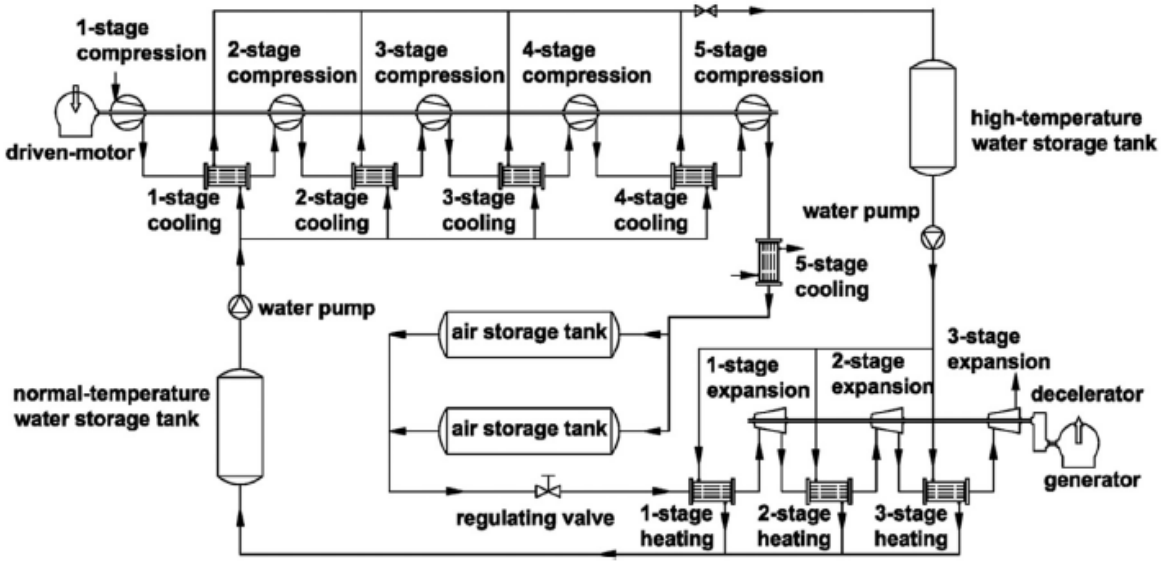


*Figure 2.12: Detailed schematic diagram of the experimental pilot "TIC-500", Chinese Academy of Sciences [39].*

Table 2.5 synthesizes the main operation characteristics of relevant previous researches on this system. All of these studies share the same configuration. It is built up from the following elements (see also Figures 2.11 and 2.12):

1. Multiple compression and expansion stages.
2. Throttling valve that reduces the maximum storage pressure to the input pressure of turbine (minimum pressure).
3. TES Storage tank at high temperature (HT-TES) that accumulates the water flowing from the cooling exchangers during the compression phase.

4. TES Storage tank at low temperature (LT-TES) that retains the water mass flow leaving the preheating heat exchanger of turbines.

The modeled round-trip efficiency varies in the range of 50%-64% (Table 2.5) according to the selection of design parameters of the equipment cited above. However, the pilot "TICC-500" designed by Wang et al. [39] (Figure 2.12) achieved experimentally an efficiency of 22.6% with five compression stages driven by a motor of 315 kW, three expansion stages connected to a generator of 500 kW, air tanks with storage pressure ranging from 25 MPa to 95 MPa, and pressurized water as thermal energy storage at 108˚C. The designed round-trip efficiency of the plant was higher at 40.7 % .This difference in these values was attributed to the unsteady operation of compressors and the performance of TES system. Note that the dynamic variation of the most relevant operating parameters of the pant are also reported in this publication.

Referring to Table 2.5, owing to the fact that the global compression ratio is higher than of the expansion ratio, and conceding that the performances of charging and discharging components are similar, the number of expansion stage is generally lower than of the expansion, except for the configuration of Szablowski et al. [46] on which the heat associated with the last charging HEX is lost to the environment.

On the other hand, for the same reason pointed above, the temperature of each expansion stage remains higher than the ambient temperature so that the temperature of LT-TES reservoir is also higher (reaches values from 42˚C to 80˚C) which means a loss of this heat energy. In this context, Zhang et al. [48] investigated the effect of thermal energy storage on the efficiency of A-CAES and found that a proportion of heat is left in TES which could be used to improve the efficiency. Zhou et al. [49] studied the effect of recovering the exhaust heat released from the output of the last stage turbine on the system efficiency of conventional CAES and A-CAES. The improvement on A-CAES is not significant because of the low value of the temperature of the exhaust flow. Luo et al. [45] proposed an optimisation of the classical configuration by integrating a recovery HEX downstream each preheating HEX and upstream each turbines. The efficiency improvement was found at 2.6%.

As for TES materials, pressurized water is the most popular owing to its very low cost and its excellent thermal proprieties. Thermal oil was also selected when the TES temperature becomes at higher levels.

The choice of the maximum storage pressure should be selected according to the geotechnical proprieties of the caverns and maximum allowable stress of artificial reservoirs; however, it has been chosen arbitrary by the authors and it is commonly fixed to around 70 bars in underground reservoirs (at large scale) and up to 100 bars for steel reservoirs.

The minimum pressure is governed by the admissible pressure of turbine which is related to the plant scale .Conventional gas turbine is designated at power scale of MW so that the minimum pressure is around 43 bars (Table 2.5), while it is lower for small scales (hundreds of kW) since gas turbines are not commercially available at this scale (first line of Table 2.5), for example the

pilot “TICC-500” used a radial inflow turbine developed by Key laboratory of cryogenics, TIPC, Chinese Academy of Sciences [39].

## 2.6 Trigenerative Compressed Air Energy Storage T-CAES

Previously, it has been demonstrated that CAES is adaptable to produce heating and cooling energy [13,16,19,20,21,50,51] by changing the preheating energy in the discharge phase, hence the trigenerative compressed air energy storage T-CAES has been introduced. Here, we mention that the consideration of the quantity of heat left on A-CAES (see the previous section) point out the importance of this concept. Besides, for the cooling energy T-CAES system could replace trithermal refrigeration cycles (absorption machines) characterized by expensive components and sometimes toxic materials such as Li-Br [21].

From a thermodynamic point of view, T-CAES differs from the A-CAES by a partial use or disuse of the compression heat as preheating energy of the expander. There is limited number of studies on this system. Many configurations have been proposed, which differ according to the manner in which the compression heat is used. Two types can be distinguished:

1. The first type devotes the heat produced during the charge phase for heating purposes while the electricity and the cooling energy are generated in the discharge phase, as proposed by Facci et al. [13], Lv et al. [19], Liu and Wang [20] and Arabkoohsar et al. [50]. Figure 2.13 illustrates the arrangement of the component of the discharge phase.
2. The second type is based on using an amount of heat stored during the expansion to increase the electrical efficiency while keeping the possibility to produce cooling and heating energy. This is suggested by Jannelli et al. [16], Li et al. [21] and Han and Guo [51]. Figure 2.14 shows the proposed configurations.

*Table 2.5: Main characteristics of LT-A-CAES as proposed by relevant research studies*

| | Status | Power (MW) | | Stages numb | | Pressure (bar) | | TES | | | Efficiency |
|---|---|---|---|---|---|---|---|---|---|---|---|
| | | Comp | Exp | Comp | Exp | Out Comp | In Exp | Materials | $T_{hot,TES}$ (°C) | $T_{Cold,TES}$ (°C) | |
| **Wang et al. [39]** | experimental pilot | 0.315 | 0.5 | 5 | 3 | 93 | 25 | Pressurized water | 108 | 45 | 22.6 |
| **Wolf and Budt [44]** | research project | 50 | 30 | 4 or 8 | 4 | 150 | 100 | Pressurized water | 150 | | 52-60 |
| **Grazzini and Milazzo[43]** | theoretical study | 1 | 1 | 6 | 6 | Var from 20 to 140 | | Pressurized water | 106 | 42 | around 58 |
| **Luo et al. [45]** | theoretical study | 60 | 290 | 4 to 6 | 4 to 6 | 70 | 43 | Pressurized water | around 130 | 52 to 67 | 59 to 64 |
| **Szablowski et al. [46]** | theoretical study | 60 | 161 | 2 | 3 | 70 | 43 | Synthetic oil (Therminol 55) | 300 | 80 | 50 |

.

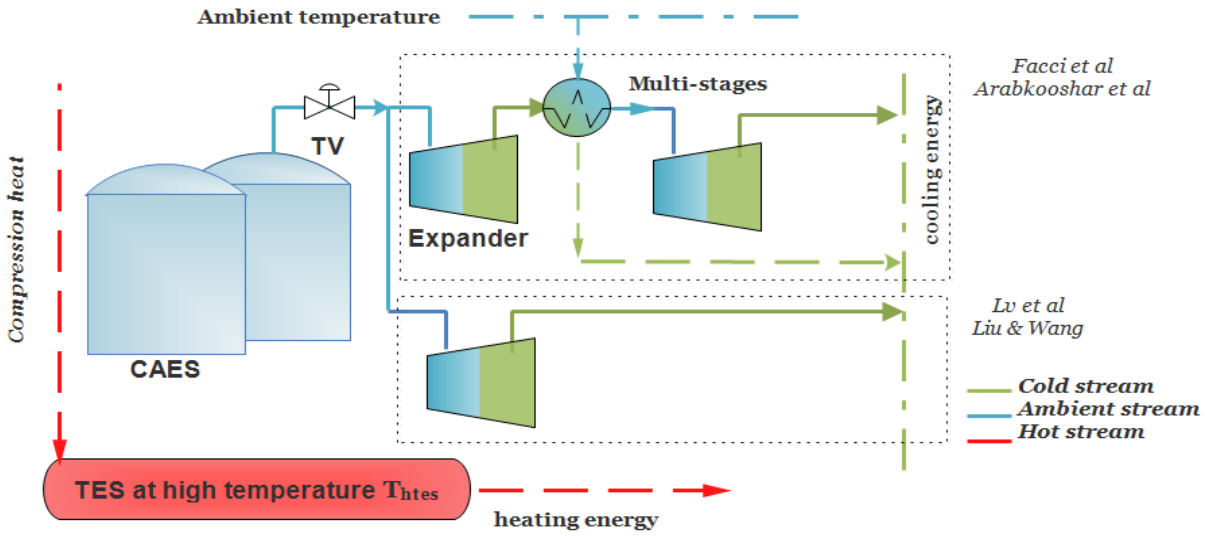


*Figure 2.13: T-CAES without preheating as proposed by Facci et al.[13], Lv et al.[19], Liu and Wang [20] and Arabkoohsar et al.[50].*

T-CAES is studied for small and large scales. In addition to the electric energy production, the cooling and heating energy demand of users is targeted for small applications, while district heating and cooling are intended for large applications [50,51]. Facci et al. [13] proved the compatibility of the system with small size civil applications by means of satisfying peak shaving, heating and cooling demand. Jannelli et al. [16] developed a design methodology of the storage system by applying it on a small scale stand-alone power station (telecommunication base station) with photovoltaic energy production. The system was able to satisfy the energy demand in terms of electricity and cooling. Apart from that, Li et al. [21] investigated a configuration of the system for load shifting and for meeting the cooling and heating demands of an office building located in Chicago (USA). As for large scales, Arabkoohsar et al. [50] demonstrated the potential of this system to support district heating and cooling and reserve services in electricity market for a typical large-scale application of the system in wind farms in Denmark.

In order to analyze and discuss the proposed configurations, the main operation parameters of air side components and TES components were collected and shown in Tables 2.6 and 2.7 respectively. In the two types of configurations (with or without preheating), the compression phase is as the same as for A-CAES. It can be noticed from Table 2.6 that the number of stages rises with the maximum storage pressure to keep a lower level of TES temperature as well as for electric efficiency purposes. Apart from that, the compression ratio was varied continuously according to the air pressure in the reservoir by some authors without investigating or accurately accounting the effect of this variation on the thermal energy storage devices. On the other hand, Arabkoohsar et al. [50] varied the compression ratio and the number of stages discontinuously. They used the three-compression stage in parallel (equivalent to one stage in terms of compression ratio) when the air pressure is lower than 5 bars, then two stages until the pressure reaches 25 bars and then three stages.

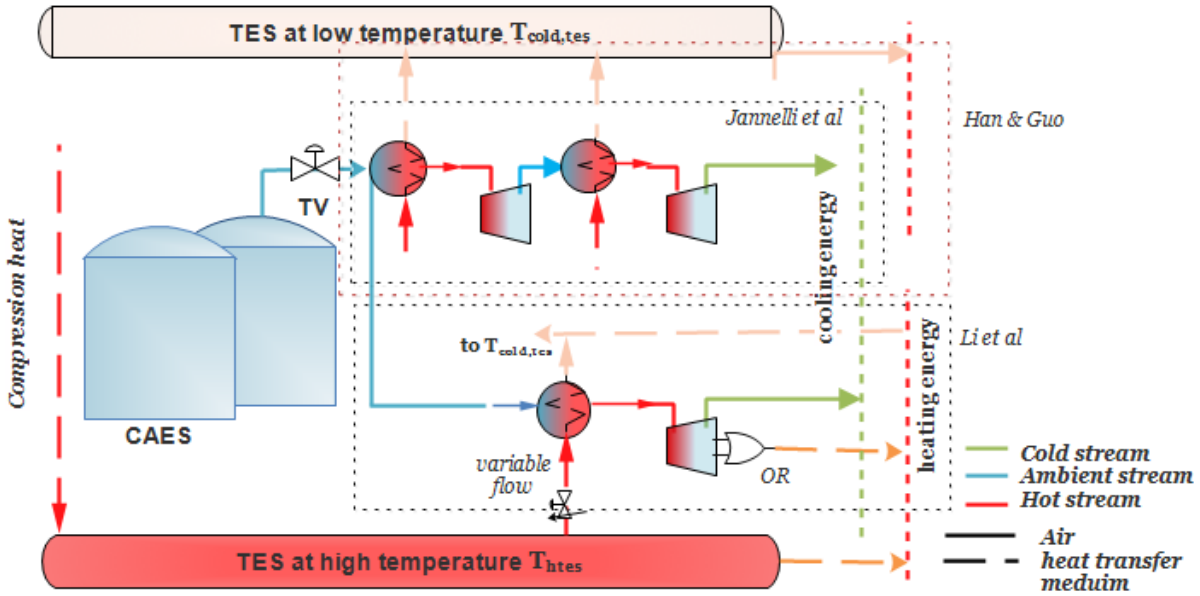


*Figure 2.14: T-CAES with preheating as proposed by Jannelli et al.[16], Li et al. [21] and Han and Guo [51].*

It can be noticed that there is not a principle which governs the choice of the maximum storage pressure by the authors, for instance it was fixed to 125 bars by Arabkoohsar et al. [50] without demonstrating that it is compatible with a specific cavern, and it was chosen arbitrary for small scale applications such as 35 bars by Jannelli et al. [16], 50 bars by Facci et al. [13]. However, it is generally fixed at lower level for large applications (60 or 125 bars) and at higher levels (up to 300 bars) for small ones since higher mass density is required for small applications.

The difference between configurations appears in the discharging phase. In the first type, the temperature of TES is chosen to suit the temperature of space heating system (75˚C for Facci et al. [13]) or the district heating requirements (120˚C for Arabkoohsar et al. [50]). The inlet of expanders is at the ambient temperature. Hence, there is always a possibility to produce cold energy at the exit of each stage (Figure 2.14).

Depending on the operating pressure of expanders and its minimum allowable output temperature, expansion process can be composed of one or more inter-heating stages, while the cold air on the upstream of each stage is heated by the air stream at room temperature. Using multistage is intended to increase the overall electrical efficiency of the system and limit the temperature at the output of each stage.

In the second type, the choice of the temperature of TES was not concerned by the authors, its level was rather as a result of imposing the number of compression stages and the mass flow rate of transfer medium so that it varies from 147˚C to 307˚C (Table 2.7). Jannelli et al. [16] and Han and Guo [51] settled the output temperature of each expansion stage lower than the ambient temperature to produce cooling energy, while this later was taken only from the last stage. Meanwhile the input temperature of each turbine is higher than the ambient temperature but still

lower than of the TES. A multi turbine stages are used in order to improve the overall efficiency of the system and to ensure that the input temperature of turbines is adaptable with $T_{hot,TES}$.

Alternatively, Li et al. [21] suggested to regulate the input temperature of the turbine (and subsequently its output) by varying the mass flow rate of the preheating HEX so that the system is able to produce whether cooling energy if the exhaust temperature of air is below the ambient temperature, or heating energy when the temperature is higher.

In the majority of the configurations of the second type, the stored heat is not completely used as preheating energy so that the temperature output of heat transfer medium of preheating HEX is higher than the ambient temperature which leads to have $T_{cold,\,TES} > T_{amb}$ . The potential heat related to cold,TES reservoir (for the majority of configurations) and to the exhaust flow of the turbine (configuration of Li et al. [21]) are used for heating purposes.

In the two types of configurations, the input pressure of expanders was widely different. Liu and Wang [20] referred to scroll expanders with expansion ratio of 5.5. Li et al. [21] employed syngas turbines and settled the pressure input when the turbine operates at its maximum efficiency. Han and Guo [51] refer to conventional gas turbines. By contrast, the other studies admitted the input pressure value theoretically. Similarly, the minimum allowable temperature output of the expander was ignored by some authors. Besides, the efficiency of compressors and expanders in a considerable proportion of these studies was taken arbitrary. However, it can be noticed (from Table 2.6) and agreed that for large scale applications the efficiency of machinery is higher.

Some authors have considered that the expansion ratio is variable [13, 21]. These assumptions do not necessarily take into account technological aspects and generate a variable input and output temperature at the expander level.

It can conclude from this analysis above that the majority of the studies have not taken the technological aspects and the operational constraints for all the system components at the same time, which explains the large differences between operation parameters.

*Table 2.6: Operation parameters of air side components of T-CAES as proposed by related authors.*

| | **Power (kW)** | | **Stage's number** | | **Pressure (bar)** | | **polytropic coefficient (>1) or efficiency (<1)** | | **Temperature (˚C)** | | | |
|---|---|---|---|---|---|---|---|---|---|---|---|---|
| | **Comp** | **Exp** | **Comp** | **Exp** | **Out Comp** | **In Exp** | **Comp** | **Exp** | **In Comp or ambient** | **Out Comp** | **In Exp** | **Out Exp** |
| **Facci et al.** [13] | 18 | 18 | 3 | 3 | varies from 20 to 50 (continuous) | varies from 48 to 19 | 0.7 | 0.7 | 25 | vary with comp ratio (<99) | around 25 | vary with exp ratio (>-46) |
| **Arabkooshar et al.** [50] | up to 10,000 | up to 10,000 | varies from 1 to 3 | varies from 1 to 3 | varies from 5 to 125 (discrete) | varies from 125 to 5 | 0.85 | 0.65 | max 30 | 238(*) | max 30 | min -100 (*) |
| **Liu and Wang** [20] | --- | --- | 1 | 1 | varies from 5.5 to 18 (continuous) | 5.5 | 1.25 | 1.25 | 30 | max 267 (*) | 30 | -57 |
| **Jannelli et al.** [16] | 3.7 | 1.35 | 3 | 2 | 35 | 25 | 0.85 | 0.75 | [8;25] | 159 | 130 | 3 |
| **Li et al. (winter)** [21] | | 45.8 | 4 | 1 | varies from 7 to 300 (continuous) | 7 | 1.25 | 1.25 | 4 | | 327 | 104 |
| **Li et al. (summer)** [21] | | 76.3 | 4 | 1 | varies from 13.4 to 300 (continuous) | 13.4 | 0.9 | 0.9 | 26 | 124 | 16 | -111 |
| **Han and Guo** [51] | 80,000 | 100,000 | 2 | 2 | 60 | 40 | 0.85 | 0.85 | 20 | max 460 | 114 | -33 |

*Table 2.7: Characteristics of TES components of T-CAES as proposed by the mentioned authors.*

| | Material | Temperature (°C) | | HEX |
|---|---|---|---|---|
| | | $T_{h,TES}$ | $T_{cold,TES}$ | Effectiveness |
| **Facci et al.** [13] | Water | 75 | not applicable | |
| **Arabkooshar et al.** [50] | Oil | 120 | not applicable | 0.8 |
| **Liu and Wang** [20] | | up to 147 | not applicable | 0.75 |
| **Jannelli et al.** [16] | Thermal oil | 164 | 8 | 0.95 |
| **Li et al.** [21] | Thermal oil | around 300 | $>T_{amb}$ | |
| **Han and Guo** [51] | Therminol 66 | 307 | around 87 | 0.7 |

### 2.6.1 Evaluation of the performances of T-CAES

T-CAES is not a simple technology, it has several roles such as an electrical storage technology and meets heating and cooling demands. In order to assess this system, the round-trip electrical efficiency defined by the ratio of electrical output to electrical input (Equation 2.1) is no longer sufficient to evaluate it.

$$\eta_{el} = \frac{E_{out,el}}{E_{in,el}} \tag{2.1}$$

Many approaches are possible to evaluate the performances. The first approach is based on the first principle of thermodynamics where electrical, heating and cooling energies are considered as outputs of the system, so that the coefficient of performance becomes:

$$COP_g = \frac{Q_{heat} + Q_{cool} + E_{out,el}}{E_{in,el}} \tag{2.2}$$

Where $Q_{cool}$ is the cooling energy and $Q_{heat}$ is the heating energy.

In order to study separately the contribution of the cooling and the heating energy separately on system performances, Equation 2.2 can be modified to derive the performance index shown in Equations 2.3.a and 2.3.b.

$$COP_{el,heat} = \frac{Q_{heat} + E_{out,el}}{E_{in,el}} \tag{2.3a}$$

$$COP_{el,cool} = \frac{Q_{cool} + E_{out,el}}{E_{in,el}} \tag{2.3b}$$

These coefficients of performances enable to evaluate the energy benefits of the system relative to the energy provided. However, COP index overestimates the performance values, and also the addition of energy values with different types is improper. Within this framework, the adoption of exergy efficiency can be used. However, it underestimates the performance [21] due to the fact that the exergy analysis appeals to the efficiency of an optimal Carnot cycle which always overestimates the efficiency of real cycles. In addition, this analysis is used rather for

thermodynamic optimization of the system. Therefore, Li et al. [21] introduced a new index named the comprehensive efficiency defined by :

$$\eta_g = \frac{\frac{Q_{heat}}{COP_{ref,heat}} + \frac{Q_{cool}}{COP_{ref,cool}} + E_{out,el}}{E_{in,el}} \quad (2.4)$$

where $COP_{ref,heat}$ and $COP_{ref,cool}$ are the performance coefficients of conventional heat pumps for heating and cooling, respectively. As a first approximation, they are considered equal to 4 and 3 [16].

The first two terms of the numerator of Equation (2.4) show the equivalent electrical energy needed to produce the heating and cooling energy by a conventional heat pump. Hence, the comprehensive efficiency reflects the ratio between the two following terms: (1) the sum of the output electrical energy and the equivalent electrical energy needed to generate the heating and the cooling energies, (2) the electrical energy input. Thus, we prefer to employ the term "global equivalent electrical efficiency" instead of "comprehensive efficiency". Here, we put the emphasis on this efficiency, which is the most important index in order to compare the T-CAES technology with other storage technologies such as electrochemical batteries.

Table 2.8 presents the performance criteria collected or calculated from the studies conducted on the T-CAES.

*Table 2.8: Performances achieved by the studies conducted on T-CAES. (*) refers to calculated values, (˙) refers to assumed values.*

| | $\eta_{el}$ | $COP_{cool,el}$ | $COP_{heat,el}$ | $COP_g$ | $COP_{cool,ref}$ | $COP_{heat\ ref}$ | $\eta_g$ |
|---|---|---|---|---|---|---|---|
| **Facci et al.** [13] | 0.3 | 0.45(*) | 1.18(*) | 1.38(*) | 3(˙) | 4(˙) | 0.6(*) |
| **Arabkooshar et al.** [50] | 0.3 | 0.63(*) | 1.23(*) | 1.56(*) | 3(˙) | 4(˙) | 0.64(*) |
| **Liu and Wang** [20] | 0.31 | 0.57 | 0.92 | 1.18 | 3(˙) | 4(˙) | 0.55 |
| **Jannelli et al.** [16] | 0.57 | 0.62 | not applicable | 0.62 | 3 | not applicable | 0.59 |
| **Li et al.** [21] **(winter)** | 0.43(*) | not applicable | 0.59 | 0.59 | not applicable | 4 | 0.47(*) |
| **Li et al.** [21] **(summer)** | 0.24(*) | 0.51 | not applicable | 0.51 | 3 | not applicable | 0.51(*) |
| **Han and Guo** [51] | 0.41 | 0.49(*) | 0.71(*) | 0.8 | 3(˙) | 4(˙) | 0.51(*) |

As a preliminary evaluation, It can be seen that the round trip electrical efficiency achieved by the system vary from 0.24 to 0.57 according to the configuration type and the design parameters (shown in Tables 2.6 and 2.7). As expected, regardless of these parameters, as expected the electrical efficiency of the configurations with preheating is always higher (see lines 4, 5 and 7) of Table 2.8). By contrast, the values of the equivalent electric efficiency (comprehensive efficiency) are comparable which point out the importance of the cooling production on improving the overall performances. Generally, the contribution of the generation of heat and cold can varies between 10% and 30%.

In addition, it can be concluded that the efficiency is strongly related to difference on operating pressure of compressor and expanders, for instance by comparing the results of Li et al. [21] in the summer and winter seasons, the electrical efficiency drops significantly as soon as the input pressure of expander drops from 13.4 bars to 7 bars.

It is expected that the electrical efficiency of the T-CAES is smaller than the large-scale system A-CAES (which can reach 70%), which is due to the difference between the pressure input of expander and the partial use of preheating energy. In addition, the efficiency of the system becomes lower at small-scales which is known for energy systems. Nevertheless, the performance values seem interesting, especially when the cooling and heating energies are considered. An overall equivalent electrical efficiency value that can reach 60% approaches to that of electrochemical batteries (60%-90%) and seems very interesting.

### 2.6.2 Optimization studies on Adiabatic and T-CAES.

Despite the difference between A-CAES and T-CAES in terms of preheating energy, technical and technological aspects, the thermodynamic and thermal modelling and analysis approach are similar.

Start with A-CAES, recent research investigations put the accent on the influence of the efficiency of turbines and compressors as well as the storage pressure on the system performances. Hartmann et al. [52] proved that the round trip efficiency of polytropic configuration is 10% lower than the isentropic configuration at 70%. Mozayeni et al. [53] showed that the storage pressure has a significant effect on the amount of energy stored and found that the round-trip electric efficiency increases from 35% to 74% by increasing the efficiency of the compressors and turbines from 0.65 to 0.95. In agreement with this, Luo et al. [45] developed a detailed model for A-CAES and focused on the system efficiency optimization via a parametric analysis. The main conclusion is that the system efficiency is mainly dominated by the isentropic efficiency of compressors and turbines and the heat transfer rate of heat exchangers (on other terms the effectiveness). Based on energy and exergy analysis, Szablowski et al. [46] found out, for a large scale system, that the major exergy destruction occurs in the compressors and turbines, and an important exergy loss is located at the throttling valve relaxing the air from 70 to 43 bars.
It is known that the operating pressure of turbomachinery is confined to a small range around its design input/output pressure so that the maximum and minimum pressure are taken as constant in the majority of the studies. However, little attention has been paid to the partial load operation of turbomachinery, He et al. [54] studied the compression phase with variable pressure ratio and optimized the compression efficiency keeping it above 80% by varying the blade inlet angle and the rotational speed. Guo et al. [47] developed a dynamic model of A-CAES operating between 4.2 MPa and 7 MPa taking into consideration part-load operations of compressors and turbines and demonstrated that those components are also the main responsible for the exergy destructions. Finally, Grazzini and Milazzo [43] focused on the optimisation of the design parameters of heat exchangers dedicated for A-CAES and they proposed in [55] an optimization strategy by using different arrangements of the compressors and expanders from parallel to series according to the pressure of the air reservoir.

In order to reduce the system losses, many researchers proposed innovative solutions. Houssainy et al. [56] proposed a patented novel hybrid high temperature thermal energy storage and low temperature A-CAES including a turbocharger unit that provides supplementary mass flow rate which contribute to decrease the storage pressure/volume and reducing the system cost. Kim [57]

carried out an energy and exergy analysis of different configurations of CAES with adiabatic or quasi-isothermal compression and expansions, constant volume and constant pressure air storage. The results demonstrated that the configuration with constant pressure and isothermal process presents the higher performances. In line with this, as mentioned previously, They proposed a patented constant-pressure compressed air energy storage (CAES) system combined with pumped hydro storage [32]. Mazloum et al. [58] proposed an innovative constant isobaric A-CAES including multistage adiabatic compression and expansion which achieved a round trip electrical efficiency of 53.6%.

As regards to the T-CAES, Facci et al. [13] investigated the effect of the design parameters on the efficiencies of the system such as the number of compression and expansion stages, turbines and compressors efficiency, maximum storage and expansion pressures. Apart from that, Minutillo et al. [59] optimized the configuration proposed by Jannelli et al. [16] (see previous section) considering it in different climate zones. Their results highlighted that the best performances are achieved by choosing both the lowest average pressure and the highest operating pressure range between maximum and minimum pressure of the air tank. By contrast, Liu and Wang [20] demonstrated that the decrease of the maximum storage pressure and the polytropic coefficient of the expanders, while increasing its expansion ratio improves significantly the coefficient of performance of the T-CAES. Finally, Han and Guo [51] focused on optimizing the system by operating the expanders under variable pressure.

To sum up, the main optimization parameters investigated in the literature are the following:

- Number of compression/expansion stages.
- Efficiency of compressors/expanders.
- Effectiveness of heat exchangers.
- Maximum and minimum storage pressures.
- Design parameters of heat exchangers such as the length, number and the diameters of tubes.

## 2.7 Conclusions and Problematic

In the past years, research and development has been being conducted on adiabatic and trigenerative compressed air energy storage, thanks to the improvement made by the use of compression heat. Furthermore, the system gained attention for small scales applications in favor of applying artificial reservoirs without relying on specific geological underground characteristics.

Research has been focusing on A-CAES at low temperature of thermal energy storage, which presents a good efficiency in the range of 50%-65%. Meanwhile the efficiency of the T-CAES seems to be interesting, especially after applying the heating and cooling potentials.

A-CAES approaches a stage of maturity that allows to develop its different configurations, the laws that govern its operation and its optimization paths. Although, the T-CAES system has not yet reached this stage of maturity. It has been considered recently and is characterized by a multitude of potential configurations. Besides, studies on T-CAES focused on introducing its concept, suggestion of configurations, demonstrating its adaptability to specific applications and

invoking some optimization opportunities. Nevertheless, the proposed configurations are not based on a rigorous thermodynamic analysis, and the related modeling and optimization studies do not sufficiently account for technological aspects and technical constraints. This problematic will be handled in the two next chapters.

The majority of the optimization studies on these two systems has been carried out without taking into account all the relations between system compounds and the evaluation criteria. This point will be explained and covered in Chapter 4.

Finally, available experimental studies concentrate on validating numerical models of sub-systems such as air caverns and thermal energy storage, or to show the real behavior of the system without a solid relationship with theoretical models. The coupled experimental/modeling approach is the subject of Chapter 5.

# CHAPTER 3 - THERMODYNAMIC CONCEPT AND ENERGETIC ANALYSIS OF THE TRIGENERATIVE COMPRESSED AIR ENERGY STORAGE

## 3.1 Objectives and originality

As discussed in the latter chapter, in the literature, the configurations proposed for the T-CAES are studied to demonstrate the importance of its concept, whereas they are not based on a complete rigorous thermodynamic analysis to justify these configurations set-up.

In this chapter, the fundamental principle of the T-CAES system is formulated in order to derive its possible configurations and deduce the key elements that influence system performances.

The invoked analysis is based on the first principle of classical thermodynamics or in another terms, it is an energy analysis based on energy equations balance in terms of work and heat. The thermodynamic process is considered as ideal focusing on energy equations of air flow, while the heat transfer in heat exchangers is described only qualitatively so as to comply with the principles of heat transfer.

This approach is similar to the analysis of conventional thermodynamic cycles to establish its maximum theoretical efficiency. It has been used by Kim [57] to analyze the different concepts of CAES such as the isothermal and adiabatic as well as isobaric or isochoric storage. Besides, Wolf and Budt [44] refer to this approach to demonstrate that the level of thermal storage is independent of theoretical thermodynamic efficiency (without taking into account irreversibility). In our context, the approach is very useful to bring a better understanding of the T-CAES concepts and it is furthermore extended to derive different T-CAES configurations.

## 3.2 Methodology

Since the objective of this part is to figure out the thermodynamic concept without going into depth in the real behavior of the process, the following simplifying assumptions are considered:

- Air is considered as a perfect gas.
- Compression and expansion processes are supposed adiabatic reversible (isentropic).
- Pressure losses, thermodynamic to electrical conversion efficiency are not considered.
- Heat transfers with the environment are excluded.
- No constraints were imposed on heat exchanger effectiveness so that it can tend to one.

In the T-CAES or A-CAES, the process is composed from three main phases:

1. Charging phase: it is the compression process on which the energy is absorbed to produce heat and pressurized air.

2. Storage phase where the energy is conserved. Following the previous assumptions, no losses are considered with the environment.
3. Discharging phase: it is the expansion process on which the air and the stored heat are combined to produce the output energy.

As for any thermodynamic cycle's analysis, the energy equations should be written in each transformation. In the following, the equations of each phase are presented, then the global energy balance of the system is established with the aim of elaborating its different possibility in an energetic point of view.

## 3.3 Governing thermodynamic equations

Figure 3.1 and Figure 3.2 present the nomenclature used for the parameters in the charging and discharging phases.

### 3.3.1 Charging phase

#### *Compression chain*

The compression ratio of each stage is the same, and is determined by Equation 3.1 as a function of the maximum tank pressure and the number of stages.

$$\beta_{c,i} = \left(\frac{P_{max}}{P_a}\right)^{1/N_c} \tag{3.1}$$

During an isentropic compression, the temperature output of each stage is calculated by Equation 3.2.

$$T_{out,c,i} = \beta_{c,i}^{\frac{\gamma-1}{\gamma}} . T_{in,c,i} \tag{3.2}$$

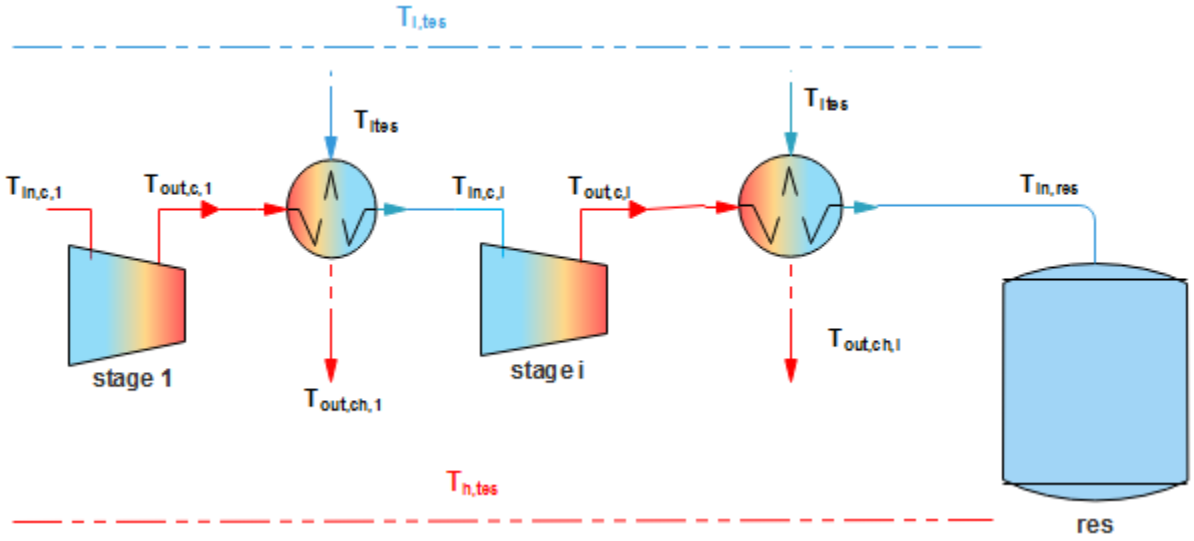


*Figure 3.1: Scheme of the charging phase.*

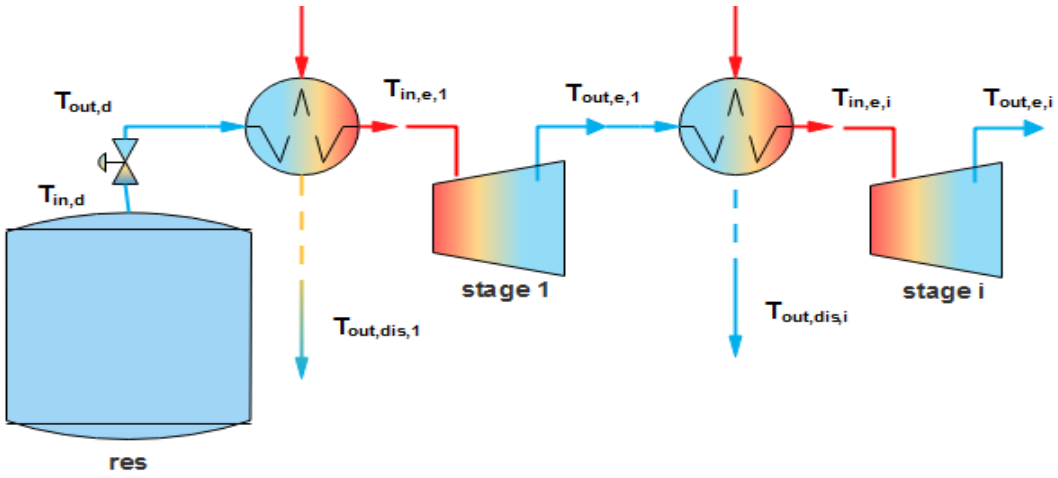


*Figure 3.2: Scheme of the discharging phase.*

The electric power is transformed to the thermodynamic power by Equation 3.3

$$\dot{W}_c = N_c . \dot{m}_c . C_{p,a} \left(T_{out.c,i} - T_{in,c,i}\right) \tag{3.3}$$

The mass flow rate of compression is derived from the two last equations, as follows:

$$\dot{m}_c = \frac{\dot{W}_c / N_c}{C_{pa} \left(T_{out.c,i} - T_{in,c,i}\right)} \tag{3.4}$$

### *Intercooling heat exchangers*

Since the counter-flow heat exchanger is characterized by high performances, it is designated throughout this thesis. The heat provided by the heat source (air flow) is expressed by:

$$\dot{Q}_{air} = \dot{m}_c . C_{p,a} . \left(T_{out,c,i} - T_{in,c,i+1}\right) \tag{3.5}$$

In this part, it is assumed that the heat exchanger is ideal so that the temperature input of each stage approach the ambient temperature, so that: $T_{in,c,i} = T_{amb}$

The latter equation becomes:

$$\dot{Q}_{air} = \dot{m}_c . C_{p,a} . \left(T_{out,c,i} - T_{amb}\right) \tag{3.6}$$

The heat absorbed by the heat sink (TES heat transfer fluid) is expressed by:

$$\dot{Q}_{fluid} = \dot{m}_f . C_{p,f} . \left(T_{h,TES} - T_{l,TES}\right) \tag{3.7}$$

Applying energy balance in heat exchangers, the heat provided by the air is equal of that absorbed by the fluid ($\dot{Q}_{fluid} = \dot{Q}_{air}$). The heat delivered by each heat exchanger is absorbed by the thermal energy storage fluid, so this amount of heat is expressed as:

$$\dot{Q}_{s,i} = \dot{m}_c . C_{p,a} . \left(T_{out,c,i} - T_{amb}\right) \tag{3.8}$$

The thermal energy stored per time unit (thermal power) resulted from the total number of heat exchangers is then:

$$\dot{Q}_s = N_c.\dot{m}_c.C_{p,a}.\left(T_{out,c,i} - T_{amb}\right) \tag{3.9}$$

### *Stored compressed air mass during the charge phase*

As mentioned in the last chapter, the air cannot be expanded beyond the operating pressure of the expander. Hence, the air pressure in the air reservoirs varies in the range of the input expander pressure $P_{min}$ and the maximum storage pressure $P_{max}$ , and the stored compressed air mass at the ambient temperature is expressed by:

$$m_s = \frac{P_{max} - P_{min}}{r.V_{res}.T_{amb}} \tag{3.10}$$

Here, the time required to charge and discharge can be deduced from Equations 3.11 and 3.12 respectively:

$$t_{ch} = \frac{m_s}{\dot{m}_c} \tag{3.11}$$

$$t_{dis} = \frac{m_s}{\dot{m}_e} \tag{3.12}$$

## 3.3.2 Discharging phase

### *Expansion chain*

Remember that the air in the reservoir is throttled from the storage pressure to the admission pressure of the turbine. The throttling process is considered as isenthalpic. Hence:

$$T_{out,d} = T_{in,d} = T_{amb} \tag{3.13}$$

The thermodynamic of expansion phase is similar to that of compression. The expansion ratio of each stage, the temperature output and the expansion power are expressed in Equations 3.14, 3.15 and 3.16 respectively.

$$\beta_e = \left(\frac{P_{min}}{P_a}\right)^{1/N_e} \tag{3.14}$$

$$T_{out,e,i} = \beta_e^{\frac{1-\gamma}{\gamma}}.T_{in,e,i} \tag{3.15}$$

$$\dot{W}_e = \sum_{i=1}^{Ne} \dot{m}_e.C_{p,a}.\left(T_{in,e,i} - T_{out,e,i}\right) \tag{3.16}$$

### *Preheating heat exchangers*

The preheating energy is obtained from the ambient temperature when the temperature input of heat exchanger is lower than $T_{amb}$ and the associated energy can be used as cooling energy as expressed by Equation 3.17:

$$\dot{Q}_{cool,i} = \dot{m}_e . C_{p,a} . \left(T_{amb} - T_{out,e,i-1}\right) \quad (3.17)$$

When the air temperature achieves the ambient temperature, the heat is recovered from the heat stored, and the preheating energy is equivalent to the recovered or recuperated heat $Q_r$. This heat is the crucial parameter which leads to have many system configurations. Hence, it is considered as an imposed parameter.

The heat absorbed per time unit of each heat exchanger is a function of the imposed recuperated energy, the number of expansion stages and the discharge time. It is calculated from Equation 3.18.

$$\dot{Q}_{dis,i} = \frac{Q_r}{N_e . t_{dis}} \quad (3.18)$$

The input temperature of each expansion stage is a function of the output temperature of the preceding one and the heat recovered, as expressed by Equations 3.19.a and 3.19.b.

If $T_{out,e,i-1} > T_{amb}$

$$T_{in,e,i} = \frac{\dot{Q}_{dis,i}}{\dot{m}_e . C_{pa}} + T_{out,e,i-1} \quad (3.19.a)$$

If $T_{out,e,i-1} \leq T_{amb}$

$$T_{in,e,i} = \frac{\dot{Q}_{dis,i}}{\dot{m}_e . C_{pa}} + T_{amb} \quad (3.19.b)$$

### 3.3.3 Global system assessment

As mentioned above, the recovered heat is one of the key elements to anticipate the capability of the system to produce different types of energy (cooling, heating and electricity). Since the recovered heat represents a part of the heat stored, it is more convenient to define an input parameter which is the ratio of the heat recovered to the stored one (Equation 3.20). Once this ratio is imposed, the recovered heat is known.

$$C_{rs} = \frac{Q_r}{Q_s} \quad (3.20)$$

Taking the thermal energy storage as a control volume, the heating energy is the difference between the heat stored and the heat recovered. On the other hand, taking the air side as a control volume, an unavoidable heat can occur at the exhaust air flow and its temperature is higher than the ambient temperature, so that the energy related to this airflow can be used also for heating purposes. Hence, the heating energy becomes:

$$Q_h = Q_s - Q_r + Q_{N_e} \quad (3.21)$$

where $Q_{N_e}$ is the heat taken from the last expansion stage, with the condition of: $Q_{N_e} = 0$ if $T_{out,e,N_e} \leq T_{amb}$.

Equation 3.22 is the reformulated form of Equation 3.21.

$$Q_h = (1 - C_{rs}).Q_s + \dot{m}_e.C_{pa}.\left(T_{out,e,N_e} - T_{amb}\right).t_{dis} \quad (3.22)$$

The cooling energy is calculated from Equation 3.23.

$$Q_{cool} = \sum_{i=1}^{Ne} \dot{Q}_{cool,i}.t_{dis} \quad (3.23)$$

Finally, the round-trip electrical efficiency is expressed by Equation 3.24.

$$\eta_{el,g} = \frac{\dot{W}_e.t_{dis}}{\dot{W}_c.t_{ch}} \quad (3.24)$$

To sum up, Figure 3.3 presents a block diagram of the equations and input output parameters shown above.

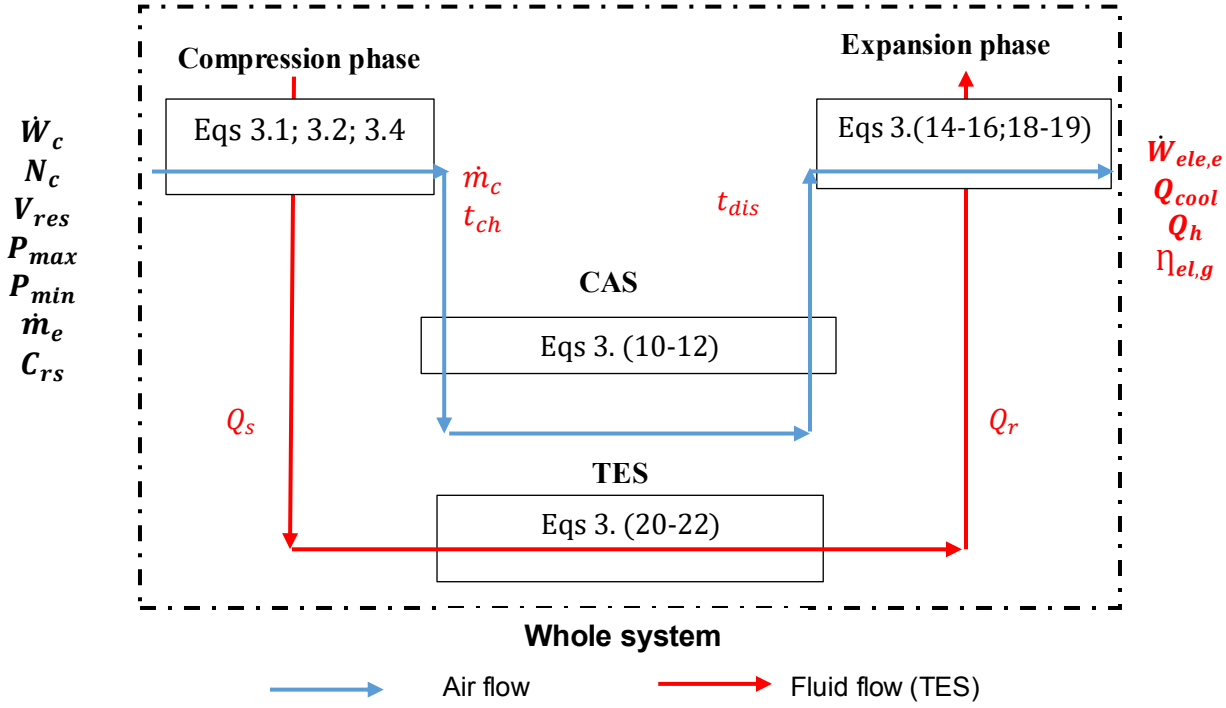


*Figure 3.3: Block diagram of the thermodynamic equations of the T-CAES.*

## 3.4 Thermodynamic concept

### 3.4.1 Adiabatic concept

In order to figure out rigorously the thermodynamic concept of the A-CAES, Table 3.1 shows a simple example of an ideal adiabatic system. The expansion mass flow rate is taken equals to the compression one with the aim of isolating the effect of discharging and charging time. Since the system is adiabatic, all the heat stored is recuperated in the discharge phases so that $C_{rs}$ is fixed to one. Hence, the global expansion ratio should be equal to the expansion ratio in order to satisfy the later condition ($C_{rs} = 1$).

Firstly, it can be noticed that an ideal A-CAES is achieved only when the compression ratio is equal to the expansion one which means that the storage should be isobaric. This proves the results of Zhang et al. [48] (see the previous chapter), which is: on A-CAES a quantity of heat is left and not used. Besides, this highlights that the isobaric CAES is the best choice in terms of maximum efficiency.

In the second place, when the number of compression stages increases, it is obvious that the temperature output of each stage decreases which means the drop of the temperature of thermal energy storage. By contrast, the global electric efficiency stays constant at 100%. Hence, it can be deduced that the temperature of TES does not affect the maximal achievable electric efficiency.

In conventional thermodynamic cycles (engine cycles), the maximum efficiency is governed by the maximum process temperature $T_{max}$. By the contrary, as shown in P-V diagram in Figure 3.4, the A-CAES is simply composed of a compression and an expansion so that $T_{max}$ is independent from the system efficiency. This concept is the idea behind low temperature LT-A-CAES introduced by Wolf and Budt [44].

However, one can say that in A-CAES the global compression and expansion ratio are not equals and the temperature of thermal energy storage may affect the value of the electric efficiency. Here, this effect cannot be attributed to the temperature of the thermal energy storage itself, but rather to the temperature difference between the expansion input and compression output. This effect will be explicated in next chapters.

Finally, it should be noted that the rise of the number of compression stage leads to the increase of the compression flow rate due to the fact that the compression efficiency increases since it approaches the isothermal process (Figure 3.4).

*Table 3.1: Numerical example of an ideal A-CAES.*

| **Fixed parameters** | | | | |
|---|---|---|---|---|
| | Compression power (kW) | | | 100 |
| | Global compression ratio | | | 20 |
| | Ambient temperature (°C) | | | 30 |
| | $C_{rs}$ | | | 1 |
| **Studied parameters** | | | | |
| **Compression phase** | Number of compression and expansion stages | 1 | 2 | 3 |
| | flow rate (kg/s) | 0.25 | 0.32 | 0.35 |
| | Output temperature of each stage (°C) | 440 | 191 | 130 |
| **Expansion phase** | Global expansion ratio | 20 | 20 | 20 |
| | Expansion mass flow rate (kg/s) | 0.25 | 0.32 | 0.35 |
| | Output temperature of each stage (°C) | 30 | 30 | 30 |
| | Electric power of each stage (kW) | 100 | 50 | 33.3 |
| | Total electric power (kW) | 100 | 100 | 100 |
| **Global electric efficiency** | | 1 | 1 | 1 |

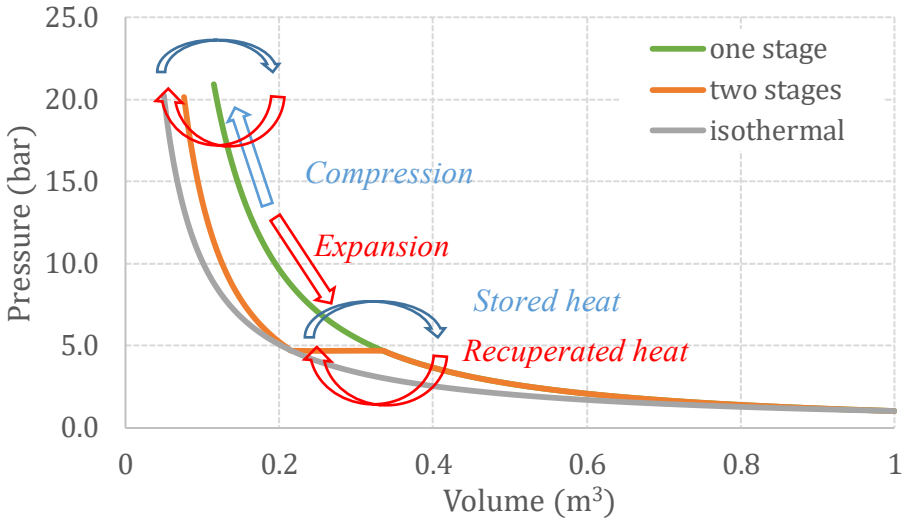


*Figure 3.4: A-CAES representation on the Clapeyron diagram.*

### 3.4.2 Trigenerative concept

Once the global expansion ratio is lower than the global compression, the ratio of the recuperated to stored heat achieves a value lower than one. Here, the question becomes how the value of $C_{rs}$ govern the system operation. In order to illustrate this effect, the input expansion pressure and other values shown in Table 3.2 are fixed. The variation of the input and output temperature of the expander, heat stored, heating energy as well as the cooling energy as a function of $C_{rs}$ are shown in Figure 3.5. The electric efficiency variation is presented in Figure 3.6.

*Table 3.2: Imposed parameters to study the T-CAES.*

| **Imposed parameters** | |
|---|---|
| Ambiant temperature (°C) | 25 |
| Compression power (kW) | 3.17 |
| Global compression ratio | 300 |
| Storage volume (m³) | 0.29 |
| $N_c$ | 1 |
| $N_e$ | 1 |
| Global expansion ratio | 30 |
| $C_{rs}$ | [0;0.85] |

As the recovered heat increases, the inlet temperature of the expander increases which leads to the rise of its output temperature (Figure 3.5 left). Hence, the enthalpy difference between the inlet and the outlet of the expander rises linearly which rises the expansion work and the electric efficiency (Figure 3.6).

The maximum value reached by the electric efficiency is 67% as $C_{rs}$ equals to 0.83, which corresponds to the maximal achievable temperature of the input of the expander. Above this value the temperature of this later exceeds that of the compressor outlet. The maximum efficiency value is lower than 100% due to the difference between expansion and compression ratio which induces an exergetic losses associated to pressure.

The examination of Figure 3.5a enables to identify the three following system operations:

1. When $C_{rs} < 0.4$ : the three form of energy (cooling, heating and electricity) can be produced. This is the concept of the trigenerative compressed air energy storage.
2. When $C_{rs} \geq 0.4$ : the cooling energy is disabled and the output expander temperature becomes higher than the ambient temperature (Figure 3.5b). Thus, the system is cogenerative. As the expansion ratio approaches the compression one $C_{rs}$ rises and the system tends to be adiabatic, as shown in the previous section.

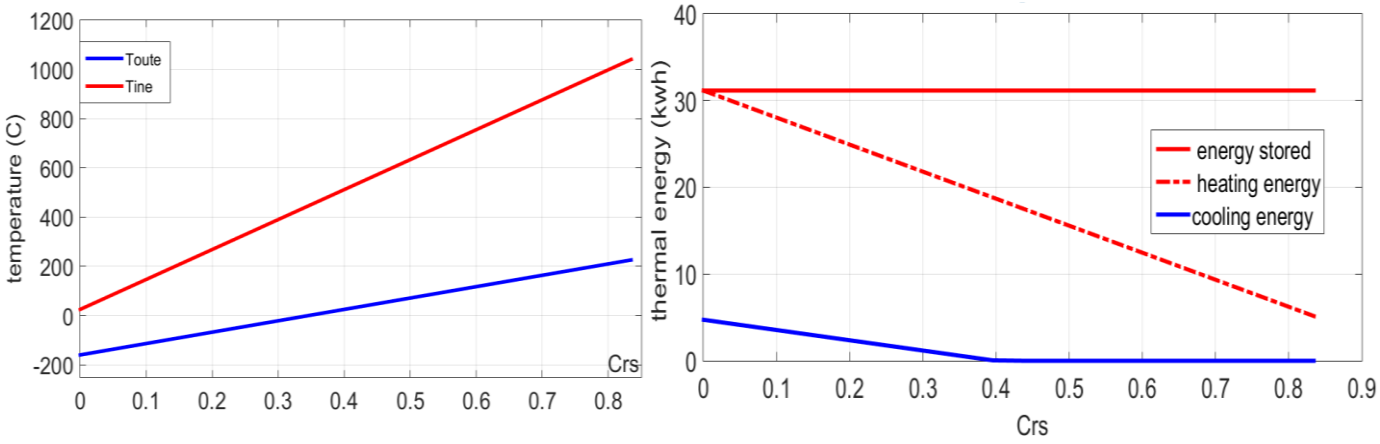


*(a)* *(b)*

*Figure 3.5: (a) Input and output temperature variation and (b) energy distribution as a function of the heat recuperated to stored ratio.*

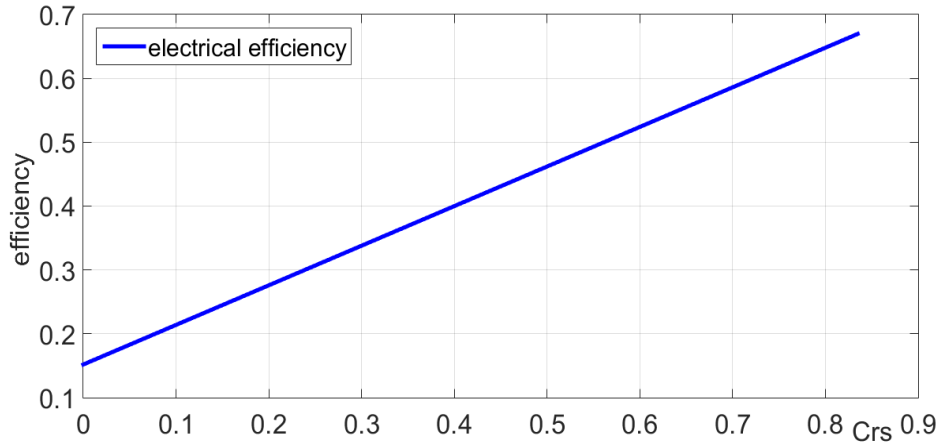


*Figure 3.6: Electrical efficiency variation as a function of the heat recuperated to stored ratio.*

The main conclusions which can be summed up from the previous analysis are:

1. The amount of recovered heat is the key element which improves the electric efficiency and governs the production amount of heating and cooling energy. However, any amelioration of the electric efficiency is charged by a decrease of heating and cooling energy.
2. The main obstacle to achieve the maximum heat recuperation rate (in other words $C_{rs}$=1) and the maximum efficiency is the pressure difference between expander input and

compressor output. However, this deficiency can be compensated by the cooling and heating energy productions (the trigeneration concept).

## 3.5 Trigenerative Compressed Air Energy Storage possible configurations

### 3.5.1 Energy analysis method

Based on the results of the previous section, the recuperated to stored heat is related directly to the input and output temperature of expansion stages. Hence, the analysis of the possible configurations can be performed by investigating $C_{rs}$ value for a desired value of outlet or inlet temperature of the expansion stage. However, It was decided to fix the value of the outlet $T_{out,e,i}$ for following reasons :

- The value of $T_{out,e,i}$ governs the opportunity to produce or not the cooling energy.
- Once $T_{out,e,i}$ achieves the ambient temperature value the air re-achieves its initial state which means the compression/expansion cycle is performed.
- The simulation experiences of the authors in T-CAES admitted that the value of $T_{out,e,i}$ is very relevant to ensure heat transfer medium of TES mass conservation.

The configurations arrangement is based on inspecting the temperature levels at the expansion stages levels. Then, they are evaluated by calculating the output energy. Figure 3.7 explicits the resolution algorithm. The method begins with imposing the last expansion stage temperature ($T_{cond}$ in the algorithm), the method of resolution consists in iterating the $C_{rs}$ value (initialized to one) until that the two following conditions are satisfied:

(a) Condition 1: the temperature at the outlet of the last expansion stage is equal to the imposed value.
(b) Condition 2: the temperature at the inlet of each expansion stage is smaller than the temperature at the outlet of the compressor stages.

The number of compression and expansion stages are fixed to 3, and the global compression and expansion ratio are fixed to 300 and 50 respectively. Besides, three cases were studied by imposing the last stage output temperature to $T_{amb}$+50°C, $T_{amb}$ and $T_{amb}$-50°C. As a first approximation, the preheating energy was assumed to be symmetrically distributed between the expansion stages.

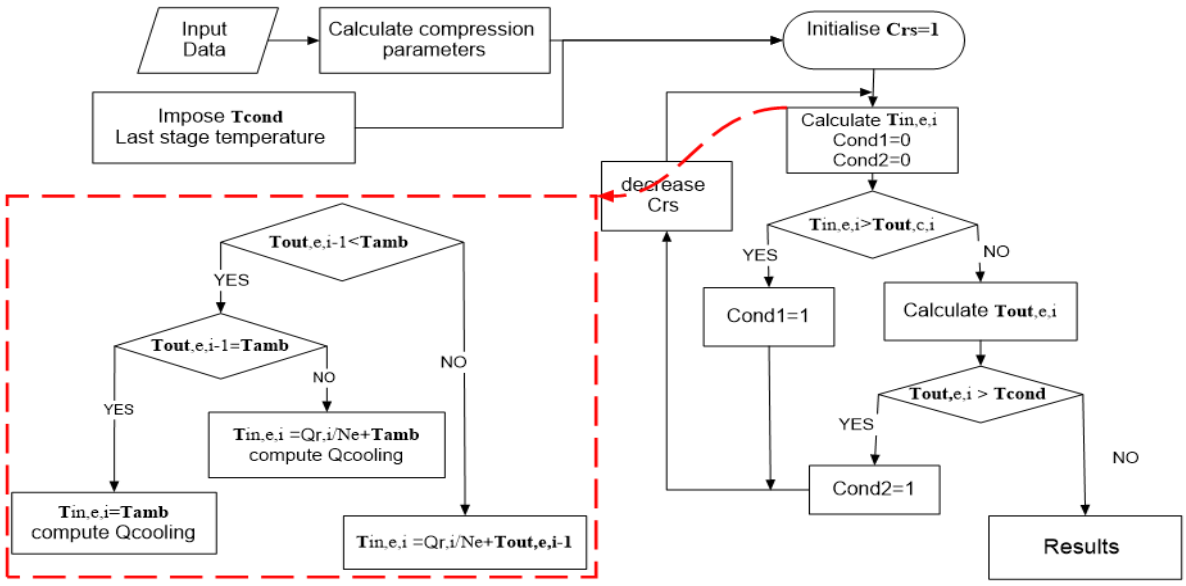


*Figure 3.7: Resolution algorithm to derive the possible configurations of the T-CAES.*

### 3.5.2 Possible configurations

According to the value of the output temperature imposed, three configurations are deduced. Tables 3.3 and 3.4 present the energy values and the temperature distribution respectively. Figure 3.8 presents the differences between the 3 configurations that were derived from Table 3.4.

*Table 3.3: Numerical values of energy flows of an ideal T-CAES.*

| **Configurations** | **1** | **2** | **3** |
|---|---|---|---|
| Last expansion stage temperature | $T>T_{amb}$ | $T=T_{amb}$ | $T<T_{amb}$ |
| | 75.0 | 25.0 | -25.0 |
| Heat recuperated to stored ratio $C_{rs}$ | 0.8 | 0.62 | 0.3 |
| Input electric energy (kWh) | 15.2 | 15.2 | 15.2 |
| Output electric energy (kWh) | 10.7 | 9.5 | 7.9 |
| Heating energy (kWh) | 4.6 | 5.7 | 10.9 |
| Cooling energy (kWh) | 0.0 | 0.0 | 3.54 |
| Electric efficiency (%) | 70.0 | 62.6 | 52.0 |

*Table 3.4: Temperature input and output of the discharge phase of the three T-CAES configurations.*

| | **Expansion input and output temperatures** | **Stage 1** | **Stage 2** | **Stage 3** |
|---|---|---|---|---|
| **Configuration 1:** | Input temperature (°C) | 191 | 213 | 229 |
| **$T>T_{amb}$** | Output temperature (°C) | 47 | 62 | 73 |
| **Configuration 2:** | Input temperature (°C) | 159 | 159 | 159 |
| **$T=T_{amb}$** | Output temperature (°C) | 25 | 25 | 25 |
| **Configuration 3:** | Input temperature (°C) | 87 | 87 | 87 |
| **$T<T_{amb}$** | Output temperature (°C) | -25 | -25 | -25 |

Comparing the value of the electric efficiency of the three configurations, it can be deduced that the increase of the level of the temperature input/output of each expansion stage leads to rise the

electric efficiency. This is due to the fact that the expansion is undergoing at high average value of temperature. Besides, the difference in the values of efficiency between the first and the second configuration (at 7.4%) is lower than of the difference between the second and the third ones (10.6 %) in spite of the same deviation on the output temperature (almost 50°C). This can be attributed to the fact that: in the second configuration the heat of compression is exploited at high level in a way that the air flow achieves its initial state at ambient temperature and pressure, in other words the enthalpy of the inflow entering the system is equal to of the outflow.
As expected, the production of the cooling energy (in the third configuration) and the improvement of the electric (by comparing the three configurations) reduces the heating energy production.

Concerning the temperature level of the streams of each configuration:

- In the first configuration: multi-levels of the temperature output of preheating HEX as well as the TES medium mass flow rate are expected which complicates further the study, notably the HEX design.
- In the second and the third configuration, the temperature distribution is symmetrical which simplify the design. Besides, the temperature of cold, TES reservoir is close to the ambient temperature which enables the use of this later directly in the charging phase.

The cold production (third configuration) is characterized by a number of heat exchanger which is double of the other configurations which could increase the investment cost.

It can be easily relate the obtained configurations to those proposed in the literature: the first one is equivalent to the A-CAES with excess heat production, while the third one is similar to the configuration of Jannelli et al. [16] and Hand and Guo [51], with a difference that those authors take into consideration only the cold from the last expansion stage.

To conclude, the analysis based on the heat recuperation rate brings to have three main configurations which differs mainly on its efficiency, design complexity and cooling production. The optimal choice would refer to the energy needs for a specific application.

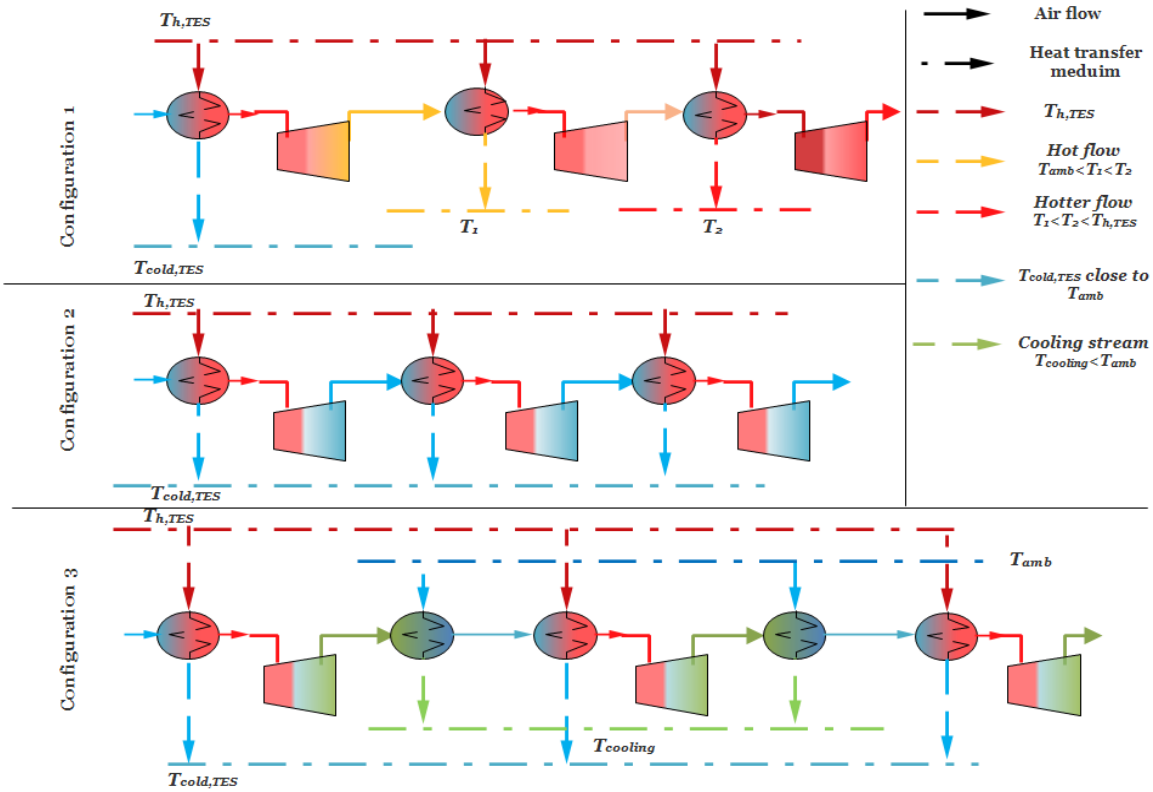


*Figure 3.8: Discharging phase of the three configurations of the T-CAES.*

### 3.5.3 Basic configurations

The possibility to have many configurations gives rise of the question of which configuration is the more adaptable for a given energy needs. Notwithstanding, further analysis of the results of the previous section drive to investigate on the possibility to have a general configuration which combine the advantageous of the three configurations and to be adjustable to satisfy energy demands.

It can be concluded from the previous analysis that a high temperature level when the expansion takes place is associated with higher efficiency. Hence, the heat can be exploited on the first successive stages so that the high expansion temperature is ensured, then the cooling can be exploited on the other successive stages.

Based on this latter idea, Figure 3.9 shows the suggested basic configurations. The first basic configuration (top schema of Figure 3.9) can be seen as a combination between the second and the third configurations discussed in the previous sections. When the cooling is not needed, the suggested configuration is equivalent to the second configuration of Figure 3.8, whereas when the cooling is required it is released simply by by-passing the third heat exchanger and supply the remaining inter-heat HEX by the stream at the ambient temperature. Here, the importance of this configuration is its flexibility to meet the requirements both in summer and winter seasons.

In order to demonstrate the benefit of this basic configuration, Table 3.5 shows the simulation results. Aiming to keep the same cooling energy produced, three expansion stages with a global expansion ratio of 7.05 is required, while the first expansion stage can be divided into two stages

due to the lower expansion ratio. The gain achieved by comparison with the third configuration of Figure 3.8 is about 2%, thanks to the higher temperature expansion level at 120˚C.Meanwhile, the efficiency drops by 4.3 % by comparison with the second configuration (summer seasons), which is due to the low level of input temperature (87˚C) of the last three stages. However, this problem can be optimized by connecting the two last stages and preheating them by one HEX at once. Here, we will not go into details furthermore since it is intended to show a guideline to adopt the proper configuration, and because of the results are based on simplified equations.

*Table 3.4: Numerical values of energy streams of the first basic configuration.*

| | **Without cooling** | **With cooling** |
|---|---|---|
| Output temperature of the last three expansion stages | T=Tamb<br>25.2 | T<Tamb<br>-25.0 |
| Input temperature of the expansion stages<br>First two stages/last three stages | 120/86 | 120/25 |
| Input electric energy (kWh) | 15.25 | 15.25 |
| Output electric energy (kWh) | 8.38 | 8.81 |
| Heating energy (kWh) | 7.13 | 6.44 |
| Cooling energy (kWh) | 0.00 | 3.54 |
| Electric efficiency (%) | 58 | 54 |

The aim of the second basic configuration (in the bottom of Figure 3.9) is to increase the electric efficiency, so that it differs from the first basic one by the fact that the temperature input of each stage is the highest possible, so that it is close to the temperature of TES. On the other side, the temperature output of the second expansion stage is high (Figure 3.9) so that an additional re-cooling heat exchanger is needed to extract the heat when the cooling is needed. Otherwise, it is equivalent to the first configuration of Figure 3.8.

The comparison of these two basic configurations should be based on a detailed thermodynamic model and it is discussed in details in the following sections.

## 3.6 Conclusion

In this chapter, the basic thermodynamic equations that governs the T-CAES are presented. A rigorous analysis based mainly on analyzing the ratio of the heat recuperated to the heat stored enables to conclude three possible configurations. However, a further discussion based on the grade of the input temperature of expansion phase and the application energy needs leads to conclude two basic configurations.

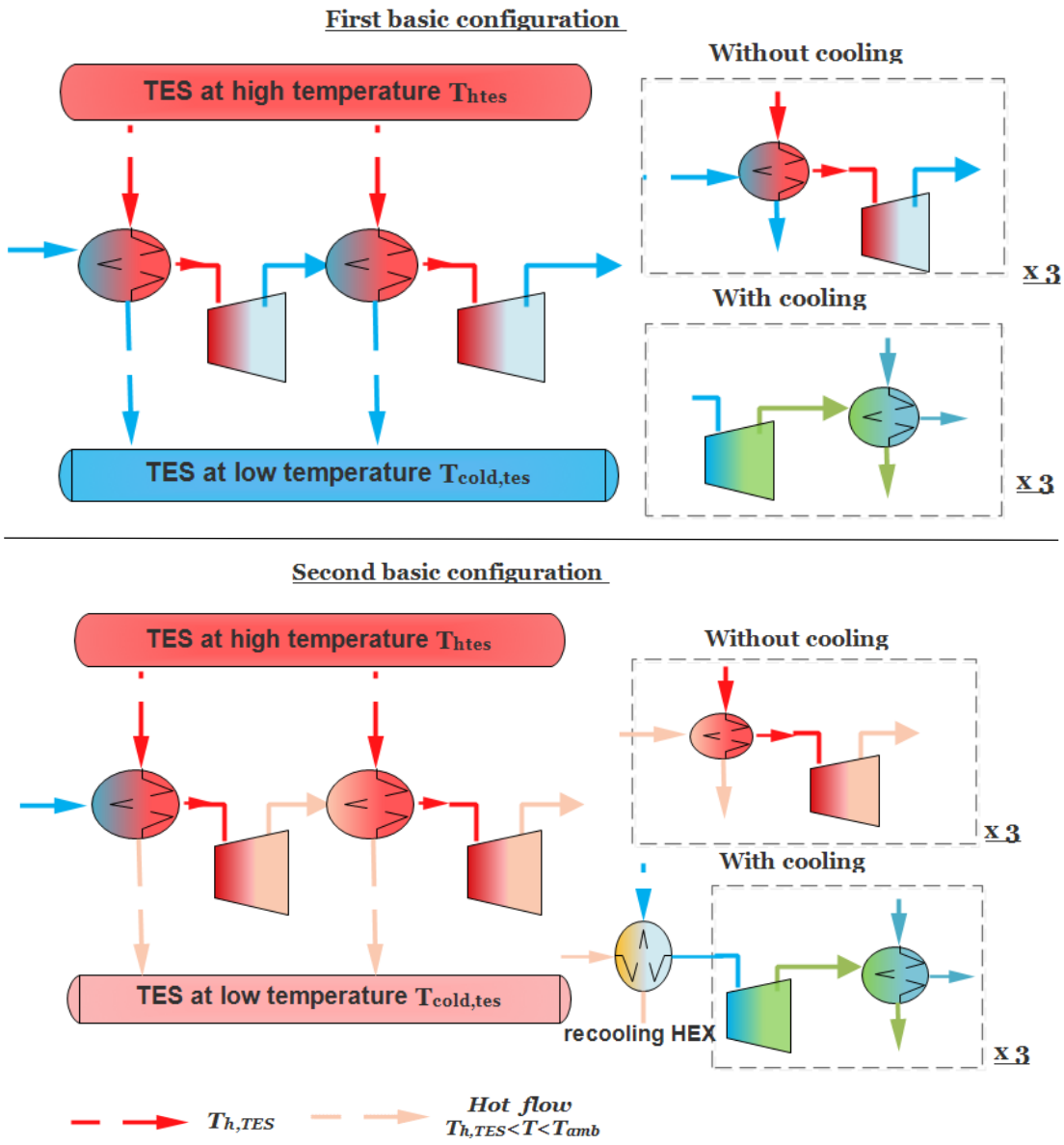


*Figure 3.9: General basic configurations deduced for T-CAES.*

The discharge phase of the basic configurations is generally formed by two parts of expansion stages: the first part is formed by an expansion stages preheated by the thermal energy storage TES while the expansion stages of the second part are preheated by the ambient stream if the cooling is needed or by the TES if the cooling is not required. The amount of cold production can be adjusted by varying the pressure input of the second part of the expansion stages.

The detailed model of the components of the system is necessary to predict the real performances of the configurations of the T-CAES. This will be the subject of the next chapter.

# CHAPTER 4 – DESCRIPTION AND MODELLING OF THE TRIGENERATIVE COMPRESSED AIR ENERGY STORAGE.

## 4.1 Objectives

In this chapter, the basic configurations deduced from the previous chapter are well established taking into consideration the technological issues of each component. Then, an accurate causal steady-state model (input/output modelling) of the T-CAES system is developed paying attention to the following aspects, which make up the originality of this study:

- Technological issues and technical constraints.
- Interrelation between components especially heat exchangers integration as well as temperature levels of the thermal energy storage tanks.
- Integration of the evaluation criteria of EES technologies deduced from Chapter 2 in the model to assess the T-CAES.

Firstly, the descriptions of the configurations are presented, justifying the choice of devices. Secondly, general hypothesis of the thermodynamic model are illustrated. Thirdly, the thermodynamic model of each component is developed. Finally, the global thermodynamic model is deduced.

## 4.2 System description

Figures 4.1 and 4.2 show the schematic diagram of the novel tri-generation system proposed based on the basic configurations discussed in the previous chapter.

As mentioned in the previous chapter, during the charging phase, ambient air is compressed via multistage compressors. The compressed air is cooled after each compression stage in a heat exchanger (HEX) by thermal energy storage medium. Volumetric compressors are suitable for limited mass flow rates and high-pressure ratios [60, 61], so they are the most suitable for small scale system .

Regarding the thermal energy storage medium TES, as demonstrated in the previous chapter , the approach of low-temperature A-CAES presented by Budt and Wolf [44], where the temperature level of TES is below 200˚C is adopted. As for the materials used, referring to chapter 2 phase change material could be used in favor of high energy density and constant storage temperature. However, in order to offer flexibility in control and reduce the system cost, sensible heat storage is preferred. Among heat transfer medium such as thermal oil [16, 21], water [43] or Therminol 66 [51] (see Chapter 2) pressurized water remains adequate for our application because of the low cost, the high thermal capacity and conductivity and being environmental friendly [31,45]. Hence, it is selected here.

In order to achieve a high energy recuperation rate, the counter-flow heat exchangers remain the best choice. On the other hand, shell and tube HEX exhibit a high design flexibility for different values of heat capacity and mass flow rates, high adaptability to high values of pressure and temperature [62]. By combining the advantages of these two types of HEX, a shell and tube heat

exchanger with one shell and tubes pass and counter flow arrangement is selected in the present study.

In the discharge phase, as shown in Figure 4.1, the air pressure is reduced by a throttling valve (TV) in order to be compatible with the expansion machinery and to ensure a high energy density of the air stored at constant volume. The role of the heat exchanger installed just after the throttling valve is explained later since it requires a further understanding of the process.

Existing small scale pilot scale applications rely on volumetric expanders [20]. These later are considered as an ideal choice for small-scale CAES because of its low costs and low operational speed rotation [63]. In the other hand, existing volumetric expanders ratios are limited between 8 and 14 for piston expanders and 5 for scroll type as reported by Lemort et al. [64]. However, it is well known that a low expansion ratio lowers the electric efficiency of the system (see Chapter 2) so the expansion machine should be designed to handle high input pressure.
Recently, the Deprag company in collaboration with the University of Applied Science Amberg-Weiden (Germany) [65] developed a micro axial turbine which could work with an input pressure going to 25 bars. Thus, the first expansion stages are selected as axial turbines and the last stage as a volumetric machinery.
This latter could be selected as piston or scroll expander. Scroll machines exhibit higher performances [12,64], whereas they are restricted to small pressure ratios without handling high values of pressure and temperature [65]. Hence, it seems to be advantageous in this application. Notwithstanding, piston expanders can be designed to handle higher pressure (like reciprocating compressors) which is important for prospective CAES application. Regardless of the fact that commercially available piston air motor (AM) are designed for maximum pressure input of 8 bars, it is decided to employ the AM and investigate its behavior owing to the research opportunity to develop an AM with higher pressure ratio.

As explained in the previous chapter, referring to the basic configuration, the heat stored should be exploited at the highest possible level to increase the electric efficiency, so the heat is deployed in the first expansion stages. The second part of the expansion chain should meet the requirements of producing cooling energy when needed. It corresponds to the air motor (AM) and may contains one or more than turbine stages. However, as a first evaluation of the system it is decided to fix the ability of the system for cooling energy production by fixing the pressure input of the second expansion part. Consequently, this latter represents the air motor (AM).

The two basic configurations discussed in the previous chapter leads to have the two configurations shown in Figure 4.2.

In the first configuration: the aim is to simplify the design and use the water temperature of cold TES directly in the charge phase so that the cold TES temperature should be as low as possible (close to ambient temperature). The water temperature of cold TES should be as low as possible (close to ambient temperature) in order to use it in the charge phase (Figure 4.2a). Consequently, as expected, the output temperature of each turbine is close to the ambient temperature and the cooling is achieved by releasing the outlet air of turbines directly at the input of the air motor. This can be achieved by minimizing the water mass flow rate in the preheating heat exchangers so that

the remaining water in hot TES tank is used directly for heating purposes (this point will be figured out throughout the modeling equations).

In the second configuration: the goal is to maximize the system electric efficiency by maximizing the air preheating. The air input temperature should be as high as possible, close to the hot TES temperature. As a result, the output temperature of each expansion stage would be higher than the ambient temperature (Figure 4.2b), leading to adding a cooling HEX just before the AM (nominated by HEX rc in Figure 4.2b) to produce cooling energy when needed. This design concept induces a high value of the water temperature at the outlet of the HEX (orange colors in Figure 4.2 right), which is used to satisfy the heating demand. Furthermore, as explained later in this chapter, there will be no water remaining in the hot-temperature reservoir of TES.

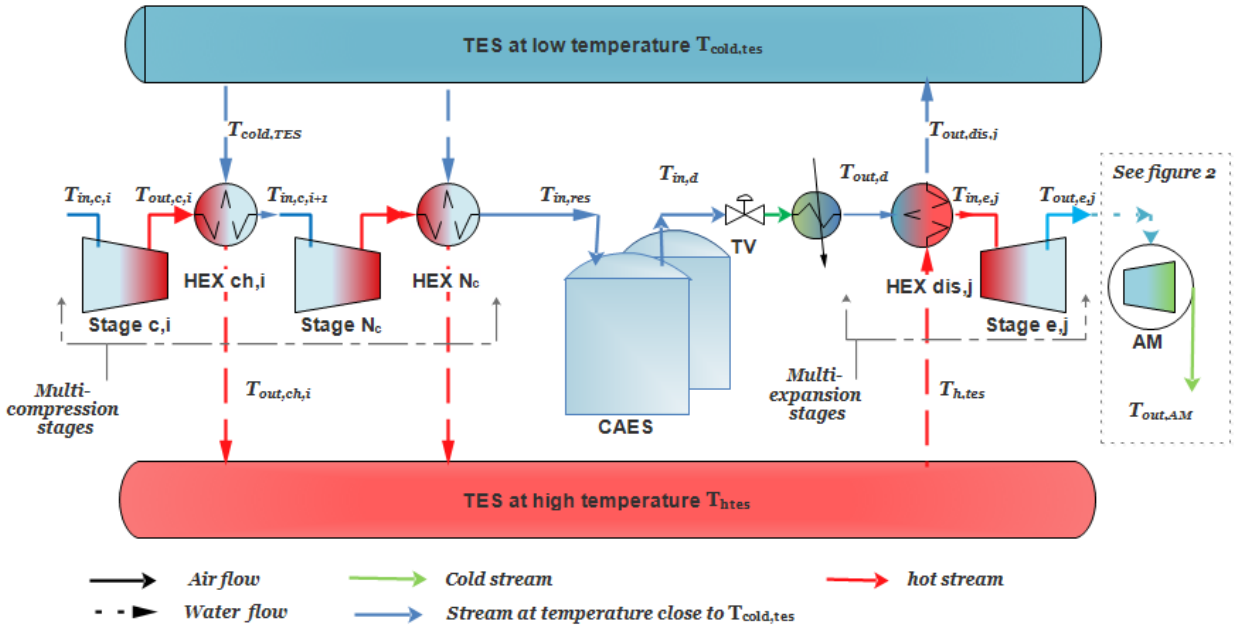


*Figure 4.1: Schematic diagram of the proposed trigenerative compressed air energy system with the notations.*

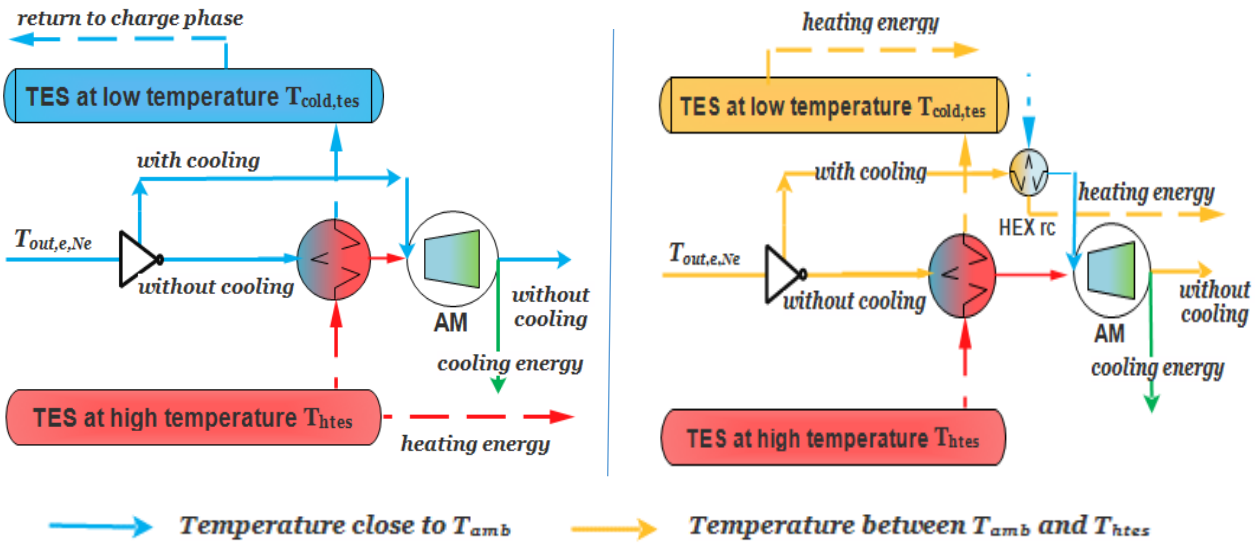


*(a) First configuration.* *(b) Second configuration.*

*Figure 4.2: Schematic diagram of the last expansion stage subsystem (the air motor AM) and temperature levels of streams for the first configuration (a) and the second configuration (b).*

## 4.3 Modeling of the T-CAES process

### 4.3.1 Modeling assumptions

Remember that CAES principle is divided into three phases: (1) charge or compression phase, (2) storage phase and (3) discharge or expansion process. The perspective application of the model is to use it for the assessment of performances and the optimisation of the configuration of the T-CAES. A steady state approach allows a fast calculation time and enables to assess the effect of design parameters, so it is targeted throughout this study. On the other hand, in the second phase- as its name imply- the physical parameters are variable as a function of time. Hence, dynamic model is needed for this phase.

In order to reduce the modelling complexity, general assumptions are introduced:

- Air is considered as an ideal gas expect inside the throttling valve.
- The heat capacity of the compressed air is constant, independently of the pressure variation.
- Pressure losses in the pipes are negligible.
- It can be noticed from the tables giving the thermal properties of pressurized water that the effect of temperature on the heat capacity may be ignored.
- Since operating pressure of expansion is much lower than of compression phase and pressure losses in HEX are proportional to the operating pressure as shown later in Equation 4.10, the pressure losses in HEX of discharge phase are neglected compared with the losses in HEX of discharge phase.
- The temperature of the cold TES reservoir in the charge phase is at the ambient temperature. It is basically saying that: in the first configuration, the water at $T_{cold,TES}$

(which is slowly higher than the ambient temperature) achieved the room temperature just at the beginning of the charge phase by losing its small amount of heat to the environment. In the second configuration, all the heating energy is used so that the temperature of water supply of the cold TES reservoir is at the room temperature.

It is important to mention that, there are another simplifying hypothesis related to each component. They are cited later since they are related to the modeling process.

The modeling of the T-CAES is not simple and the model of each component depends on each other. However, in order to simplify the understanding of the modeling process. The air side and the water side components are separated. If there is a relation (1) required to model a given component (A), for example compressor, which depends on the model of component (B), for example HEX, the relation (1) is used directly on the modeling of (A) and will be demonstrated in the modeling section of (B). Consequently, the modeling process is separated as follow:

- Modeling of the air side component: it includes the model of the charge phase, storage phase and discharge phase.
- Modeling of the water side components: the model of heat exchangers and thermal energy storage as well as the calculation of energy outputs are presented.

### 4.3.2 Modelling of the charge phase

#### *Compressors*

Volumetric compressors can operate with variable or constant global compression ratio. Since the variation of this later may induces a variable air mass flow rate, which open the question of the operation and control of heat exchanger. A constant global compression ratio is considered. In addition, Pressure losses at the admission, through the discharge valve are neglected compared to of the heat exchanger.

Dynamic compressors whose efficiency reflects the internal heat and the isentropic term are the most commonly used, volumetric compressors are characterized by some amount of heat lost to the environment which is implicitly expressed by a polytropic coefficient $n_c < \gamma$. Thus, the output temperature of each stage is written as:

$$T_{out,c,i} = T_{in,c,i}.\beta_{c,\mathrm{i}}^{\frac{n_{c,i}-1}{n_{c,i}}} \tag{4.1}$$

Where $\beta_c$ is the compression ratio.

Thermodynamic work of one compression stage is calculated by integrating $d(P.V)$ throughout the thermodynamic cycle which gives:

$$W_{th,c,i} = \frac{n_{c,i}}{n_{c,i}-1}.m_c\,.r.\left[T_{out,c,i} -.T_{in,c,i}\right] \tag{4.2}$$

The thermodynamic power of one compression stage is deduced from Equation 4.2 by introducing Equation 4.1 and expressing the ideal gas constant as a function of heat capacity:

$$\dot{W}_{th,c,i} = \frac{\gamma-1}{\gamma}\frac{n_{c,i}}{n_{c,i}-1}.\dot{m}_c.C_{p,a}.T_{in,c,i}\,.\left[\beta_c^{\frac{n_{c,i}-1}{n_{c,i}}} - 1\right] \tag{4.3}$$

Input temperature of each stage depends only on the previous compression stage output temperature and previous heat exchanger. As demonstrated later in Section 4.6, heat exchanger effectiveness is defined by:

$$\varepsilon_i = \frac{T_{out.c,i} - T_{in,c,i+1}}{T_{out,c,i} - T_{amb}} \tag{4.4}$$

By reformulating Equation 4.4:

$$T_{in,c,i+1} = T_{amb} + \Delta T_i \tag{4.5}$$

Where

$$\Delta T_i = \left(1 - \varepsilon_{c,i}\right)\left(T_{out,c,i} - T_{amb}\right) \tag{4.6}$$

Consequently, the input temperatures of the compressors are equal to the ambient temperature plus a value $\Delta T_i$, which expresses the effect of heat exchanger effectiveness.

Adding the electrical efficiency and mechanical efficiency, and replacing Equation 4.6 in Equation 4.3, the total electric power consumption for $N_c$ stages is calculated as:

$$\dot{W}_{el} = \frac{1}{\eta_e.\eta_m}.C_{p,a}.\dot{m}_c.\sum_{i=1}^{Nc}\frac{\gamma-1}{\gamma}\frac{n_{c,i}}{n_{c,i}-1}\left((T_{amb} + \Delta T_{i-1}).\beta_{c,\mathrm{i}}^{\frac{n_{c,i}-1}{nc_i}} - 1\right) \tag{4.7}$$

However, the electric power is delivered by renewable energy resources and it is imposed as an input parameter, so that the mass flow rate is the output value. It is derived from Equation 4.7 as:

$$\dot{m}_c = \frac{\eta_e.\eta_m\dot{W}_{el}}{C_{p,a}.\sum_{i=1}^{Nc}\frac{\gamma-1}{\gamma}\frac{n_{c,i}}{n_{c,i}-1}\left((T_{amb} + \Delta T_{i-1}).(\beta_{c,\mathrm{i}}^{\frac{n_{c,i}-1}{nc_i}} - 1)\right)} \tag{4.8}$$

For constant global compression ratio, the optimal distribution of compression ratio of each stage $\beta_{c,i}$ is symmetrical [66], so that:

$$\beta_{c,optimal} = \left(\frac{P_{in,res}}{P_{atm}}\right)^{1/N_c} \tag{4.9}$$

As for pressure losses $\Delta P_l$ in heat exchangers, an accurate account of them should refer to the calculation of the mass flow rate and design parameters of HEX, which is an advanced design task. Herein, the approximation formula (1) of $\Delta P_l$ for each HEX of intercoolers reported by Jubeh and Najjar [67] and Liu and Wang [20] is used.

$$\Delta P_{l,c,i} = \frac{0.0083\varepsilon_{c,i}}{1-\varepsilon_{c,i}}P_{out,c,i} = \frac{0.0083\varepsilon_{c,i}}{1-\varepsilon_{c,i}}\beta_{c,optimal}^{\ i}.P_{atm} \tag{4.10}$$

The required output pressure of each compression stage used to compensate the pressure losses $\Delta P_{l,c,i}$ is shown in Equation 4.11 and the actual compression ratio of each stage $\beta_{c,i}$ is calculated by Equation 4.12.

$$P_{out,c,i} = \beta_{c,optimal}{}^{i}.P_{atm} + \Delta P_{l,c,i} \tag{4.11}$$

$$\beta_{c,i} = \frac{P_{out,c,i}}{\beta_c{}^{i-1}.P_{atm}} \tag{4.12}$$

### *Air tank*

The minimum pressure $P_{min}$ of the air storage is limited by the operating pressure of the turbines, thus a residual amount of air remains in the reservoir:

$$m_{residual} = N_{res}\frac{P_{min}V_{res}}{r.T_{res}} \tag{4.13}$$

The air mass that could be stored is limited by the maximum pressure allowed in the storage tank and calculated by Equation 4.14 using the ideal gas law. Furthermore, during the charge phase it is assumed that the temperature into the tanks is uniform. In other words, the temperature into a tank is the same as at the entrance of the tank: $T_{res} = T_{in,res}$.

$$m_s = N_{res}\frac{(P_{max} - P_{min}).V_{res}}{r.T_{in,res}} \tag{4.14}$$

The time required to completely charge the reservoir is calculated by:

$$t_{ch} = \frac{m_s}{\dot{m}_c} \tag{4.15}$$

It should be noted that the reservoir insulation is not expected to account for the increasing energy density for a given storage pressure. Heat transfer between the environment and the compressed air occurs for any phase. Consequently, the air storage temperature and pressure variation are accounted for only during the storage phase. The following assumptions are made:

1. The heat capacity of the compressed air is constant, independently of the pressure variation.
2. The temperature gradient inside the storage tank is negligible.
3. The thermal resistance of the wall thickness is negligible compared to that due to natural convection.

Heat transfer to the environment induces a decrease of the air storage temperature, which results in the following governing equation:

$$\frac{m_s C_{pa}}{N_{res}}\frac{dT}{dt} = \frac{(T_{amb} - T)}{R_{th}} \tag{4.16}$$

The first order differential Equation 4.16 is solved. The time-temperature variation is expressed by Equation 4.17a and the pressure is computed simply by the ideal gas law:

$$T(t) = T_{amb} + \left(T_{(t=0)} - T_{amb}\right)e^{\frac{-N_{res}.t}{m_s.C_{pa}.R_{th}}} \tag{4.17.a}$$

However, the ambient temperature may vary with time. In this case, by discretizing time, the new solution gets:

$$T_{(t_{(j)})} = T_{amb(t_{(j-1)})} + \left(T_{(t_{(j-1)})} - T_{amb(t_{(j-1)})}\right) e^{\frac{-N_{res}.\Delta t}{m_s.C_{pa}.R_{th(j-1)}}} \quad (4.17.b)$$

where $\Delta t$ is the time step.

The average thermal resistance of the natural boundary layer is defined as:

$$R_{th_a} = \frac{1}{h\pi(D+2d)H} \quad (4.18)$$

The average heat convection coefficient for a cylinder is defined as:

$$h = \lambda_a \frac{Nu}{H} \quad (4.19)$$

where $H$ is the height of the cylinder and $Nu$ is the Nusselt number expressed by the empirical formula reported by Bejan [68].

$$Nu = \frac{4}{3}\left[\frac{7.Ra_H.Pr}{5.(20+21.Pr)}\right]^{0.25} + \frac{4.(272+315.\mathrm{Pr})\mathrm{H}}{35.(64+63.Pr).D} \quad (4.20)$$

To sum up, Figure 4.3 presents the block diagram of the mathematical model of the air components of charging and storage phase.

### 4.3.3 Modelling of the discharge phase

In the same way, as for the charge phase, the discharge time can be calculated by:

$$t_{dis} = \frac{m_s}{\dot{m}_e} \quad (4.21)$$

#### *Pressure regulator*

The physical law that governs the pressure reduction (throttling of compressed air) is the Joule-Thomson Law on which the enthalpy remains constant and the internal energy decreases as:

$$\Delta U = \Delta PV \quad (4.22)$$

The majority of CAES modelling has considered compressed air as an ideal gas throughout this component which leads to constant temperature. However, this assumption is no longer true when the pressure reduction magnitude is important. Temperature variation may be expressed by the Joule-Thomson coefficient:

$$\mu_T = \left(\frac{\partial T}{\partial P}\right)_h \quad (4.23)$$

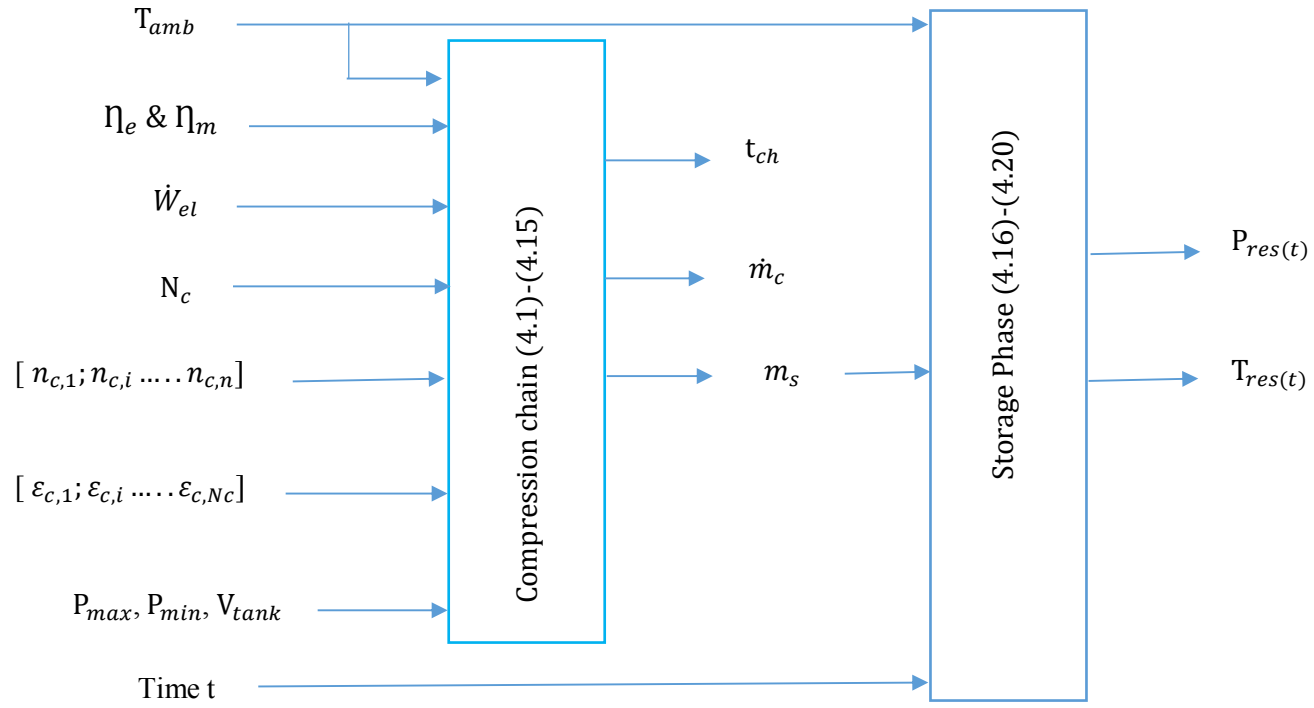


*Figure 4.3: Block diagram of the model of air side of the charge and storage phase.*

The isenthalpic curves of gases used in the chemical industry can be obtained from chemical textbooks, but the curves for compressed air were not found. Consequently, in order to find the isenthalpic curves and evaluate their slopes given by $\mu_T$, experiments were conducted by Hoxton [69]. This last author covered a wide range of pressure (from 25 to 150 atm). His semi-empirical approximation is given by [69]:

$$\frac{\Delta T}{\Delta P} = \frac{50.1 + 0.0297P}{T} + \frac{14830 - 1.674P}{T^2} + \frac{366000 - 19093P}{T^3} - (0.122 - 0.0000157P) \qquad (4.24)$$

Equation 4.24 can be written as:

$$\frac{\Delta T}{\Delta P} = 2.a.P + b \qquad (4.25)$$

where

$$a = \frac{1}{2}\left(\frac{0.0297}{T_{in,d}} - \frac{1.674}{{T_{in,d}}^2} - \frac{19093}{{T_{in,d}}^3} + 0.0000157\right)$$

$$b = \frac{50.1}{T_{in,d}} + \frac{14830}{{T_{in,d}}^2} + \frac{366000}{{T_{in,d}}^3} - 0.122$$

Temperature variation versus pressure is obtained by integration of Equation 4.25, so that it depends on the initial pressure and temperature of the air and the reduced pressure.

$$T(P) = a.P^2 + b.P + c \qquad (4.26)$$

where c accounts for the family of isenthalpic curves and is calculated by:

$$c = T_{in,d} - a.{P_{in,d}}^2 - b.P_{in,d} \tag{4.27}$$

It can be deduced from Equation 4.27 that the temperature output of the throttling valve varies with the pressure of the compressed air so that a dynamic model is needed to account these temperature variations. On the other hand, the objective of the study is to predict the performance of the system and conduct an optimization study, and the study-state model is simpler and more sufficient for these objectives. In order to deal with this issue, the model of the expansion valve is validated experimentally in the next chapter for future use in the research field, but for this study, it was assumed that the heat exchanger installed after the throttling valve (Figure 4.1) is able to maintain the temperature input of the first preheating heat exchanger $T_{in,e,1}$ at the ambient temperature. Besides, the associated cooling potential of this heat exchanger is not taken into account.

### *Modelling of turbines*

Throughout the turbine, the thermodynamic energy of compressed air expressed by its enthalpy is transformed to kinematic energy in the stator, then to mechanical energy by the rotor. It is known that heat transfer is negligible in turbomachinery and the ideal process corresponds to an isentropic one, ideal power is written as:

$$\dot{W}_{e,ideal} = \dot{m}_e.\left(h_{0,in} - h_{0s,out}\right) = \dot{m}_e.C_{p,a}.T_{0s,in,e}.\left(1 - (\frac{P_{0,in,e}}{P_{0,out,e}})^{1-\gamma/\gamma}\right) \tag{4.28}$$

where $T_0$ and $P_0$ are the stagnation temperature and pressure respectively and the index s refers to isentropic transformation.

Due to irreversibility induced by internal heat, the output temperature is actually higher than $T_{0s,out}$, thus real power is indeed:

$$\dot{W}_{e,real} = \dot{m}_e\left(h_{0,in} - h_{0,out}\right) = \dot{m}_e C_{p,a}\left(T_{0,in,e} - T_{0,out,e}\right) \tag{4.29}$$

The ratio between the real and ideal work stands for the thermodynamic efficiency. However, the exit fluid velocity of the rotor is not at zero and the associated kinematic energy (named exhaust loss) should not be ignored so that the terms total to total efficiency $\eta_{tt}$ and total to static efficiency $\eta_{ts}$ have been employed [70]. The former efficiency does not include the kinematic energy whereas it is considered by the latter.

Owning that the kinematic energy can be converted in the subsequent turbine stage or the air motor, $\eta_{tt}$ is considered in this study, hence:

$$\eta_{tt} = \frac{\left(T_{0,in,e} - T_{0,out,e}\right)}{T_{0s,in,e}.\left(1 - (\frac{P_{0,in,e}}{P_{0,out,e}})^{1-\gamma/\gamma}\right)} \tag{4.30}$$

$\eta_{tt}$ is classically determined according to the two dimensionless parameters flow coefficients and stage load [70], which vary depending on design parameters and operation parameters (pressure ratio and flow rate). Performance curves can be found in text books, nonetheless those curves are

developed using experimental tests on common and commercialized turbines at medium or large scale [70,71].

In this study, the turbine used is recently developed and it is difficult to account for the performance characteristics. Notwithstanding, a value of 57% for the total to static efficiency is provided by the designer in which the compressed air is the working fluid and the expansion ratio is 10 [72]. This value was assumed in this study and considered as constant independently of operating conditions (pressure ratio, flow rate). At the same time, exhaust losses in turbines are estimated at around 3% to 5% of total losses [70], so that $\eta_{tt}$ was deducted from $\eta_{ts}$, equal to $1.05\ \eta_{ts}$.

To conclude, the output temperature and electric power are derived from Equations 4.29 and 4.30 as follows:

$$T_{out,e,j} = T_{in,e,j} - \eta_{tt}.T_{in,e,j}\left(1 - {\beta_{e,j}}^{1-\gamma/\gamma}\right) \tag{4.31}$$

where $\beta_e$ is the expansion ratio of each expansion stage:

$$\beta_{e,j} = \frac{P_{in,e,j}}{P_{out,e,j}} = \frac{P_{min}}{P_{in,AM}}^{1/N_e} \tag{4.32}$$

$$\dot{W}_{el,e} = \eta_{el,e} \sum_{j=1}^{j=N_e} \eta_{m,e}\eta_{tt}\dot{m}_e C_{p,a}(T_{in,e,j} - T_{out,e,j}) \tag{4.33}$$

$\eta_{m,e}$ is the mechanical conversion efficiency estimated to 95% for small scales turbines, and $\eta_{el,e}$ is the electric efficiency of the generator.

Now, it is the question of how to determine the temperature input of each expansion stage. The answer depends on the design method as following.
For the second configuration, the temperature input of each stage is designed as higher as possible and is calculated by:

$$T_{in,e,j} = T_{h,TES,dis} - Pinch_e \tag{4.44}$$

The relation between the pinch point temperature difference $Pinch_e$ and HEX effectiveness is derived later in the heat exchanger modeling section. It is expressed by:

$$Pinch_e = (1 - \varepsilon_e)\left(T_{h,TES,dis} - T_{out,e,j-1}\right) \tag{4.45}$$

Before we proceed to assess the temperature input of the first configuration, It is important to figure out that the number of expansion stages $N_e$ play a key role in the design of T-CAES (note that $N_e$ denotes the number of expansion stages without the air motor because AM was devoted for cooling purposes). With this intention, let us consider the second configuration: for an imposed value of the temperature of TES, the input temperature of each expansion stage $N_e$ is related to $T_{h,TES,dis}$ and the effectiveness of HEX (see Equations 4.44 and 4.45). A lower number of expansion stages $N_e$ results in a decrease of the output temperature and furthermore to decrease the electric efficiency, or in another words the decrease of the average expansion temperature leading to decrease the efficiency (see Chapter 3 for further information). Here, It can be easily

seen that there is a critical number of $N_e$ (called $N_{e,critical}$) from which the output temperature of each stage become higher than the ambient temperature.

Taking into account the first configuration, at this value of $N_{e,critical}$ the input temperature of each expansion stage should be lowered to achieve the design condition of $T_{out,e,i} = T_{amb}$ . Increasing $N_e$ beyond $N_{critical}$ means a further decrease of the input temperature of each stage and consequently the electric efficiency. As a conclusion, the optimal number of expansion stages $N_{e,optimal} = N_{e,crtical}$.

It is true that in the second configuration, the electric efficiency may increase if $N_e > N_{e,crtical}$. However, it can be noticed from the results of the previous study of Luo et al. [45] that the global electric efficiency $\eta_e$ increases slightly above a value of $N_e$ corresponding to $T_{out,e,i}$ close to $T_{amb}$. Moreover, many simulations were carried out and proved the latter achievement. Besides, it is more valuable to compare the two configurations for the same number of stages. The flow diagram of the method of finding $N_{e,optimal}$ is presented in Figure 4.4. It is found by an iteration procedure by increasing the value of $N_e$ , and calculating the output temperature of turbine stages $T_{out,e,i}$. The iteration stops as soon as $T_{out,e,i}$ becomes higher than $T_{amb}$.

Now, $N_{e,optimal}$ and the temperature input and output of turbines for the second configuration are known, by contrast, in the first configuration, the temperature input of each stage should satisfy the condition of $T_{out,e,j} = T_{amb}$. As a result, $T_{in,e,j}$ could be expressed by using Equation 4.31 as:

$$T_{in,e,j} = \frac{T_{amb}}{1 - \eta_{tt}.\left(1 - \frac{P_{in,e,j}}{P_{out,e,j}}^{1-\gamma/\gamma}\right)} \tag{4.46}$$

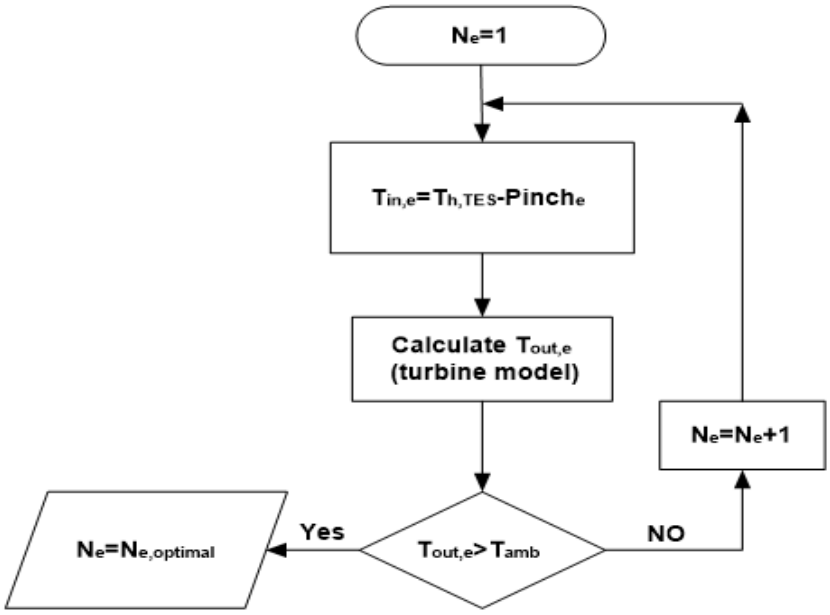


*Figure 4.4: Algorithm developed to select the optimal number of expansion stages.*

### *Modelling of air motor*

By analogy with compression, the output temperature and the thermodynamic power of the ideal expansion cycle are obtained as follows:

$$T_{out,AM} = T_{in,AM}.\beta_d^{\frac{1-n_e}{n_e}} \tag{4.47}$$

where $T_{in,AM} = T_{in,e,j}$

$$\dot{W}_{th,AM} = \frac{\gamma-1}{\gamma}\frac{n_e}{n_e-1}.\dot{m}_e.C_{p,a}.T_{in,AM}.\left[1-\beta_e^{\frac{1-n_e}{n_e}}\right] \tag{4.48}$$

where $\beta_{e,AM} = \frac{P_{in,AM}}{P_a}$

In order to account for the deviation between real and ideal thermodynamic cycles and also mechanical losses, the thermodynamic or pneumatic mechanical efficiency is introduced:

$$\eta_{th,m} = \eta_m.\eta_{th} = \frac{\dot{W}_{m,AM}}{\dot{W}_{th,AM}} \tag{4.49}$$

Mechanical shaft power and mass flow rate variations versus shaft rotation speed are generally provided for each operating pressure by the manufacturer. Thus, shaft power curves versus mass flow rate for each input pressure can be deduced. By polynomial interpolation of the obtained function $\dot{W}_{m,AM}(\dot{m}, P_{in})$, the thermodynamic-mechanical efficiency is obtained via Equation 4.49.

Finally, accounting for the electrical efficiency, the electrical power can be calculated as:

$$\dot{W}_{el,AM} = \eta_{el,AM}.\eta_{th,m,AM}.\dot{W}_{th,AM} \tag{4.50}$$

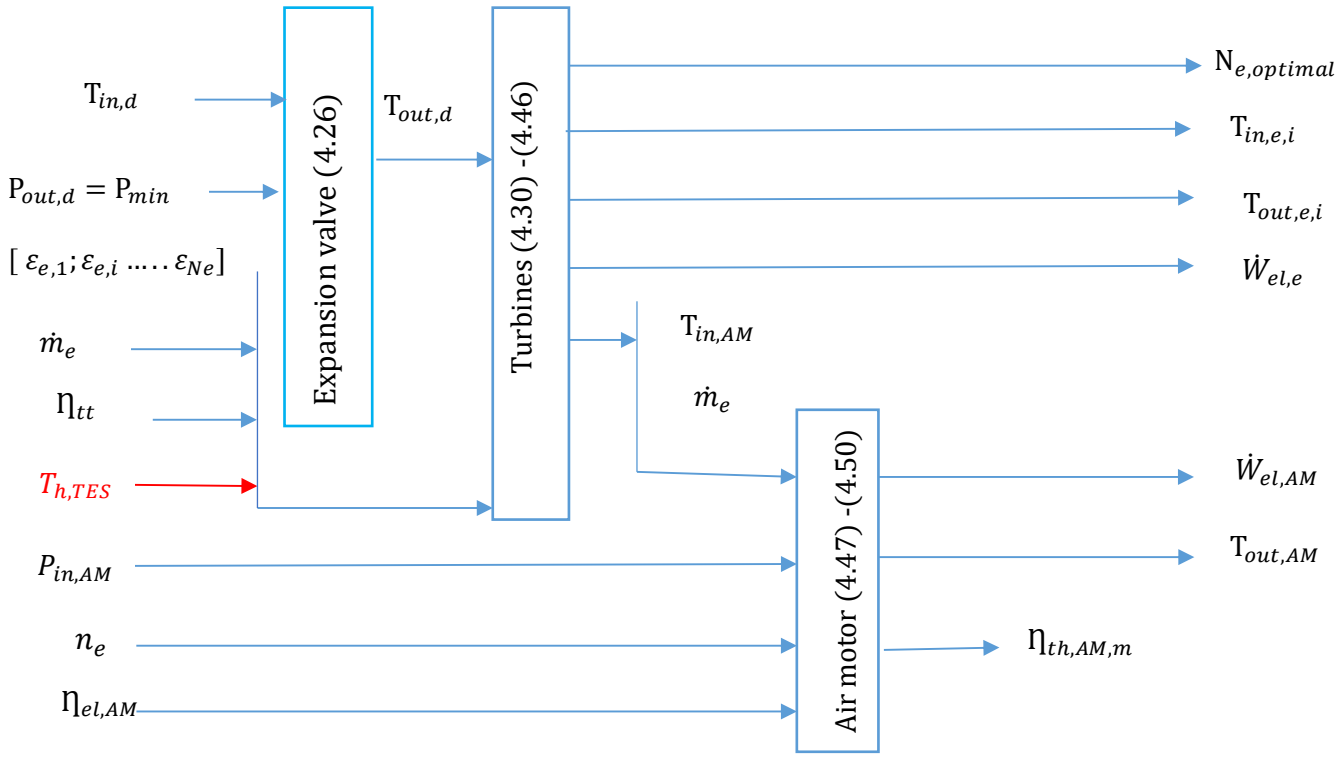


*Figure 4.5: Block diagram of the model for the air side of discharge phase.*

### 4.3.4 Modelling of heat exchangers and thermal energy storage

Typical input design parameters of HEX are mass flow, heat capacity and outlet temperatures of hot and cold fluids [62].

$$\varepsilon = \frac{C_{hot}.\left(T_{in,hot} - T_{out,hot}\right)}{C_{min}\left(T_{in,hot} - T_{in,cold}\right)} \qquad (4.51.a)$$

or

$$\varepsilon = \frac{C_{cold}.\left(T_{out,cold} - T_{in,cold}\right)}{C_{min}\left(T_{in,hot} - T_{in,cold}\right)} \qquad (4.51.b)$$

where $C$ is the thermal capacity of the flow, which equals the product of the mass flow rate of the flow and its heat capacity.

In the charge phase, in order to maximize the cooling efficiency of the compressed air and consequently the global electric efficiency, the minimal thermal capacity is to be attributed to the air side.

As a result, $C_{min} = \dot{m}_{a,c}.C_{p,a}$ and $C_{max} = \dot{m}_{w,ch,i}.C_{p,w}$

Hence, the effectiveness is expressed by:

$$\varepsilon_{ch} = \frac{T_{in,c,i} - T_{in,c,i+1}}{T_{in,c,i} - T_{cold,TES}} \qquad (4.52)$$

For the optimization study, the effectiveness of heat exchangers is considered the same so that $\varepsilon_{c,i} = \varepsilon_{ch}$. Besides, it was assumed that $T_{cold,TES} = T_{amb}$. Hence, Equation 4.4 is obtained.

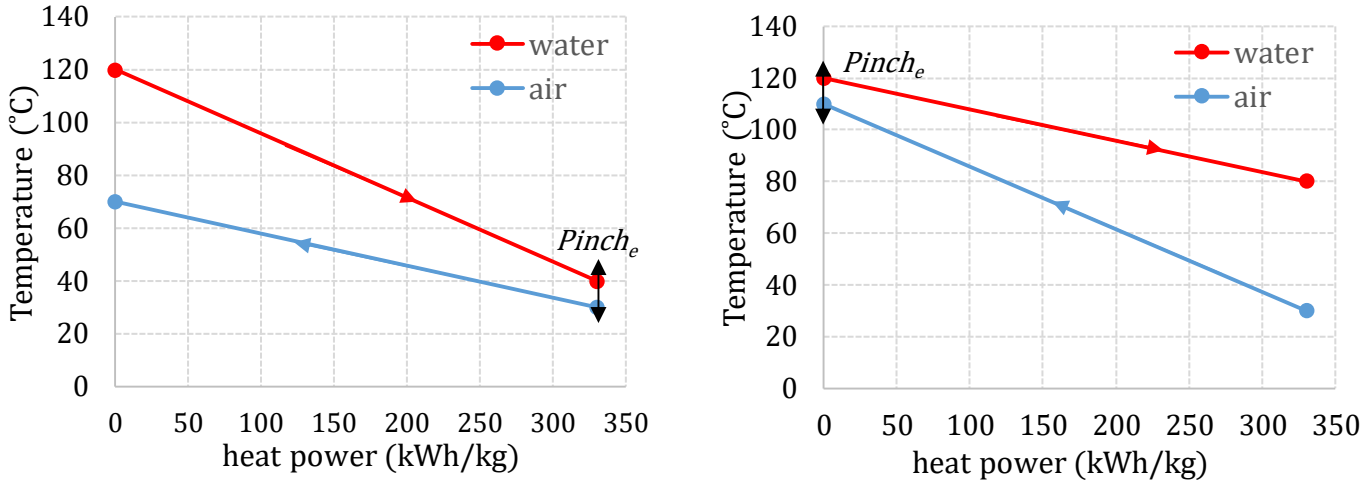


*(a) First configuration.* *(b) Second configuration.*

*Figure 4.6. Temperature variations of air and water versus heat duty for the first configuration (a) and second configuration (b).*

In the discharge phase, Figure 4.6 shows the difference between the two designs concepts by means of temperature variation for an imposed heat duty.

As mentioned earlier, in the first configuration the output temperature of water flow should be the minimal possible value. Consequently, $C_{min}$ belongs to the water side and $C_{max}$ to the air side.

As a result, $C_{max} = \dot{m}_{a,e}.C_{p,a}$ and $C_{min} = \dot{m}_{w,dis,j}.C_{p,w}$

The effectiveness gets:

$$\varepsilon_{e,1} = \frac{T_{h,TES} - T_{out,dis,j}}{T_{h,TES} - T_{out,e,j-1}} = \frac{C_{max}(T_{out,e,j-1} - T_{in,,e,j})}{C_{min}(T_{h,TES} - T_{out,e,j-1})} \qquad (4.53.a)$$

In the second configuration, the input temperature of the air flow at the air turbine should be chosen the maximum possible, thus $C_{min}$ belongs to the air side and the effectiveness become:

$$\varepsilon_{e,2} = \frac{T_{in,e,j} - T_{out,e,j-1}}{T_{h,TES} - T_{out,e,j-1}} = \frac{C_{max}(T_{h,tes} - T_{out,dis,j})}{C_{min}(T_{h,TES} - T_{out,e,j-1})} \qquad (4.53.b)$$

where $C_{min} = \dot{m}_{a,e}.C_{p,a}$ and $C_{max} = \dot{m}_{w,dis,j}.C_{p,w}$

For the first configuration the pinch occurs at the output of water flow, whereas for the second configuration the pinch takes place at the input of water flow, so that:

$$for\ the\ 1^{st}\ config:\ Pinch_e = T_{out,dis,j} - T_{out,e,j-1} \qquad (4.54.a)$$

$$for\ the\ 2^{nd}\ config:\ Pinch_e = T_{h,TES} - T_{in,e,j} \qquad (4.54.b)$$

By replacing Equation 4.54 by 4.53, $Pinch_e$ is related to the effectiveness of HEX as expressed below:

$$Pinch_e = (1 - \varepsilon_e)\left(T_{h,TES} - T_{out,e,j-1}\right) \tag{4.55}$$

The later Equation 4.55 is very useful to derive the temperatures at the input/output of HEX as seen later in this section. Besides, It is important to note that this equation is equivalent to Equation 4.6 where $Pinch_c = \Delta T_i$.

The number of transfer unit NTU is a function of heat exchanger efficiency, flow arrangements, $C_{min}$ to $C_{max}$ ratio and HEX type (for example number of shell and tube passes, cross flow HEX). The NTU approach and relations for different types of HEX are reported in details in [62]. In this study, shell and tube HEX with one shell and tube pass and counter flow arrangements was considered. The corresponding NTU relations are given by Equations 4.56:

$$for\ z < 1 : \text{NTU} = \frac{\ln\left(\frac{1 - z.\varepsilon_j}{1 - \varepsilon_j}\right)}{\ln(1 - z)} \tag{4.56.a}$$

$$for\ z = 1 : \text{NTU} = \frac{\varepsilon_j}{1 - \varepsilon_j} \tag{4.56.b}$$

where $z = \frac{C_{min}}{C_{max}}$

Following the NTU method, the HEX footprint is expressed by:

$$(UA) = NTU.C_{min} \tag{4.57}$$

The charge phase is common to both configurations so the same model is used. During the charge phase, once $T_{h,TES,ch}$ is imposed, heat balance between air and water sides enables the calculation of water mass flow rate of each HEX as follows:

$$\dot{m}_{w,ch,i} = \frac{C_{min}(T_{in,c,i} - T_{in,c,i+1})}{C_{p,w}(T_{h,TES} - T_{cold,TES})} \tag{4.58}$$

where $C_{min} = \dot{m}_{a,c}.C_{p,a}$ and $C_{max} = \dot{m}_{w,ch,i}.C_{p,w}$.

It should be noted that the maximum value of $T_{h,TES}$ is to be chosen such as $C_{min} \leq C_{max}$, thus $T_{h,TES}$ should satisfy the following condition:

$$T_{h,TES} \leq (T_{in,c,i} - T_{in,c,i+1}) + T_{cold,TES} \tag{4.59}$$

The total mass flow of water that can be stored at the temperature $T_{h,TES}$ is the sum of the flows leaving HEX, the total mass of stored water and the necessary volume of the storage tank are expressed in Equations 4.60 and 4.61.

$$m_{TES} = \sum_{i=1}^{N_c} \dot{m}_{w,ch,i}\,.\,t_{ch} \tag{4.60}$$

$$V_{res,TES} = \frac{m_{TES}}{\rho_w} \tag{4.61}$$

In the end, the total thermal energy that could be stored could be computed from the air side or water side by Equation 4.62.

$$Q_s = \sum_{i=1}^{i=Nc} \dot{m}_c . C_{p,a} . \left(T_{out,c,i} - T_{in,c,i+1}\right) . t_{ch} \; = \sum_{i=1}^{i=Nc} \dot{m}_{w,ch,i} . C_{p,w} . \left(T_{cold,TES} - T_{h,TES}\right) . t_{ch} \tag{4.62}$$

During the storage process, it is obvious that the water mass is conserved, but the temperature of TES drops due to heat transfer with the environment. One can account this loss by integrating a model of the TES reservoir. However, it is supposed that the TES tank is sufficiently isolated to achieve a high thermal efficiency of 95% with a short storage period (range of hours). The thermal efficiency is defined as:

$$\eta_{TES} = \frac{m_{TES} C_{p,w} \left(T_{h,TES,dis} - T_{amb}\right)}{m_{TES} C_{p,w} \left(T_{h,TES} - T_{amb}\right)} = \frac{T_{h,TES,dis} - T_{amb}}{T_{h,TES} - T_{amb}} \tag{4.63}$$

The temperature of TES in the discharge phase is calculated by:

$$T_{h,TES,dis} = \eta_{TES} \left(T_{h,TES} - T_{amb}\right) + T_{amb} \tag{4.64}$$

Heat loss is then:

$$Q_{loss} = m_{TES} C_{p,w} \left(T_{h,TES} - T_{h,TES,dis}\right) \tag{4.65}$$

Next, modifications were included in the model depending on the configuration of the discharge phase.

Equations of the discharge phase for the 1st configuration:

In the discharge phase, for the first configuration the output temperature of water flow $T_{out,dis,j}$ in HEX is governed by its effectiveness or its pinch point temperature difference $Pinch_e$ as expressed by Equation 4.66.a, while the mass flow rate is determined by the heat balance between each flow of the HEX (Equation 4.66.b).

$$T_{out,dis,j} = T_{out,e,j-1} + Pinch_e \tag{4.66.a}$$

where the relation between $Pinch_e$ and the HEX effectiveness is shown earlier in Equation 4.54.a.

$$\dot{m}_{w,dis,j} = \frac{C_{max} (T_{in,e,j} - T_{out,e,j-1})}{C_{p,w} (T_{h,TES,ch} - T_{out,dis,j})} \tag{4.66.b}$$

where $C_{min} = \dot{m}_{w,dis,j} . C_{p,w}$ and $C_{max} = \dot{m}_{a,e} . C_{p,a}$ for the first configuration.

By applying the heat and mass balance, the accumulated mass of the outflow water of preheating HEX and its temperature, the remaining mass in high TES temperature tank and also the heating energy potential are presented on Equations 4.66.c, 4.66.d and 4.66.e.

$$m_{cold,TES} = \sum_{i=1}^{N_e+x} \dot{m}_{w,dis,j} \,.\, t_{dis} \qquad (4.66.c)$$

$$m_{rem,h,TES} = m_{heating} = m_{TES} - \sum_{i=1}^{N_e+\bar{x}} \dot{m}_{w,dis,j} \,.\, t_{dis} \qquad (4.66.d)$$

where: $\bar{x} = 1$ if the cooling is activated, otherwise $\bar{x} = 0$.

$$Q_{heat,1} = m_{rem,h,TES}.\, C_{p,w}.\, (T_{h,TES} - T_{amb}) \qquad (4.66.e)$$

Equations of the discharge phase for the 2nd configuration:

For the second configuration, one can design the HEX such as the temperature variation in the air side is the same as the water side which decreases the temperature difference between the two sides and the required footprint. In order to minimize this latter, the maximum mass flow rate and the least possible temperature output of water flow should be chosen (Figure 4.6). This is achieved by pumping all the water of the hot temperature reservoir to the reservoir at low temperature. Consequently, the water mass flow is determined by applying the mass balance on TES (Equation 4.67.b). The heat balance in the HEX enables the calculation of the output water temperature (Equation 4.67.a).

$$T_{out,dis,j} = T_{h,TES,dis} - \varepsilon_{e,j}.\frac{C_{min}}{C_{max}} (T_{h,TES} - T_{out,e,j-1}) \qquad (4.67.a)$$

$$\dot{m}_{w,dis,j} = \frac{m_{TES}}{(N_e + x) t_{dis}} \qquad (4.67.b)$$

where: $x = 0$ if the cooling is activated, otherwise $x = 1$.

$C_{min} = \dot{m}_{a,e}.\, C_{p,a}$ and $C_{max} = \dot{m}_{w,dis,j}.\, C_{p,w}$ for the second configuration.

Returning to TES, as mentioned above:

- In the first configuration, an amount of water is remaining in the hot TES tank which is used for heating and the temperature return of preheating HEX approaches the ambient temperature.
- In the second one, the return temperature of TES is sufficiency high to be used for heating purposes and the reservoir at high temperature is fully empty by the end of the discharge phase.

By applying the mass balance, it can be concluded that:

$$m_{cold,TES} = m_{heating} = m_{h,TES} \qquad (4.67.c)$$

$$m_{rem,h,TES} = 0 \qquad (4.67.d)$$

$$Q_{heat,2} = m_{cold,TES}.\, C_{p,w}.\, (T_{cold,TES} - T_{amb}) + x.\, C_{max,Ne+1} (T_{out,dis,Ne+1} - T_{amb}).\, t_{dis} \qquad (4.67.e)$$

where the second term of the Equation 4.67.e accounts for the energy required in order to recool the outlet air of the last turbine stage before it is introduced in the air motor AM to produce cooling energy. This term will be void if the cooling energy is not activated.

It is important to note that $\dot{m}_{w,dis,j}$ is sufficiently high to verify the design method based on $\dot{m}_{w,dis,j}.C_{p,w} \geq \dot{m}_{a,e}.C_{p,a}$:

$$\dot{m}_{w,dis,j} \geq \frac{C_{min}}{C_{p,w}} \tag{4.68}$$

Equations of the cold TES for the 1st and 2nd Configurations:

The temperature $T_{cold,TES}$ of the returning water can be calculated by applying energy balance as shown in Equation 4.69.

$$T_{cold,TES} = \sum_{i=1}^{N_e+x} \frac{\dot{m}_{w,dis,j} T_{out,dis,j}}{m_{cold,TES}} t_{dis} \tag{4.69}$$

In the end, the thermal energy recuperated to preheat the air before expansion can be computed from the air side or water side by Equation 4.70 and cooling energy is deduced by Equation 4.71.

$$Q_r = \sum_{i=1}^{i=Ne+\bar{x}} \dot{m}_e.C_{p,a}.\left(T_{out,e,j-1} - T_{in,e,j}\right).t_{dis} = \sum_{i=1}^{i=Ne+\bar{x}} \dot{m}_{w,dis,j}.C_{p,w}.\left(T_{h,TES} - T_{out,dis,j}\right).t_{dis} \tag{4.70}$$

where $T_{out,e,0}$ is the temperature input of the first HEX.

$$Q_{cool} = \bar{x}.\dot{m}_e.C_{p,a}.\left(T_{amb} - T_{out,AM}\right).t_{dis} \tag{4.71}$$

where: $\bar{x} = 1$ if the cooling is activated, otherwise $\bar{x} = 0$.

## 4.4 Evaluation criteria

As mentioned in the state of the art, electrical energy storage technologies are evaluated by many evaluation criteria such as: technical maturity, energy density, efficiency, cost and others criteria. Hence, the criteria which can be accounted for by the thermodynamic modelling are well established in this study and listed as follows:

**Energy density $E_d(kWh/m^3)$** is defined by the amount of output energy provided per unit of volume as expressed by Equation 4.72. This criterion is of crucial importance, as higher energy density requires a small volume which makes the system more compact and may reduce its cost.

$$E_d = \frac{E_{out,el,e}}{V_{res}} \tag{4.72}$$

where $E_{out,el,e}$ is the output electrical energy and is accounted by:

$$E_{out,el,e} = \dot{W}_{el,e}.t_{dis} \tag{4.73}$$

**Round trip electrical efficiency** or simply **electrical efficiency**: it is defined by the ratio of energy output to energy input.

$$\eta_{el} = \frac{E_{out,el}}{E_{in,el}} = \frac{\dot{W}_{el,e} t_{dis}}{\dot{W}_{el,c} t_{ch}} \tag{4.74}$$

Since our system produces heating and cooling energy, the coefficient of performance defined by Equation 4.75 accounts for these elements. By contrast, it is more appropriate to compare our system with other electrical energy storage technologies, so the **comprehensive efficiency** defined by Equation 4.76 is used on which the cooling and heating energy are replaced by the equivalent electrical energy to produce the heating and cooling energy by a conventional heat:

$$COP_g = \frac{Q_s + Q_{cool} + E_{out,el}}{E_{in,el}} \tag{4.75}$$

$$\eta_g = \frac{\frac{Q_{heat}}{COP_{ref,heat}} + \frac{Q_{cool}}{COP_{ref,cool}} + E_{out,el}}{E_{in,el}} \tag{4.76}$$

where $COP_{ref,heat}$ and $COP_{ref,cool}$ are the performance coefficients of conventional heat pump functioning on heating and cooling mode respectively.

The **cost of the system** is a vital criterion to be assessed. It begins with finding the characteristics of each component of the system including the number of compression and expansion stages, heat exchangers footprints, reservoir volume and operating pressures. All these parameters will be discussed for the sake of reducing the cost of the system in Chapter 6, and the estimation of the cost of each component will be developed in Chapter 7. Finally, the system is also assessed in term of the time of charge and discharge which have a useful practical significance.

To sum up the thermodynamic model and the evaluation criteria, Figure 4.7 shows the block diagram of the T-CAES system model with the main input and output parameters.

## 4.5 Conclusion

In this chapter, a whole thermodynamic model of the T-CAES system was developed. The design parameters of each compound are settled as input parameters, while the output parameters consist of a set of evaluation criteria (such as system performances and energy density), parameters reflecting the cost (heat exchanger footprints and the number of compression and expansion stages) as well as other useful parameters which are important for prospective engineering applications (such as the charge or discharge times, pressures and temperatures at the inlet/outlet of each component). The main uncertainties of the model rely on ignoring the cooling energy between the throttling valve output and the first heat exchanger of the discharge phase in order to predict the performances by a steady-state model.

According to the design methodology of heat exchangers and the need, whether to maximize the round-trip electric efficiency or reduce the total heat exchanger area, two configurations are deduced. The first configuration is intended to simplify the design by reducing the number of heat

exchangers and by reusing the water of the discharge process in the charge process, while the aim of the second configuration is to optimize the electric efficiency by maximizing the preheating energy before the expanders.
Finally, it is demonstrated that there is an optimal number of expansion stages, which can be found by a numerical iteration procedure.

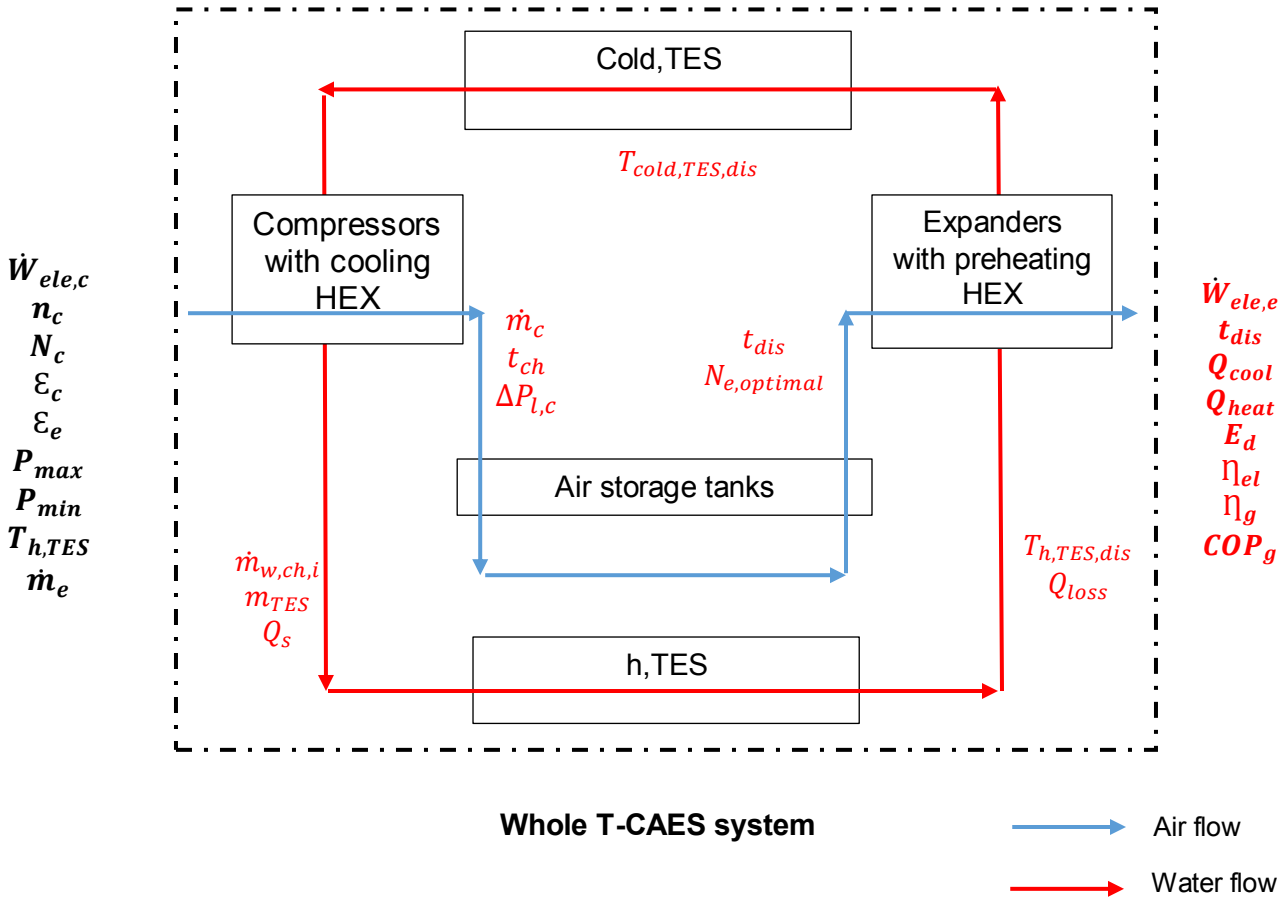


*Figure 4.7: Block diagram of the thermodynamic model of the whole T-CAES system with main input parameters (black) and output parameters (red).*

# CHAPTER 5 - EXPERIMENTAL TESTS AND MODEL VALIDATION OF A SMALL SCALE TRIGENERATIVE COMPRESSED AIR ENERGY STORAGE SYSTEM

## 5.1 . Objectives and originality

As mentioned in Chapter 2, very few experimental studies are focused on micro or small scale CAES. Experimental studies on medium scale A-CAES presented by Geissbühler et al. [40] and Becattini et al. [41] were performed to validate numerical models of air cavern and thermal energy storage without developing an experimental/modeling approach for the whole system. In the second place, concerning the A-CAES pilot plant "TICC-500", experimental data reported by Wang et al. [39] are insufficiently correlated with the developed model. The experimental round-trip efficiency was 22.6% compared to the designed one at 40.7%, which means a relative error of 44.4%. The errors were attributed to the unsteady working operation of compressors, low performances of TES without a clear relation between these errors to the model of each component.

The objective of this chapter is to characterize a small-scale compressed air energy storage pilot unit (4 kW compressor's power and 2 kW expander's power) built by the GEPEA laboratory at IMT Atlantique, Nantes (France). An experimental campaign was realized in order to determine its energy performances, limitations and perspectives of improvement. The originality of the study presented in this chapter is to adopt a combined thermodynamic/experimental approach to validate the model of the T-CAES air side components developed in the last chapter.

This chapter is organized as follows:

- Firstly, the experimental small-scale pilot (4 kW compressor's power and 2 kW expander's power) built in GEPEA laboratory at the IMT Atlantique (France) is described.
- Secondly, the air side components model is validated experimentally by paying a careful attention to each component.
- Thirdly, a particular attention is paid on the throttling valve and air motor in order to provide further knowledge about the system behaviors and performances.
- Finally, conclusions are drawn on the model limitations and the optimization opportunities of the T-CAES.

## 5.2 Experimental Setup

This section begins with a general layout of the experimental bench. Then, a detailed description of each component and the experimental procedure and operating parameters are presented.

### 5.2.1 . General description

To study the characteristics of the CAES system, an existing industrial pilot unit has been previously built in GEPEA laboratory at the IMT Atlantique, France. The process instrumentation diagram and photograph are shown in Figures 5.1 and 5.2.

The rated power of the compressor driven-motor (1) is 4 kW with a maximum global compression ratio of 325. Compressed air is stored in six reservoirs (2) with a capacity of 50 L each. The air stored is expanded through an air motor (5) coupled to a DC generator of 2 kW maximum power. The admission air motor pressure could vary in the range [2-8] bars (absolute values). The pressure at the entrance of the air motor is controlled manually via a pressure regulator (3). The pilot is equipped with sensors for continuous monitoring of power, pressure, temperature and mass flowrate (4).

Experimental uncertainties associated with the measurements have been determined from the manufacturer's data of the temperature probes (+/- 1.6°C), pressure probes (between 0.05% to 0.1% of the measure range), and airflow meters (0.08% of the measure range).

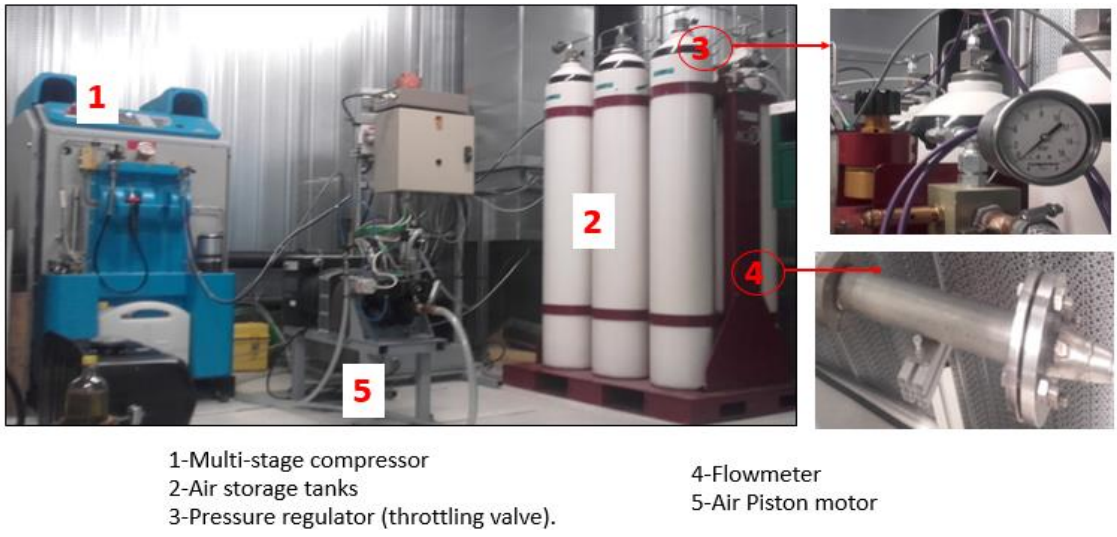


*Figure 5.1: Photograph of the CAES pilot unit at IMT Atlantique, France.*

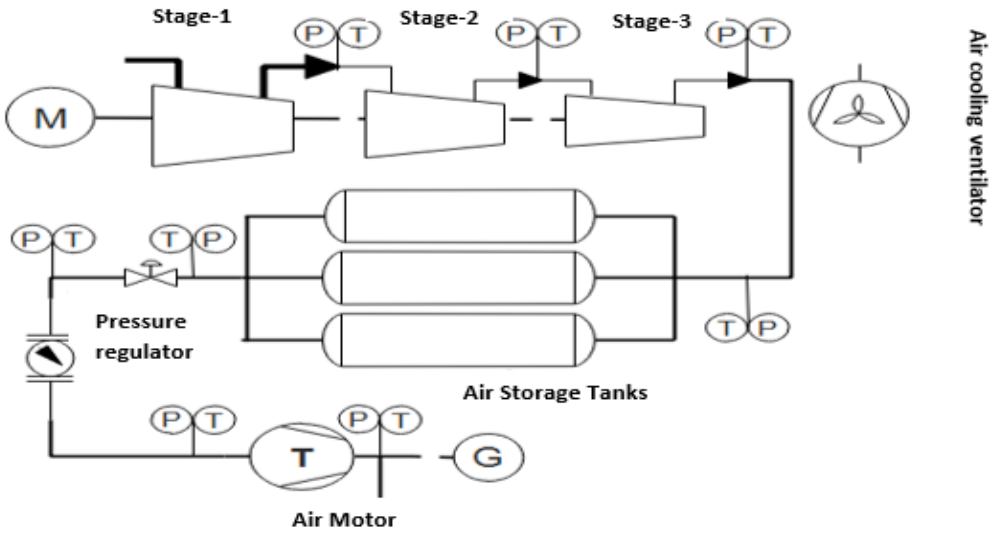


*Figure 5.2: PID of the CAES pilot unit at IMT Atlantique, France.*

### 5.2.2 . Compressor chain

As shown in Figure 5.3, the piston reciprocating compressor is a three-stage compressor arranged in a W form, cooled by air-air heat exchanger between two consecutive stages. The cooling air flow is forced by one ventilator. The pressure ratios of the first 2 stages are 7.6 and 5.6 respectively but the pressure ratio of the third stage varies from 4.08 to 7.2 according to the state of charge. It should be noticed that for a fixed global pressure ratio, the optimal distribution is symmetrical [66], which is different from the manufactured compressor. This is due to a variable global pressure ratio. Air humidity is ignored because the compressor is equipped with a dehumidifier. Table 5.1 shows the main characteristics of the compressor chain.

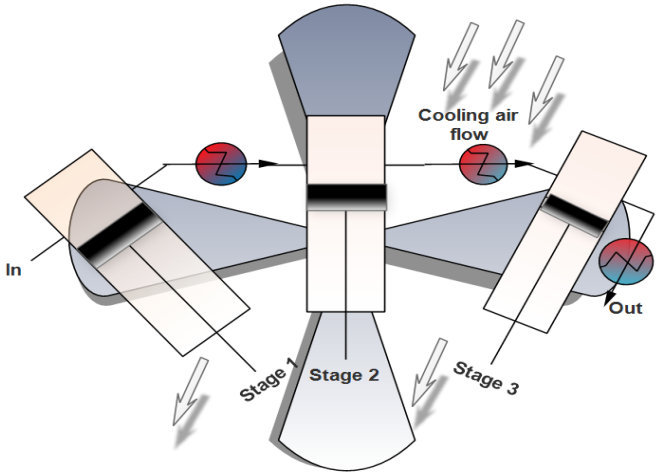


*Figure 5.3: Representative scheme of the intercooled air compressor.*

During the charge phase, the values of pressure, temperature, power and mass flow rate are recorded every 20 minutes, which is accurate enough regarding their temporal variations.

After measuring the temperatures, the effectiveness of the heat exchanger is calculated using Equation 4.4 (see Chapter 4), and the polytropic coefficient, after algebraic manipulation, is calculated as:

$$n_c = \frac{1}{1 - \frac{\ln\left(\frac{T_{out,i}}{T_{in,i}}\right)}{\ln\left(\beta_c\right)}} \tag{5.1}$$

Unfortunately, we do not know the exact mechanical efficiency $\eta_m$ and electrical efficiency $\eta_e$. The latter depends on the nominal power and standard efficiency of the motor. The electrical efficiency usually ranges between 0.75 and 0.83 for a 4 kW motor as stated by [73]. An average value of 0.8 is then considered here. Similarly, a value of 0.9 is taken for the mechanical efficiency which is estimated in the range of [0.88-0.95] by [61]. It is important to mention that the different parameters displayed in Table 4.1 are obtained for a fixed pressure ratio.

Finally, as shown in Table 5.1, there is a heat transfer with the environment, which occurs at the air connection. The resulted difference in terms of temperature was integrated in the model.

*Table 5.1: Experimental characteristics of compression chain. (*) refers to calculated values.*

| Parameter | 1-stage | 2-stage | 3-stage | Pipe connection | Storage tank |
|---|---|---|---|---|---|
| Inlet pressure [bar] | 1.013 | 7.9 | 44.4 | | 181 to 315 |
| Outlet pressure [bar] | 7.7 | 44.4 | 181 to 315 | | |
| Pressure ratio (*) | 7.6 | 5.6 | 4.08 to 7.2 | | |
| Inlet temperature [°C] | 22 | 62.0 | 58.0 | 43.3 | 33 |
| Outlet temperature [°C] | 118.0 | 198.7 | 152.0 | 33 | |
| Mechanical efficiency | | | 0.88-0.95 (0.9) | | |
| Electric efficiency | | | 0.75-0.83 (0.8) | | |
| Shaft Power [kW] | | | 3.19 | | |
| Polytropic coefficient (*) | 1.16 | 1.25 | 1.22 | | |

| HEAT EXCHANGERS | | | |
|---|---|---|---|
| Parameter | 1-stage | 2-stage | 3-stage |
| Effectiveness, ε (*) | 0.583 | 0.796 | 0.836 |

### 5.2.3 . Storage reservoir

The total capacity of the six tanks is 0.3 $m^3$, and the maximum allowed pressure is 350 bars. Nevertheless, for security purpose, the compressor stops automatically as soon as the air pressure reaches 315 bars. A high value of the storage pressure is chosen to account for the fact that to store a given air mass, the cost consequences of operating at low maximum pressure is more severe than at too high pressure [14]. The minimum operating pressure of the air storage is chosen at 5 bars, which corresponds to the input air motor pressure in order to facilitate the control of the pressure manually.

During the storage phase, the air temperature and pressure inside the tank are collected to validate the model.

### 5.2.4 . Air motor and pressure regulator

Three types of experiments were carried out:

- Firstly, the pressure input of the air motor (AM) was manually monitored and regulated to 5 bars throughout the discharge phase. The procedure for obtaining the physical variables is the same as for the charge phase with a record frequency of 1 minute, which is acceptable compared to the discharge time (around 2 hours).
- Secondly, we focused on the temperature change across the throttling valve. It was rigorously accounted and acquired once the pressure of the air tanks varies, allowing a validation of the model.
- Finally, the impact of pressure, temperature and mass flow at the inlet of the AM on its efficiency was investigated.

For these two later experiments, the operating conditions in terms of pressure and temperature are obtained according to the state of discharge of the stored air while the valve is constantly regulated.

The mass flow rate or in other words the speed of rotation of the air motor shaft is controlled by changing the load electric resistance.

It is noticeable that a significant unavoidable amount of heat transfer occurs from the environment to the air flowing in the flow meter, inducing an unpredicted value of the air temperature at the entrance of the air motor. For validation purpose, an average value of this temperature is taken into account.

The electrical efficiency of the generator used is 0.83. Table 5.2 shows the characteristics of the discharge phase. The polytropic coefficient of the air motor is determined by:

$$n_e = \frac{1}{1 + \frac{\ln(\beta_{AM})}{\ln(\frac{T_{out,AM}}{T_{in,\mathrm{AM}}})}} \tag{5.2}$$

*Table 5.2: Experimental characteristics of the discharge phase. (*) refers to calculated values.*

| Parameter | Expansion valve | Flow meter | Air Motor |
|---|---|---|---|
| Inlet pressure [bar] | 300-9 (max 300) | 5 | 5 |
| Outlet pressure [bar] | 5 | 5 | 1.031 |
| Inlet temperature [°C] | 24 | -22<T<14 | -5<T<24 (10 on average) |
| Outlet temperature [°C] | -22<T<14 | -5<T<24 (10 on average) | |
| Mass flow rate [kg/h] | | 49.28 | 49.28 |
| Polytropic coefficient | | | 1.1 (*) |

## 5.3 . Experimental results and model validation

Model and experiment results are compared and summarized in Tables 5.3 and 5.4. It can be seen that the reservoir is completely charged at a maximum pressure of 181 bars after 4 hours and 20 minutes, compressors consume 13.72 kWh with a heating energy that can be stored of 5.72 kWh. The air motor provides 0.437 kW for one hour and 8 minutes while the reservoir is completely discharged. The electrical round-trip efficiency is very low at 3.6%, whereas the comprehensive efficiency or the global equivalent electrical efficiency is higher and equal to 15.16 % owning the values of heating energy and cooling energy (0.8 kWh).

The parameters predicted by the model such as the air mass flow rate in the compressor, the charge and discharge times and also the electrical and comprehensive efficiencies are in good agreement with the experimental results. The maximum error is 13.1%, which is calculated by:

$$error(\%) = \frac{|model\ result - experimental\ result|}{Maximum(model\ result, experimental\ result)} \tag{5.3}$$

Finally, a detailed analysis for the charge, storage and discharge phases was conducted to study and illustrate the behavior of each component.

### 5.3.1 . Charge phase

The charge phase was conducted at the room temperature of around 22˚C. Figures 5.4 and 5.5 present respectively the input and output pressure and temperature variations during the charge phase. Two operation periods can be identified according to the global pressure ratio variations.

During the first period, the pressure output of each stage is constant with a small fluctuation at the outlet of the third stage due to instabilities when opening and closing the exhaust valve.

According to Figure 5.5, the temperatures of each component and of the stored air increase, then stabilize. This transitional period for the compressor and heat exchangers lasts around 40 minutes and is due to the heat exchange taking place with the environment.

The stabilization duration of the compressed air temperature is longer (around two hours) due to the fact that the initial amount of air (at 8.8 bars and ambient temperature) acts to cool the stored air. The constant value of the temperature after 2 hours proves that the heat exchange with the environment could be neglected compared to the mass heat transfer through the charge air flow, as proposed in the model.

Similar behaviours for the temperature and pressure profiles can be found in the experimental results reported by Wang et al. [39] though the stabilization of the air temperature inside the reservoir was not achieved in their case. This can be explained by a more important initial air mass in the study of Wang et al. [39] (around 38% of the total mass stored).

As it can be seen on Figure 5.6, the absorbed electric power is constant as well as the air mass flow (apart from weak fluctuations). The air pressure in the reservoir increases linearly from 8.8 bars to 181 bars in 4 hours and 20 minutes, which demonstrates the adequacy of the perfect gas relation to model the stored air.

According to Table 5.3, the values of the air flow and charge time predicted by the model are accurate with an error which does not exceed 12%. These errors are caused by the pressure losses not being accounted, uncertainties regarding the mechanical and electric efficiencies and mostly by the transitional regime which is not considered by the model.

*Table 5.3: Experimental and model results of the charge phase.*

| | **F.CH.S @ 181 bars First period** | | | **F.CH.S @ 315 bars Second period** |
|---|---|---|---|---|
| Parameters | Experiment | Model | Error (%) | Experiment |
| Air flow rate [kg/h] | 14.4 | 15.09 | 4.6 | 14.18 |
| Charge time [h] | 4.3 | 3.79 | 11.9 | 7 |
| Consumed electric energy [kWh] | 13.72 | 12.09 | 11.9 | 22.86 |
| Potential heating energy [kWh] | 5.27 | 4.87 | 7.6 | 8.61 |

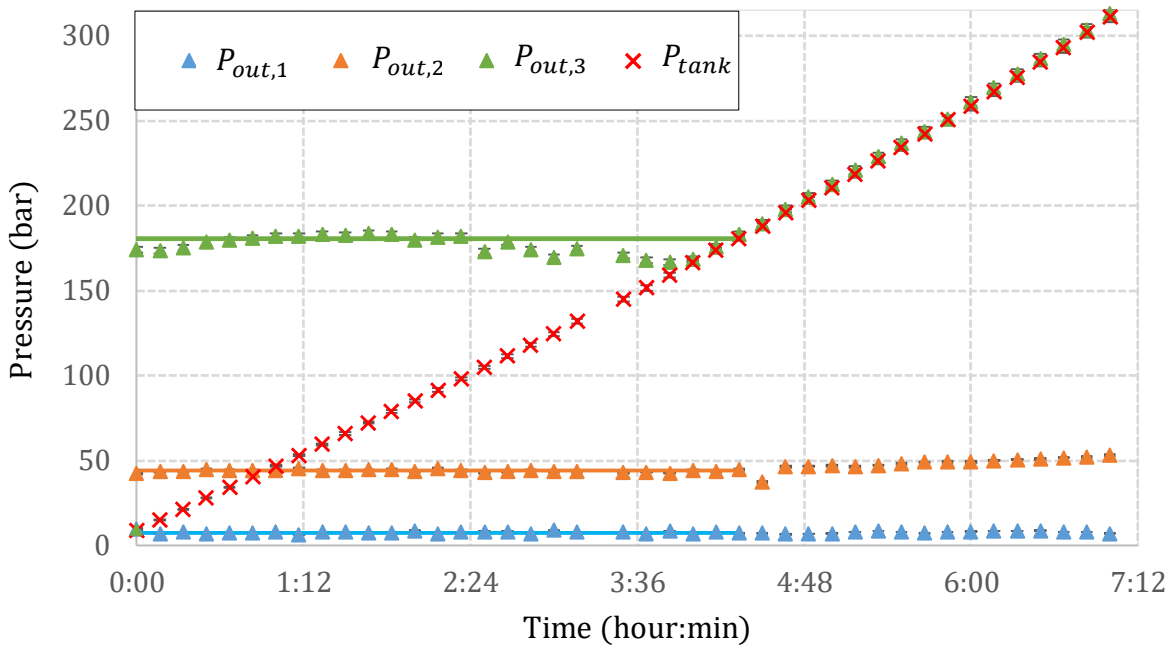


*Figure 5.4: Pressure variations during the charge phase (lines represent the model and points for experimental).*

During the second period, the pressure ratio of the first stage remains constant and that of the second stage slowly increases. At the same time, this ratio increases according to the reservoir pressure for the third stage (Figure 5.4).

As shown in Figure 5.5, the outlet temperatures of the last two compression stages raise which implies an increase of the outlet temperature of all HEX since the efficiency of each HEX remains almost constant.

The driven motor is asynchronous, the increase in global pressure ratio means an increase of the shaft torque and a slow decrease in the rotation speed. Thus, as it can be observed in Figure 5.6, the air mass flow slightly decreases until 13.6 kg/h and the input power increases reaching a maximum value of 3.6 kW for an air pressure of 315 bars.

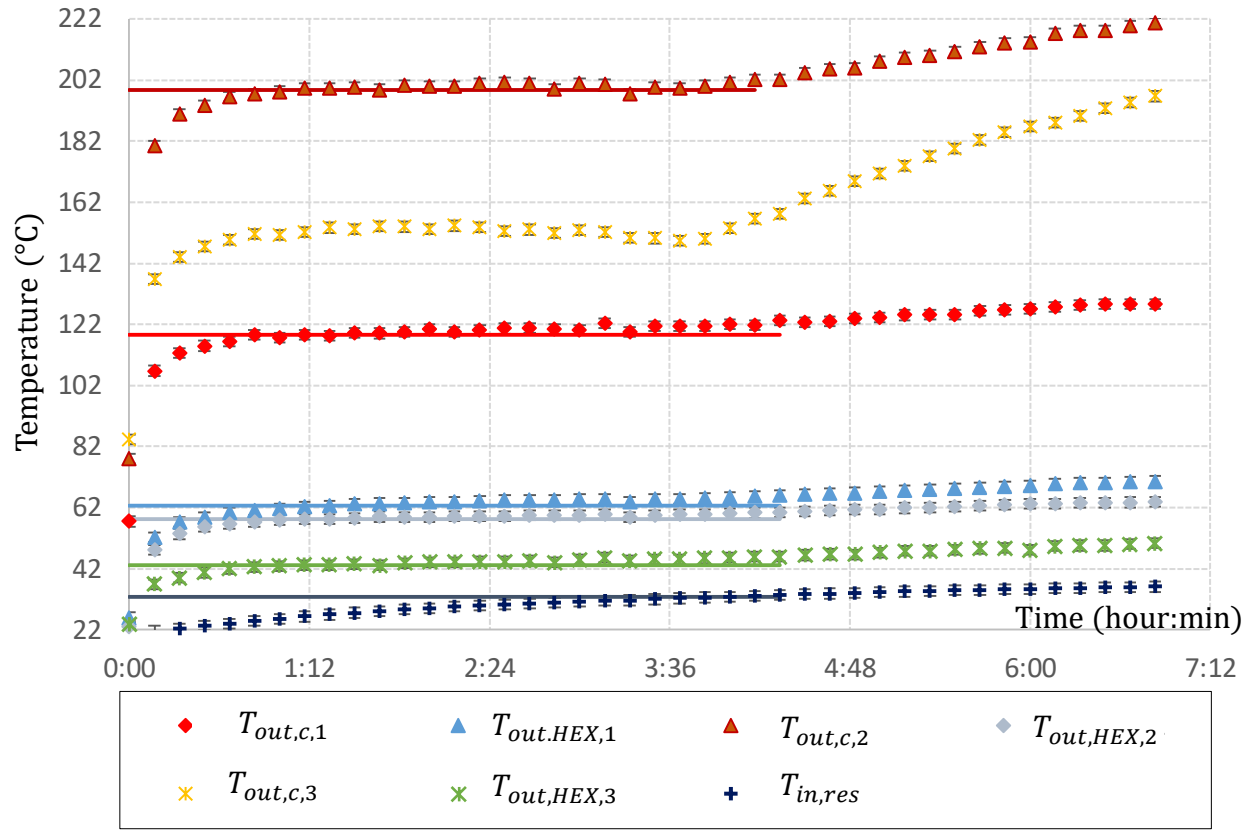


*Figure 5.5: Input and output temperatures of each component during the charge phase (lines represent the model and points for experimental).*

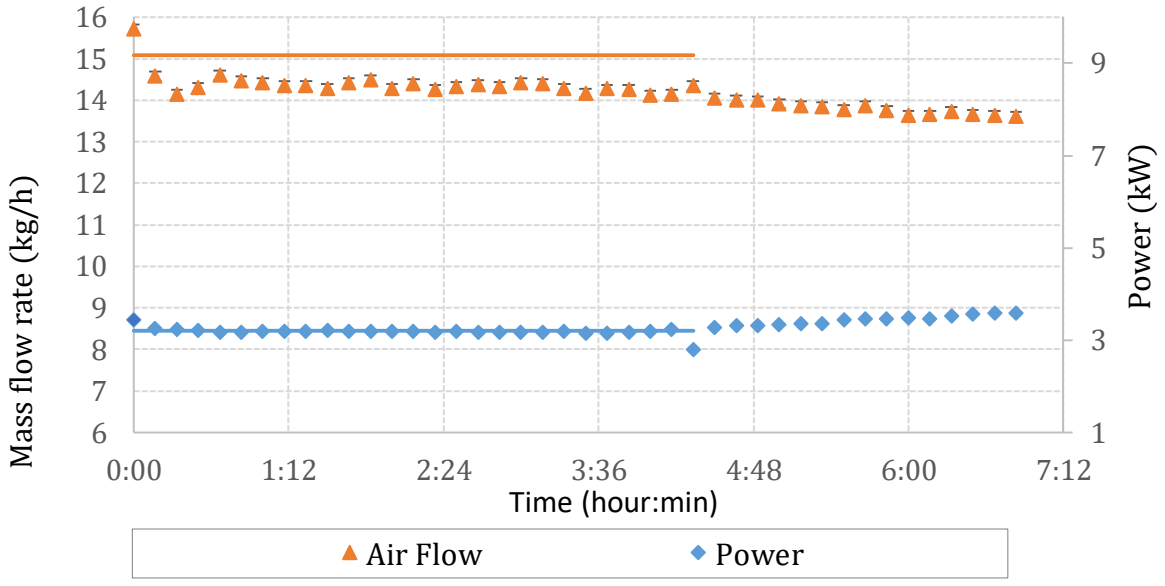


*Figure 5.6: Air mass flow and compressor power during the charge phase (lines represent the model and points for experimental).*

### 5.3.2 . Storage phase

The experimental and modeling results are illustrated in Figure 5.7 for the storage phase. The predicted temperature and pressure variations are in line with the measured ones. The stored air temperature decreases exponentially and achieved the ambient temperature after a storage duration of around 5 hours. The pressure drop is similar and reaches 296 bars which is slightly lower than the predicted one (301 bars), representing an error of 1.6 %.

It should be noticed that the change of heat capacity with pressure was introduced and investigated and it is found that it reduces insignificantly the percentage of error. Hence, potential error sources could be identified as:

- Storage tanks are closely placed and natural boundary layers may be mixed contrary to the model assumptions.
- Real air properties and humidity (even if partial humidification occurs) are not taken into consideration.

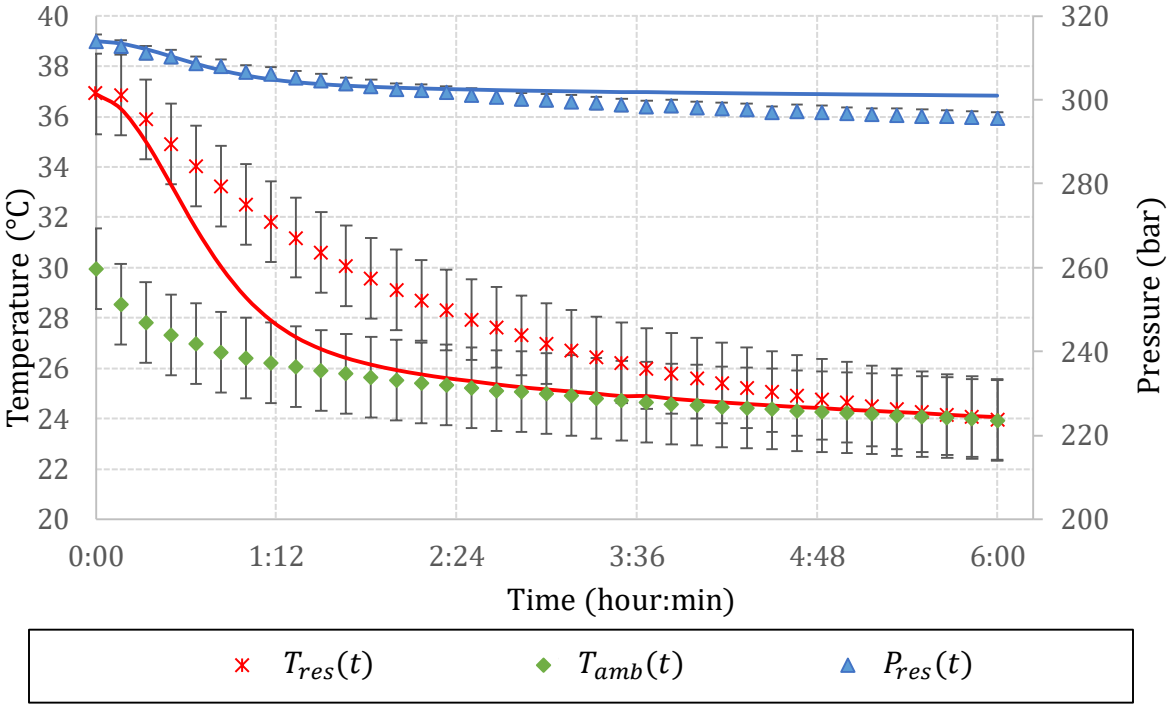


*Figure 5.7: Pressure and temperature of the stored air during the storage phase.*

### 5.3.3 . Discharge phase

The discharge phase is examined at the room temperature of 26.4˚C. As outlined previously, the input pressure of the air motor is regulated continuously at 4 bars (gauge pressure), its fluctuation can be observed in Figure 5.8. In practice, the air pressure does not expand to the atmospheric pressure. Consequently, the pressure output of the AM remains always above this level (Figure 5.8). The air reservoir pressure decreases almost linearly from 301 bars to around 9 bars during this phase which takes 1 hour and 40 minutes.

Figure 5.9 displays the temperature variations with time. Two types of profiles can be observed. During the first 10 minutes, the outlet temperatures of the expansion valve and consequently of the AM decrease which is inconsistent with the Joule-Thomson law, saying that the temperature should rise when the pressure input decreases. This variation can be explained by the fact that the exhaust air serves to cool the stored air as it can be noticed from its temperature profile. Afterwards, the temperature rises as expected.

*Table 5.4: Experimental and model results of the discharge phase.*

| | **I.DIS.S @ 181 bars Experiment n°1** | | | **I.DISCH.S @ 300 bars Experiment n°2** |
|---|---|---|---|---|
| Parameters | Experiment | Model | Error (%) | Experiment |
| Average power [kW] | 0.437 | 0.432 | 1.1 | 0.435 |
| Discharge time [h] | 1.13 | 1.16 | 2.6 | 1.66 |
| Produced electric energy [kWh] | 0.49 | 0.50 | 1.5 | 0.72 |
| Cooling energy [kWh] | 0.80 | 0.78 | 1.9 | 1.14 |
| Round trip electric efficiency (%) | 3.6 | 4.1 | 13.1 | 3.2 |
| COP | 0.48 | 0.51 | 6.0 | 0.46 |
| Comprehensive efficiency (%) | 15.16 | 16.4 | 7.5 | 14.24 |

Table 5.4 shows a comparison between the model and the experimental results of the discharging. Concerning the first experiment, the initial pressure was set to181 bars, despite the fact that the average air mass flow rate equals to 49.28 kg/h is higher than that of compression. The power output was equal to 0.437 kW (see Table 5.4). It is even lower than the power input since the electric efficiency is very low (3.6%). The poor performance of the system ($\eta_{el} = 0.032$ ; $COP = 0.48$) is justified by the difference of the operating pressures during the compression and expansion processes and is clearly apparent in the exergy losses or the irreversibilities in the throttling valve. It should be noted that the real performance is higher since the cooling potential between the expansion valve and the air motor input is not evaluated (see Chapter 4).

Errors in terms of the discharge time and the power output are very low (maximum 2.6%) caused by the average value of the input air temperature of the air motor introduced in the model and the fluctuation of the pressure input due to the manual regulation. Owning to the error during the charge phase, the maximum error was for the round-trip efficiency (13.1%), which remains quite acceptable.

Finally, when the discharge occurs from the initial state of 300 bars (experiment n°2), the electric efficiency and comprehensive efficiency are slightly lower (3.2% and 14.24% respectively). These values result from two effects: a higher value of compression ratio lowers the performance meanwhile; the variable compression ratio contributes to an increase of the efficiency.

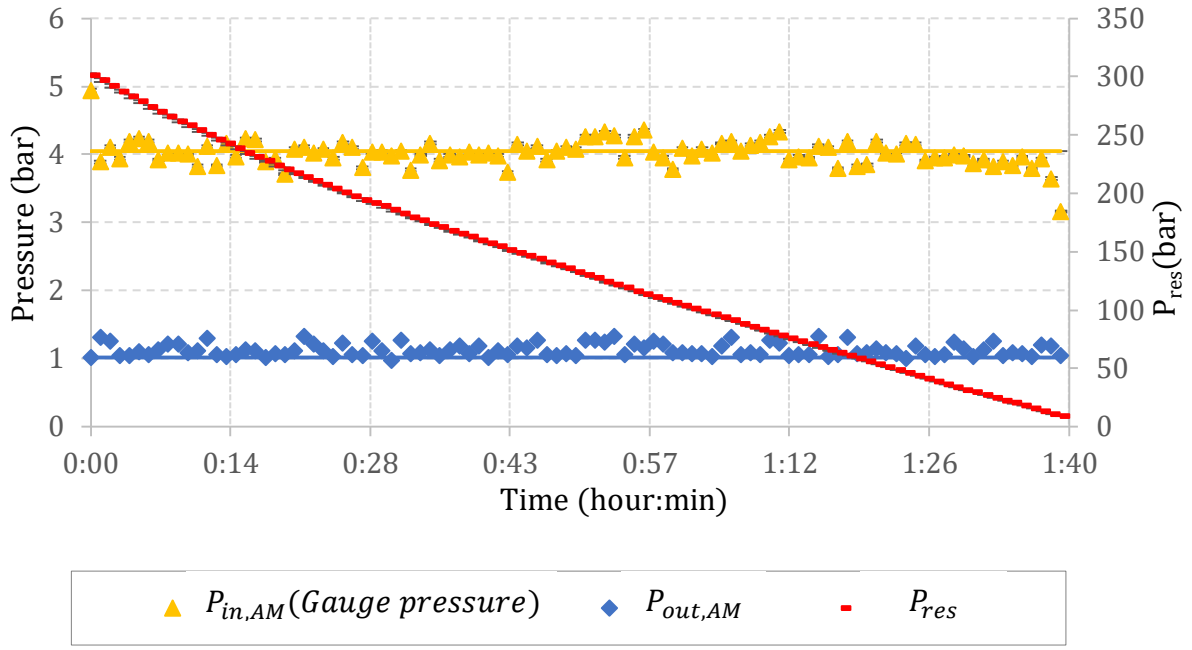


*Figure 5.8: Pressure variations during the discharge phase (lines represent the model and points for experimental).*

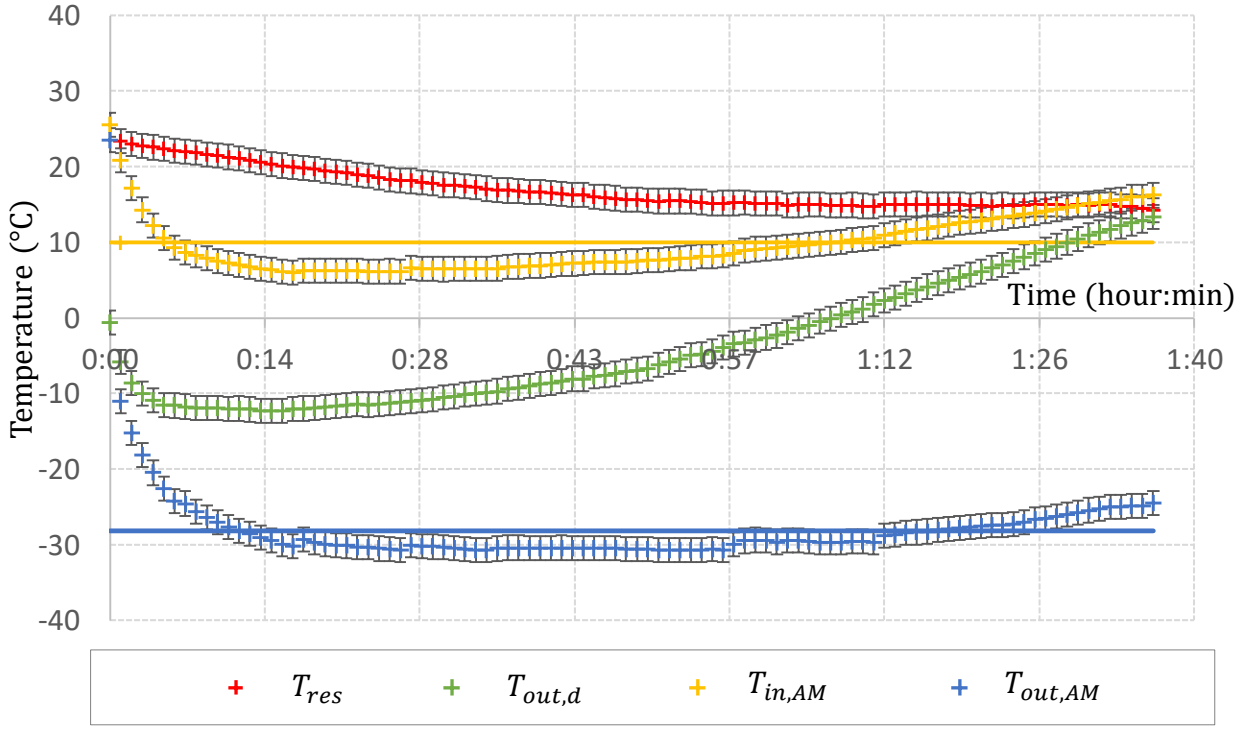


*Figure 5.9: Input and output temperatures of each component during the discharge phase (lines represent the model and points for experimental)..*

## 5.4 Experimental Focus on the throttling valve and the air motor

In this section, we investigate more in-depth the effect of the operation characteristics of these two components.

### 5.4.1 . Throttling valve

Using the approximation of Noel [32] expressed in Equations 4.24 and 4.25 in Chapter 4, isenthalpic curves are plotted and compared to the experimental results in Figure 5.10. By throttling the stored air to 5 bars, it can be concluded that when the initial pressure is higher the temperature drops is larger. The maximum error of the calculated values is around 11% and is recorded when the initial pressure at 245 bars is out of the range of this approximation [25 atm; 150 atm]. Nonetheless, this error means an insignificant difference of 1˚C or 2˚C. As a result, the approximation of Noel remains accurate enough to model the pressure regulator for the pressure range considered here.

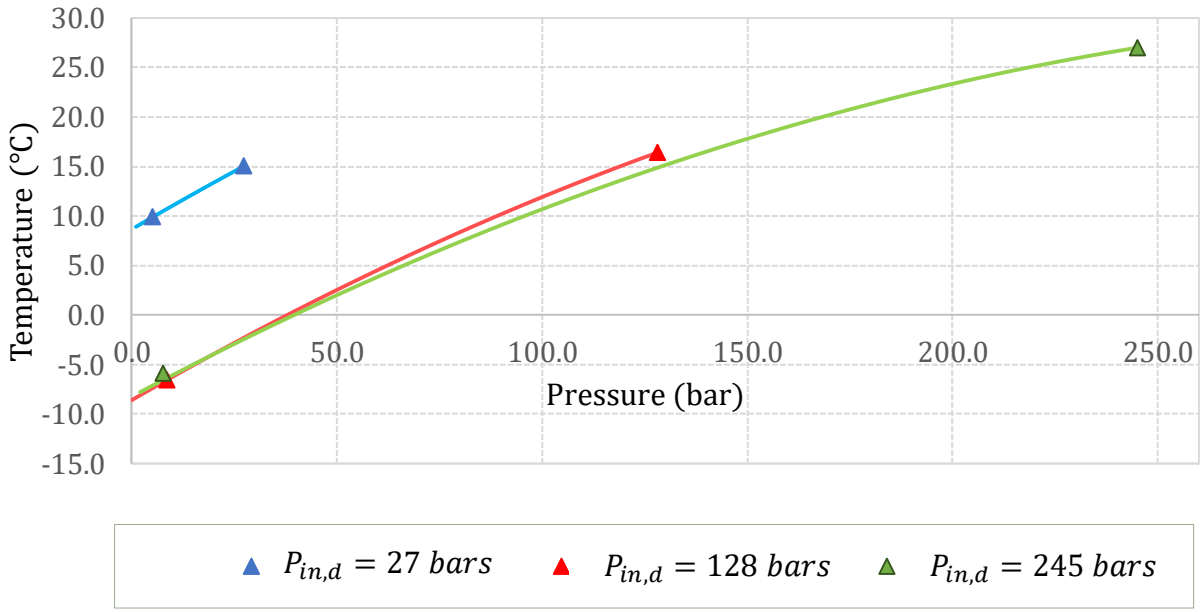


*Figure 5.10: Isenthalpic curves of throttling in the pressure regulator (lines represent the model and points for experimental).*

### 5.4.2 . Air Motor

Since the polytropic coefficient is associated with the amount of heat transfer from the environment to the expanding air, it depends on several factors such as the ambient temperature and the input pressure and temperature. The effect of the ambient temperature is not explored in this study since it did not substantially change during the experimental campaign. By comparison of the different values of the polytropic factor, it is found that $n_e$ is independent of the operating conditions. For instance, it is equal to 1.12 for ($P_{in,e} = 4\ bars$ ; $T_{in,e} = 1^{\circ}C$) and 1.1 for ($P_{in,e} = 6\ bars$ ; $T_{in,e} = 13^{\circ}C$). Consequently, the value of 1.1 was selected.

It is of great importance to derive the thermodynamic to electrical efficiency conversion independently of the temperature input, which is done in Figure 5.11 using Equation 4.49. Regardless the operating pressure, the efficiency is optimal for a certain value of RPM, denoted $RPM_{optimal}$ but still not high enough (around 25%) and lower than the value achieved with a scroll expander (reported as higher than 70% [7, 64]). Similar conclusions and values can be found in the works of Yu et al. [74] and Lemoufet-Gasti [75]. The low-efficiency values can be attributed mainly to the air leaks at small RPM [76] and to mechanical losses at high RPM.

Low operation pressures are linked to an efficient thermodynamic electrical conversion due to fact that the displacement volume is no longer sufficient to expand the air to the atmospheric pressure. For instance, the air expands to 1.05 bar when the input pressure is 3 bars whereas it expands to 1.12 bar for 4 bars pressure input (see Table 5.5).

*Table 5.5: Power and pressure output of the air motor for different operating conditions.*

| $P_{in}$ (bar) | $T_{in}$ (°C) | RPM | $Power_{EXP}$ (kW) | $Power_{model}$ (kW) | $P_{out}$ (bar) | Error (%) |
|---|---|---|---|---|---|---|
| 3 | 19 | 897 | 0.3 | 0.34 | 1.05 | 11.8 |
| 3 | 5.6 | 892 | 0.283 | 0.34 | 1.05 | 16.8 |
| 4 | 18.5 | 898 | 0.447 | 0.45 | 1.12 | 0.7 |
| 4 | -2 | 881 | 0.39 | 0.45 | 1.12 | 13.3 |

In order to examine the effects of the operating conditions of the air motor on the output power provided by the manufacturer, these curves are compared to the experimental results in Figure 5.11 for different mass flows, input pressures and temperatures. The experimental values are consistent with the power curves with a difference varying between 0.7 % and 16.8% according to the input temperature. As detailed in Table 5.5, when the temperature approaches the ambient temperature, the error is reduced. This is because the manufacturer curves of the air motor are made for industrial applications for which the maximum air storage pressure does not exceed 30 bars and therefore the input temperature is close to the room temperature. This point out that the thermodynamic to mechanical efficiency of the air motor depends also on the input temperature of the AM.

## 5.5 . Conclusions and perspectives

In this chapter the compressed air energy storage pilot unit existing at IMT Atlantique was described. Several experimental tests were carried out in order to investigate the real behavior of our system, focusing on the discharge phase. Experimental results were found to be in good agreement with the model results of air side components presented in Chapter 4, with an error which does not exceed 13.2 %.

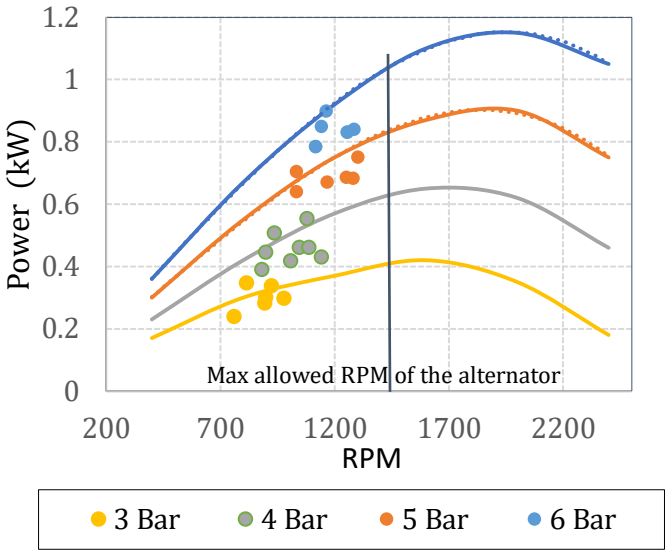


*(a) Power variations.*

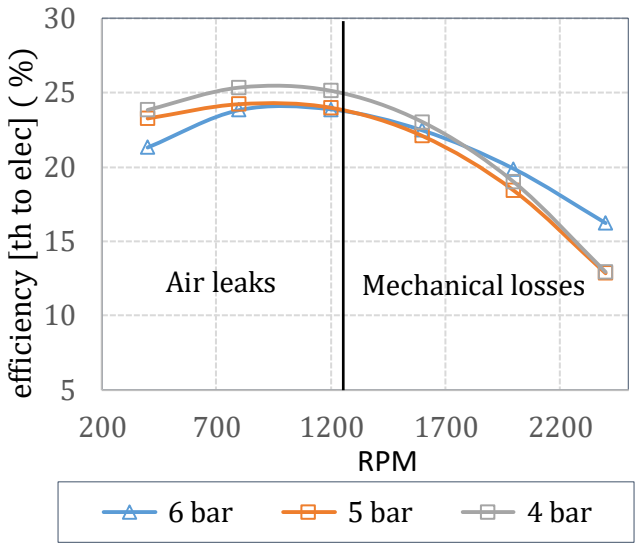


*(b) Efficiency variations,*

*Figure 5.11: Power versus RPM of the air motor (a) and thermodynamic to electrical conversion (b) (lines represent the model and points the experiments).*

The model developed for air component enables an accurate prediction of the system performance and provides relevant output parameters for practical applications. It is the first reliable model validated with experimental data for small-scale compressed air energy storage system.

The main model limitations are the following:

- Errors induced by the following assumptions:
  1. The transitional regime during the charge phase was ignored.
  2. Real air properties and humidity were not accounted in the storage phase.
  3. The effect of air input temperature of the air motor was not accounted.
- The developed model is steady-state. Nonetheless, a dynamic is necessary for particular cases:
  1. When the compression ratio is variable.
  2. In order to assess properly the cooling potential and the output power, the transient nature of the discharge process should be accounted for.

However, since the objective of this thesis is to provide the investigation of prospective system performances and its thermodynamic optimization, the developed steady state model still reliable and sufficient in this scope.

**During the charge phase**, the consumed electric energy of 13.72 kWh was 12% higher than the model of 12.1 kWh. The error was caused mainly by the transitional regime required to stabilize compressed air temperature.

The transitional regime during the charge phase takes about 40 minutes. Pressure and temperature in the air tank during this phase were accounted, the temperature stabilizes at a particular level which differs from the results of Wang et al. [39]. It highlights in particular the prime importance of the initial mass of stored air.

**During the storage phase**, the air temperature as well as the pressure were modelled and found in good agreement with the experimental measurements. Unfortunately, it has not been possible to provide those variations during the discharge phase because of the influence of the cold exhaust air of the air motor flowing around our system.
**During the discharge process,** the output electric energy of 0.49 kWh was 1.5 % less than the model of 0.5 kWh.
A particular attention was paid to every compound in this phase.
It has been demonstrated that the Joule-Thomson effect governs the temperature change across the pressure regulator and the assumption of constant temperature is no longer true as stated in previous models of compressed air energy storage system.
A comprehensive analysis of the air motor efficiency was presented to clarify its performance curves. The reported high values of the power output associated with higher input temperatures provide a first evidence of the benefit of preheating.

On the other hand, the existing industrial pilot does not allow to validate the model of all the components of the configurations proposed in Chapter 4 such as the water side of heat exchangers and turbines. One or different improvements can be made to upgrade the experimental pilot:

1. Replacement of the air-cooling fan of the compressor by three heat exchangers installed after each stage.
2. Install a thermal energy storage unit composed from a pressurized water circuit, as proposed in Chapter 4.
3. Install the micro air turbine proposed in the last chapter.
4. Install a preheating heat exchanger before the air motor in order to investigate the effect of input temperature in the output power and the polytropic coefficient.

Since a significant difference between the charge pressure at 181 bars and discharge pressure at 5 bars takes place, the round-trip electrical efficiency is very low at 3.6% and the comprehensive efficiency which represents the equivalent electrical storage efficiency reaches 15.6% underlying the importance of the trigeneration concept.

Apart from increasing the expansion ratio until 25 in virtue of the axial micro-turbine proposed in Chapter 4, two different potential strategies could be applied also in a future work to reduce losses in the throttling valve and improve the performance of the system:

1. Replacing the throttling valve by a Ranque-Hilsch vortex tube or a cascade of vortex tubes. These devices have indeed the capability to relax the air to reduce the maximum inlet pressure allowed by current micro-turbines, while producing a hot and a cold stream. The produced cooling power would be then reinjected within some heat exchangers of the compressed air energy storage system.
2. Adding a supersonic ejector after the throttling valve to mix the air from tanks at different pressures (which would reduce the cost of the storage tanks) and guarantee a more constant pressure at the inlet of the turbine. It has been successfully applied by Chen et al. [43] for a large-scale adiabatic compressed air energy storage system.

# CHAPTER 6 - PARAMETRIC OPTIMIZATION OF SMALL SCALE TRIGENERATIVE COMPRESSED AIR ENERGY STORAGE

## 6.1 Objectives and originality

Previous optimization studies on the A-CAES and T-CAES identified different optimization opportunities such as varying the number of compression/expansion stages, increasing the effectiveness of heat exchangers and changing the storage pressure and other parameters stated above. Authors focused on one or more aspects and investigated the potential performance improvement. However, they overlooked or not clearly addressed the relations between the design parameters of the equipment. For instance, when the number of compression stages is changed the number of expansion stages was kept constant and when the water mass flow rate of intercooling heat exchangers HEX is changed (which changes the thermal energy storage temperature) the flow of the preheating HEX is fixed. Another limitation that could be highlighted in some studies when considering a variable pressure ratio is that the thermal energy storage is inadequately correlated to other compounds. This leads to an inaccurate estimation of the efficiency improvement.

In addition, the system was evaluated based on one or many evaluation criteria separately without taking into account most of them at the same time. As an example, when the round-trip efficiency was concerned the energy density and other parameters reflecting economic criteria were often discounted.

The objective of this study is to derive an optimal design guideline of the trigenerative compressed air energy storage based on parametric optimization, focusing at the same time on all interdependent design parameters of equipment and paying attention to the majority of assessment criteria at once. The contributions and novelties turn out as follows:

- The parametric optimization focuses on the mutual effect of the design parameters in the case where the choice of one of them is conditional on others. In addition, the effect of the thermal of energy storage is quantified for the first time.
- The study applies various criteria used to assess the energy storage technologies such as energy density, heat exchanger footprints, round trip electric efficiency and the comprehensive efficiency in the optimization of the T-CAES.

The chapter is arranged as follows: section 6.2 presents the methodology of the optimization procedure. Section 6.3 analyzes the results, then the optimal design guidelines is derived. Based on this latter, the characteristics of the small-scale T-CAES are deduced in section 6.4. Finally, the important conclusions are summed up in section 6.5.

## 6.2 Methodology of the parametric optimization

Generally speaking, the optimization of energy systems can be conducted by using thermo-economic analysis, multi-objective optimization or parametric study [77]. However, our system is recently proposed and the analysis via parametric study figure out the key drivers for the optimization of the performances of the T-CAES.

This analysis starts by identifying the design parameters and dissect their effect on the performances of the system. The relevant parameters were retained from the thermodynamic model. Table 6.1 lists the base values of the fixed parameters used in our study.

*Table 6.1: Fixed parameters and variable parameters of the parametric study.*

| **Fixed parameters** | **Value** | **Reference** |
|---|---|---|
| Ambient temperature [˚C] | 30 | -- |
| Input power [kW] | 3.17 | Experimental pilot |
| Polytropic coefficient of compressors | 1.25 | [20] |
| Compressor mechanical efficiency | 0.9 | Average value of the range (0.85;0,95) [61] |
| Motor electric efficiency | 0.9 | Premium motor efficiency [73] |
| Total volume of 6 air storage reservoirs [$m^3$] | 0.29 | Experimental Pilot |
| Dimension of each air reservoir (height X diameter) [m] | 1.4 X 0.21 | Experimental Pilot |
| Storage time [h] | 5.5 | Time required to Stabilize the temperature and pressure (experimental results). |
| Thermal efficiency of TES | 0.95 | --- |
| Expansion mass flow [kg/s] | 0.0183 | --- |
| Minimum pressure of compressed air [bar] | 25 | [72] |
| Total to total efficiency of turbines | 0.63 | [72] |
| Mechanical efficiency of turbines | 0.95 | [70] |
| Generator electric efficiency | 0.9 | Like motors |
| Minimum allowed temperature output of AM [˚C] | -20 | [20] |
| Input pressure of AM (bar) | 6 | Analysis of AM data |
| Polytropic coefficient of AM | 1.1 | Experimental results |
| Thermodynamic to mechanical efficiency conversion of AM | 0.304 | Experimental results |
| $COP_{heat\ pump}$ (heating mode) | 4 | [20] |
| $COP_{heat\ pump}$ (cooling mode) | 3 | [20] |

| **Varying parameters** | **value ranging** |
|---|---|
| Temperature of hot TES [˚C] | [70; 150] |
| Effectiveness of HEX | [0.65; 0.97] |
| Maximum pressure of compressed air [bar] | [30; 350] |
| Number of compression stages | [2; 7] |

Herein, firstly, input power scale and reservoir volumes correspond to a small scale unit in accordance with Jannelli et al. [16] and the experimental pilot described in Chapter 5. Secondly, the output temperature of the air motor should be upper than the minimum allowed temperature specified by the designer (-20˚C according to [78]). Owning that the minimum ambient temperature on which the cooling energy should be activated is 25˚C, a simple calculation gives that an output temperature of air motor at -20˚C corresponds to a pressure input of 6 bars (absolute value). The expansion mass flow rate at 0.0183 kg/s corresponds to the maximum efficiency of the air motor at the fixed pressure, while at the same time it is ensured its adaptability to air turbines and to produce a total output power (ranging from 1.5 kW to 2 kW) to meet the need of a small scale electric load. In the end, the values of the performance parameters of machinery such as

efficiency were collected from available commercial data (where the highest values are taken) or from the estimated values in the literature.

Table 6.1 also presents the design varying parameters and their ranges of variation. These parameters are varied one at a time or many at the same time to study their effects on the system performances. As an illustration, when the temperature of TES is varied the number of compression stages and HEX effectiveness are constant (the parameters are varied one at a time). On the other hand, when the number of compression stages is varied the effectiveness of HEX is constant, while the thermal energy storage temperature should be changed (many parameters are changing at the same time). In addition, the effect each parameter was evaluated by taking into consideration the impact of each parameter in others. Each case will be explained further in the results sections.

Once those effects are well known, the optimal design solutions are derived and the two configurations deduced in chapter 4 are compared. The cooling energy was initially activated in all cases and then disabled to investigate its effect.

## 6.3 . Results and discussions

### 6.3.1 . Effects of the temperature of the thermal energy storage

The following parameters are fixed:

1 Number of compression stages $N_c = 3$.
2 Maximum pressure $P_{max} = 200$ bars.
3 The effectiveness of HEX: $\varepsilon_c = \varepsilon_e = 0.85$.

The variation of electric and comprehensive efficiencies and also the optimal number of expansion stages, HEX footprints and finally the temperature of cold TES and the output temperature are shown in Figures 6.1.a, 6.1.b and 6.1.c respectively.

In the discharge process, in order to satisfy the condition of the output temperature of the turbine close to the ambient temperature, a higher level of $T_{h,TES}$ means a low number of expansion stages which decreases at a critical values of $T_{h,TES}$ at 80˚C and 130˚C (see Figure 6.1.a).

According to Figure 6.1.a, in the second configuration, the electrical efficiency and the comprehensive efficiency increase continuously a little due to the fact that the input temperature of turbines increases with $T_{h,TES}$. In the other hand, in the first configuration those efficiencies raises only as from the critical values of $T_{h,TES}$ (corresponding to a change of $N_e$).the maximum increase of the electrical efficiency and comprehensive efficiency is about 8.5% and 3.6% respectively of its initial values at 14.6% and 26%. These values have proved that the cogeneration option increases the global efficiency (by about 11.4 % in this case) and the temperature of TES have a minor impact on the electric efficiency as stated by Wolf and Budt [44].

Before analyzing the required HEX footprints, it is known that the total footprint of a number of HEX is governed by the logarithmic mean temperature difference (LMTD) of each HEX and obviously the number of HEX.

In the charge process, once the temperature of thermal energy storage is changed while keeping the HEX effectiveness as constant, the water mass flow rate should decrease and the logarithmic mean temperature difference (LMTD) of each HEX decreases. As a result, the total footprint of the three intercooling HEX in compression phase increases (see Figure 6.1.c).

In the discharge phase, it can be observed also from Figure 6.1.c that the general trend of the discharge phase HEX footprint decreases as $T_{h,TES}$ increases due to the fact that the number of expansion stages decreases. However, a further inspection says that at the critical values of $T_{h,TES}$ the footprint has its maximum value for the first configuration and its minimum values for the second configuration. Afterwards, the footprint of the first configuration decreases significantly (of an average value of 3.15 W/K/˚C) which results from the increasing the LMTD of each HEX exchanger, whereas the footprint of the second configuration increases slowly (of an average value of 0.39 W/K/˚C) which is linked also for the little decrease of the LMTD.

In totality, the total footprint of all the HEX is mainly influenced by the HEX of the discharge phase (see the trend of the red line in Figure 6.1.c). It takes its minimum values always in the first configuration due the additional recooling HEX in the second configuration. The minimal possible of 103 W/K was achieved at $T_{h,TES} = 120˚C$ in the first configuration, while the values were ($130˚C$; 215 W/K) for the second configuration.

From Figure 6.1.c, it can be seen that the temperature of cold TES is almost constant at 10˚C higher than the ambient temperature which is linked to the pinch point temperature difference $Pinch_e$. By contrast, in the second configuration, since $Pinch_e$ is related to $T_{h,TES}$, $T_{cold,TES}$ increases almost linearly versus $T_{h,TES}$ for a fixed number of expansion stages and presents discontinuities with varying $N_e$. Its value is always above 60˚C which is suitable for heating purposes.

Finally, as can be predicted from the design methodology, the output temperature of air motor is constant at -15 (where the ambient temperature is 30˚ C) for the first configuration but it is a little higher in the range of [-12;-15.2] in the second configuration which is attributed to the effectiveness of the recooling HEX. It should be noted that the heating and cooling energy shows a very little difference between the 2 configurations (data are not shown because of the minor effect).

To summarize, generally speaking, an increase in the temperature of TES results in a decrease of the required expansion stages and the required HEX footprint but a slight increase of the electric and comprehensive efficiency. Besides, there are critical values of $T_{h,TES}$ to be avoided (80˚C and 130˚C for the first configuration) in order to reduce the HEX footprints without a much decrease of the efficiencies of the system. Eventually, the first configuration is simpler and better from an economical point of view (based on HEX footprints).

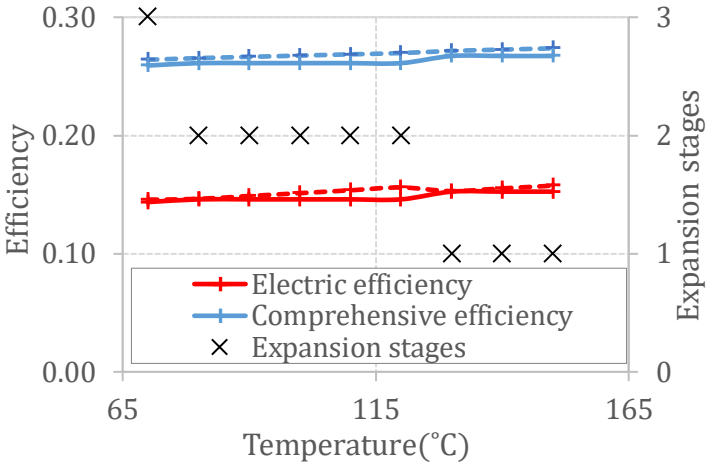


*Figure 6.1.a. T-CAES efficiencies (left axis) and the optimal number of expansion stages (right axis) as a function of the temperature of TES*

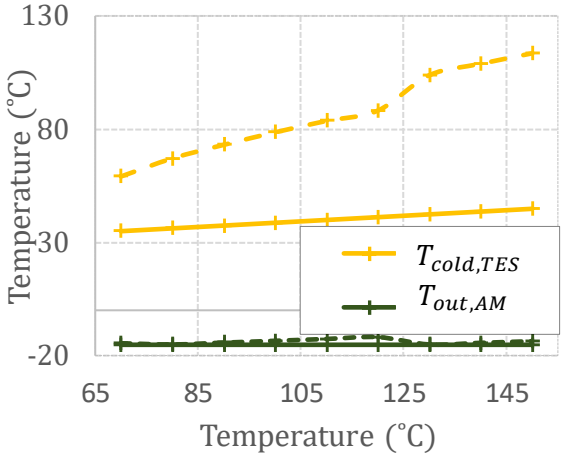


*Figure 6.1.b. The temperature of AM and of the cold TES as a function of the hot temperature of TES.*

*(Solid lines for the first configuration and dashed lines for the second one).*

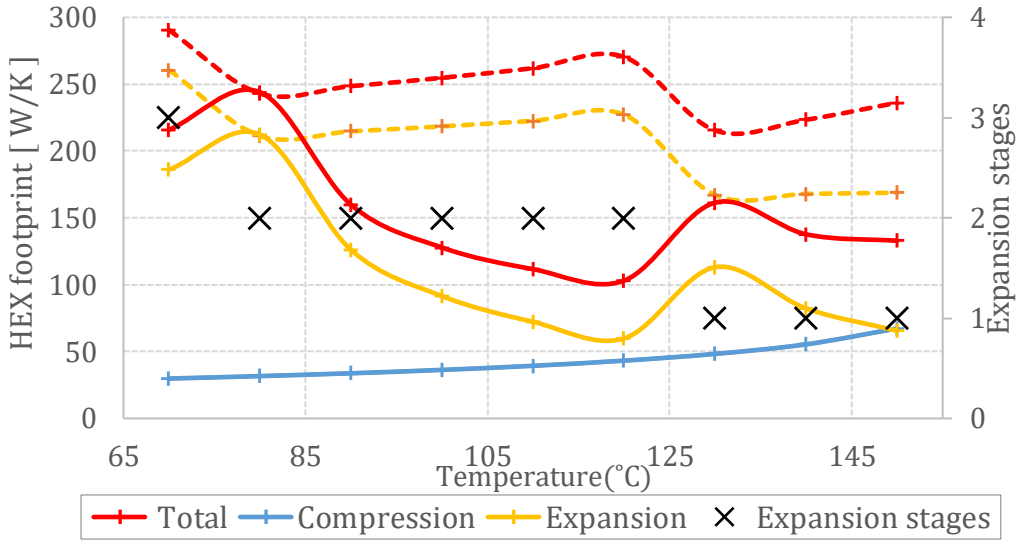


*Figure 6.1.c. Required HEX footprints (left axis) and the number of expansion stages (right axis) as a function of the hot temperature of TES (solid line for first configuration and dashed line for the second).*

*Figure 6.1: Effect of the thermal energy storage temperature.*

### 6.3.2 . Effects of the number of compression stages

The effect of this parameter is studied in the literature taking into account a constant temperature of TES [13] or constant mass flow rate of intercooling HEX [45] and with a constant number of expansion stages. It is important to reinforce the analysis by integrating a reasonable choice of $T_{h,TES}$ and varying the number of expansion stages. In this work, this temperature is varied according to the results obtained in section 6.3.1, it is chosen in order to reduce the system

complexity (number of expansion stages and total HEX footprints) and simplify our analysis. Consequently, $T_{h,TES}$ was selected the maximum possible value (in other words $C_{min} = C_{max}$ for intercooling HEX) which matches these objectives (see Figure 6.1.b).

The other parameters were fixed as follows:

1 Maximum pressure $P_{max} = 200$ bars.
2 The effectiveness of HEX: $\varepsilon_c = \varepsilon_e = 0.85$

As evident from Figure 6.2.a the rise of the number of compression stages implies an increase of the expansion stages going from critical values (passing from three compression stages to two and from 6 to 7), meanwhile the temperature of TES is reduced which is a consequence of the decline of the temperature output of each compression stage.

Figure 6.2.c displays the variation of the ratio of discharge time to charge time and the heat stored as a function of the number of compression stages. It is known from the literature that a higher number of $N_c$ increases the compression efficiency which means a reduce of the time of charge for a fixed electric power input, thus it can be seen that the ratio $t_{dis}/t_{ch}$ augments with $N_c$ substantially (around 19%) at the beginning (passing from 2 to 4 stages) and slightly (about 3%) afterwards. Turning to the heat stored, $N_c$ has a marginal effect on it. Similarly, heating and cooling energy hardly varies (data are not shown here).

Figure 6.2.b reports the variation of the efficiencies of the system. Since the time of charge is decreased, the electric and comprehensive efficiencies increase and share the same behaviors as the $t_{dis}/t_{ch}$ ratio, with a little increase when the number of compression stages are above three or four. These variations are consistent with that of Luo et al. [45] and Facci et al. [13] with a difference on the values of the electrical efficiency.

The required HEX footprints are given in Figure 6.2.d. Generally speaking, the rise of compression stages, as well as expansion stages and HEX are behind the increase of the total footprints. Adding that the required footprints of the second configuration are always higher than the first one. Nevertheless, some exceptional cases occur, for instance, the total footprint for the first configuration is slightly lower when $N_c$ increases from 6 to 7 which can be attributed to a higher LMTD of HEX in the discharge phase.

To conclude, there is an optimal choice of the number of compression stages, which corresponds to a compromise between increasing the electrical efficiency and decreasing the system complexity and costs (stem from the number of stages and total footprints). The configuration with three compression stages is an optimal solution in our case.

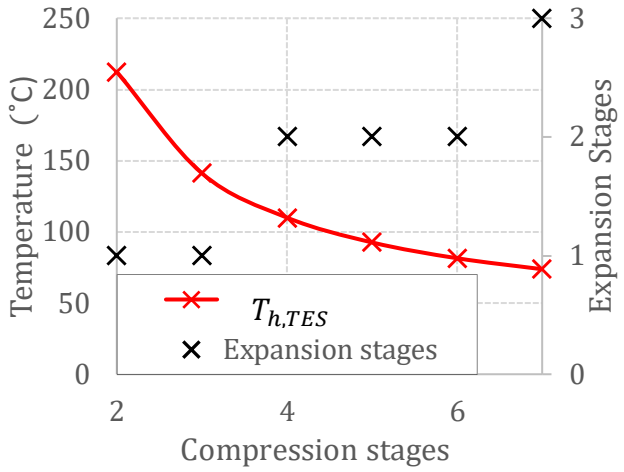


*Figure 6.2.a. Temperature of hot TES (left axis) and required expansions stages (right axis) as a function of the number of compression stages.*

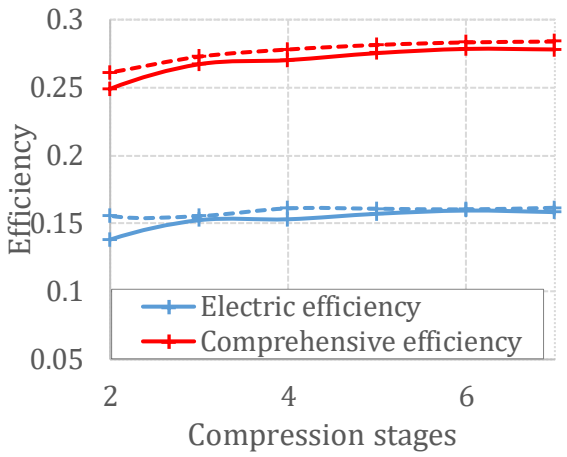


*Figure 6.2.b. T-CAES efficiencies as a function of the number of compression stages.*

*(Solid lines for the first configuration and dashed lines for the second one)*

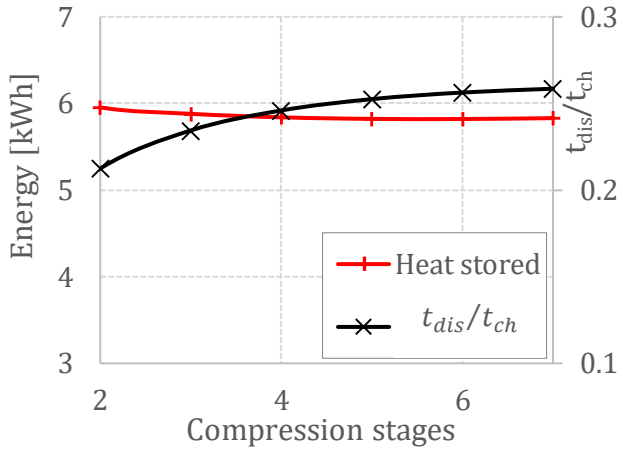


*Figure 6.2.c. Heat stored (left axis) and the discharge to charge time ratio (right axis) as a function of the number of compression stages*

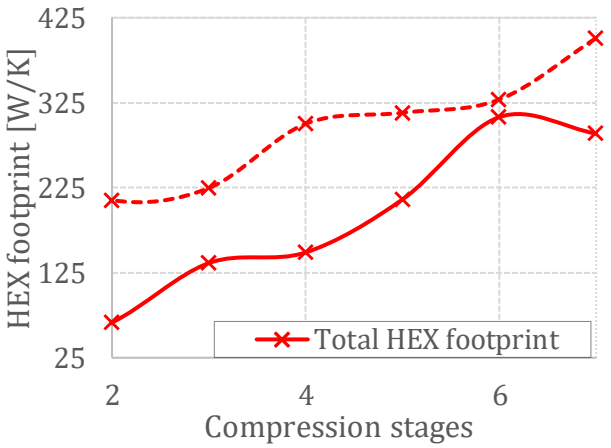


*Figure 6.2.d. The total required HEX footprints as a function of the number of compression*

*(Solid lines for the first configuration and dashed lines for the second one)*

*Figure 6.2: Effect of the number of compression stages.*

### 6.3.3 . Effect of the effectiveness of intercooling HEX

As outlined in Chapter 2, the theoretical investigation of this parameter has been the subject of the study of Han and Guo [51]. Notwithstanding, their analysis is based on variable compression and expansion ratios. Alternatively, in this study, the effect of HEX effectiveness was carried out with a constant design temperature of TES respecting the current practical applications of HEX.

Based on the previous results, the following parameters are fixed:

1 Number of compression stages $N_c = 3$.
2 Maximum pressure $P_{max} = 200$ bars.
3 The effectiveness of expansion HEX $\varepsilon_e = 0.85$
4 The temperature of the hot TES is fixed to 140˚C.

Since the charge parameters of the two configurations are the same, only the results of the first configuration are presented in Figures 6.3.a, 6.3.b and 6.3.c.

Figure 6.3.a shows that the energy density grows linearly with the effectiveness which arises from the drop of the temperature of the air inlet flowing to the air reservoir. In addition, the discharge to charge time ratio surges steadily with the effectiveness at the beginning, then it remains almost constant when the effectiveness is between 0.79 and 0.85 and it drops sharply when the effectiveness is above 0.93. The rise of this ratio mainly comes from the decrease of the charge time due to the growing of the air mass flow rate, and also to the increase of the discharge time due to the growing of the energy density. On the other hand, the decline of this ratio is due to the pressure losses that affect adversely the airflow and the charge time.

It is obvious that the improvement of the effectiveness increases proportionally the heat delivered by each HEX. By combining this with the rise of the charge time, the heat stored and the heating energy increase significantly as can be seen from Figure 6.3.b. Another conclusion which can be revealed from this figure is that the cooling energy increases linearly ascribed to the rise of the discharge time.

In Figure 6.3.c, the gain in the heat energy stored yields to the increase in the heat recuperated which gives rise to the electrical efficiency. As well, this increment with the increasing of the heating and cooling energy originates in the improvement of the comprehensive efficiency. Comparing Figures 6.3.a and 6.3.c shows that the discharge to the charge ratio and the electrical and comprehensive efficiency share the same behavior due to the fact that the compression and expansion powers are constant. All in all, the electrical and comprehensive efficiency increase moderately about 8% and 14.5% respectively from their initial values when the effectiveness goes from 0.65 to 0.85. It's important to note that these behaviors still in line with the results of Han and Guo [51] despite of the difference in the simulation conditions.

Finally, as can be found in Figure 6.3.c, the total HEX footprints rise moderately (26% of its initial value) when the effectiveness goes from 0.65 to 0.83 and then significantly (41 % of its initial value) when the effectiveness is above 0.85.

These analyses below allow us to conclude that the effectiveness of intercooling HEX should be chosen as an optimal trade-off between the system performances (efficiencies, cooling and heating energy) and the required footprints. In our cases, the optimal effectiveness is a value in the range of 0.77 to 0.86.

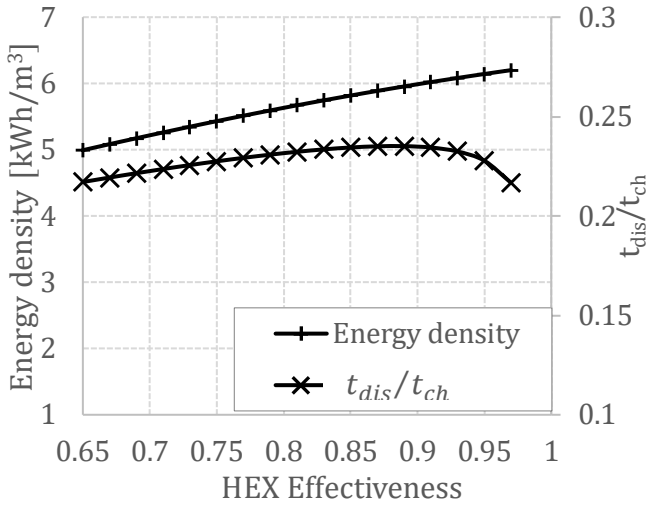


*Figure 6.3.a. Energy density (left axis) and discharge to charge time ratio (right axis) as a function of the effectiveness of intercooling HEX.*

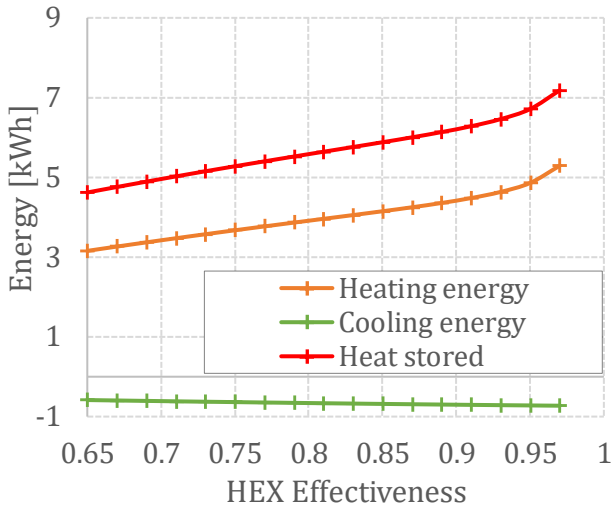


*Figure 6.3.b. Heating, cooling and stored energy as a function of the effectiveness of intercooling HEX.*

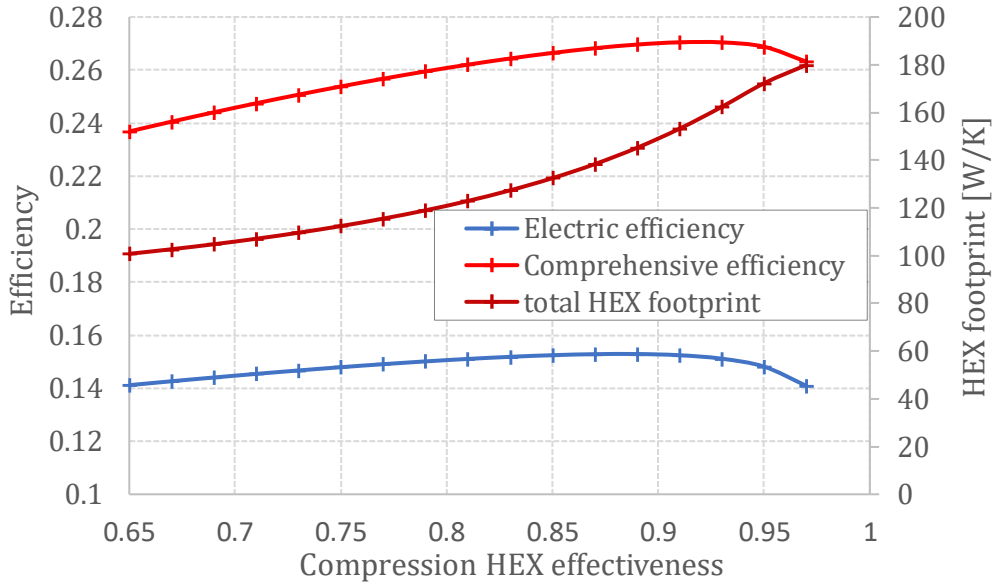


*Figure 6.3.c. T-CAES efficiencies (left axis) and the total HEX footprints (right axis) as a function of the effectiveness of intercooling HEX.*

*Figure 6.3: Effect of the effectiveness of intercooling HEX.*

## 6.3.4 . Effect of the effectiveness of discharge phase HEX

Here, the same fixed parameters of the previous section 6.3.3 were adopted with the exception of taking $\varepsilon_c = 0.85$ and $\varepsilon_e$ varying in the range [0.65-0.97].

Figures 6.4.a and 6.4.b report the simulation results in terms of the heating and cooling energy and performances respectively. The first important point to underline is that there is a critical value of the effectiveness at 0.79 on which the number of turbines can be reduced from two to one. In the two range of variation of effectiveness ([0.65; 0.77] and [0.79; 0.97]) the parameters variations are similar.

In the first configuration, it can be noticed that there is a linear rise of 27.6W/0.01 for the heating energy upon a decline of about 1˚C/0.01 of the temperature of the cold TES, which results in a total drop from 66.5˚C to 33.13˚C. This is originated from the proportional relation between $\varepsilon_e$ and $Pinch_e$ on the hand, and the heating energy on the other hand. Physically speaking, at low levels of HEX effectiveness the drop of the heating energy is elicited by the heat wasted from the cold TES reservoir to the environment. As for cooling energy, it is predicted that it remains constant as the temperature input of AM is unchanged. Owning that the temperature input and output of each turbine are also unchanged, the electrical efficiency remains constant at 14.5% then 15.2 % (Figure 6.4.b). On the other hand, the comprehensive efficiency increases a few as 2.5%, which is accounted for the heating energy.

In the second configuration, in Figure 6.4.a, the cold TES temperature declines as long as the effectiveness rises. The heating energy and also the cooling energy barely increase when $\varepsilon_e$ is below 0.77 and adversely when $\varepsilon_e$ is above 0.77. Those effects are related in the first place to the rise of the preheating energy delivered to the air side and the increase of the amount of heat of the recooling HEX before the AM in the second place. For these reasons also, according to Figure 6.4.b, the electrical efficiency and the comprehensive efficiency slowly go up with a slope of 0.5%/0.15 and 0.3%/0.15 respectively.

Finally, the total footprints of HEX in the two configurations slowly rises as the effectiveness is below 0.83, by contrast it increases dramatically as the effectiveness is above 0.85.

To conclude, it is crucial to choose the effectiveness of HEX above a critical value (at 0.79 in our case) in order to reduce the number of expansion stages. The overall efficiencies can be kept as high as expected even if the effectiveness is at moderate values ([0.79; 0.85] in our case). Furthermore, in the first configuration, an additional option to economize in terms of the area of HEX is to impose the effectiveness as lower as possible conditionally upon using the water mass of cold TES reservoir for heating purposes.

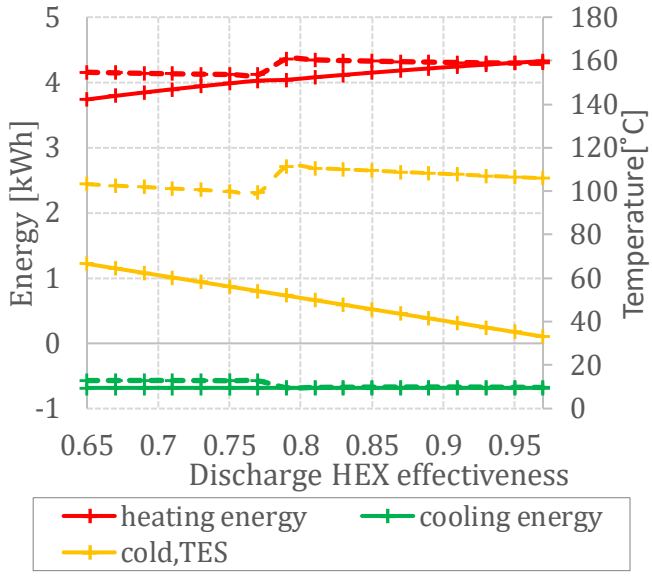


*Figure 6.4.a. Temperature of cold TES (right axis), heating and cooling energy (left axis) as a function of the effectiveness of discharge phase*

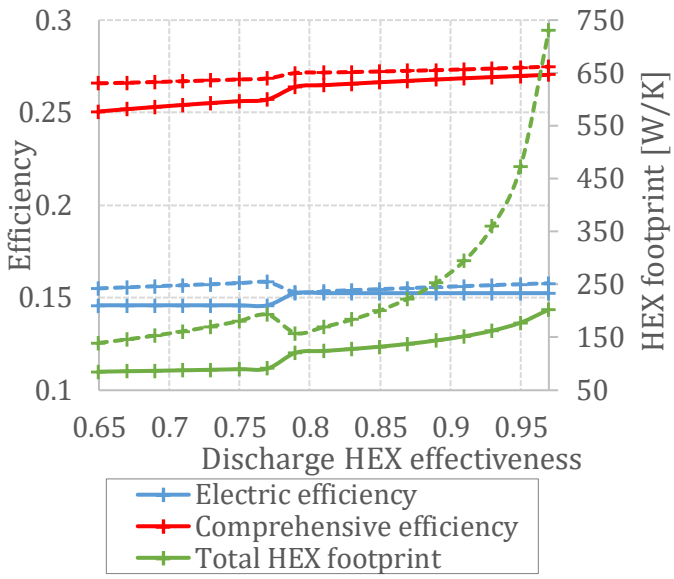


*Figure 6.4.b. T-CAES efficiencies (left axis) and the total HEX footprints (right axis) as a function of the effectiveness of discharge phase HEX.*

(Solid lines for the first configuration and dashed lines for the second one)

*Figure 6.4: Effect of the effectiveness of discharging HEX.*

### 6.3.5 . Effect of the maximum storage pressure

In order to isolate the effect of the number of compression stages they are fixed to two and the other parameters are chosen as follow:

1 The minimum pressure is $P_{min} = 25$ bars.
2 The effectiveness of HEX $\varepsilon_e = \varepsilon_c = 0.85$
3 $T_{h,TES}$ is the maximum possible value ($C_{min} = C_{max}$ for intercooling HEX).

Based on the perfect gas relation, the stored air mass and the time of charge are proportional to the maximum storage pressure so that the energy density rises linearly as evident in Figure 6.5.a. On the other side, the required charge time is greater than of the discharge one because of the former is proportional to $\beta^5$ (see equation 4.8), evidence for this is in Figure 6.5.a where the discharge to charge ratio declines mostly from 30 to 180 bars.

The inspection of Figure 6.5.b indicates that the heat stored and the heating energy increase significantly with the maximum storage pressure, which is originated from two major effects: the increase of the charge time and the rise of the heat power (due to the increase of the temperature output of each compression stage). Besides, the heat recuperated in the discharge phase increases, it can be seen by regarding the difference between points of the graph of the heat stored and of the heating energy in Figure 6.5.b. Simultaneously, for the past reasons, in Figure 6.5.c, the electric and the comprehensive efficiencies plunge down over than 36% and 23% respectively from their initial values at 23.2% and 33.5% as the pressure goes from 30 bars to 130 bars. Afterwards the

two electric and comprehensive efficiencies decrease moderately with a proportion of 12% and 8% respectively.

Regarding to the required HEX footprints shown in Figure 6.5.c, the total footprint decreases as high as 50% when the pressure rises to 130 bars and then as lower as 11%.

To sum up, increasing the ratio of maximum to minimum reservoir pressure $\delta$ below than 5.2 (which correspond to $P_{max} < 130$ when $P_{min} = 25$ ) entails substantial decrease on the system performance and the required footprints, while the energy density increases linearly. It is difficult to find a trade-off between the performances and the energy density so that the choice of the maximum pressure will be governed by the system application and cost.

However, Proczka et al. [14] showed that the cost consequences of operating a pressure vessel at too low pressure are more severe than at too high. As a result, keeping a low value of the ratio $\delta$ of the maximum to minimum pressures, let us say 2.5, and increasing the maximum and minimum pressure, as the simulation results illustrated in Figure 6.6, the efficiency drop is prevented while having the opportunity to achieve a high energy density as long as the maximum pressure increases. It is important to stress that this optimization opportunity entails the study of the possibility to construct a turbine or an AM, which operates at high pressures.

Finally, it is convenient to compare our results with the literature despite of the difference in the system configuration. The maximum pressure effect is in line with of Liu and Wang [20] and Facci et al. [13] but it was found by Facci et al. [13] that the ratio $\delta$ has a minor effect which caused by an assumption of variable pressure ratio of machinery.

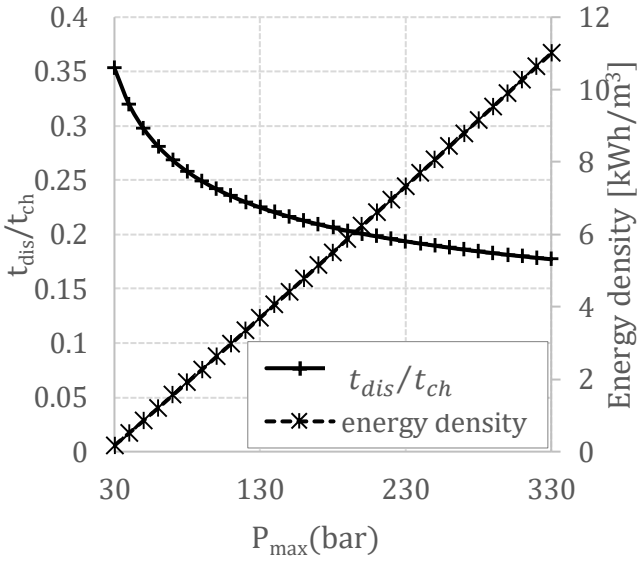


*Figure 6.5.a. Discharge to charge time ratio (left axis) and energy density (right axis) as a function of the maximum storage pressure.*

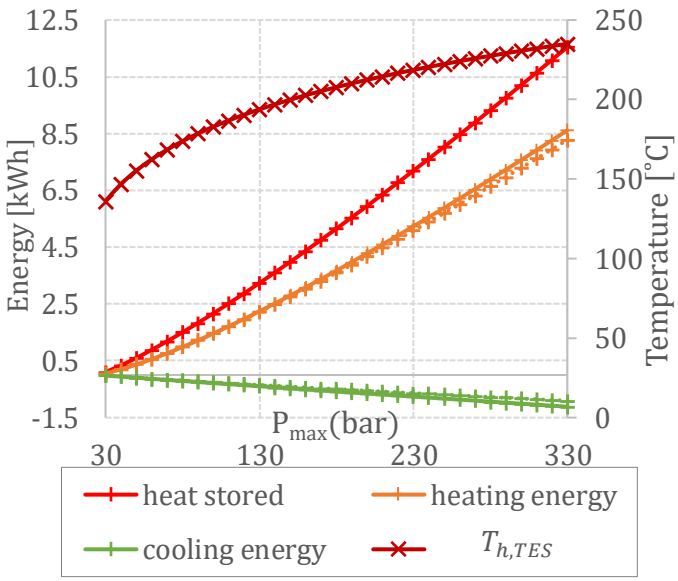


*Figure 6.5.b. High temperature of TES (right axis) and heating, cooling and stored energy (left axis) as a function of the maximum storage pressure.*

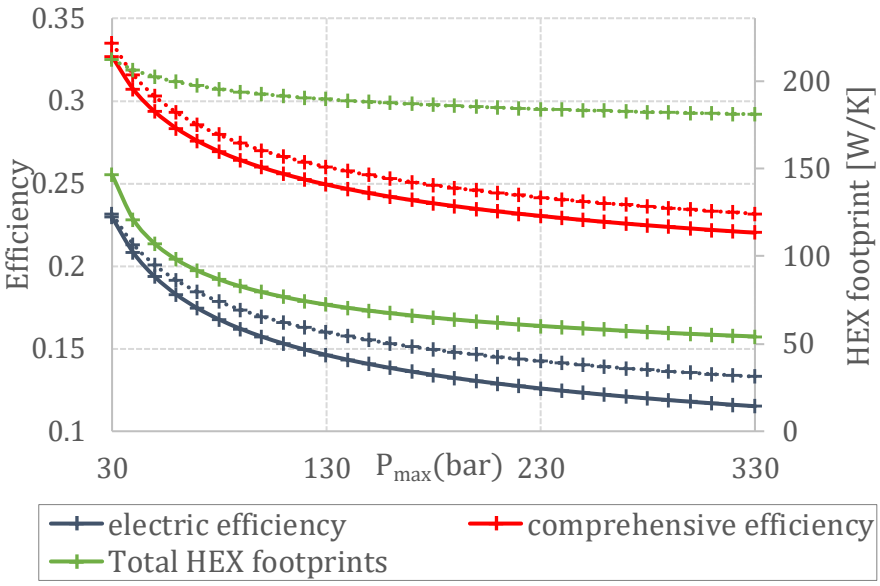


*Figure 6.5.c T-CAES efficiencies (left axis) and the total HEX footprints (right axis) as a function of the maximum storage pressure.*

(Solid lines for the first configuration and dashed lines for the second one)

*Figure 6.5: Effect of the maximum storage pressure.*

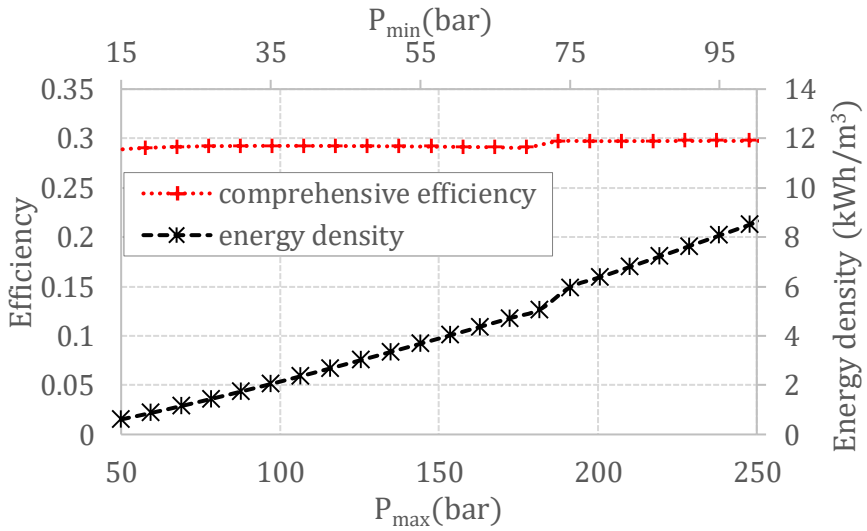


*Figure 6.6: Comprehensive efficiency (left axis) and energy density (right axis) at constant maximum to minimum pressure ratio as a function of the maximum storage pressure (the variation of the minimum storage pressure is shown in the secondary x-axis on the top)*

### 6.3.6 . Effect of the cooling energy

Based on the simulations results in the above sections, an optimal selection (stressing that an optimal and not the optimal) of the above parameters is listed in Table 6.2 where the maximum storage pressure is chosen by giving preference to the energy density.

Table 6.3 summarizes the effect of disabling the cooling energy on system energy output, performances and HEX footprints. Similarly, the efficiencies of the second configuration are very slowly higher than of the first configuration in all cases. Comparing the first two lines for each configuration, when the system operates without cooling the electrical efficiency is improved by 1.5% but the comprehensive efficiency is dropped by 4%, which underlines that the heating and cooling energy have greater effect on the comprehensive efficiency. Another important conclusion which can be deduced is that when the system is intended for a site without cooling demand the second configuration is more advantageous economically since the total HEX footprint is 22% lower than the first configuration, and when the cooling is needed in the system the opposite is true.

*Table 6.2: Optimal solution of the design parameters.*

| Parameters | value |
|---|---|
| Temperature of h,TES [˚C] | 140 |
| effectiveness of compression HEX | 0.85 |
| effectiveness of expansion HEX | 0.82 |
| Maximum pressure of compressed air [bar] | 200 |
| Number of compression stages /expansion stages | 3/one turbine stage and an AM |

*Table 6.3: Energy outputs, efficiencies and total HEX footprints of the two configurations with and without enabling the cooling energy.*

| | Cooling energy (kWh) | Electrical efficiency (%) | Comprehensive efficiency (%) | Total HEX footprint (W/K) | Heating energy (kWh) |
|---|---|---|---|---|---|
| **First configuration** | 0 | 16.66 | 22.53 | 193.8 | 2.61 |
| | 0.68 | 15.25 | 26.53 | 125.1 | 4.10 |
| **Second configuration** | 0 | 16.90 | 23.75 | 149.2 | 3.04 |
| | 0.67 | 15.40 | 27.19 | 177.4 | 4.34 |

## 6.4 . Characteristics of the micro-scale T-CAES

It is of great practical importance to derive all the parameters of the subsystems so that the output parameters of each compound are illustrated in the Tables 6.4, 6.5 and 6.6 for the first configuration enabling the cooling production. The optimal parameters given in Table 6.2 are adopted.

As illustrated previously in Table 6.3, the electric round trip efficiency is low at 15.25%. Evidences for that can be found in Table 6.4 and the main causes are as follows:

1 The electric energy input was 11.09 kWh but the heat stored was 52 % lower at 5.9 kWh. This is not only related to the effectiveness of HEX but mainly to the unavoidable heat lost by the volumetric compressors (expressed by its polytropic coefficient).
2 Since the compression to expansion pressure ratio is high, the ratio of the heat recuperated at 1.22 kWh to the heat stored at 5.9 kWh is at about 21%. In other words, important losses are located on the expansion valve restricting the use of available heat. Justifications of that were illustrated in Chapters 3 and 5.
3 Referring back to the thermodynamic to the existing mechanical conversion of turbine and air motor, which are 0.62 and 0.30 respectively. Thus, it is predictable to have a low round trip efficiency, which is on good agreement with the founding of the optimization studies previously mentioned in Chapter 2: the electric efficiency is mainly affected by the efficiency of turbines and compressors.

In addition, in spite of the electric power output of expanders (2.06 kW) is 65% lower than of the compressors (3.17 kW), the discharge time (51 minutes) was 24 % lower than of the charge phase which is related to the poor electric efficiency.

In Table 6.5, as predicted in the model, the pressure losses in the two first intercooling heat exchangers can be neglected compared to the last HEX. Consequently, the pressure losses in the discharge phase HEX can be ignored when the minimum to maximum pressure ratio $\delta$ is high. An important feature which can be noticed which is the heat exchanger footprint of the first HEX is higher than the last one due to the fact that: in spite of the same value of effectiveness, the LMTD changes according the temperature levels. Hence, the effectiveness of the last HEX can be much higher in order to increase the energy density and the round-trip efficiency of the system (see Section 6.3.3).

In Table 6.6, in spite of the expansion ratio of the turbine is lower than the AM, the power delivered by the turbine is higher than of the AM, which is linked to the low expansion temperature of the AM (see chapter 3 for further explications) and its lower efficiency of conversion. Since the mass flow rate of the discharge phase is higher than of the charge phase, the heat duty of the discharge HEX is greater. Thus, the footprints of this later are the most important (about three times of the charge HEX).

*Table 6.4: Output parameters of the charge phase for the first configuration.*

| | **Stage 1** | | **Stage 2** | | **Stage 3** | | **Air tank** |
|---|---|---|---|---|---|---|---|
| **Compressors** | **in** | **out** | **in** | **out** | **in** | **out** | **in** |
| | | **HEX 1** | | **HEX 2** | | **HEX 3** | |
| **HEX** | | **in** | **out** | **in** | **out** | **in** | **out** |
| Pressure [bar] | 1.01 | 6.18 | 5.90 | 35.97 | 34.35 | 209.41 | 200.00 |
| Pressure drop [bar] | | 0.28 | | 1.62 | | 9.41 | |
| Density [kg/m$^3$] | 1.17 | 4.95 | 6.37 | 27.04 | 36.59 | 155.41 | 212.47 |
| Air temperature [˚C] | 30.00 | 161.97 | 49.79 | 190.38 | 54.06 | 196.50 | 54.98 |
| Water mass flow [kg/s] | | 0.0011 | | 0.0013 | | 0.0013 | |
| HEX footprint [W/K] | | 23.16 | | 16.49 | | 15.79 | |
| Heat Power [kW] | | 0.483 | | 0.587 | | 0.610 | |

*Table 6.5: Output parameters of the discharge phase for the first configuration.*

| | HEX-1 | | HEX-2 | | | |
|---|---|---|---|---|---|---|
| **HEX** | **in** | **out** | **in** | **out** | | |
| | | **Turbine** | | **AM** | | |
| **Expanders** | | **in** | **out** | **in** | **out** | |
| Power [kW] | | 1.347 | | 0.715 | | |
| Pressure [bar] | | 25.00 | 6.00 | 6.0 | 1.01 | |
| Air temperature [˚C] | 30.00 | 111.0 | 30.0 | 30.0 | -15.2 | |
| Water temperature [˚C] | 48.8 | | 0 | | | |
| Heat recuperated [kW] | 1.488 | | 0 | | | |
| Water mass flow [kg/s] | 0.004 | | 0 | | | |
| HEX footprint [W/K] | 70.66 | | 0 | | | |

*Table 6.6: Main output parameters of the model for the first configuration.*

| **Charge phase** | |
|---|---|
| charge time [h] | 3.5 |
| air mass flow [kg/s] | 0.0043 |
| air stored [kg] | 54.1 |
| water stored [kg] | 46 |
| **End of Storage phase** | |
| temperature of TES [˚C] | 134.5 |
| air temperature [˚C] | 30 |
| air pressure [bar] | 186.7 |
| **Discharge phase** | |
| discharge time [h] | 0.82 |
| water remained on h,TES tank [kg] | 12.26 |
| water pumped to cold,TES tank [kg] | 33.73 |
| **Energy balance** | |
| electric energy input [kWh] | 11.1 |
| heat stored [kWh] | 5.88 |
| heat loss [kWh] | 0.562 |
| recuperated heat [kWh] | 1.22 |
| heating energy [kWh] | 4.1 |
| cooling energy [kWh] | 0.68 |
| electric energy output [kWh] | 1.7 |

## 6.5 . Conclusions and perspectives

Based on the two configurations of the trigenerative compressed air energy storage proposed in chapter 4. An optimization via a parametric study is conducted for the two configurations in order to provide a guideline for an optimal selection of the design parameters. The main contribution of this study is that the optimization is based on the investigation of the mutual effect of the parameters and their impact on the criteria listed above. The following conclusions could be drawn:

1 The temperature level of the hot thermal energy storage has a marginal effect on the system efficiencies (not more than 1.5%). However, the accurate temperature level should be high to ensure a minimal number of expansion stages and to lower the total heat exchanger footprints at constant number of stages (120˚C or 150˚C and 90˚C or 130˚C were the optimal values for the first and second configurations respectively).

2 The optimal choice of the number of compression stages and the effectiveness of heat exchangers is based on a compromise between the system efficiencies (comprehensive efficiency and electrical efficiency) on one side, and the number of expansion stages and the heat exchangers footprints on the other side. Three compression stages were sufficient when the maximum pressure reaches 200 bars.

3 The choice of the maximum storage pressure has a significant effect on the system efficiencies (with a deviation of up to 12%) and the energy density. There is no trade-off between these criteria and the optimal choice will be based upon the cost and the benefits of the system.

4 There is no need to design the heat exchanger with very high effectiveness since it leads to an adverse effect on the whole system efficiency (because of pressure losses) and rises the required footprints. The optimal range of effectiveness is found between 0.79 and 0.85.

5 Enabling the cooling energy at the last expansion stage has a greater effect on the comprehensive efficiency (rises by 4%) than the electrical efficiency (drops by 1.5%) which provides support to the benefits of the system configurations without preheating in the discharge phase proposed previously in the literature.

6 The two configurations studied present low differences in terms of global efficiencies. On the other hand, it is economically more viable in terms of heat exchangers footprints to adopt the first configuration when the system is intended to produce cooling energy and the second configuration otherwise.

At micro scale applications, based on existing technologies and applying an optimal choice of the design parameters, the electrical efficiency is low at 17%. On the other hand, the cooling and heating energy improves the system efficiency by almost 11.5%. The main causes of the low values of efficiencies and the possible solutions are illustrated as follow:

1. In order to keep a high energy density, the maximum storage pressure should be high so that the losses in the throttling valve are significant. This can be avoided by:
   - Keeping a low ratio of the maximum to minimum pressure while increasing the values of this later. This raises the question to develop a new expansion micro-scale machinery which operates at high pressure.
   - Applying a machinery with variable expansion pressure ratio as proposed by Han and Guo [51]. However, the study of the technical feasibility in terms of technology and coupling the thermal energy storage compound of such solutions are needed.
2. At a micro-scale, the efficiency of turbines and notably the air motor are very low. Increasing the scale of the system and replacing the air motor with a scroll expander (despite its low expansion ratio) makes the application more interesting in terms of the global efficiencies.

Finally, it can be deduced that the parametric optimization procedure developed based on the mutual effect of parameters is able to provide optimal solutions for the design of trigenerative compressed air energy storage systems. The importance of this optimization procedure lies in its

ability to be extended to optimize the adiabatic compressed air energy storage since this later form a part of the configuration introduced here. Next chapter will focus on the integration of an economic model with the aim of finding the accurate optimal techno economic solutions, especially for the maximum storage pressure.

# CHAPTER 7 - TECHNO ECONOMIC STUDY OF T-CAES

## 7.1 . Introduction

The development of cost models for innovative electrical energy storage technologies has received limited attention in the literature, especially for CAES, whereas it is a crucial step for its commercialization.

For large scale A-CAES, let us remember that the cost of A-CAES is not well reported and quantified as shown in Table 2.3 of Chapter 2. However, Rogers et al. [1] conducted a thermodynamic and economic review on different CAES technology, the cost of A-CAES in 2012 varied in a wide range, between 850 and 1870 USD/kW. The studies proposed in the literature show different conclusions in regards to the economic perspective of the A-CAES depending on the application context (site location and application on load shifting or renewable energy integration), the design condition (such as expansion and compression ratio) and the system configuration. Kapila et al. [79] developed an economic model for PHS, C-CAES and A-CAES based on the accounting for the cost of each component as a function of the output power plant scale ranging from 298 to 498 MW. The A-CAES was evaluated on the basis of maximum storage pressure at 160 bars and global expansion ratio of 140. It was found that A-CAES is not attractive with a cost of 375-480 USD/kWh.year. In line with this, Huang et al. [80] carried out a techno-economic study of C-CAES and A-CAES with roundtrip efficiency of 52.6% and 64.7% respectively and an electric output power of 140 MW. These systems were studied in the North-Ireland electricity market context for peak-hours shifting. The specific capital investment cost was found very high at 738 euro/kW for C-CAES and 907 euro/kW for A-CAES.
On the contrary, Meng et al. [81] performed a process design and economic study on applying the A-CAES on a wind farm. Their results concluded that the total annual cost per kWh (named levelized cost of electricity) of the system is lower than conventional power plants (natural gas combustion turbine) and some renewable energies such as hydropower.

For small scale CAES, little study concerning the economic modeling and evaluation of the T-CAES was published, expect for the T-CAES proposed by Lv et al. [19] (see Chapter 2). The economic profit in terms of annual cost saving was evaluated without paying attention to the investment cost of the system.

Concerning the techno-economic optimization, in the hybrid system of A-CAES and thermal energy storage TES proposed by Houssainy et al. [56] (see Chapter 2), with the objective of minimizing the investment cost and maximizing the efficiency. A parametric optimization was conducted on the pressure input of turbocharger and the required distribution of energy between thermal and compressed air. A trade-off solution was found and it is demonstrated that the system is competitive from a capital cost perspective.
Yao et al. [82] performed a thermodynamic and economic modeling of a system composed from a gas engine, small scale CAES and a refrigeration cycle based on ejector. The economic model is expressed as a function of the equipment size such as the power rating of compressors and turbines and the area of heat exchangers. Then, the study focused on multi-objective optimization to find an optimal solution between economic and thermodynamic performances.

From this short literature review, we can conclude that a rigorous economic model of the component of the T-CAES, as well as an optimal techno-economic solution of the design parameters are important points to solve.

Hence, this chapter focuses on the following aspects:

1. Developing an economic model of the cost of equipment of T-CAES plant at small scales.
2. Analyzing the cost model in order to deduce the main parameters influencing its cost.
3. Performing the techno-economic optimization via parametric study.
4. Comparing the plant cost with its actual competitive solution such as electrochemical batteries.

Since the context of our study is to apply our system in off-gird northern sites in Canada, we proceed to omit the cooling energy. Consequently, the air motor is eliminated and the output pressure of the last turbine stage is at the ambient pressure.

## 7.2 . Economic Modeling of the components of the T-CAES

### 7.2.1 . General Method

The most accurate cost estimate of the capital cost of equipment is provided by a current price quotes from vendors. However, quotes do not provide the variation of the cost of equipment with its size. Another alternative is to use approximations or graphs available in chemical engineering textbooks or related softwares.

Based on different approximation methods and data from specific vendors. Many cost estimation programs can be used such as AspenPEA, CapCost, EconExpert [83,84]. However, these programs may not involve all the equipment of T-CAES, especially the new developed turbines and pressurized air vessels so that, it is more convenient to use the approximation formulas.

In this study, the cost model of compressors and heat exchangers are based on the data reported in [84] which are taken from Richardson Engineering Services, Inc. On the other hand, vendor quotes are taken on for other components (turbine and pressure vessels).

Nevertheless, Feng and Rangaiah [83] compared the results of five cost estimation programs and found that there is a significant deviations between each programs for equipment which is attributed to the cost data sources. In order to cope with this problem, the result obtained from the model presented in this study were compared to available cost data obtained at discrete points from Matches Company [85]. In cases where a significant deviation between the results of our model and of Matches, a correction factor is used in order to maintain an error less than $\pm$ 25 %. Note that Matches is a reliable source which provides competitive cost engineering studies for process development design and for first commercial applications.

As a general rule, the cost of each component depends on the capacity, the operation pressure, the materials used and finally it should be adjusted to the time of purchase. In the following sections, we discuss each of these points and the approximations used.

### *Effect of capacity*

The cost of equipment does not increase proportionally to the capacity. The most common relation between these two parameters is provided by Equation 7.1. Once the cost $C_{A_0}$ at a defined capacity $A_0$ is known, the cost at any capacity can be found.

$$C_A^0 = C_{A0}^0 . \left(\frac{A}{A_0}\right)^z \tag{7.1}$$

where C denotes the capital cost, A the capacity and z ($z \leq 1$) is the cost exponent which depends on the type of equipment.

Based on cost data obtained from vendors, a more accurate approximation formula (Equation 7.2) has been used in cost estimation programs [83],[84].

$$\log_{10}(C_A^0) = K_1 + K_2 \log_{10}(A) + K_3 [\log_{10}(A)]^2 \tag{7.2}$$

In order to express explicitly the cost vs capacity. Equation 7.3 derived from Equation 7.2 is as follows:

$$C_A^0 = 10^{K_1} A^{K_2} e^{K_3 . \frac{[\ln(A)]^2}{\ln(10)}} \tag{7.3}$$

where $K_1, K_2 \; and \; K_3$ are constants depending on each component.

### *Effect of system pressure and materials*

The capital cost $C_A^0$ mentioned in previous section refers to a defined base condition of pressure and carbon steel as construction material. Deviation from these conditions are handled by multiplying the base cost $C_A^0$ by factors accounting to materials and maximum design pressure. In textbooks, this method is called the equipment module costing technique and the multiplication factors are named the bare module cost factors. Equation 7.4 is used to calculate the actual equipment cost.

$$C_A = C_A^0 . F_p . F_M \tag{7.4}$$

where $C_A$ is the capital cost at the application conditions, $C_A^0$ is the cost at base conditions. $F_p$ and $F_M$ are the bare module factors of operating pressure and material respectively.

The material factors can be found directly from tables in textbooks. However, compressed air and pressurized water does not require specific materials, thus it is convenient to employ the carbon steel so that: $F_M = 1$.

The pressure factor varies according to Equation 7.5 in the same form of Equation 7.3.

$$F_p = 10^{K_{p1}} P^{K_{p2}} e^{Kp_3 . \frac{[\ln(P)]^2}{\ln(10)}} \tag{7.5}$$

where $K_{p1}, K_{p2} \; and \; K_{p3}$ are constant values varying with each component.

The pressure factor of pressurized vessel is quite different from other components due to the fact that the pressure influences significantly the required materials to manufacture the vessel. Based

on the ASME code (American Society of Mechanical Engineers) for pressure vessel design, the expression of pressure factor of carbon steel vessels as reported in [84] is shown in Equation 7.6.

$$F_{P,res} = \frac{\frac{(P+1)D}{2[850-0.6(P+1)]} + 0.00315}{0.063} \qquad for\ t_{res} > 0.0063m \tag{7.6}$$

$$F_{P,res} = 1 \qquad for\ t_{res} < 0.0063m$$

where t refers to thickness and D the diameter of the reservoir (or tank).

The relation is strictly validated when $t_{res} < {}^{D}/_{4}$, which means for $D < 0.4\ m$ the pressure should be lower than 320 bars.

### *Effect of time of purchase*

It's obvious that the cost of products increases as a result of the rise of the cost of wages, services and raw materials. This change of economic conditions is known by the term of cost inflation. It is expressed by the cost index which varies each year.it can be accessed from chemical engineering issues or the website mentioned in [86].

Once the cost of equipment at any time is known, the cost at a desired time is achieved by applying Equation 7.7.

$$C_{y,i} = C_{y_o} \frac{I_{y_i}}{I_{y_0}} \tag{7.7}$$

where C is the cost and I is the cost index. Subscripts: $y_i$ refers to the year of purchase and $y_o$ refers to base year when cost is known.

## 7.2.2 . Application of the method on T-CAES plant.

### *Calculation and Analyzing of Pressure factors*

Beginning with compressors and turbines. It is equal to 1 for turbines and compressors according to the reference [84]. Notwithstanding, it was found that it is equal to 1.3 for compressors when the pressure ratio is higher than 69 bars according to data of Matches [85].Since higher pressure is associated with using more materials, It seems that the result of this latter is more accurate, so it is taken into account.

The required coefficients for the calculation of the pressure factor (see Equation 7.5) of heat exchangers are shown in Table 7.1. It can be seen that the cost of the last heat exchanger is the highest and can achieve a value of more than 3 times of the cost of the previous HEX.

*Table 7.1: Pressure factors of heat exchangers [6].*

| $k_{p1}$ | $k_{p2}$ | $k_{p3}$ | **Pressure Range (bars)** | $F_{p,HEX}$ |
|---|---|---|---|---|
| 0 | 0 | 0 | <5 | 1 |
| -0.00164 | -0.00627 | 0.0123 | [5;140] | [1;1.1] |
| 13.1467 | -12.6574 | 3.0705 | [140;300] | [1.33;3.4] |

As to pressurized vessel, the effect of the maximum storage pressure on the rise of the pressurized tank cost is shown in Figure 7.1 (by plotting the function of Equation 7.6 for D=0.21 m). When the pressure is higher than 26 bars, the pressure factor rises dramatically (almost linearly) and achieves a value of 8.67 at 320 bars. Hence, comparing this with other components, the operation pressure has a major effect not only on the cost of air storage volume but also on the cost of the T-CAES plant. Thus, an optimal economic value of storage pressure is highly needed.

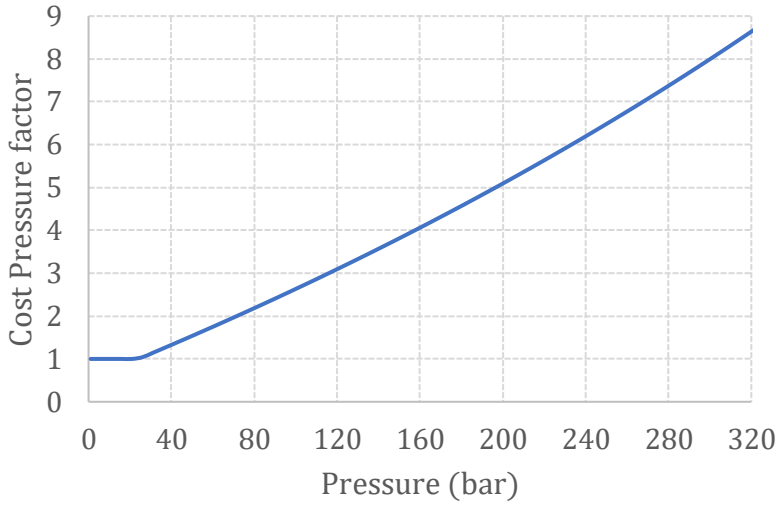


*Figure 7.1: Variation of cost pressure factor of tank versus maximum storage pressure (fixing the tank diameter at 0.21 m).*

## *Capital Cost calculation*

Above all, it should be noted the capital cost values are taken from the approximation presented in [84] and [85] with the base years 2001 and 2014 respectively. In this study, the costs were adjusted for the year 2017 due to the inflation data availability. They are adjusted by using Equation 7.7. Based on ref [86]:the cost index for the base years 2001 in [84], 2014 in [85]) and our base year 2017 are the following:

$I_{y_{,2001}} = 397, I_{y_{,2014}} = 576.1 \; and \; I_{y_{,2017}} = 567.5$

**Mechanical components**

The micro-turbines employed in our system does not correspond to classical turbines so that cost data are not available in textbooks. Alternatively, they were collected from DEPRAG Company [87] and plotted in Figure 7.2. The values were interpolated in order to have an equation in the form of Equation 7.1 (power function) thus, the approximation formula of the cost of turbine is:

$$C_{A,turbine} = 2012{,}2\, A^{0.814} \tag{7.8}$$

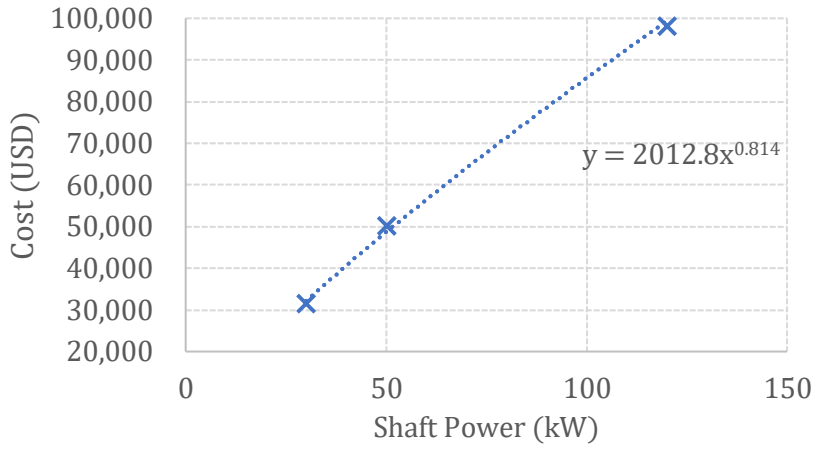


*Figure 7.2: Values and interpolated function of the cost of micro-turbines versus shaft power.*

As for compressors and HEX, the constant coefficients required to account the capital cost are retrieved from ref [84] and presented in Table 7.2.

*Table 7.1: Coefficients required for the calculation of capital cost of mechanical components (base year 2001 for compressors and HEX [6]).*

| | | Equation 7.1 | | | | | Equation 7.3 | |
|---|---|---|---|---|---|---|---|---|
| | **type** | **$k_1$** | **$k_2$** | **$k_3$** | **Capacity** | **Range** | **z** | **range** |
| **Compressor** | reciprocating, centrifugal | 2.2897 | 1.36 | 0.1027 | fluid power (kW) | >450 | 0.84 | <450 |
| **Heat exchanger** | double pipe | 3.344 | 0.2745 | -0.0472 | area($m^2$) | [1;10] | 0.59 | <1 |
| | shell and tube | 4.3247 | -0.303 | 0.1634 | area($m^2$) | 30 | 0.59 | >10 |
| **Turbine** | radial, axial | | | | shaft power (kW) | | 0.814 | <500 |

**Air reservoirs**

As regards to the cost of air reservoirs, Proczka et al. [14] carried out a detailed study on the material and manufacturing cost of cylindrical vessels. They found that for a fixed storage pressure, the cost declines with the increase of the length to radius ratio. Though, the cylinder length is limited by shipping and manufacturing constraints [14] and its value should be fixed. Consequently, for a fixed reservoir volume and length, using higher number of pressure vessels with small diameter is more economical than using one reservoir with larger diameter [14].
To conclude, for a desired storage volume, each vessel should be chosen with the highest length to radius ratio and the total volume is acquired by the number of the vessels.

Consulting the technical data of vessels from many manufacturers, it is found that the length to radius ratio is around 6 and the length ranges from 1 to 2. These dimensions correspond to the dimensions of tanks used in the experimental set up (L/D=6.6 and L=1.4m), thus they were adapted.

Based on multiple vendors (Fjords Processing, KS Industries, Modern Custom Fabrication Inc.), Houssainy et al. [56] reported that the cost of tanks is proportional to the volume as expressed by Equation 7.9 (consistent with Equation 7.1 with z=1). By replacing the total volume with the product of the number of reservoirs and the volume of each one, and multiplying by the pressure factor the actual cost of air storage device is calculated by Equation 7.10.

$$C_{V,res}^{0} = 1000.V_{res} \tag{7.9}$$

$$C_{V,res} = 1000.F_{P,res}N_{res}V_{res,i} \tag{7.10}$$

where the index i refers to tank i.

## 7.3 . Methodology of the technoeconomic analysis and cost model validation

### 7.3.1 . Methodology

Based on the results presented in chapter 6, the second configuration is more beneficial for the T-CAES without cooling. Thus, the system can be regarded as an A-CAES with excess energy heating production. Besides, the procedure of finding the optimal design remains applicable in this case.

In practical applications, we are interested on investigating the system cost as a function of its power and energy output.

Remember that in the model developed in Chapter 4, the power output is settled as an output parameter and the mass flow rate in the discharging phase is an input parameter. In order to inverse the role of these two parameters, the iteration procedure presented in Figure 7.3 is integrated in the model. The mass flow rate is increased from its initial value until finding the value of the desired output power.

The air volume required to satisfy the output energy demand is accounted by Equation 7.11. The number of reservoirs is calculated by Equation 7.12.

$$V_{total} = \frac{\dot{m}_e.t_{dis}.r.T_{amb}}{P_{\max(t)} - P_{min}} \tag{7.11}$$

$$N_{res} = \frac{V_{total}}{V_{res,i}} \tag{7.12}$$

where $V_{res,i}$ is the volume of each reservoir. $P_{\max}(t)$ is the maximum storage pressure at the end of the storage phase.

The analysis of the cost model presented in the previous section demonstrates that the maximum storage pressure has the principal effect on the system cost. Consequently, this parameter is the subject of the techno-economic optimization.

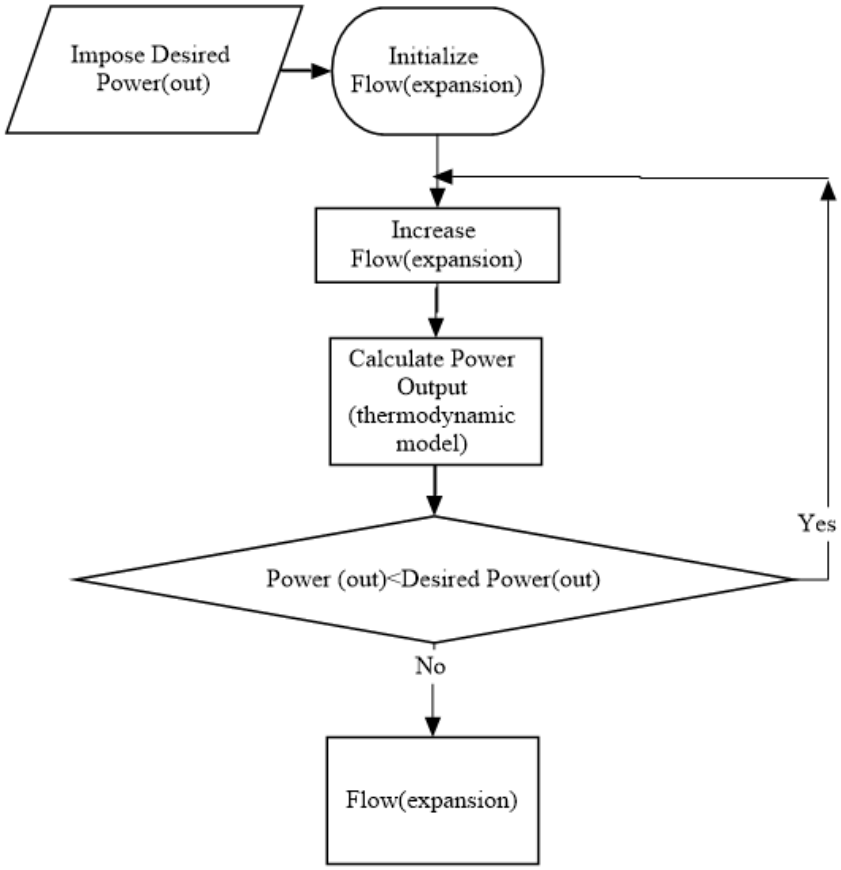


*Figure 7.3: Algorithm of finding the expansion mass flowrate for an imposed power output.*

The mass of stored air can be achieved whether by increasing the maximum air pressure with decreasing the volume (number of tanks) or by rising the volume with reducing the air pressure (see Equations 7.11 and 7.12). In line with this, Equation 7.10 points out that the cost is a function of these two factors (number of reservoirs and pressure factor). This reveals a potential solution to minimize the air storage cost, whilst always taking account of the round-trip efficiency of the T-CAES. Thus, the question is how the storage pressure affect the number of reservoirs and the cost of air storage. This will be answered by conducting a parametric study on the storage pressure.

Since the thesis context is to adopt the system at small scale applications, it is mandatory to define rigorously the range of power of this latter. As seen in Chapter 2 the rated power of small scale above-ground CAES was defined in the range of 0-3 MW. However, this general definition is no longer true when it comes to relate the system power scale to the turbine scale. Thus, it is more convenient to define the power scale according to the turbine.

It is known that small or micro scales turbines differs from the conventional gas turbines by the admission pressure. By consulting technical data of many manufacturers of micro-turbines such as Capstone and Siemens, the input pressure still lower than 25 bars. The highest micro-turbine pressure input is of that developed by Deprag Company, as stated in Chapter 4.

Returning to the micro-turbine scale definition, Backman and Kaikko [88] stated that there is no unique assessment of this scale in the literature, it is defined lower than 1MW, 500 kW, 100 kW or even 15 kW. In this study, we adopt the scale of [1;500] kW.

The total to total isentropic efficiency of radial micro-turbines was reported by Galanti and Massardo [89] in the range of 25-500 kW. Their results show that the turbine efficiency is almost constant at 0.86 when the power is higher than 100 kW, otherwise it varies between 0.84 and 0.86. As a first approximation, in this study, the power range [1;500] is separated according to the turbine type and its total to total efficiency, as follow:

1. Axial micro turbine: $\eta_{tt} = 0.65$ for $\dot{W}_{el,e} < 30\ kW$ (see Chapter 4).
2. Radial micro turbine: $\eta_{tt} = 0.85$ for $\dot{W}_{el,e} > 30\ kW$.

Once the optimal pressure is determined, it is important to dissect the cost of each component as a function of energy scales, power scales, and time of discharge to charge ratio. Owing to practical applications of the system, the power output and the time of discharge are considered to be the conditions on which the system will be designed.

By adopting the optimization procedure used in Chapter 6, the optimal design parameters are derived. Besides, the following parametric analysis were performed:
In the first place, in order to dissect the cost variation of each component in the same scale range, the electric power of compression and expansion were assumed to be equals. The time of discharge is considered to be 3 hours.
In the second place, a potential application of the system is considered with a discharge time of 6 hours and charging time of 8 hours (discharge to charge time ratio of 0.75). These values were assumed anticipating an excess of renewable energy of 8 hours and a need for a desired value of output power during 6 hours. The compressor power is calculated by Equation 7.11, derived from Equation 4.72.

$$\dot{W}_{el,c} = \alpha . \frac{\dot{W}_{el,e}}{\eta_{el,g}} \tag{7.11}$$

where $\alpha$ is the discharge to charge ratio.

Finally, the system will be compared to its competitive storage solution, which is the commonly used lead-acid electrochemical battery. The comparison is based on the annual capital cost expressed by (USD/kWh.year) for a supposed time of 30 years. The prospective T-CAES is purchased once due to its long life time (30-40 years), while the batteries should be bought 6 times taking into account its lifetime of 5 years.
The comparison will be carried out in regards to the comprehensive and the electric efficiency of the T-CAES. In other terms, the output energy is taken, for the first time, equals to the electric energy delivered by turbines, and for the second time, the equivalent electric energy of heating (Equation 7.12) is added in order to assess the benefit of the trigeneration option.

$$E_{el,out,equivalent} = \dot{W}_{el,total} . t_{dis} = \left( \frac{\dot{Q}_{heting}}{COP_{ref}} + \dot{W}_{el,e} \right) . t_{dis} \tag{7.12}$$

### 7.3.2 . Model reliability

The cost model was developed from many sources of information; thus, the results should be compared in order to verify the model reliability. Since the pressurized tanks and turbines costs were based on quotes, there is no need to verify. On the other hand, for compressors and heat exchangers, the cost data collected from Match Company were compared to the model results and shown in Table 7.3.

The deviation between the costs of compressors does not exceed 11.5% and becomes lower when the compressor power range increases. Similarly, the cost difference of shell and tube heat exchanger (when the area is higher than 10 $m^2$) is lower than 21.2 %. At the beginning, the cost results are overestimating by comparison to cost data of Matches, then it decreases and becomes lower estimating as the values of heat exchanger area are high. For double pipe heat exchangers, the cost results were consistent (deviation lower than 25%) after multiplying by a correction factor of ½. Otherwise, the cost model results when the heat exchanger type is changed (at an area of 10 $m^2$) would shows a significant increase which seems illogical (see cost curves on any textbooks).

*Table 7.2: Comparison between the results of the cost model and cost data of Matches Company.*

| | **Present model** | **Matches Company** | **Deviation (%)** |
|---|---|---|---|
| **Power (kW)** | Compressor (pressure ratio 70 - N stages[1]) | | |
| 29.4 | 33,530 | 37,900 | -11.5 |
| 75 | 73,634 | 78,900 | -6.7 |
| 147 | 129,570 | 137,300 | -5.6 |
| 463 | 339,716 | 343,800 | -1.2 |
| **Area ($m^2$)** | Heat exchanger (30 bars) | | |
| 0.4 | 919 | 1,100 | -16.5 |
| 1 | 1,578 | 1,200 | 24.0 |
| 10 | 2,664 | 2,300 | 13.7 |
| 20 | 19,279 | 17,100 | 11.3 |
| 30 | 24,489 | 24,100 | 1.6 |
| 80 | 43,680 | 55,400 | -21.2 |

## 7.4 . Results and discussions

### 7.4.1 . Optimal storage pressure range

Fixing the energy output at 30 kWh, the required number of reservoirs and its cost as well as the electric efficiency are shown in Figures 7.4 and 7.5. The number of reservoirs decreases substantially as the pressure decreases from 40 bars to 125 bars, and then it declines slowly. This due to the fact that the pressure and the volume are inversely proportional for a fixed air mass. Figure 7.5 reveals that the cost required to store the compressed air is mostly governed by the volume when the pressure is lower than 120 bars. Afterwards, the cost drops slowly as the pressure reaches 200 bars and remains almost constant in the range of [200; 300] before it slightly grows up when the pressure is higher than 300 bars. This due to the gradual decrease of the reservoir number (Figure 7.4) and the rise of the pressure cost factor. As long as the electric efficiency have only gradual decrease from 120 bars, the optimal storage pressure is in the range of [120; 200] from a techno-economic point of view.

On account of Equation 7.10, the cost variation is independent of the initial conditions (initial volume), thus the optimal range of storage pressure remains the same whatever the output energy as demonstrated in Figure 7.6.

[1] The number of stages N is not provided by Matches Company

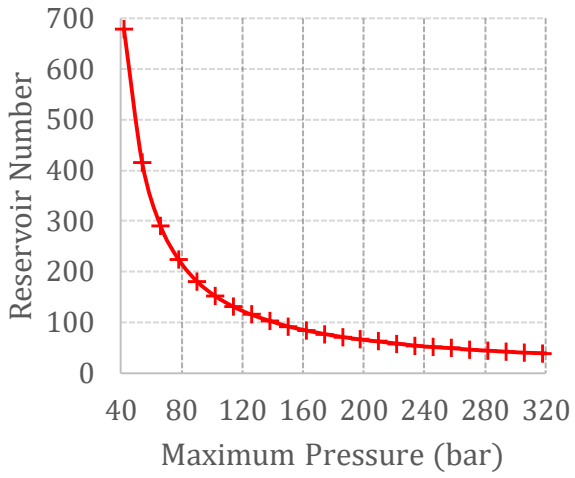


*Figure 7.4: Variation of reservoir number as a function of maximum storage pressure (output energy of 30 kWh).*

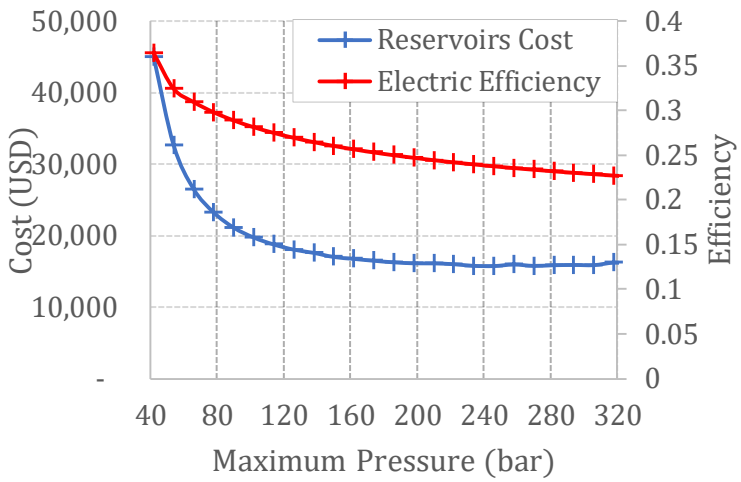


*Figure 7.5: Variation of reservoir costs and electric efficiency as a function of maximum storage pressure (output energy of 30 kWh).*

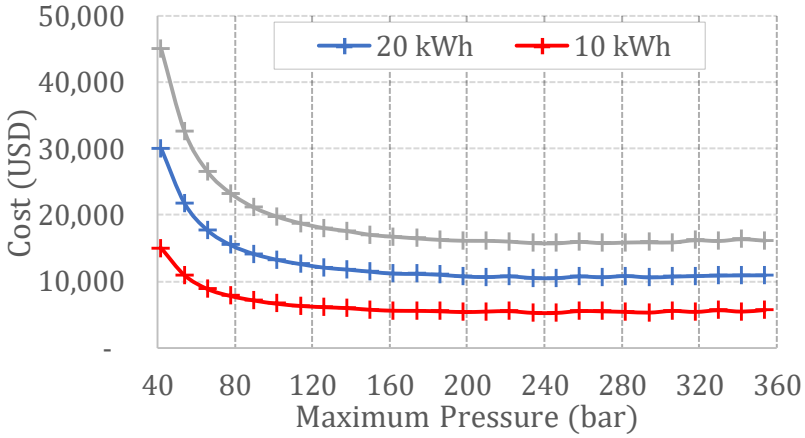


*Figure 7.6: Variation of reservoir costs as a function of maximum storage pressure and output energy.*

## 7.4.2 . Cost of the components and the plant

Based on the above section, the storage pressure can be chosen in the range of [120; 200]. However, the cost of the plant is studied in the following sections with the aim of minimizing the capital cost and use standardized pressure vessels, so the maximum pressure is fixed to 200 bars. The design parameters at this pressure were shown in Table 6.2, with a difference of changing the AM by a turbine stage.

The round-trip electric efficiency and comprehensive efficiency are shown in Table 7.4. Owing to the use of air turbine instead of the air motor, the efficiencies are higher than of those obtained in Chapter 6. The results are separated according to the power range [1;30] and [30;450]. A higher value of performances in the second range are achieved due to the enhancement of turbines efficiency.

*Table 7.3: Round trip electric efficiency and comprehensive efficiency of the proposed system.*

| Output Power range (kW) | Electric efficiency (%) | Comprehensive efficiency (%) |
|---|---|---|
| [1;30] | 21.2 | 32.5 |
| [30;450] | 32.3 | 40.5 |

### *1st Case: Same input and output power*

In this case, only the first range of power [1; 30] is studied. Taking into account the round-trip electric efficiency of 21.2 %, the required charging time is approximately 14 hours. The variations of the cost of each component per kWh versus the output energy are shown in Figure 7.7.

Firstly, with a fixed time of charge and discharge, it is apparent that the electric power and the energy output vary proportionally. Secondly, as expected, the cost of one kWh of all components (expect the reservoirs) decrease sharply as the power grows until approximately 15 kW, then the cost declines gradually. The cost of turbines is a little higher than of the compressors which could be attributed to the commercial maturity of this latter at small scales. In spite of the fact that the total heat exchangers area of the expansion phase is higher than of the compression phase (see Chapter 6), the opposite is true when it comes to the cost as the operation pressure of heat exchangers in the charging phase is bigger.

It is important to underline that the reservoir cost per kWh is the highest and stays the same owing to the proportional relation between the output energy and the mass of compressed air.

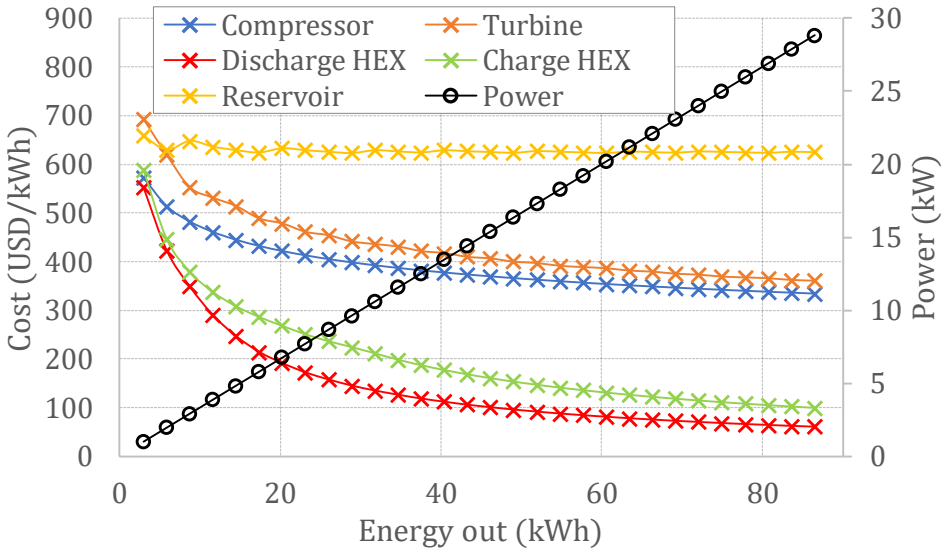


*Figure 7.7: Variation of the output power and the cost of each component as a function of the output energy with a discharge to charge ratio of 0.21.*

The previous conclusion raises the question of how could the CAES be economical at large scale. Figure 7.8 displays the cost of fictive caverns as a function of its volume (according to Garvey and Pimm [90]) . The marginal cost here comes from the drilling expenses and increases slightly with the cavern size or system capacity so that the cost of air storage per unit of energy decreases with the scale as well as the mechanical equipment.

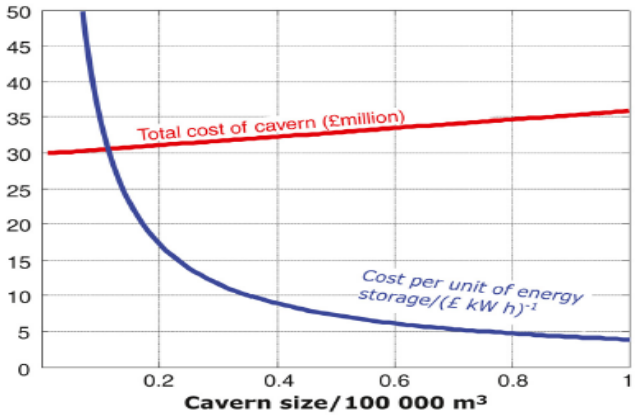


*Figure 7.8: The cost of caverns in large scale CAES (y axis is the y-axis is either cost/£106 or cost per unit/£ (kWh) [11].*

## *2nd case: discharge to charge time of 0.75*

In real applications of energy storage technologies, the time of discharge to charge ratio does not reach a very low values such as in the previous case, so that in this case the time of discharge is fixed to 8 hours and of the charge to 6 hours. Here, we stress that this case is studied to highlights the economic aspect for potentials applications. The equipment costs are studied in the two power range [1;30] and [30;450], and they are presented separately in the two Figures 7.9.a and 7.9.b.

Before we proceed to analyze the cost curves, By replacing $\alpha$ and $\eta_{el,e}$ by its values in Equation 7.11, we can conclude that the required electric compressor power is equal to 3.75 times the output power when this latter is lower than 30 kW, while it is 2.35 times at higher output power scale which results from the increment of the roundtrip electric efficiency.

As expected, in Figures 7.9.a and 7.9.b, the trend of cost variations is in line with of the previous studied case with a difference on the component cost shares. For an output power lower than 5 kW (Figure 7.9.a), the compressor accounts for a larger cost share which arises from its significant power. Afterward, the air reservoirs cost has again the highest cost as a result of the decline of the cost of compressor per kWh. At the same time, the cost of this latter stays higher than of the other equipment.

We observe from Figure 7.9. b that the cost of reservoirs and compressors plunge as a result of the drop of the value of compression power and the amelioration of the power conversion of stored air mass. In other terms the air mass needed drops for a certain energy output due to the increase of the turbine efficiency.

The total plant cost per kWh is presented in Figure 7.10. The cost of 1 kWh decreases as long as the plant scale decreases, it declines substantially at the beginning from 6 to 92 kWh (from 1 to 15 kW in term of output power) and slightly afterwards. These variations can be explained by the significant decrease of mechanical components costs for a power lower than 15 kW (see the first case study) and the unchanged cost of reservoirs. Obviously, the total cost of the plant increases as long as the system scale rises.

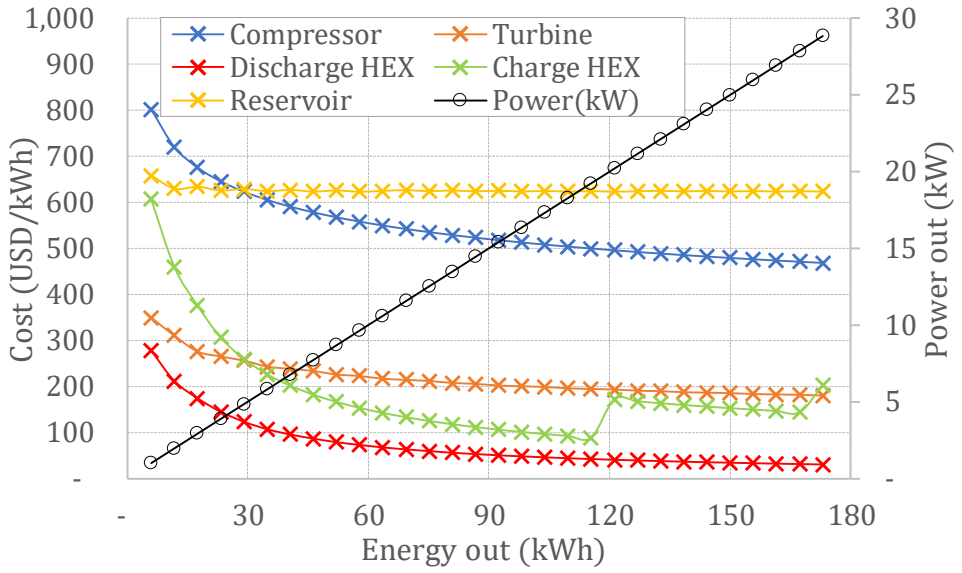


*Figure 7.9.a: Variation of the output power and the cost of each component as a function of the output energy with a discharge to charge ratio of 0.75 and power less than 30 kW.*

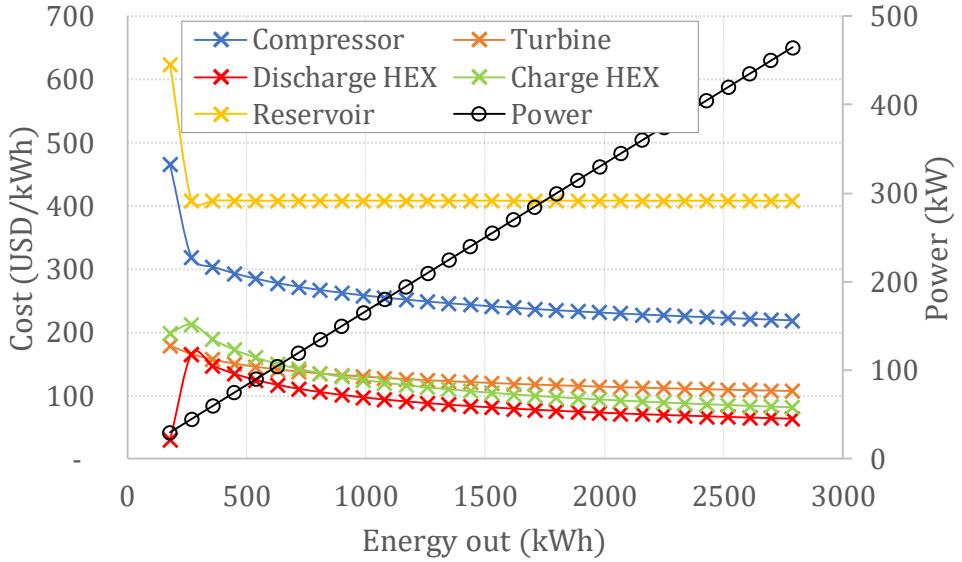


*Figure 7.9.b: Variation of the output power and the cost of each component as a function of the output energy with a discharge to charge ratio of 0.75 and power higher than 30 kW.*

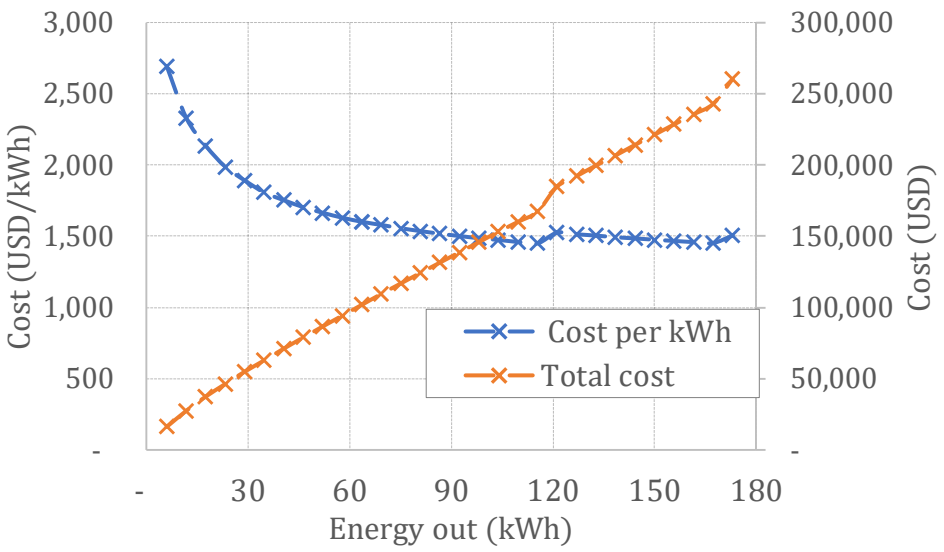


*Figure 7.10: Variation of the total costs of the plant as a function of the output energy.*

### 7.4.3 . Comparison of the T-CAES with batteries

In general, there is no clear relation between battery costs against its capacity. The estimation cost ranges are different in the literature. In this study, we assume the cost to be 300 USD/kWh as an average value of the cost range of [200; 400] reported by Luo et al. [2] (see Chapter 2). However, it can be seen from the data collected in [91] and shown in Figure 7.11 that the cost increases with battery size contrary to what is found for T-CAES. Consequently, it should be kept in mind that our system become more competitive as its scale increases.

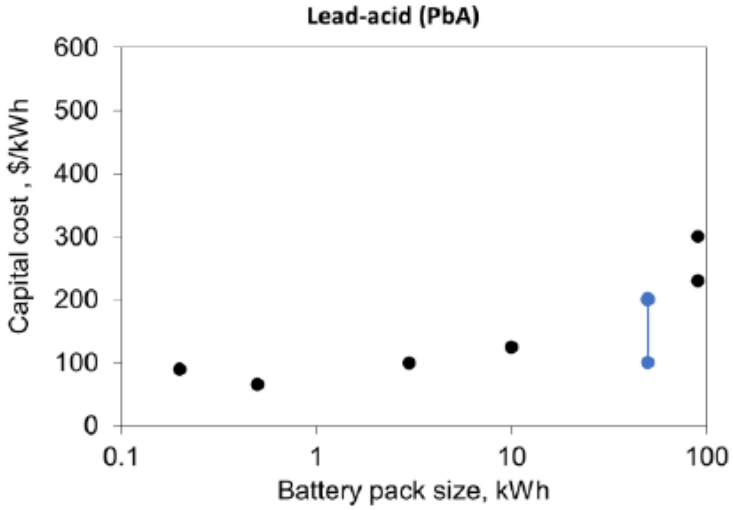


*Figure 7.11: Capital cost of Pb-Acid batteries against typical capacity (on logarithmic scale) as reported by companies (black) and according to industry standards (blue).*

Figure 7.12 shows a comparison between the T-CAES and batteries in terms of cost per kWh for a power range less than 30 kW. In case where system is applied without need for heating, Figure 7.12 (left) shows that it becomes less costly than batteries as the electric power is higher than 5.8

kW. On the contrary, if the heating energy is required in the application, the T-CAES becomes a lower cost solution whatever the power scale (Figure 7.12 right). In the two cases, the economic benefit of the T-CAES grows steeply until a power scale at about 15 kW is reached, then the reservoir cost maintain the plant at an almost constant cost per kWh, which limits its competitiveness .The cost difference benefit stabilizes at around 12 $/kWh.year without heating energy, but it is 2.6 times higher (around 32 $/kWh.year) if the heating is considered. This improvement is linked to the free gain of energy obtained from the same air capacity with the same components. This highlights the major contribution of the trigeneration option in enhancing the cost-benefit.

Figure 7.13 presents the cost benefit of our system for a power scale above 30 kW. As discussed previously, the improvement of turbine efficiency (above 30 kW) leads to an improvement of around 10% on global system efficiency and in reducing of the plant capital cost. the cost trend shares the same behavior as the previous case but it re-stabilizes at around 30$/kWh.year (when the power is higher than 255 kW). This value means that the cost benefit by comparison with batteries increases 2.5 times as the system efficiency is enhanced by 10% at higher power scale.

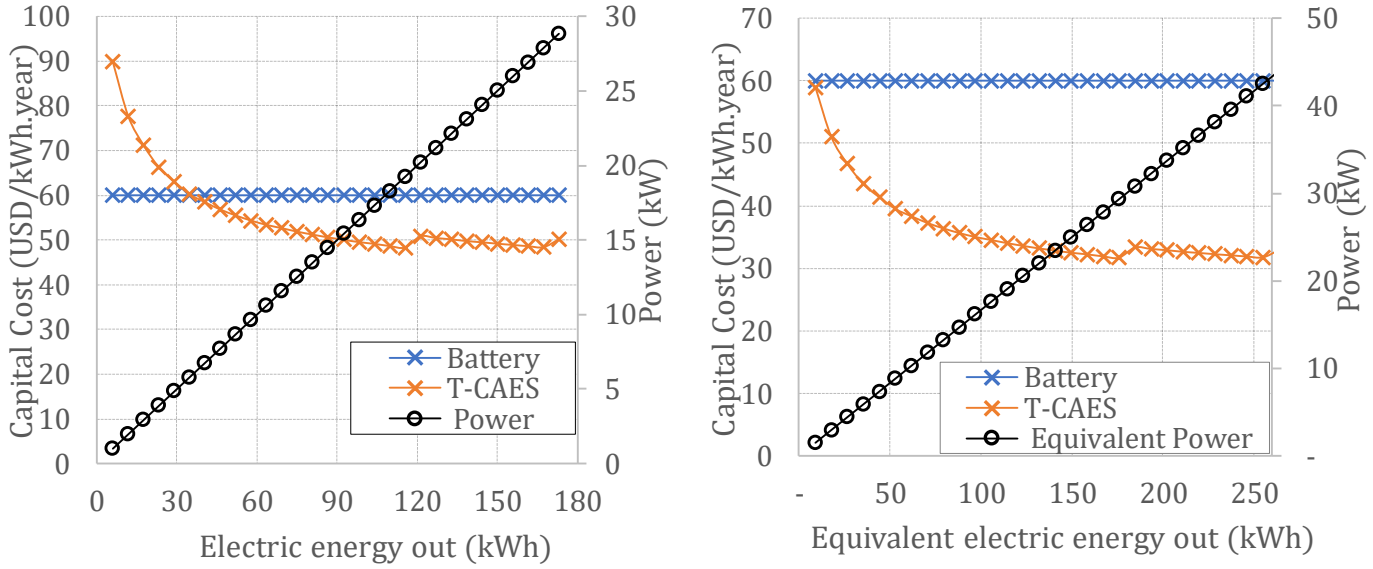


*Figure 7.12: Capital cost of lead acid battery and T-CAES against electric energy output, without considering the heating energy(left) and with taking the equivalent electric energy of this latter (right).*

Finally, it is very important to remember that the round-trip electric efficiency of the batteries is high at 60-90% (see Chapter 2) while the T-CAES is low at 21-32%. For a desired electric output, the difference on efficiency results in higher requirement of excess of energy of renewable energy in the case of T-CAES which could involve an additional cost of renewable energy installation per comparison to batteries. Besides, in the case of the application of the system for peak-load shifting, T-CAES is advantageous only when the electricity price in peak hours is 3.12-4.7 times higher (or 2.4-3.12 times when all the heat is needed) than of the normal hours.

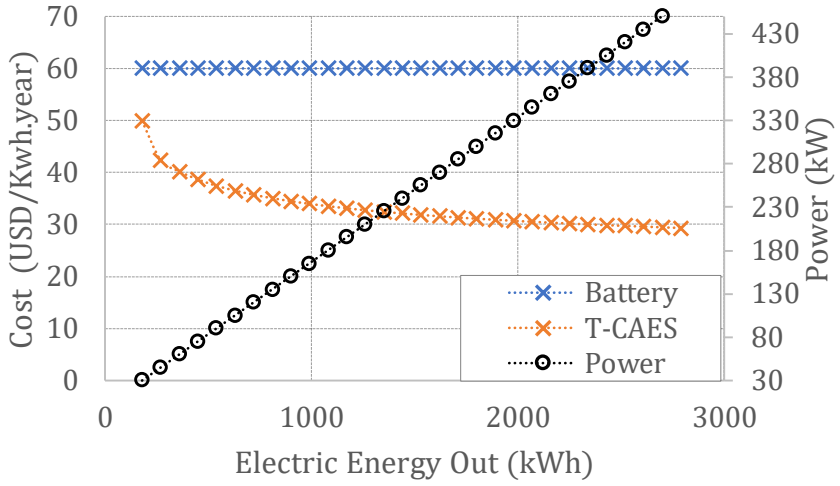


*Figure 7.13: Capital cost of lead acid battery and T-CAES against electric energy output, with a power range higher than 30 kW.*

## 7.5 Conclusions and Perspectives

In this chapter, we propose an economic model of the T-CAES which is based on cost approximations used to estimate the cost of chemical engineering plants and also on interpolation of component prices quotes. The costs of mechanical components are governed essentially by its capacity while both the storage pressure and the air volume head up the reservoir cost.

After being demonstrated that the optimal techno-economic storage pressure is in the range of [120; 200], the cost of components and the whole plant were simulated at a maximal storage pressure of 200 bars with different power and energy scales. The plant cost is then compared to its existing competitive technological solution: the lead acid batteries assuming a life time of 30 years. The main conclusions which can be drawn are the following:

1. The cost of the plant reduces from 90 USD/kWh.year to 30 USD/kWh.year as the energy scale grows up from 1 kWh to 2.7 MWh due to the scale raise and the enhancement of turbine efficiency at high power scales.
2. The cost of the plant is mainly related to the cost of air storage reservoirs which limits the reduction of the plant capital cost per kWh with rising the power or energy scale.
3. For long term of 30 years, the T-CAES becomes more economical than $P_bA$ batteries when the power is higher than 5.8 kW considering a discharge time of six hours.
4. The trigeneration option reduces drastically the system cost (1.67 times) as the additional heat energy (or even cooling energy) can be seen as zero-cost energy production.

The T-CAES is under development, and apart from research and developments needed to improve its efficiency, an inexpensive way to store air rather than pressurized tank is needed. Oak Ridge National Laboratory (ORNL) [92] has been developing a low-cost, high pressure, steel/concrete pressure vessel technology for storage of compressed gaseous hydrogen . In future investigations, this under-development solution could be adopted for compressed air with the aim of increasing its economical profitability.

# CHAPTER 8 – CONCLUSIONS AND PRESPECTIVES

## 8.1 Conclusions (en français)

Le système C-CAES classique ou conventionnel a été établi et appliqué dans les installations de Huntorf (Allemagne) et de McIntosh (États-Unis). Le concept est basé sur l'utilisation de la production excédentaire d'électricité pour comprimer l'air, le stocker dans des cavernes souterraines et le restituer lors de la phase de détente. Le principal défaut de cette technologie est la faible valeur de rendement dû au gaspillage de la chaleur de compression.

Au fil des dernières années, des travaux de recherche et de développement ont été menés sur l'amélioration de l'efficacité du système C-CAES par l'utilisation de la chaleur de compression pour préchauffer l'air détendu, ce qui mène au développement d'une nouvelle génération nommée adiabatique A-CAES. De plus, l'utilisation de réservoirs artificiels qui peuvent être installés sur n'importe quel site, ainsi que la possibilité de produire de l'énergie supplémentaire pour le chauffage et le refroidissement génèrent une génération appelée système trigénératif de stockage d'énergie par l'air comprimé à petite échelle T-CAES. Ce système semble être prometteur et même compétitif par rapport aux solutions conventionnelles à petite échelle comme les batteries en vertu de : temps de stockage prolongé, densité énergétique élevée, longue durée de vie avec un très faible coût de maintenance et un temps de réponse acceptable.

A-CAES a approché une phase de maturité en termes de détermination de ses différentes configurations, ses équations gouvernantes et les voies d'optimisation. Son rendement est compris entre 50% et 65% aux basses températures de stockage de l'énergie thermique (TES), et peut atteindre 70% aux températures élevées de TES.
D'autre part, T-CAES a été récemment évoqué. Les configurations proposées ne sont pas basées sur une analyse thermodynamique rigoureuse, les études de modélisation et d'optimisation ne tiennent pas suffisamment en compte les aspects technologiques et les contraintes techniques. Les critères d'évaluation tels que le rendement et la densité énergétique ne sont pas suffisamment étudiés et comptabilisés.

Dans le cadre de cette thèse, une investigation détaillée sur les configurations possibles du T-CAES a été réalisée tout d'abord. Deuxièmement, la modélisation thermodynamique de chaque composant a été conduite. Troisièmement, les caractéristiques du système ont été examinées et le modèle des composants côté air a été validé expérimentalement en effectuant des essais expérimentaux sur le pilote industriel existant à IMT-Atlantique, France. Ensuite, une optimisation paramétrique a été menée afin d'obtenir une directive de conception optimale du système. Finalement, une évaluation économique ainsi qu'une optimisation technico-économique du système sont effectuées.

Au Chapitre 3, les équations thermodynamiques simplifiées qui régissent les systèmes adiabatique et trigénérative CAES ont été développées afin de comprendre le concept thermodynamique de chaque technologie. En se basant sur le rapport de chaleur récupérée à la chaleur stockée et sur la température moyenne de détente, deux configurations de base de T-CAES ont été déduites.

Dans les deux configurations, la phase de décharge est formée de deux parties principales : la première partie est composée d'un multi-étage de détente préchauffés par le dispositif de stockage thermique, la deuxième est dédiée au refroidissement si cela est requis sinon, elle est équivalente à la première partie. La quantité d'énergie de refroidissement produite peut être contrôlée en fonction de la pression d'entrée de la dernière partie.
La différence entre les deux configurations repose sur le fait que : la première configuration a été proposée dans le but de simplifier la conception, tandis que l'optimisation de rendement électrique globale fait l'objectif de la seconde configuration.

Dans le Chapitre 4, un modèle thermodynamique détaillé du T-CAES a été développé, en justifiant le choix technologique de chaque composant et en prenant en compte les contraintes techniques. Le modèle est exprimé en fonction de : des paramètres d'entrée qui représentent les variables de conception, des paramètres de sortie qui comprennent les critères d'évaluation (tels que les performances du système et la densité énergétique), ainsi que des paramètres indiquant le coût (empreintes des échangeurs de chaleur et nombre des étages de compression et de détente) et autres paramètres utiles pour des applications pratiques futures (tels que les temps de charge et de décharge, pressions et températures aux entrées et sorties des différents composants).
Par ailleurs, une importante conclusion a été obtenu en démontrant qu'il existe un nombre optimal des étages de détente, que l'on peut trouver par une itération numérique.
Les principales incertitudes du modèle reposent sur sa limitation au régime permanent, ce qui conduit à ignorer certains effets tel que l'énergie de refroidissement induit par la vanne de détente. De plus, l'étude a été limitée en donnant la priorité au rendement électrique en fixant la production de l'énergie frigorifique.
La différence entre les deux configurations a été expliquée en vertu de l'analyse détaillée, la simplicité de la première configuration est justifiée par la réduction du nombre d'échangeurs de chaleur et par la réutilisation de l'eau dans le procédé de charge, tandis que la seconde configuration vise à optimiser le rendement électrique en maximisant le préchauffage avant les détenteurs.

Dans le Chapitre 5, des essais expérimentaux ont été effectués sur un pilote existant à IMT, Atlantique, France, composé de : un compresseur à 3 étages refroidis par des échangeurs de chaleur air-air, réservoirs d'air comprimé, vanne de détente et un moteur pneumatique. Le modèle des composants côté air a été validé expérimentalement en termes de débit massique d'air de compression, de puissance électrique de phase de décharge et de rendement électrique global. L'erreur maximale était de 13,2 %, ce qui est acceptable pour prédire les performances du système. Il s'agit du premier modèle fiable validé avec des données expérimentales pour un système de stockage d'énergie à air comprimé à petite échelle.

Les différences entre le modèle et les résultats expérimentaux sont principalement dues au fait que le modèle ne tient pas en compte du régime transitoire pendant la phase de compression, des propriétés réelles de l'air pendant la phase de stockage et de l'effet de la température à l'entrée du moteur pneumatique.
Par ailleurs, des études expérimentales supplémentaires ont été menées sur la vanne de détente et le moteur pneumatique. Comme prévu, l'effet de Joule-Thomson induit une baisse de la température au niveau de la vanne, qui ne peut pas être ignorée. De plus, les courbes de conversion

thermodynamique à mécanique ainsi que l'effet de la température d'entrée du moteur pneumatique sont expliquées et reliées aux phénomènes physiques.
Le rendement électrique global du dispositif expérimental à 3.6 % était très faible en raison de la différence significative (qui vaut 176 bars) entre les pressions de stockage maximale et minimale. D'autre part, le rendement électrique équivalent a atteint 15.6%, ce qui prouve l'importance du concept trigénératif.

Au Chapitre 6, l'optimisation paramétrique des deux configurations proposées précédemment a été réalisée. L'originalité de cette optimisation par rapport aux études antérieures dans la littérature est la prise en considération de l'effet mutuel des paramètres et les critères d'évaluation en même temps.
Des résultats importants concernant le choix des paramètres de conception ont été obtenus :
Premièrement, la pression maximale de stockage a un effet significatif sur le rendement du système (jusqu'à 12%) et la densité énergétique. La solution optimale devrait être basée sur une optimisation technico-économique.
Deuxièmement, le niveau de température du stockage de l'énergie thermique a un effet marginal sur le rendement du système (pas plus de 1.5 %). Une température plus élevée peut réduire les coûts en minimisant le nombre des étages de détente et l'empreinte totale des échangeurs thermique.
Troisièmement, le choix optimal du nombre d'étages de compression peut être trouvé comme un compromis entre les performances du système et d'autres paramètres reflétant le coût tels que : le nombre d'étages de détente et l'empreinte total des échangeurs thermique.
Enfin, l'efficacité des échangeurs de chaleur doit être choisie à un niveau modéré compris entre 0.79 et 0.85 afin d'éviter des valeurs excessives de pertes de charge et des surfaces d'échange.
Sur la base de ces valeurs optimales, pour des applications à l'échelle micro, le rendement électrique de système est faible à 17%. D'autre part, l'énergie de refroidissement et de chauffage améliore l'efficacité du système environ de 11.5 %. Ces faibles valeurs sont principalement liées au faible rendement de conversion des machines de détente et au bas niveau de pression à l'entrée des micro-turbines existantes à 25 bars.
Il a été démontré que la première configuration est privilégiée lorsque l'énergie de refroidissement est requise et que la deuxième est préférable dans le cas contraire. En outre, il est justifié que l'activation de l'énergie de refroidissement a un effet plus important sur le rendement global (augmentation de 4%) que sur le rendement électrique (diminution de 1,5%).

Dans le Chapitre 7, nous proposons un modèle économique du T-CAES basé sur des approches de coûts utilisées pour estimer le coût des équipements des procédés chimiques et également sur l'interpolation des prix obtenus par des devis. Les coûts des composants mécaniques sont essentiellement régis par leur capacité, tandis que la pression de stockage et le volume d'air sont les deux facteurs prépondérants dans le coût des réservoirs.
Un modèle économique du T-CAES à petite échelle a été développé en fonction de son échelle de puissance et des paramètres d'opérations tel que la pression de fonctionnement. La valeur optimale de pression maximale de stockage est déduite via une optimisation technico-économique, elle se situe dans le rang de [120 bars- 200 bars].

Après avoir fixé la pression maximale à 200 bars, les résultats de la simulation ont démontré que le coût de 1kWh diminue significativement de 90 USD à 30 USD lorsque l'échelle de système passe de 1kWh à 2.7 MWh, puis le coût diminue très légèrement. Le coût le plus élevé est lié aux réservoirs d'air qui est proportionnel à l'échelle énergétique.
En outre, sur une longue période de 30 ans, la solution T-CAES s'avère économiquement avantageuse par rapport aux batteries (avec un gain de 30 USD/kWh) dans la mesure où l'échelle de puissance est supérieure à 5.8 kW. Un avantage supplémentaire de notre système était justifié par la gratuité de la production d'énergie de refroidissement et de chauffage. D'autre part, en raison du faible rendement électrique du T-CAES, il n'est avantageux que lorsque le prix de l'électricité aux heures de pointe est 3.12-4.7 fois plus élevé (ou 2.4-3.12 fois lorsque toute la chaleur est nécessaire) que celui des heures normales, et lorsque l'excédent de production des énergies renouvelables est peu pris en compte en termes de coût des investissements.

L'importance de la méthodologie et des résultats de cette thèse se concrétise dans : l'illustration du concept de systèmes CAES trigénératif et adiabatique, l'étude des différentes configurations possibles du T-CAES, le développement d'un modèle thermodynamique et économique fiable pour les recherches futures dans le domaine CAES, la proposition d'une méthodologie d'optimisation techno-économique qui peut être appliquée pas seulement sur T-CAES, mais aussi sur A-CAES avec quelques légères modifications.
Enfin, cette étude peut être fortement impliquée dans les systèmes CAES isobares, puisqu'une pression d'entrée constante des turbines a été adoptée.

Comme **perspectives**, pour les applications à petite échelle, sur la base des technologies existantes des machines, le rendement électrique du système est faible, de 17 % à 21,2 % aux micro-échelles (inférieures à 30 kW) et maximum de 32,3 % aux plus grandes échelles. Les travaux futurs devraient se focaliser sur une amélioration du rendement du système. Plusieurs recommandations sont proposées comme suit :

- Développement technologique de machines de détente pour fonctionner sous pression variable avec une pression élevée d'entrée. Les moteurs pneumatiques à piston pourraient être un bon choix puisque les moteurs existants fonctionnent avec une pression variable et pourraient être conçues avec une haute pression d'entrée similairement aux compresseurs.
- Étude de faisabilité du couplage des échangeurs de chaleur et de stockage d'énergie thermique avec le côté air fonctionnant à des pressions, températures et débits massiques variables. C'est complémentaire aux études théoriques proposées dans la littérature.
- Étude de la possibilité de remplacer la vanne de détente par un tube à vortex. Ce dispositif est capable de réduire la pression maximale dans la phase de détente et de produire simultanément : un courant chaud qui peut alimenter la turbine, et un courant froid qui peut être utilisé à des fins de refroidissement.

Étant donné que le modèle développé est un modèle en régime permanent, les travaux de recherche futurs devraient être ciblés sur l'élaboration de modèles dynamiques tenant compte des aspects technologiques afin d'évaluer les améliorations potentielles apportées par les solutions proposées ci-dessus. En outre, le modèle dynamique est incontournable pour étudier les opérations aux charges partielles du système.

D'un point de vue économique, il a été démontré que les réservoirs sous pression ne sont plus économiquement rentables lorsque l'échelle énergétique de l'installation augmente. Les réservoirs sous pression en acier/béton en cours de développement, étudiés par l'Oak Ridge National Laboratory (États-Unis), peuvent être considérés comme une solution d'avenir pour réduire le coût d'investissement.

## 8.2 . Conclusions (in English)

Classical or conventional C-CAES was established and applied in the Huntorf plant (Germany) and the McIntosh plant (USA). The concept is based on using the excess electricity production to compress the air, store it in underground caverns and release it in the expansion phase. The main draw-back of this technology is the low-efficiency due to the waste of compression heat.

In the past years, research and development has been being conducted on the improvement of the efficiency of the C-CAES by the use of compression heat to preheat the expanded air, which leads to develop a new generation named Adiabatic A-CAES. Furthermore, by using artificial tanks that can be installed at any site, as well as the opportunity to produce supplementary heating and cooling energy generates a new generation named small scale trigenerative compressed air energy storage T-CAES. This system appears to be encouraging and even competitive with conventional small-scale solution as batteries by virtue of: prolonged storage time, high energy density, long lifetime with a very low maintenance cost, acceptable response time.

A-CAES approached a stage of maturity in terms of defining its different configurations, governing equations and optimization paths. Its efficiency ranges at 50%-65% with low temperature of thermal energy storage (TES), and reaches 70% with high temperature of TES.

On the other hand, T-CAES has been considered recently. Its proposed configurations are not based on a rigorous thermodynamic analysis, the related modeling and optimization studies do not sufficiently account for technological aspects and technical constraints. The evaluation criteria such as the efficiency and the energy density are not rigorously studied and accounted.

Throughout this thesis, firstly a detailed investigation on the possible configurations of the T-CAES was performed. Secondly, the thermodynamic modeling of each component was carried out. Thirdly, the system characteristics was investigated and the model of the air side components was validated experimentally by handling experimental test on the Industrial Pilot existing at IMT-Atlantique, France. Then, a parametric optimization was performed in order to derive an optimal design guideline of the system. Finally, an economic assessment as well as techno-economic optimization of the system are realized.

In Chapter 3, the basic simplified thermodynamic governing equations of the Adiabatic and trigenerative CAES were developed in order to figure out the thermodynamic concept of each technology. By analyzing the heat recuperated to the heat stored rate and the average expansion temperature, two basic configurations were deduced.
In the two configurations, the discharge phase is formed by two main parts: the first part is composed by a multi expansion-stages preheated via thermal energy storage, while the second part is dedicated for cooling energy production if it is needed otherwise, it is equivalent to the first part.

The amount of cooling energy production can be controlled according to the pressure input of the last part.
The difference between the two configurations turns out in the fact that: the first configuration was proposed with the aim of simplifying the design, while the maximization of the global electric efficiency was the priority of the second configuration.

In Chapter 4, a detailed thermodynamic model of the T-CAES was developed, justifying the technological choice of each component and taking into account the technical constraints. The model is expressed as a function of : input parameters which represents the design ones, output parameters which consists of the evaluation criteria (such as system performances and energy density), parameters reflecting the cost (heat exchanger footprints and the number of compression and expansion stages) as well as other useful parameters which are important for prospective engineering applications (such as the charge or discharge times, pressures and temperatures at the inlet/outlet of each component).
Besides, an important funding was achieved by demonstrating that there is an optimal number of expansion stages, which can be found by a numerical iteration procedure.
The main uncertainties of the model rely on limiting it to a steady state model, which leads to ignore some effects such as the cooling energy outlet of the throttling valve. In addition, the study was limited by giving priority to the electric efficiency by fixing the cooling energy production.
The difference between the two configurations was figured out in virtue of the detailed analysis, the simplicity of the first configuration was justified by reducing the number of heat exchangers and by reusing the water of the discharge process in the charge process, while the second configuration sill intended to optimize the electric efficiency by maximizing the preheating energy before the expanders.

In Chapter 5, experimental tests were performed on an existing pilot at IMT, Atlantique, France composed from: 3 stage compressors intercooled by air-air heat exchangers, pressurized air tanks, throttling valve and an air motor. The developed steady state model of air side component was validated experimentally in terms of air compression mass flow, electrical output power, and global electric efficiency. The maximum error was at 13.2%, which is acceptable to predict the system performances. It is the first reliable model validated with experimental data for small-scale compressed air energy storage system.
The model and experimental result differences were caused mainly by the disregard of the model of: the transitional regime in the compression phase, the real air properties in the storage phase and the effect of input temperature of the air motor.
In addition, further experimental investigations were carried in regards to the throttling valve and the air motor. As predicted by the model, the effect of Joule-Thomson across the throttling valve induces a drop of the temperature, which cannot be ignored. As regards the AM, the thermodynamic to mechanical conversion curves as well as the effect of input temperature of the air motor were well correlated to its physical phenomena.
The round-trip electrical efficiency of the experimental set-up at 3.6% was very low due to the significant difference at 176 bars between the maximum and the minimum storage pressure. On the other hand, the equivalent electrical efficiency reached 15.6%, which proves the importance of the trigenerative concept.

In Chapter 6, the parametric optimization of the two configurations proposed previously was carried out. The originality of this optimization among of that conducted in the literature is the investigation of the mutual effect of design parameters and accounting at once the evaluation criteria.
Important achievements regarding the choice of the design parameters were found:
Firstly, the maximum storage pressure has the significant effect on the system efficiency (up to 12%) and energy density. The trade-off solution should be based on techno-economic optimization.
Secondly, the temperature level of the hot thermal energy storage has a marginal effect on the system efficiencies (not more than 1.5%). Higher level of the temperature can lead to lower cost via minimizing the minimal number of expansion stages and the total heat exchanger footprints.
Thirdly, the optimal choice of the number of compression stages can be found as a compromise between the system performances and other parameters reflecting the cost such as: the number of expansion stages and the heat exchanger footprints.
Finally, the heat exchanger effectiveness should be chosen at moderate level ranging from 0.79 to 0.85 in order to prevent excessive values of pressure losses and footprints.
The optimization results were able to conclude the optimal values of design parameters. A set of values were found such as: the maximum pressure at 200 bars, the temperature of TES at 140˚C, the effectiveness of discharging and charging HEX at 0.85 and 0.82 respectively.
Based on these optimal values, at micro scale applications, the electrical efficiency is low at 17%. On the other hand, the cooling and heating energy improves the system efficiency by almost 11.5%. These low values are mainly related to the low conversion efficiency of expansion machinery and low-pressure input of micro-turbine at 25 bars.
It was demonstrated that the first configuration is preferable when the cooling energy is needed and the second one otherwise. Besides, it was justified that enabling the cooling energy has a greater effect on the comprehensive efficiency (rises by 4%) than the electrical efficiency (drops by 1.5%).

In Chapter 7, an economic model of the T-CAES is proposed which is based on cost approximations used to estimate the cost of chemical engineering plants and also on interpolation of component prices quotes. The costs of mechanical components are governed essentially by its capacity while both the storage pressure and the air volume head up the reservoir cost.
An economical model of the small-scale T-CAES as a function of its capacity and design parameters such as the operating pressure was developed. The optimal techno-economic of the maximum storage pressure was found in the range of [120 bars- 200 bars].
After fixing the maximum pressure to 200 bars, the simulation results demonstrated that the cost of 1 kWh decreases significantly from 90 USD to 30 USD as the energy scale rises from 1kWh to 2.7 MWh, then the cost decreases very slightly. The highest cost is related to the air reservoirs and is proportional to the energy scale.
In addition, for long term of 30 years, the T-CAES solution was found economically beneficial compared to batteries (by 30 USD/kWh) as the power scale is higher than 5.8 kW. An additional benefit of our system was justified by the free cost of cooling and heating energy production. On the other hand, owing to the low electric efficiency of the T-CAES , it is beneficial only when the

electricity price in peak hours is 3.12-4.7 times higher (or 2.4-3.12 times when all the heat is needed) than of the normal hours, and when the excess of renewable energy production is not highly considered in terms of capital cost.

The importance of the methodology and finding throughout this thesis turns out in: clarifying further the concept of the trigenerative and adiabatic CAES, investigating the different possible configurations of the T-CAES, developing a reliable thermodynamic and cost model for future research in the CAES field, proposing a methodology of techno-economic optimization which can be applied not only on T-CAES but also on A-CAES with minor modifications.
Finally, this study can be strongly implicated in the isobaric-CAES, since a constant input pressure of turbines was adopted in this thesis.

As **future perspectives**, for small scales applications, based on existing technologies of machineries, the electrical efficiency of the system is low at 17%-21.2% at micro-scales (lower than 30 kW) and at maximum of 32.3 % at higher scales. Future work should focus on increasing the round-trip efficiency of the system. Many recommendations are proposed as follow:

- Technology development of expander machineries to work under variable pressure with high input pressure. The air piston expanders would be a good candidate since the existing expanders operates with a variable pressure and could be designed with high pressure input analogous to the compressors.
- Investigation on the feasibility study of coupling the heat exchangers and thermal energy storage with the air side operating at variable pressures, temperatures and mass flowrates as a complementary to the theoretical studies proposed in the literature.
- Investigation on the possibility of replacing the throttling valve by vortex tube. This device is able to reduce the maximum pressure in the expansion phase and producing at the same time: a hot stream which can supply the turbine, and a cold stream which can be used for cooling purposes.

Since the developed model is a steady-state model, future research should focus on developing a dynamic modeling taking into account technological aspects in order to assess the potential improvements of the above proposed solutions. Besides, dynamic model is mandatory in order to investigate the partial load operations of the plant.

In an economic point of view, it was demonstrated that pressure vessels are no longer economically beneficial when the plant energy scale grows up. The under-development Steel/concrete pressure vessel investigated by Oak Ridge National Laboratory; USA can be considered as a future prospective to reduce the investment cost.

# PUBLICATIONS

The studies done throughout this thesis were published in two peer-review journal papers and one conference paper as follows:

1. M. Cheayb, M. Marin Gallego, M. Tazerout and S. Poncet, "Modelling and experimental validation of a small- scale Trigenerative Compressed Air Energy Storage system", *Applied Energy*, vol. 239, pp.1371-1384, 2019.

2. M. Cheayb, S. Poncet, M. Marin Gallego, M. Tazerout, "Parametric optimization of a trigenerative small scale compressed air energy storage system", *Conference: 27th Canadian Congress of Applied Mechanics (CANCAM 2019)*, Sherbrooke, Canada, May 27-30, 2019.

3. M. Cheayb, M. Marin Gallego, S. Poncet, M. Tazerout, "Micro-scale trigenerative compressed air energy storage system: Modelling and parametric optimization study", *Journal of Energy Storage*, vol. 26, 100944, 2019.

# REFERENCES


[1] A. Rogers, A. Henderson, X. Wang, and M. Negnevitsky, "Compressed air energy storage: Thermodynamic and economic review", in *2014 IEEE PES General Meeting" Conference & Exposition*, National Harbor, MD, USA, 2014, pp. 1–5.

[2] X. Luo, J. Wang, M. Dooner, and J. Clarke, "Overview of current development in electrical energy storage technologies and the application potential in power system operation", *Applied Energy*, vol. 137, pp. 511–536, 2015.

[3] D. Wolf, "*Methods for design and application of adiabatic compressed air energy: storage based on dynamic modeling*", PhD thesis, University of Bochum, Oberhausen Laufen, 2011.

[4] H. Chen, T. N. Cong, W. Yang, C. Tan, Y. Li, and Y. Ding, "Progress in electrical energy storage system: A critical review", *Progress in Natural Science*, vol. 19, no. 3, pp. 291–312, 2009.

[5] Y. Zhou, L. Wang, and J. D. McCalley, "Designing effective and efficient incentive policies for renewable energy in generation expansion planning", *Applied Energy*, vol. 88, no. 6, pp. 2201–2209, 2011.

[6] H. Ibrahim, « *Étude et conception d'un générateur hybride d'éléctricité de type éolien-diesel avec élément de stockage d'air comprimé* », PhD thesis, Université du Québec à Chicoutimi, 2010.

[7] M. Peker, A. S. Kocaman, and B. Y. Kara, "Benefits of transmission switching and energy storage in power systems with high renewable energy penetration", *Applied Energy*, vol. 228, pp. 1182–1197, 2018.

[8] I. Orlandi, N. Tyabji, J. Chase, "Off Gird Solar Market Trends Report" Bloomberg New Energy Finance and Lighting Global, 2016.

[9] J. Royer, "Status of Remote/Off-Grid Communities in Canada", Natural Resources Canada, 2011.

[10] S. A. Papathanassiou and N. G. Boulaxis, "Power limitations and energy yield evaluation for wind farms operating in island systems", *Renewable Energy*, vol. 31, no. 4, pp. 457–479, 2006.

[11] D. Zafirakis and J. K. Kaldellis, "Autonomous dual-mode CAES systems for maximum wind energy contribution in remote island networks", *Energy Conversion and Management*, vol. 51, no. 11, pp. 2150–2161, 2010.

[12] X. Luo, J. Wang, M. Dooner, J. Clarke, and C. Krupke, "Overview of Current Development in Compressed Air Energy Storage Technology," *Energy Procedia*, vol. 62, pp. 603–611, 2014.

[13] A. L. Facci, D. Sánchez, E. Jannelli, and S. Ubertini, "Trigenerative micro compressed air energy storage: Concept and thermodynamic assessment", *Applied Energy*, vol. 158, pp. 243–254, 2015.

[14] J. J. Proczka, K. Muralidharan, D. Villela, J. H. Simmons, and G. Frantziskonis, "Guidelines for the pressure and efficient sizing of pressure vessels for compressed air energy storage", *Energy Conversion and Management*, vol. 65, pp. 597–605, 2013.

[15] H. Ibrahim, A. Bourji, M. Ghandour, and A. Merabet, “Optimization of compressed air storage’s volume for a stand-alone wind-diesel hybrid system” in *Electrical Power & Energy Conference (EPEC), 2013 IEEE*, Hailfax, Canada, pp. 1–7, 2013.

[16] E. Jannelli, M. Minutillo, A. Lubrano Lavadera, and G. Falcucci, “A small-scale CAES (compressed air energy storage) system for stand-alone renewable energy power plant for a radio base station: A sizing-design methodology”, *Energy*, vol. 78, pp. 313–322, 2014.

[17] A. Abdon, X. Zhang, D. Parra, M. K. Patel, C. Bauer, and J. Worlitschek, “Techno-economic and environmental assessment of stationary electricity storage technologies for different time scales”, *Energy*, vol. 139, pp. 1173–1187, 2017.

[18] X. Luo and J. Wang, “Overview of current development on compressed air energy storage”, EERA technical report, *School of Engineering, University of Warwick, UK*, 2013.

[19] S. Lv, W. He, A. Zhang, G. Li, B. Luo, and X. Liu, “Modelling and analysis of a novel compressed air energy storage system for trigeneration based on electrical energy peak load shifting”, *Energy Conversion and Management*, vol. 135, pp. 394–401, 2017.

[20] J.-L. Liu and J.-H. Wang, “Thermodynamic analysis of a novel tri-generation system based on compressed air energy storage and pneumatic motor,” *Energy*, vol. 91, pp. 420–429, 2015.

[21] Y. Li, X. Wang, D. Li, and Y. Ding, “A trigeneration system based on compressed air and thermal energy storage,” *Applied Energy*, vol. 99, pp. 316–323, 2012.

[22] S. Weitemeyer, D. Kleinhans, T. Vogt, and C. Agert, “Integration of Renewable Energy Sources in future power systems: The role of storage,” *Renewable Energy*, vol. 75, pp. 14–20, 2015.

[23] M. Beaudin, H. Zareipour, A. Schellenberglabe, and W. Rosehart, “Energy storage for mitigating the variability of renewable electricity sources: An updated review,” *Energy for Sustainable Development*, vol. 14, no. 4, pp. 302–314, 2010.

[24] Internationnal Hydropower Association, “Hydropower status report”, 2018.

[25] M. J. Anjois, S. A. Gabriel, and C. Guerra, “L’énergie au Québec et au Canada : un document pour engager la conversation”, Report, Institut de l’énergie Trottier, Polytechnique Montréal, 2015.

[26] A. Gil, M. Medrano, I. Martorell, L. Ana, D. Pablo, Z. Belen, L. F. Cabeza, “State of the art on high temperature thermal energy storage for power generation. Part 1—Concepts, materials and modellization”, *Renewable and Sustainable Energy Reviews*, vol. 14, no. 1, pp. 31–55, 2010.

[27] L. Moens and D. M. Blake, “Advanced heat transfer and thermal storage fluids”, *Proceedings of International Solar Energy Conference*, pp. 791–793, Florida, USA, 2005.

[28] H. Zhang, J. Baeyens, G. Cáceres, J. Degrève, and Y. Lv, “Thermal energy storage: Recent developments and practical aspects,” *Progress in Energy and Combustion Science*, vol. 53, pp. 1–40, 2016.

[29] B. Wu, R. Reddy, and R. Rogers, "Novel ionic liquid thermal storage for solar thermal electric power systems," *Proceedings of Solar Forum 2001*, pp. 445–452, Washington DC, 2001.

[30] M. F. Demirbas, "Thermal Energy Storage and Phase Change Materials: An Overview," *Energy Sources, Part B: Economics, Planning, and Policy*, vol. 1, no. 1, pp. 85–95, 2006.

[31] M. Budt, D. Wolf, R. Span, and J. Yan, "A review on compressed air energy storage: Basic principles, past milestones and recent developments," *Applied Energy*, vol. 170, pp. 250–268, 2016.

[32] Y. M. Kim, D. G. Shin, and D. Favrat, "Operating characteristics of constant-pressure compressed air energy storage (CAES) system combined with pumped hydro storage based on energy and exergy analysis," *Energy*, vol. 36, no. 10, pp. 6220–6233, 2011.

[33] Hydrostor Company, "Hydrostor A-CAES Terra-Brochure", Brochure, accessed https:// www.hydrostor.ca/, 2017.

[34] H. Wang, L. Wang, X. Wang, and E. Yao, "A Novel Pumped Hydro Combined with Compressed Air Energy Storage System," *Energies*, vol. 6, no. 3, pp. 1554–1567, 2013.

[35] E. Yao, H. Wang, L. Liu, and G. Xi, "A Novel Constant-Pressure Pumped Hydro Combined with Compressed Air Energy Storage System," *Energies*, vol. 8, no. 1, pp. 154–171, 2014.

[36] T. P. L. Camargos, D. L. F. Pottie, R. A. M. Ferreira, T. A. C. Maia, and M. P. Porto, "Experimental study of a PH-CAES system: Proof of concept," *Energy*, vol. 165, pp. 630–638, 2018.

[37] A. Odukomaiya, A. Abu-Heiba, S. Graham, and A. M. Momen, "Experimental and analytical evaluation of a hydro-pneumatic compressed-air Ground-Level Integrated Diverse Energy Storage (GLIDES) system," *Applied Energy*, vol. 221, pp. 75–85, 2018.

[38] RWE Power AG, "ADELE – Adiabatic Compressed Air Energy Storage For Electricity Supply", Brochure, Germany, 2010.

[39] S. Wang, X. Zhang, L. Yang, Y. Zhou, and J. Wang, "Experimental study of compressed air energy storage system with thermal energy storage," *Energy*, vol. 103, pp. 182–191, 2016.

[40] L. Geissbühler, V. Becattini, G. Zanganeh, S. Zavattoni, M. Barbato, A. Haselbacher and A. Steinfeld, "Pilot-scale demonstration of advanced adiabatic compressed air energy storage, Part 1: Plant description and tests with sensible thermal-energy storage," *Journal of Energy Storage*, vol. 17, pp. 129–139, 2018.

[41] V. Becattini, L. Geissbühler, G. Zanganeh, A. Haselbacher, and A. Steinfeld, "Pilot-scale demonstration of advanced adiabatic compressed air energy storage, Part 2: Tests with combined sensible/latent thermal-energy storage," *Journal of Energy Storage*, vol. 17, pp. 140–152, 2018.

[42] A. Sciacovelli, *Y. Li, H. Chen, Y. Wu, J. Wang, S. Garvey, Y. Ding,* "Dynamic simulation of Adiabatic Compressed Air Energy Storage (A-CAES) plant with integrated thermal storage – Link between components performance and plant performance," *Applied Energy*, vol. 185, pp. 16–28, 2017.

[43] G. Grazzini and A. Milazzo, "A Thermodynamic Analysis of Multistage Adiabatic CAES," *Proceedings of the IEEE*, vol. 100, no. 2, pp. 461–472, 2012.

[44] D. Wolf and M. Budt, "LTA-CAES – A low-temperature approach to Adiabatic Compressed Air Energy Storage," *Applied Energy*, vol. 125, pp. 158–164, 2014.

[45] X. Luo, J. Wang, C. Krupke, Y. Wang, Y. Sheng, J. Li, Y. Xu, D. Wang, S. Miao and H. Chen, "Modelling study, efficiency analysis and optimisation of large-scale Adiabatic Compressed Air Energy Storage systems with low-temperature thermal storage," *Applied Energy*, vol. 162, pp. 589–600, 2016.

[46] L. Szablowski, P. Krawczyk, K. Badyda, S. Karellas, E. Kakaras, and W. Bujalski, "Energy and exergy analysis of adiabatic compressed air energy storage system," *Energy*, vol. 138, pp. 12–18, 2017.

[47] C. Guo, Y. Xu, H. Guo, X. Zhang, X. Lin, L. Wang, Y. Zhang, H. Chen, "Comprehensive exergy analysis of the dynamic process of compressed air energy storage system with low temperature thermal energy storage," *Applied Thermal Engineering*, vol. 147, pp. 684–693, 2019.

[48] Y. Zhang, K. Yang, X. Li, and J. Xu, "The thermodynamic effect of thermal energy storage on compressed air energy storage system," *Renewable Energy*, vol. 50, pp. 227–235, 2013.

[49] S. Zhou, J. Zhang, W. Song, and Z. Feng, "Comparison Analysis of Different Compressed Air Energy Storage Systems," *Energy Procedia*, vol. 152, pp. 162–167, 2018.

[50] A. Arabkoohsar, M. Dremark-Larsen, R. Lorentzen, and G. B. Andresen, "Subcooled compressed air energy storage system for coproduction of heat, cooling and electricity," *Applied Energy*, vol. 205, pp. 602–614, 2017.

[51] Z. Han and S. Guo, "Investigation of discharge characteristics of a tri-generative system based on advanced adiabatic compressed air energy storage," *Energy Conversion and Management*, vol. 176, pp. 110–122, 2018.

[52] N. Hartmann, O. Vöhringer, C. Kruck, and L. Eltrop, "Simulation and analysis of different adiabatic Compressed Air Energy Storage plant configurations," *Applied Energy*, vol. 93, pp. 541–548, 2012.

[53] H. Mozayeni, M. Negnevitsky, X. Wang, F. Cao, and X. Peng, "Performance Study of an Advanced Adiabatic Compressed Air Energy Storage System," *Energy Procedia*, vol. 110, pp. 71–76, 2017.

[54] Y. He, H. Chen, Y. Xu, and J. Deng, "Compression performance optimization considering variable charge pressure in an adiabatic compressed air energy storage system," *Energy*, vol. 165, pp. 349–359, 2018.

[55] G. Grazzini and A. Milazzo, "Thermodynamic analysis of CAES/TES systems for renewable energy plants," *Renewable Energy*, vol. 33, no. 9, pp. 1998–2006, 2008.

[56] S. Houssainy, M. Janbozorgi, and P. Kavehpour, "Thermodynamic performance and cost optimization of a novel hybrid thermal-compressed air energy storage system design," *Journal of Energy Storage*, vol. 18, pp. 206–217, 2018.

[57] Y. M. Kim, “Novel concepts of compressed air energy storage and thermo-electric energy storage", PhD thesis, Ecole Polytechnique Fédérale de Lausanne, 2012.

[58] Y. Mazloum, H. Sayah, and M. Nemer, “Dynamic modeling and simulation of an Isobaric Adiabatic Compressed Air Energy Storage (IA-CAES) system,” *Journal of Energy Storage*, vol. 11, pp. 178–190, 2017.

[59] M. Minutillo, A. Lubrano Lavadera, and E. Jannelli, “Assessment of design and operating parameters for a small compressed air energy storage system integrated with a stand-alone renewable power plant,” *Journal of Energy Storage*, vol. 4, pp. 135–144, 2015.

[60] D. H. Robison and P. J. Beaty, “Compressor Types, Classifications, And Applications,” in *Proceedings of the 21st Turbomachinery Symposium*, Texas A&M University, pp.183-188, 1992.

[61] H. P. Bloch, *A practical guide to compressor technology*, 2nd edition, Hoboken, N.J.: Wiley-Interscience, 2006.

[62] W.M. Kays and A.L. London, *"Compact heat exchangers",* Third edition, McGraw Hill, USA, 1997.

[63] W. He and J. Wang, “Optimal selection of air expansion machine in Compressed Air Energy Storage: A review,” *Renewable and Sustainable Energy Reviews*, vol. 87, pp. 77–95, 2018.

[64] V. Lemort, L. Guillaume, A. Legros, S. Declaye, and S. Quoilin, “A comparison of piston, screw and scroll expanders for small scale Rankine cycle systems,” in *Proceedings of the 3rd International Conference on Microgeneration and Related Technologies*, Napoli (Italy), 2013.

[65] A. P. WeiB, “Volumetric expander versus turbine–which is the better choice for small ORC plants,” in *3rd ASME ORC Conference,* Brussels (Belgium), 2015.

[66] P. Vadasz and D. Weiner, “The optimal intercooling of compressors by a finite number of intercoolers,” *Journal of Energy Resources Technology*, vol. 114, no. 3, pp. 255–260, 1992.

[67] N. M. Jubeh and Y. S. H. Najjar, “Green solution for power generation by adoption of adiabatic CAES system,” *Applied Thermal Engineering*, vol. 44, pp. 85–89, 2012.

[68] A. Bejan,"*Convection heat transfer"*, Fourth edition, Hoboken, New Jersey, Wiley, 2013.

[69] L. G. Hoxton, “The Joule-Thompson Effect for Air at Moderate Temperatures and Pressures,” *Physical Review*, vol. 13, no. 6, p. 438, 1919.

[70] S. L. Dixon and C. A. Hall, *"Fluid mechanics and thermodynamics of turbomachinery",* Seventh edition, Butterworth-Heinemann, UK, 2014.

[71] S. F. Smith, “A Simple Correlation of Turbine Efficiency,” *Journal of the Royal Aeronautical Society*, vol. 69, no. 655, pp. 467–470, 1965.

[72] P.W. Andreas and Z. Gerd, “Micro turbine generators for waste heat recovery and compressed air energy storage”, *15th conference on Power System Engineering, Thermodynamics & Fluid Flow-ES-2016*, Pilsen, Czech Republic, 2016.

[73] C. M. Burt, X. Piao, F. Gaudi, B. Busch, and N. F. Taufik, “Electric motor efficiency under variable frequencies and loads,” *Journal of Irrigation and Drainage Engineering*, vol. 134, no. 2, pp. 129–136, 2008.

[74] Q. Yu and M. Cai, “Experimental Analysis of a Compressed Air Engine,” *Journal of Flow Control, Measurement & Visualization*, vol. 03, no. 04, pp. 144–153, 2015.

[75] S. Lemofouet-Gatsi, “Investigation and optimisation of hybrid electricity storage systems based on compressed air and supercapacitors”, PhD thesis, Ecole Polytechnique Fédérale de Lausanne 2006.

[76] P. Beater, "*Pneumatic drives: system design, modelling and control"*. Berlin, Springer, 2007.

[77] A. Bejan, G. Tsatsaronis, and M. J. Moran, "*Thermal design and optimization"*. New-York, Wiley, 1996.

[78] SEALL Company, Pneumatic air motors, Catalogue PDE2670TCUK, 2014.

[79] S. Kapila, A. O. Oni, and A. Kumar, “The development of techno-economic models for large-scale energy storage systems,” *Energy*, vol. 140, pp. 656–672, 2017.

[80] Y. Huang, H.S. Chen, X.J. Zhang, P. Keatley, M.J. Huang, I. Vorushylo, Y.D. Wang, N.J. Hewitt, “Techno-economic Modelling of Large Scale Compressed Air Energy Storage Systems,” *Energy Procedia*, vol. 105, pp. 4034–4039, 2017.

[81] H. Meng, M. Wang, O. Olumayegun, X. Luo, and X. Liu, “Process design, operation and economic evaluation of compressed air energy storage (CAES) for wind power through modelling and simulation,” *Renewable Energy*, vol. 136, pp. 923–936, 2019.

[82] E. Yao, H. Wang, L. Wang, G. Xi, and F. Maréchal, “Thermo-economic optimization of a combined cooling, heating and power system based on small-scale compressed air energy storage,” *Energy Conversion and Management*, vol. 118, pp. 377–386, 2016.

[83] Y. Feng and G. P. Rangaiah, “Evaluating Capital Cost Estimation Programs,” *Chemical Engineering ww.CHE.com*, pp. 22–29, 2011.

[84] R. Turton," *Analysis, synthesis, and design of chemical processes"*, 3rd edition, Upper Saddle River, N.J: Prentice Hall, 2009.

[85] Matches Company, accessed https://www.matche.com.

[86] Chemical engineering online, accessed https://www.chemengonline.com.

[87] Deprag Company, Green energy turbine, accessed https://www.deprag.com/en/green-energy/green-energy-turbine/”.

[88] J. L. H. Backman, J. Kaikko ,"Microturbine systems for *Small and micro combined heat and power (CHP) systems*", Woodhead Publishing Limited, 2011.

[89] L. Galanti and A. F. Massardo, “Thermoeconomic Analysis of Micro Gas Turbine Design in the Range 25-500 kWe”, *Proceedings of ASME Turbo Expo 2010*, pp. 317-327, Glasgow, UK, 2010.

[90] S. D. Garvey, “Chapter 5 - Compressed Air Energy Storage” *in: Trevor M. Letcher (Ed.), Storing Energy, Elsevier, Oxford*, pp. 87–111, 2016.

[91] O. S. S. Few, A. Gambhir, E. Stephenson, A. DelCore, “Energy storage trends for off-grid services in emerging markets", Technical Report, Grantham Institute- Imperial College, Shell Foundation, 2018.

[92] Z. Feng, W. Zhang, J.-A. J. Wang, and F. Ren, “Manufacturing Cost Analysis of Novel Steel/Concrete Composite Vessel for Stationary Storage of High-Pressure Hydrogen”, Report, OAK Ridge National Laboratory, USA, ORNL/TM-2013/113, 1072154, 2012.